2021 Annual Cancer Research Symposium

NCI Cancer Center

Friday | February 5, 2021

Hosted by

OU Health | Stephenson Cancer Center

OU Health Stephenson Cancer Center wishes to recognize and thank the Oklahoma Tobacco Settlement Endowment Trust (TSET) for co-sponsoring the 2021 Stephenson Cancer Research Symposium.

In 2012 TSET awarded a five-year, $30.25 million grant to Stephenson Cancer Center to establish the Oklahoma TSET Cancer Research Program. In 2017 TSET renewed this award for an additional five year period.

The mission of the Oklahoma TSET Cancer Research Program is to decrease the burden of cancer in Oklahoma and nationally through promoting, coordinating and supporting innovative cancer research. It seeks to accomplish this mission through:

- Attracting cancer researchers with grant funding from the National Cancer Institute and other national sponsors to Oklahoma
- Developing trans-disciplinary, collaborative cancer research programs
- Promoting inter-institutional partnerships to leverage unique strengths at research institutions in Oklahoma
- Enhancing research infrastructure and shared resources to enable and support innovative and nationally-competitive cancer research
- Serving as a statewide resource for researchers and institutions that conduct cancer research

The Oklahoma TSET Cancer Research Program supports a wide range of programs, shared resources and initiatives designed to accomplish these goals.

Five Year Highlights

With support from the Oklahoma TSET Cancer Research Program Stephenson Cancer Center accomplished the following:

- Increased cancer center membership from 75 to 273 members at nine academic institutions across Oklahoma
- Recruited thirty eight new cancer researchers to Oklahoma
- Funded over fifty seed and directed-research grants to cancer investigators in Oklahoma
- Enhanced five Shared Resource facilities
- Hosted over 330 research seminar speakers
- Hosted annual statewide Cancer Research Symposium that bring together over 250 researchers from around the state
- Hosted over 75 undergraduate students from 26 different universities for a summer cancer research experience
- Since the inception of the TSET grant, the SCC has enrolled more than 7,000 patients to interventional clinical trials.

Health Promotion Research Center

OU Health Stephenson Cancer Center wishes to recognize and thank the TSET Health Promotion Research Center (HPRC) for co-sponsoring the 2021 Annual Cancer Research Symposium

---

The TSET Health Promotion Research Center (HPRC; formerly the Oklahoma Tobacco Research Center [OTRC]) is a leading research program with a focus on the entire translational continuum – from the discovery of basic mechanisms of health behavior and behavior change, to the development and evaluation of novel interventions, to the dissemination and implementation of interventions, policies, and education throughout Oklahoma.

The **mission** of the HPRC is to reduce the burden of disease in Oklahoma by addressing modifiable health risk factors such as tobacco use, sedentary lifestyle, poor diet, and risky alcohol and other substance use through research, novel intervention development, and dissemination of research findings.

The HPRC contains four major resources that facilitate research: Mobile Health Shared Resource, Tobacco Treatment Research Program, Postdoctoral Fellowship Training Program, and Tobacco Regulatory Science Clinical Laboratory.

The center was established in 2007 with funding from the Oklahoma Tobacco Settlement Endowment Trust (TSET). Recognizing the investments that TSET has made in statewide and community-based cessation and intervention projects, a key feature of the HPRC is establishing partnerships with existing and future TSET-funded projects and the Oklahoma State Department of Health (OSDH) tobacco-related programs. Those partnerships directly link HPRC researchers with health-related issues and initiatives in Oklahoma.

HPRC Directors, Faculty, and Fellows

Michael S. Businelle, PhD (Director, Faculty)
Darla E. Kendzor, PhD (Director, Faculty)
Adam C. Alexander, PhD (Faculty)
Than C. Bui, MD, DrPh (Faculty)
Amy Cohn, PhD (Faculty)
Sarah Ehlke, PhD (Fellow)
Summer Frank-Pearce, PhD (Faculty)
Julia McQuoid, PhD (Faculty)
Chaelin Karen Ra, PhD. (Fellow)

TSET

OU Health | Stephenson Cancer Center

2021 Annual Cancer Research Symposium

Schedule at a Glance

10:00 – 11:30	Poster Session
11:30 – 11:45	Welcome & State of the Cancer Center
11:45 – 12:45	Keynote Address
12:55 – 1:55	Session I Geroscience & Cancer
1:55 – 2:00	Break
2:00 – 3:00	Session II Diabetes, Obesity & Cancer
3:00 – 3:05	Break
3:05 – 4:05	Session III Health Disparities & Cancer
4:05 – 4:35	Trainee Flash Presentations
4:35 – 4:50	Awards & Closing Remarks

OU Health | Stephenson Cancer Center

2021 Annual Cancer Research Symposium

Detailed Agenda

10:00 – 11:30	Poster Session
11:30 – 11:45	Welcome & State of the Cancer Center Dr. Robert Mannel
11:45 – 12:45	Keynote Address: **Hyperinsulinemia at the Cross-Roads of Obesity, Insulin Resistance, Aging, and Cancer** Dr. James Johnson
12:55 – 1:55	Session I Geroscience & Cancer Moderators: William Sonntag, Lori Jervis, Kathleen Moore **GeroOncology: The Study of the Role of How Aging Leads to Cancer and Impacts Cancer Therapies** Arlan Richardson **Chemotherapy-Induced Vascular Cognitive Impairment – A Model of Accelerated Aging** Anna Csiszar **Inhibition Of Granulocyte Colony Stimulating Remodels the Tumor Immune Microenvironment and May Enhance Efficacy of Currently Available Immune Checkpoint Blockade Therapy in Colorectal Cancer** Katherine Morris

OU Health | Stephenson Cancer Center

2021 Annual Cancer Research Symposium

1:55 – 2:00	Break
2:00 – 3:00	Session II Diabetes, Obesity & Cancer Moderators: Paul Darden, Min Li, Lacey McNally
	The Intersection of Diabetes and Cancer: Addressing Smoking as a Mutual Cause of Morbidity and Mortality Sydney Martinez
	Breast Cancer Endocrine Therapy Exhausts Adipocyte Progenitors Promoting Weight Gain and Glucose Intolerance Elizabeth Wellberg
	Imaging Biomarkers of Adiposity and Sarcopenia as Potential Predictors for Overall Survival Among Patients With Endometrial Cancer Treated With Bevacizumab Jessica Gillen
3:00 – 3:05	Break
3:05 – 4:05	Session III Health Disparities & Cancer Moderators: Rajagopal Ramesh, Paul Spicer, Priyo Mukherjee
	Evaluating Cancer Health Disparities Using the National Cancer Database (NCDB) Sara Vesley

OU Health | Stephenson Cancer Center

2021 Annual Cancer Research Symposium

Building Partnerships With Community Stakeholders to Eliminate Cancer-Related Health Disparities Among African Americans in Oklahoma
Adam Alexander

Food Insecurity in the Gynecologic Oncology Patient (FITGO)
Christina Washington

4:04 – 4:35 Trainee Flash Presentations

Tobacco Use and Treatment Preferences Among Adults Accessing Services at a Day Shelter
Laili Boozary

Single Cell Mass Spectrometry Metabolomics Studies of Cell-Cell Interactions Between Drug-Resistant Cells and Drug-Sensitive Cells in Co-Culture Systems
Xingxiu Chen

Measuring DNA Damage to Assess the Use of Electronic Cigarettes as a Tobacco Harm Reduction Strategy
Mayilvanan Chinnaiyan

Occurrence and Timing of Advanced Care Discussions in Recurrent Ovarian Cancer Patients Participating in Clinical Trials Remain to Be Optimized
Anjalika Gandhi

Regulation of Histone Demethylase JMJD2A by SET7/9-Mediated Methylation
Ruicai Gu

OU Health | Stephenson Cancer Center

2021 Annual Cancer Research Symposium

IL-1β Production Via STING Signaling Enhances Antitumor Memory Formation
Ashley Hoover

Social Determinants Of Health and Prostate Cancer Screening
Tram Le

Mass Spectrometry Metabolomics Studies of Single Cell in Multicellular Spheroids
Zongkai Peng

TICRR/TRESLIN Protein Expression is Cell Cycle Regulated by the CUL4-DDB1-DTL E3 Ubiquitin Ligase
Kimberlie Wittig

4:35 – 4:50 Awards & Closing Remarks

KEYNOTE SPEAKER

James D. Johnson, Ph.D.

Jim Johnson is Professor in the Department of Cellular and Physiological Sciences, and the Department of Surgery at the University of British Columbia, in Vancouver Canada. His laboratory is housed in the Diabetes Research Group at the Life Sciences Institute, where he is now Deputy Director.

Prior to arriving in Vancouver, he was a post-doctoral fellow at Washington University in St. Louis, under the guidance of Profs. Ken Polonsky and Stanley Misler. Johnson obtained his PhD in Physiology and Cell Biology from the University of Alberta under the supervision of Prof. John Chang.

A leader in the fundamental biology of pancreatic islets, insulin action, diabetes and their connections to co-morbidities including cancer, Prof. Johnson is the author of >135 peer-reviewed articles since starting in 2000. Prof. Johnson is Editor-in-Chief of the journal *Islets*. Prof. Johnson has won several awards, including being named the top Canadian researcher under 45 by the Canadian Diabetes Association in 2016.

In 2016, Prof. Johnson co-founded of the Institute for Personalized Therapeutic Nutrition based out of Vancouver, Canada, and is Board Chair of this non-profit dedicated to research, clinical care, and advocacy for people employing personalized diets to decrease the burden of type 2 diabetes.

From 2016-2018, Prof. Johnson was the inaugural Director of the Novo Nordisk Research Centre in Oxford, a hybrid academic-industry Institute focused on the fundamental biology of type 2 diabetes and target discovery. Prof. Johnson remains Visiting Professor of Integrated Physiology in the Radcliff Department of Medicine and Senior Fellow at Harris-Manchester College, in Oxford.

Prof. Johnson’s greatest passion is training the next generation of scientists; many of his former trainees hold academic faculty positions or are senior scientists in industry. Prof. Johnson is actively involved in science outreach on Twitter @JimJohnsonSci.

HYPERINSULINEMIA AT THE CROSS-ROADS OF OBESITY, INSULIN RESISTANCE, AGING, AND CANCER.

James D. Johnson, Ph. D.

Insulin in an anabolic hormone that is essential for life. However, accumulating evidence illustrates that it is possible to have too much of a good thing. Circulating insulin is controlled by diet and other lifestyle factors, with a large segment of the population having insulin in excess of what is required to maintain glucose homeostasis. In this lecture, Prof. Johnson will review clinical evidence and pre-clinical research using mouse models that establish the cause and effect relationships between hyperinsulinemia, and various outcomes, including insulin resistance, obesity, and type 2 diabetes. He will use this approach to demonstrate how excess insulin contributes to reduced longevity and delve into the molecular mechanisms involved. Further, he will show that hyperinsulinemia can play a causal role in pancreatic cancer initiation. Finally, he will propose an experimental framework to test related hypotheses in breast cancer and other cancers where obesity and hyperinsulinemia are associated with increased incidence and severity. These fundamental questions have the potential for significant translational impact and provide wonderful opportunities for collaborations between nations and between clinicians and basic physiologists.

Geroscience & Cancer

GEROONCOLOGY: THE STUDY OF THE ROLE OF HOW AGING LEADS TO CANCER AND IMPACTS CANCER THERAPIES

Arlan Richardson, PhD
Professor of Biochemistry & Molecular Biology, the University of Oklahoma Health Science Center, and Senior Research Career Scientist, Oklahoma City VA Medical Center

Age is the major risk factor risk for cancer with over three-quarters of the new diagnoses occurring in individuals over 55 years of age. Because of the growth of the research programs in cancer and aging at OUHSC, the Stephenson Cancer Center recently received a supplement from NCI to develop a GeroOncology Program, which will focus on three areas. (1) the molecular changes that occur with age that can impact cancer, (2) specialized cancer therapy for elderly patients, and (3) community outreach focused on elderly cancer patients in rural and tribal communities. The focus of this presentation will be on how age-related changes in several molecular processes could lead to the increased incidence of cancer observed with age.

CHEMOTHERAPY-INDUCED VASCULAR COGNITIVE IMPAIRMENT- A MODEL OF ACCELERATED AGING

Anna Csiszar[1,2], Chetan P. Ahire[1,2], Priya Balasubramanian[1], Stefano Tarantini[1], Tamas Kiss[1], Adam Nyul-Toth[1], Zoltan Ungvari[1]

1. Department of Biochemistry and Molecular Biology; 2. Department of Pathology, University of Oklahoma Health Sciences Center

Introduction: We found that in the aging brain~15% of endothelial cells undergo cellular senescence, a common DNA damage response that significantly alters cellular phenotypes. Our previous studies have proved that endothelial senescence contributes to vascular dysfunction and the pathogenesis of vascular cognitive impairment and dementia (VCID) in aging. Increasing clinical and experimental evidence suggest that chemotherapeutic agents cause similar symptoms of cognitive impairment in cancer survivors although its exact pathomechanism is unknown. The discovery of the cellular mechanisms responsible for decreased cognitive capacity after cancer treatment is ultimately expected to enhance understanding of the pathogenesis of the disease and will lead to the development of novel therapeutic interventions for prevention.

Hypothesis: The central hypothesis of this application is that chemotherapeutic agents induce endothelial senescence, which impairs cerebral blood flow, promote microvascular rarefaction and compromise endothelium-dependent neurovascular coupling responses as well as barrier integrity and contribute to the deterioration of cognitive function. This hypothesis was tested by using an innovative mouse model: senescence reporter mice treated with the chemotherapeutic drug paclitaxel (PTX), which allows the detection and selective elimination of senescent cells.

Results: We found that chemotherapy-induced activation of p16-dependent senescence program in endothelial cells increases oxidative stress and impairs vasodilator function. Elimination of senescent endothelial cells, through genetic manipulation (GCV treatment) or through translatable senolytic therapies (Navitoclax) restore neurovascular function and improve CBF in mice treated with clinically relevant PTX protocol. Chemotherapy-induced endothelial senescence compromised the maintenance of the microcirculatory network and impaired endothelial barrier function. The elimination of senescent cells increased microvascular density and restored BBB integrity. Endothelial senescence and consequential microvascular dysfunction contributed to the impairment of multiple domains of cognition as well.

Conclusion: On the basis of our data in animal models of chemotherapy-induced cognitive impairment we concluded that its pathogenesis significantly overlaps with that of age-related vascular cognitive impairment demonstrating an accelerated vascular aging phenotype.

INHIBITION OF GRANULOCYTE COLONY STIMULATING FACTOR REMODELS THE TUMOR IMMUNE MICROENVIRONMENT AND MAY ENHANCE EFFICACY OF CURRENTLY AVAILABLE IMMUNE CHECKPOINT BLOCKADE THERAPY IN COLORECTAL CANCER.

Katherine T. Morris, Anita L. Ray, Dawn Bender, Apryl Saunders, Megan Reidy, Michael Cloyde, Shaoxuan Guo, Megan Lerner, William Berry, Michael Stout, Robert A. Nofchissey

Although the incidence of colorectal cancer (CRC) is increasing among younger patients, it remains a disease of the elderly with over 90% of cases occurring in people over 50 and a mean age at diagnosis of colon cancer of 68 in men and 73 in women.
Total T cell infiltration into the tumor immune microenvironment has been shown to be a stronger predictor of disease specific survival than AJCC staging in colorectal cancer (CRC). However, many CRCs have limited T cell infiltration and currently available immune checkpoint inhibitors have shown efficacy in mismatch repair deficient colorectal cancers only. Currently we do not have a treatment regimen that will enhance T cell infiltration and activation in CRC.

Granulocyte colony stimulating factor (GCSF) is best known for effects on the mobilization and maturation of neutrophils and is used clinically to treat or prevent febrile neutropenia. However, we have shown that *inhibition* of GCSF in CRC development and metastatic models has beneficial anti-tumor effects as well as striking effects on the tumor immune microenvironment. In both the development and metastatic models, the use of functional anti-GCSF antibody (αGCSF) resulted in >2-fold increases in T cell infiltration into the TME. Because of these data, we hypothesize that inhibition of GCSF will overcome barriers to T cell infiltration in CRC and increase the number of patients who will respond to currently available ICB therapies. Here we will show new data from human specimens and mouse models that support this hypothesis in addition to preliminary data demonstrating potential differences in the immune response to CRC due to age.

Diabetes, Obesity & Cancer

THE INTERSECTION OF DIABETES AND CANCER: ADDRESSING SMOKING AS A MUTUAL CAUSE OF MORBIDITY AND MORTALITY

Sydney Martinez, PhD
Department of Biostatistics and Epidemiology, University of Oklahoma Health Sciences Center

Cigarette smoking remains the leading cause of preventable death and has been proven to cause many types of cancer as well as type 2 diabetes mellitus (T2DM). Smoking increases blood glucose concentration and insulin resistance and substantially accelerates micro and macrovascular complications of patients with T2DM. While the long-term benefits of smoking cessation for individuals with T2DM are clear, there is a complex relationship between smoking cessation and glycemic control. Previous studies have shown that smoking cessation paradoxically leads to glucose dysregulation. HbA1c has been shown to increase during the first one to three years post-cessation, which is only partially explained by post-cessation weight gain. Despite heightened risks among patients with T2DM, smoking prevalence remains high. Few studies have examined ways of improving smoking cessation in this population or ways of more effectively integrating cessation into diabetes care. To address gaps, we are conducting a series of studies to evaluate the implementation of smoking cessation in diabetes care, develop tailored smoking cessation interventions for smokers with T2DM, and understand the relationship between smoking behaviors and glucose levels to identify potential predictors of relapse. An online survey through the Oklahoma Physicians Resource/Research Network demonstrated that the level of agreement with whether smoking increases the risk or worsening of various conditions was higher for cardiovascular-related outcomes (90%) compared to T2DM (41%) and insulin resistance (26%). In a pilot randomized controlled trial we demonstrated the feasibility using a smartphone application and remote carbon monoxide (CO) sensor as part of a contingency management program for smoking cessation for smokers with T2DM. Patients perceived the accountability of the daily remote CO sensors as helpful to their quit attempt, but did not perceive smoking to affect their diabetes-related health. In order to understand the paradox between cessation and glycemic dysregulation, we are beginning a study using continuous glucose monitoring paired with our smartphone and remote CO study to observe glucose profiles before and after a smoking cessation attempt. We hope to contribute significant observational findings needed to elucidate the acute impact of smoking on glucose profiles during a smoking cessation attempt. Understanding the real-time associations between glucose levels and urges to smoke/relapse could inform the development of a T2DM-specific smoking cessation intervention.

BREAST CANCER ENDOCRINE THERAPY EXHAUSTS ADIPOCYTE PROGENITORS PROMOTING WEIGHT GAIN AND GLUCOSE INTOLERANCE

Elizabeth A. Wellberg[2,5,7,] Rebecca L. Scalzo[1,2,3], Rebecca M. Foright[4], Sara E. Hull[1], Leslie A. Knaub[1], Stevi Johnson-Murguia[5,7], Marisol Castillo-Castrejon[7], Fotobari Kinanee[5], Jeffrey Kaplan[5], Benjamin Freije[1], Ginger Johnson[1], Anni M.Y. Zhang[6], James D. Johnson[6], Paul S. MacLean[1,2,5], Jane E.B. Reusch[1,2,3], Sabrina Wright-Hobart[5]
elizabeth-wellberg@ouhsc.edu
1. Division of Endocrinology, Metabolism & Diabetes, Department of Medicine; University of Colorado Anschutz Medical Campus, Aurora, Colorado. 2. Center for Women's Health Research; University of Colorado Anschutz Medical Campus, Aurora, Colorado. 3. Rocky Mountain Regional VA Medical Center, Aurora, Colorado. 4. Department of Anatomy and Cell Biology, University of Kansas Medical Center, Kansas City, KS; 5. Department of Pathology, University of Colorado Anschutz Medical Campus, Aurora, CO. 6. Diabetes Research Group, Life Sciences Institute, Department of Cellular and Physiological Sciences, Faculty of Medicine, University of British Columbia, Vancouver, BC, Canada; 7. Department of Pathology, University of Oklahoma Health Sciences Center, Stephenson Cancer Center, Harold Hamm Diabetes Research Center, Oklahoma City, OK.

Breast cancer survivors treated with anti-estrogen therapies report weight gain and have an elevated risk of type 2 diabetes. Here, we show that current tamoxifen use associated with larger breast adipocyte diameter only in women with a BMI >30 kg/m^2. To understand the mechanisms behind these clinical findings, we investigated the impact of estrogen deprivation and tamoxifen in a relevant pre-clinical model of obesity. Specifically, mature female mice were housed at thermoneutrality and fed either a low-fat/low-sucrose (LFLS) or a high-fat/high-sucrose (HFHS) diet. Consistent with the high expression of *Esr1* observed in single-cell RNA sequencing of mesenchymal stem cells from adipose tissue, endocrine therapies induced adipose accumulation and preadipocyte expansion, but resulted in adipocyte progenitor depletion only in the context of HFHS. Consequently, 7-week endocrine therapy supported adipocyte hypertrophy and was associated with hepatic steatosis, hyperinsulinemia, insulin resistance, and glucose intolerance, particularly in HFHS fed females. Metformin or pioglitazone, glucose lowering drugs used to treat diabetes, or interval exercise training prevented the effects of tamoxifen but not estrogen deprivation on adipocyte size and insulin resistance in HFHS-fed mice. This translational study suggests that endocrine therapies act via ER-alpha to disrupt adipocyte progenitors and support adipocyte hypertrophy, leading to ectopic lipid deposition that may promote hyperinsulinemia, insulin resistance and type 2 diabetes. Interventions that target insulin action should be considered for some women receiving life-saving endocrine therapies for breast cancer.

NIH R01 CA241156 (EAW); University of Colorado Center for Women's Health Research (RLS, JEBR, EAW); University of Colorado Nutrition and Obesity Research Center (RLS, JEBR, PSM, EAW) Komen Foundation Career Catalyst Research Grant (EAW); VA CDA2 (RLS).

IMAGING BIOMARKERS OF ADIPOSITY AND SARCOPENIA AS POTENTIAL PREDICTORS FOR OVERALL SURVIVAL AMONG PATIENTS WITH ENDOMETRIAL CANCER TREATED WITH BEVACIZUMAB

J. Gillen[a], K.A. Mills[b], J. Dvorak[a], B. Zheng[c], T. Thai[a], R. Salani[d], C.M. Cosgrove[d], B. Davidson[e], P.H. Thaker[b] and K.N. Moore[a]

[a]Stephenson Cancer Center at the University of Oklahoma Health Sciences Center, Oklahoma City, OK, USA, [b]Washington University School of Medicine St. Louis, MO, USA, [c]The University of Oklahoma, Norman, OK, USA, [d]The Ohio State University, James Cancer Hospital, Columbus, OH, USA, [e]Duke University School of Medicine, Durham, NC, USA

Objective: To examine associations of body mass index (BMI), subcutaneous fat area (SFA) and density (SFD), visceral fat area (VFA) and density (VFD) and total psoas area (TPA) to outcomes among patients receiving chemotherapy with or without bevacizumab for advanced or recurrent endometrial cancer (EC).

Methods: This was a multi-institutional, retrospective study of patients with EC treated with and without bevacizumab as part of front-line, platinum based chemotherapy. Demographics and clinical characteristics were collected. SFA, VFA, SFD, VFD, and TPA were determined from pre-treatment CT scans using a deep learning algorithm. Data was compared with overall survival (OS) and progression free survival (PFS).

Results: Seventy-eight patients were analyzed. The majority were Caucasian (87.2%) with a mean BMI of 34.7 kg/m^2. PFS and OS did not differ between patients with BMI, SFA, VFA, SFD, VFD, or TPA $\geq$ the 50th percentile compared to <50th percentile (p=0.91, 0.45, 0.71, 0.74, 0.60, and 0.74 respectively) and (p=0.99, 0.59, 0.14, 0.77, and 0.85 respectively). When adjusting for prognostic factors, elevated VFA trended towards shorter OS (25.1 vs 59.5 months, HR = 1.68 [0.92-3.05]).

Patients receiving bevacizumab had similar OS compared to those who did not (37.6 vs 44.5 months, p=0.409). When stratified by adiposity markers, no subset demonstrated benefit from bevacizumab.

Conclusion: Obesity has been associated with increased levels of vascular endothelial growth factor (VEGF), the main target for bevacizumab therapy. Imaging measurements of VFA may provide prognostic information for patients with EC but no adiposity marker was predictive of improved response to bevacizumab.

Health Disparities & Cancer

EVALUATING CANCER HEALTH DISPARITIES USING THE NATIONAL CANCER DATABASE (NCDB)

Vesely SK, Ikeguchi A, Machiorlatti M

The National Cancer Database (NCDB) is a joint sponsored project on the Commission on Cancer (CoC) of the American College of Surgeons and the American Cancer Society. Data for the NCDB is gathered from over 1500 hospital registries from CoC accredited hospitals. The NCDB notes that more than 70% of all newly diagnosed malignancies in the USA are captured in their database. We have used the NCDB to evaluate cancer health disparities across a range of malignancies. For example, we evaluated patients with node-positive melanoma to determine if the survival benefits of adjuvant chemotherapy demonstrated in randomized comparisons persisted across various demographic factors. We evaluate 38,189 node-positive melanoma patients diagnosed between 2004 and 2015 who were in the NCDB. We calculated descriptive statistics and used the Kaplan-Meier method to create survival curves. Cox proportional hazards models, including evaluation of interactions, were created to compare differences in survival based on demographic and baseline factors. Age group (<65 years verus ≥ 65 years), sex, insurance status, positive nodes and the Charlson-Deyo score all impacted survival. Race (Caucasian versus other) did not statistical impact survival time. Immunotherapy was significantly associated with increased survival across all demographic factors. In a multivariable analysis, only age group significantly interacted with immunotherapy. The positive survival benefit of immunotherapy was greater among those in the age group of 65 years or greater as compared to those in the age group less than 65 years of age. NCDB is an important source of data to evaluate cancer health disparities.

Ikeguchi A, Machiorlatti M, **Vesely SK**. Disparity in outcomes of melanoma adjuvant immunotherapy by demographic profile. *Melanoma Management*. 2020;7(2)

Stage III Melanoma Patients who received immunotherapy were at a decreased hazard for death. The protective effect from immunotherapy was greater for those ≥65 years of age compared to those <65 years of age.

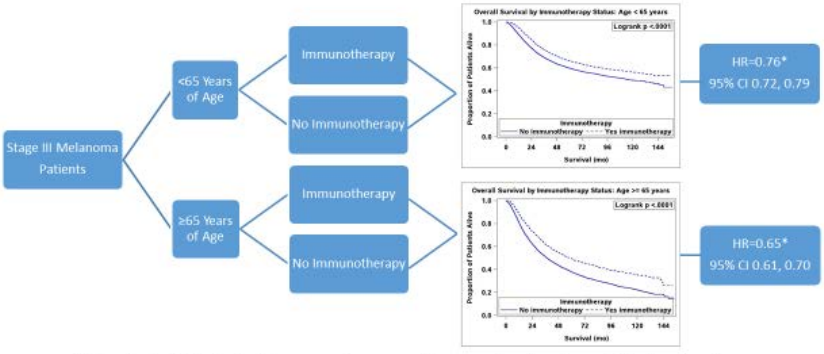

*Hazard ratio (HR) adjusted for sex, race, insurance status, number of nodes, and Charlson-Deyo Score

BUILDING PARTNERSHIPS WITH COMMUNITY STAKEHOLDERS TO ELIMINATE CANCER-RELATED HEALTH DISPARITIES AMONG AFRICAN AMERICANS IN OKLAHOMA

Adam C. Alexander (adam-alexander@ouhsc.edu)[a,b]

[a] TSET Health Promotion Research Center, Stephenson Cancer Center, University of Oklahoma Health Sciences Center, Oklahoma City, Oklahoma, United States, [b] Department of Family and Preventive Medicine, University of Oklahoma Health Sciences Center, Oklahoma

Role of funding source: The ongoing research mentioned in this presentation is supported by funds from the Oklahoma Tobacco Settlement Endowment Trust (R21-02) and Community Outreach and Engagement Core.

The Stephenson Cancer Center (SCC) is uniquely positioned to provide statewide leadership in cancer research, treatment, education, and outreach, and its central mission is to engage communities within Oklahoma to decrease cancer burden, particularly among minority and under-represented populations. However, engagement with African Americans in Oklahoma is lacking despite significant cancer disparities. The incidence and mortality rates of cancer are generally higher among African Americans than Whites in Oklahoma. Most importantly, the 5-year cancer survival rate for African Americans living in Oklahoma is 47.1%, the lowest survival rate of all racial/ethnic groups in Oklahoma. African Americans are motivated and eager to address these significant health challenges, and there is an opportunity for SCC to renew its relationship and collaborate with community stakeholders to build lasting partnerships that will shape the direction of African Americans' health in Oklahoma for decades. This presentation will provide an overview of the planned activities in 2021 to reestablish our connection with community stakeholders and African Americans in Oklahoma. Topics will include (1) establishing a research workgroup and a community advisory board for cancer disparity research with African Americans; (2) monitoring disparities associated with the COVID-19 pandemic and race-related social unrest and their impact on modifiable lifestyle-related cancer risk factors; and (3) improving cancer screening behavior among African Americans using mobile health technology and lay health educators. These efforts will serve as the foundation for building larger community-based interventions to promote cancer prevention and care and eliminate cancer-related health disparities among African Americans in Oklahoma.

FOOD INSECURITY IN THE GYNECOLOGIC ONCOLOGY PATIENT (FITGO)

C.R. Washington, J. Littlec, M. Wetherilld, J. Walkerc, S. Veselyb, B. Curryb, T. Bhushanb, L. Holmanc.

[a] *University of Oklahoma HSC, Oklahoma City, OK, USA, The University of Oklahoma Health Sciences Center, Oklahoma City, OK, USA,* [c] *The University of Oklahoma, Oklahoma City, OK, USA,* [d] *University of Oklahoma HSC, Tulsa, OK, USA*

Malnutrition is an established risk factor for poor cancer treatment outcomes, including suboptimal therapy response, complications, and survival. Food insecurity (FI), the lack of access to a healthy food supply, may contribute to malnutrition, as well as result in detrimental tradeoff decisions between paying for cancer treatment and food. Nearly 17% of Oklahoma households are FI, far exceeding the national average (11.8%), and women, racial minority, and underinsured populations are disproportionately impacted by FI. “Screen-and-intervene” strategies for FI are increasingly recognized as a standard of care for pediatrics, geriatrics and primary care population, yet less is known about best practices for FI screening within oncology populations, which face unique barriers to dietary intake due to treatment side-effects. Thus, the development and evaluation of clinic-based FI screen-and-intervene strategies for cancer settings are needed to address FI as an important modifiable risk factor for cancer outcomes. To inform this project, we initiated an ongoing quality improvement project in July 2020, to identify patients at risk for FI receiving care at the Stephenson Cancer Center Gynecologic Oncology Clinic. The screening consisted of the 2-item validated “Hunger Vital Sign” food security screener, which asks, “Within the past 12 months, 1) “…we worried whether our food would run out before we got money to buy more”, and 2), “…the food we bought just didn’t last and we didn’t have money to get more.” A third question screened for healthy food accessibility and affordability. Our preliminary analyses of the first wave of screening data (n=291 patients over 3-weeks’ time) found that one in five (21%) patients from this sample screened positive for FI risk, and 26% of all patients, irrespective of food security status, indicated difficulty with accessing affordable fruits and vegetables in their community.

The first year of this two-year study will: 1) estimate the prevalence and correlates of FI among gynecologic oncology cancer patients receiving treatment at the Stephenson Cancer Center (SCC), and 2) qualitatively explore the food needs and assistance preferences of patients at risk for FI. These data will be used to inform a clinic-based FI intervention framework for pilot implementation and evaluation during the second year of this study.

Trainee Flash Presentation

TOBACCO USE AND TREATMENT PREFERENCES AMONG ADULTS ACCESSING SERVICES AT A DAY SHELTER

Laili Kharazi Boozary, M.S.[1,4], Adam C. Alexander, Ph.D.[3,4], Joseph J. C. Waring, BPH[4], Summer G. Frank-Pearce, Ph.D., MPH [2,4], Sarah J. Ehlke, Ph.D.[4], Michael S. Businelle, Ph.D.[3,4], Amy M. Cohn, Ph.D.[4,5], and Darla E. Kendzor, Ph.D.[3,4]

[1] Department of Psychology, Cellular and Behavioral Neurobiology, The University of Oklahoma, Norman, OK, [2]Department of Biostatistics and Epidemiology, Hudson College of Public Health, The University of Oklahoma Health Sciences Center, Oklahoma City, OK, [3] Department of Family and Preventive Medicine, The University of Oklahoma Health Sciences Center, Oklahoma City, OK, [4] TSET Health Promotion Research Center, Stephenson Cancer Center, The University of Oklahoma Health Sciences Center, Oklahoma City, OK, [5] Department of Pediatrics, The University of Oklahoma Health Sciences Center, Oklahoma City, OK

Background: Although smoking rates have declined to 14% among adults in the U.S., 70-80% adults experiencing homelessness continue to smoke. Approaches are needed to address persisting tobacco-related health disparities. The current study characterized tobacco use and treatment preferences among adults accessing day shelter services.

Methods: Adults completed a survey at the Homeless Alliance Day Shelter in Oklahoma City to assess sociodemographic characteristics, tobacco history, tobacco treatment preferences, and substance use.

Results: Of participants, 75.2% (n=406) reported current smoking, and most wanted to quit (57.2%). Current smokers reported smoking 13.9 (SD=10.0) cigarettes per day (CPD; 57.1% smoked <10 CPD) and had been smoking for 23.3 (SD=12.7) years on average. Smokers were primarily male (74.9%), 45.7 (SD=11.2) years of age on average, and largely of White (41.1%, n=167), Black (25.9%, n=105), or American Indian (12.8%, n=52) race. A total of 7.2% (n=29) were veterans. The most commonly tried cessation aids included the nicotine patch (22.9%), nicotine gum/lozenges (19.0%), e-cigarettes (ECs; 14.5%), and the Oklahoma Tobacco Helpline (10.1%). Most had not previously tried any cessation aids (51.7%). Smokers most commonly endorsed cold turkey (25.1%), nicotine replacement therapy (24.6%), money or gift cards for quitting (17.2%), prescription medications (16.5%), and switching to ECs (16.0%) as offering the best chance for quitting. Participants most commonly reported cravings (54.7%), stress/mood (39.4%), habit (38.7%), and being around other smokers (36.2%) as the most difficult aspects of quitting. A total of 55.4% of all smokers reported interest in using ECs for smoking cessation and 14.5% had used ECs in the past 30 days. Smokers who reported past 30-day EC use more often used fruit/candy/other flavored (50.9%) or menthol/mint (22.0%) ECs vs. tobacco flavored (15.3%) ECs, and more frequently perceived some (39.0%) or extreme/a lot of risk (28.8%), vs. no/little risk (32.2%) associated with EC use. Past 30-day cannabis use (51.5%), heavy drinking (58.8%), and injection drug use (12.5%) were prevalent, as were mental illnesses including Generalized Anxiety Disorder (28.1%), Posttraumatic Stress Disorder (26.9%), and Major Depressive Disorder (22.5%).

Conclusion: Findings suggest that homeless shelter guests were interested in smoking cessation, though evidence-based treatments were underutilized. Smokers may benefit from education about cessation aids along with increased access. A focus on non-traditional smoking cessation approaches including EC switching and financial incentives for quitting may be warranted, and non-tobacco substance use and mental health problems may need to be considered and potentially addressed as part of a broader treatment approach.

TOBACCO USE AND TREATMENT PREFERENCES AMONG ADULTS ACCESSING SERVICES AT A DAY SHELTER

Laili K. Boozary, Adam C. Alexander, Joseph J. C. Waring, Summer G. Frank-Pearce, Sarah J. Ehlke, Michael S. Businelle, Amy M. Cohn, & Darla E. Kendzor

The University of Oklahoma Health Sciences Center, Stephenson Cancer Center, TSET Health Promotion Research Center, Oklahoma City, OK

Health Promotion Research Center

Background

- Adults experiencing homelessness have mortality rates 3x higher than the general population.
- 70-80% of homeless adults smoke despite studies showing that many 40-70%) report that they are ready to quit.
- Alternative cessation strategies may benefit those experiencing homelessness, particularly the treatments preferred by this population.

PURPOSE

- The current study describes the personal characteristics and treatment preferences of smokers accessing day shelter services.
- **Findings will inform future smoking cessation intervention approaches for adults experiencing homelessness and/or accessing shelter service.**

Methods

Participants

Eligibility Criteria

- Adults 18+ years old
- Utilizing Homeless Alliance Day Shelter

Key Measures and Scales

- Smoking Status
- Demographics
- Tobacco Use
  - Motivation to Stop Scale (Kotz et al., 2013)
  - Heaviness of Smoking Index (Kozlowski et al., 1994)
- Mental Health
  - PHQ-Depression (Spitzer et al., 1999)
  - GAD-7 (Kroenke et al., 2007)
  - Primary Care PTSD Screen (Prins et al., 2003)
- Substance Use
  - Texas Christian University Drug Screen 5 (Research, 2020)
  - Alcohol Quantity, Frequency, and Binge Drinking Questionnaire

Procedures

- Participants were approached by study staff and asked to complete surveys
- Participants were compensated for their time

Analytic Plan

- SAS 9.4
- Descriptive statistics: mean and frequency analyses
- Comparisons: chi-square and t-tests

Funding: This study was supported by funding from Oklahoma Tobacco Settlement Endowment Trust grant R21-02.

Results

Table 1: Demographic Characteristics of Smokers

Characteristic	Overall (n = 540)	Smokers (n = 406)
Age	45.65 ± 11.65	45.67 ± 11.19
Sex, Female	29.44 (159)	25.12 (102)
Race		
White	38.03 (205)	41.23 (167)
Black or African American	26.72 (144)	25.93 (105)
American Indian/Alaska Native	15.03 (81)	12.84 (52)
Latinx	11.32 (61)	10.86 (44)
Other	8.91 (48)	9.14 (37)
Currently Homeless	91.11 (492)	92.12 (374)
Marital Status, %single	82.09 (440)	84.12 (339)
Education, mean	11.53 ± 2.80	11.51 ± 2.62
Employment, % not employed	88.15 (476)	89.66 (364)
Insurance status, % uninsured	63.89 (345)	66.01 (268)
Household income, % <$5,000	69.39 (306)	70.00 (238)

Results *(cont.)*

See Table 1. Of the total sample, 75.19% (n = 406) were Smokers…

- 56.93% (n = 230) endorsed some desire to quit smoking,
- 51.29% (n = 159) of smokers were interested in a free smoking cessation program
- 25.12% (n = 102) participants endorsed Cold Turkey as offering the best chance of cessation success
- 55.38% (n = 211) were interested in using e-cigarettes as a smoking cessation strategy.
- **Top 3 Reasons for Using E-Cigarettes**: A) I can use it in places where cigarettes are not allowed (38.98%, n = 23), B) to help me quit smoking cigarettes (37.29%, n = 22), & C) to help me cut down on smoking cigarettes (37.29% n = 22)
- 71.54% (n = 186) reported a belief that God absolutely exists & (42.02 %, n = 221) participated in religious services at least once a week or more
- 22.51% (n = 88) had PHQ diagnosis of depression, 26.85% (n = 109) screened positive for PTSD, and 28.13% (n = 110) screened positive for moderate-severe GAD
- 31.20% (n = 122) screened positive for moderate or severe *SUD*
- 51.49% (n = 208) used marijuana in the past 30 days
- 23.02% (n = 90) engaged in heavy drinking
- 12.50% (n = 49) used needles to inject drugs within the past 6 months
- Only 43.10% of smokers reported owning a cell phone
- Only 41.94 (n = 164) reported that they were Extremely Confident in filling out medical forms (i.e. health literacy).
- 45.78% (n = 179) endorsed feeling anxious or uncertain about household food supply, 65.47% (n = 256) endorsed Insufficient Food Quality, and 63.17% (n = 247) endorsed Insufficient Food Intake

Results *(cont.)*

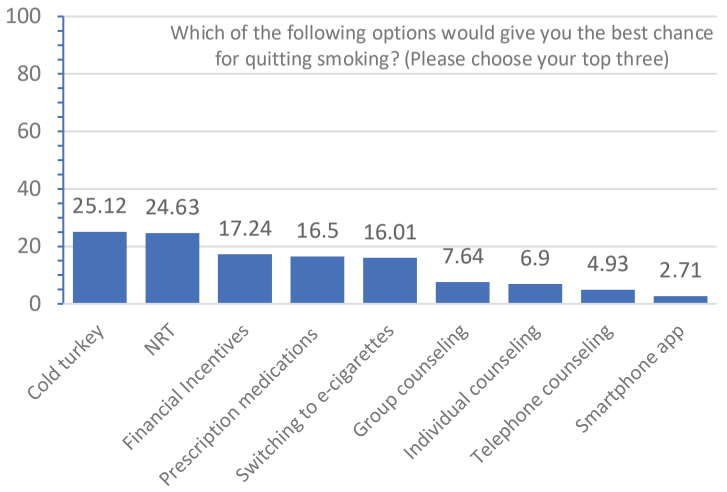

Conclusion

- Findings offer guidance about potential smoking cessation intervention strategies for adults accessing day shelter services.
- Interventions may need to provide education about effective smoking cessation treatments and incorporate alternative strategies such as financial incentives for quitting and e-cigarette switching. See Figure 1.
- Cessation intervention strategies must consider low health literacy, and high rates of mental illness, substance use, and food insecurity.

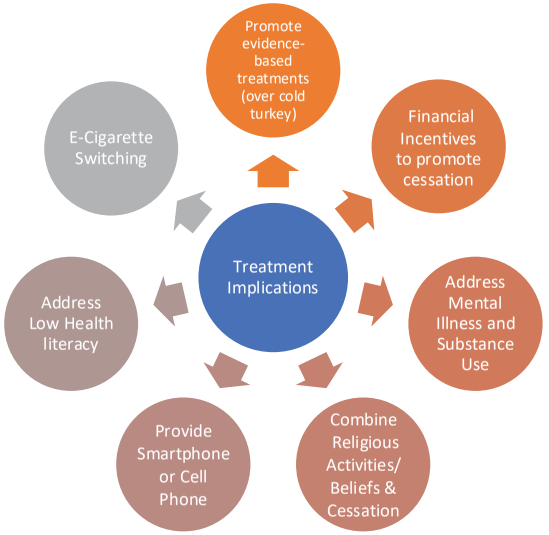

Figure 1. Implications and Recommendations for Smoking Cessation Interventions for Adults Experiencing Homelessness.

TSET

SINGLE CELL MASS SPECTROMETRY METABOLOMICS STUDIES OF CELL-CELL INTERACTIONS BETWEEN DRUG-RESISTANT CELLS AND DRUG-SENSITIVE CELLS IN CO-CULTURE SYSTEMS

Xingxiu Chen, Zhibo Yang
Department of chemistry and biochemistry, University of Oklahoma

Drug resistance is a major reason responsible for the failure in clinical cancer chemotherapy. The molecular mechanisms of drug resistance are of the great interest to researchers. It is believed that interactions between drug-resistant and drug-sensitive cells are relevant to the development of drug resistance in tumors. There are two major approaches for molecular exchange in cell-cell communication: secreting soluble molecules and transferring extracellular vesicles. A variety of *in vitro* co-culture systems, either with or without cell-cell contact, have been developed to study the mechanisms of cell-cell interactions. However, the systems without physical cell-cell contact cannot vividly mimic the actual physiological environment. Although a few techniques have been developed to study cell-cell contact, it is a great challenge to comprehensively analyze metabolomic profiles of individual cells among heterogeneous populations in such *in vitro* co-culture systems.

Mass spectrometry (MS) is a powerful tool for the analysis of cellular metabolites, which directly reflect the genetic and environmental changes of cells. To study the cell-cell interactions among different types of cells, single cell MS (SCMS) metabolomics analysis is needed. The Single-probe developed by our group is a miniaturized multifunctional device that can be coupled with MS to characterize cellular metabolites in live single cell. In this work, the Single-probe MS technique has been utilized for metabolomics studies of interactions between drug-resistant and drug-sensitive cells in co-culture systems.

Irinotecan-resistant (IRI-resistant) cells and drug-sensitive HCT 116 cells were used as models to construct the co-culture systems. MTT assay results indicate the levels of irinotecan resistance in drug-sensitive HCT 116 cells were significantly increased due to the presence of IRI-resistant cells in co-culture systems (without cell contact). To differentiate these two types of cells, HCT 116 cells with stable GFP expression (HCT 116-GFP) were used to represent the drug-sensitive cells. The SCMS studies illustrate that GFP labeling has no significant influence on cell metabolites. In the co-culture system with cell contact, metabolic profiles of HCT 116-GFP cells were significantly changed by the IRI-resistant cells. Interestingly, both types of cells tend to exhibit increased similarities of metabolomic profiles after co-culture. Investigation of cell metabolites altered by co-culture shows that a series of monosaturated lipids were significantly upregulated in HCT 116-GFP cells. We hypothesize SteaoylCoA desaturase-1 is responsible for the enhanced drug resistance of drug-sensitive cells in co-culture conditions. More experiments need to be carried out to test this hypothesis.

Single Cell Mass Spectrometry Metabolomics Studies of Cell-Cell Interactions Between Drug-resistant Cells and Drug-sensitive Cells in Co-culture Systems

Xingxiu Chen, Zhibo Yang*

Department of Chemistry & Biochemistry, University of Oklahoma

Introduction

- Drug resistance to chemotherapy medicine is a major reason for clinical cancer treatment failure.
- It is believed that interactions between drug-resistant and drug-sensitive cells are relevant to the development of drug resistance in tumors.
- A variety of *in vitro* co-culture systems, either with or without cell-cell contact, have been developed to study the mechanisms of cell-cell interactions. However, the systems without physical cell-cell contact cannot vividly mimic the actual physiological environment. Although a number of techniques have been developed to study cell-cell contact, it is a great challenge to comprehensively analyze metabolomic profiles of individual cells among heterogeneous populations in such *in vitro* co-culture systems.
- Mass spectrometry (MS) is a powerful tool for the analysis of cellular metabolites, which directly reflect the genetic and environmental changes of cells. To study the cell-cell interactions among different types of cells, single cell MS (SCMS) metabolomics analysis is needed.
- **In this work, the Single-probe MS technique has been utilized to study cell-cell interactions in a co-culture system with cells possessing different levels of anticancer drug resistance.**

Methods

- **Single-probe Mass Spectrometry**:

The Single-probe is a miniaturized multifunctional device that can be coupled with MS to characterize cellular metabolites in live single cell. The Single-probe composes of three major parts: Nano-ESI emitter, dual-bore quartz tip, and fused silica capillary.

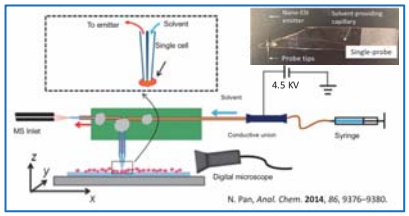

- **MTT assay for cell viability measurement:**

Drug treatments were carried out for IRI-resistant cells in 96-well plates.

MTT was added into 96-well plates for absorbance measurement (570 nm) using a microplate reader.

Methods

- **Workflow of SCMS study on Co-culture system:**

Irinotecan-resistant (IRI-resistant) cells and drug-sensitive HCT-116 cells were used as models to study the cross-communication.

Step 1: Establish co-culture system with cell contact. Stable HCT-116 cells with GFP expression (HCT-116-GFP) were used to represent the drug-sensitive cells. Both types of cells were seeded in the same well of 6-well plates, allowing for cell attachment onto gridded glass coverslips.

Step 2: Capture florescence image. To identify the two types of cells in co-culture system, fluorescence images were taken using a Nikon Eclipse Ti fluorescence microscope.

Step 3: SCMS study. The Single-probe SCMS technique was used to analyze single IRI-sensitive and resistant cells.

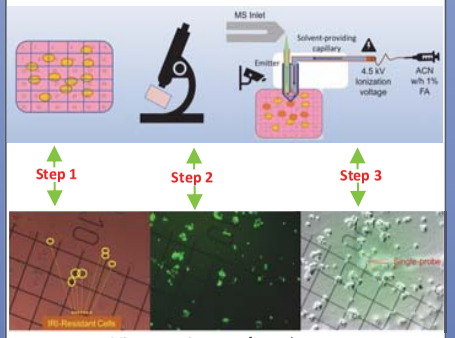

Microscopy images of co-culture system

Results

Elevated IRI-resistance of HCT 116 cells after Co-culture.

MTT assay results indicate that the levels of irinotecan resistance of regular HCT-116 cells were significantly increased due to the presence of IRI-resistant cells in the co-culture systems without cell contact (porous membrane). The drug resistance level increased along with the increase of co-culture time and the density of IRI-resistant cells .

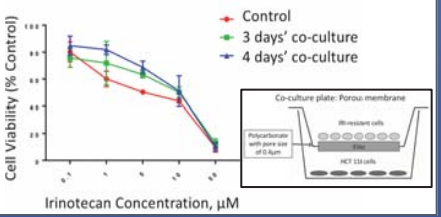

Results

GFP labeling has no significant influence on the metabolic profiles of cells.

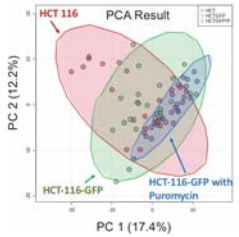

HCT 116-GFP were used to represent the drug-sensitive cells in the co-culture system with contact. The SCMS studies were carried out for HCT 116, HCT 116-GFP, and HCT 116-GFP cultured with puromycin (to maintain HCT116-GFP populations). The results illustrate that GFP labeling has no significant influence on cell metabolites.

Metabolic profiles of HCT116-GPF cells are significantly changed in co-culture system.

In the co-culture system with cell contact, metabolic profiles of HCT-116-GFP cells were significantly changed by the IRI-resistant cells. Interestingly, both types of cells tend to exhibit increased similarities of metabolomic profiles after co-culture.

PCA plot

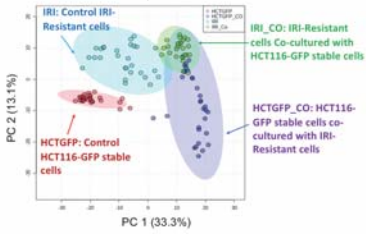

Results from student's t-test show that a series of monosaturated lipids (e.g., SM and PC) were significantly upregulated in HCT 116-GFP cells.

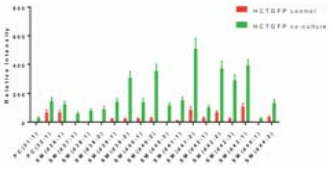

Pathway Mechanism

We hypothesize that Steaoyl-CoA desaturase-1 (SCD-1), a key enzyme in charge of producing monosaturated fatty acids from unsaturated fatty acids, is responsible for the enhanced drug resistance of drug-sensitive cells in the co-culture conditions. Yet, more experiments need to be carried out to test this hypothesis.

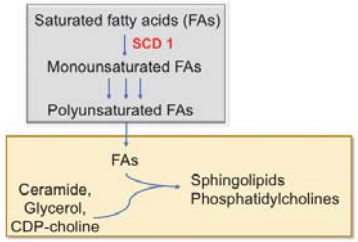

Conclusion

1. The Single-probe SCMS was successfully applied to studying cell-cell interaction in mixed co-culture systems.
2. Advantages of our biological model system: allows for cell-cell physical contact, avoids the usage of extra material in cell growth medium and the requirement of complete seal between different cell types, and more importantly, offers to analyze the individual responses of single cells in heterogenous systems.
3. The level of irinotecan resistance in regular HCT-116 cells was significantly increased due to the presence of IRI-resistant cells in the co-culture systems without cell contact. The metabolic profiles of HCT-116-GFP stable cells were significantly changed by the IRI-resistant cells in co-culture system with contact.

Acknowledgement

Dr. Yang's group members: Yanlin Zhu, Zhu Zou, Zongkai Peng, Yunpeng Lan, Tra Nguyen, Dan Chen, Zhihao Ma. Drs. Paul Sims (OU) and Chuanbin Mao (OU).
Funding: NIH (R01GM116116, R21CA204706).

MEASURING DNA DAMAGE TO ASSESS THE USE OF ELECTRONIC CIGARETTES AS A TOBACCO HARM REDUCTION STRATEGY

Mayilvanan Chinnaiyan[1], Vengatesh Ganapathy[1], Balaji Sadhasivam[1], Yan D. Zhao[2], Theodore L. Wagener[4,5], Lurdes Queimado[1,3]

Departments of [1]Otorhinolaryngology, and [2]Biostatistics & Epidemiology; [3]TSET Health Promotion Research Center, Stephenson Cancer Center, The University of Oklahoma Health Sciences Center. [4]Center for Tobacco Research, The Ohio State University Comprehensive Cancer Center, and [5]The Ohio State University Wexner Medical Center.

Background and Aims: Millions of smokers across the U.S. struggle to quit tobacco daily. Nicotine replacement and counseling are essential tools in every smoking cessation plan. Electronic cigarettes (EC) deliver plasma nicotine levels similar to that seen in smokers, and deliver less chemicals than tobacco smoke. Thus, addressing the role of ECs in tobacco harm reduction is essential. Towards that goal, we quantified DNA damage in the oral epithelial cells of exclusive combustible tobacco users and dual users of EC devices.

Methods: Adult smokers who were not planning to quit were randomized to 3 distinct groups: "Usual Brand Cigarettes" (UBC), 2nd generation ECs (G2), or 3rd generation ECs (G3), and provided free tobacco products according to assigned group. Tobacco product use details, CO level, blood, saliva, oral mucosa and urine samples were collected at each visit. DNA was extracted from oral cells and damage was quantified by q-PADDA, at 3 time point visits (Week 0, 4, 12). Data analysis was performed using ANOVA model.

Results: Data from 93 participants (UBC=35, G2=27 and G3=31) are included in this report. At enrolment (week 0), there were no significant differences in age, sex or tobacco product use across groups. At 12 weeks, CO levels and combustible tobacco use were significantly reduced in G2 and G3 dual users (UBC=18±10, G2=6±7, G3=7±7 cig/day). A significant reduction in the levels of oral mucosa DNA damage at 4 and 12 weeks (2 to 6 fold) was observed in dual users of combustible tobacco and G2 EC devices, but not G3 devices, when compared with exclusive combustible tobacco users.

Conclusion: Our study shows that when provided with EC devices, smokers significantly reduced the number of combustible cigarettes smoked. Dual users of combustible tobacco and G2 EC devices have significantly lower the levels of DNA damage in their oral mucosa compared with exclusive combustible tobacco or G3 dual users. These data suggest that 2nd generation EC devices are an effective harm reduction tool.

Grant support: NIH/NCI (R01CA204891, Wagener; R01CA242168, Queimado) and PHF (Queimado). Dr. Queimado holds a PHF Endowed Chair in Otorhinolaryngology.

MEASURING DNA DAMAGE TO ASSESS THE USE OF ELECTRONIC CIGARETTES AS A TOBACCO HARM REDUCTION STRATEGY

Mayilvanan Chinnaiyan[1], Vengatesh Ganapathy[1], Balaji Sadhasivam[1], Yan D. Zhao[2], Theodore L. Wagener[4,5], Lurdes Queimado[1,3]

Departments of [1]Otorhinolaryngology, and [2]Biostatistics & Epidemiology; and [3]TSET Health Promotion Research Center, Stephenson Cancer Center, The University of Oklahoma Health Sciences Center. [4]Center for Tobacco Research, The Ohio State University Comprehensive Cancer Center, and [5]The Ohio State University Wexner Medical Center

Background

- Millions of smokers across the U.S. struggle to quit tobacco use daily due to nicotine addiction.
- Electronic cigarettes (EC) provide an alternative mode of nicotine delivery.
- EC use has increased since users perceive them as safe. In 2020, about 3.6 million youth nationwide reported currently using ECs.
- Besides nicotine, EC aerosol contains harmful chemicals and known carcinogens.
- Studies reported that EC aerosol causes DNA damage and suppresses DNA repair proteins.

Aims

- To determine whether ECs can reduce tobacco harm, we quantified DNA damage in oral epithelial cells of exclusive combustible tobacco users and dual users of 2nd and 3rd generation ECs.

Methods

- Adult smokers who were not planning to quit in the next three months were randomized into 3 distinct groups.

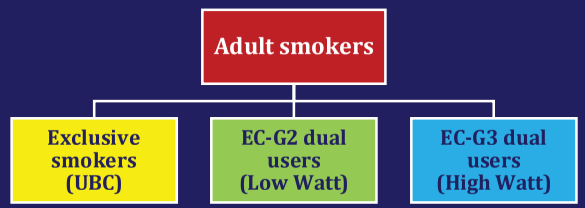

Methods

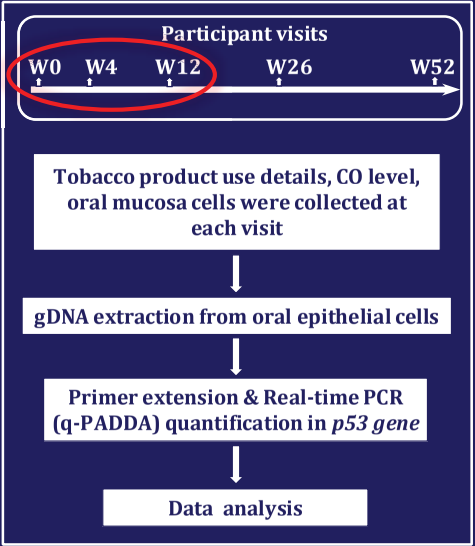

Results

	Exclusive smokers (UBC)	EC-G2 dual users	EC-G3 dual users
Cases (#)	35	27	31
Age (y)	42±12	42±13	43±14
Sex (M:F)	12:13	7:20	11:20

Table 1: Participants demographic details. There was no difference observed in age across the groups. Data shown as Mean ± SD.

Grant Support

NIH/NCI (R01CA204891, Wagener; R01CA242168, Queimado) and the PHF (Queimado). Dr. Queimado holds a PHF Endowed Chair in ORL.

Results

	Exclusive smokers (UBC)			EC-G2 dual users			EC-G3 dual users		
Weeks	W0	W4	W12	W0	W4	W12	W0	W4	W12
Tob. cigs/day	17 ± 10	18 ± 10	18 ± 10	16 ± 8	8 ± 7	9 ± 8	17 ± 7	9 ± 7	8 ± 7
E-cig puffs /day	0	0	0	0	65 ± 140	89 ± 198	0	57 ± 67	52 ± 57
Watts	-	-	-	-	7.7 ± 1.1	8.2 ± 1.0	-	26 ± 12	28 ± 16
CO (ppm)	24 ± 16	22 ± 17	23 ± 21	26 ± 14	20 ± 19	16 ± 16	26 ± 16	18 ± 12	19 ± 16

Table 2: Tobacco product use over time and markers of exposure. There was a reduction in the number of tobacco cigarettes and CO levels observed at 4 & 12 weeks in dual users of tobacco and electronic cigarette. Data shown as Mean ± SD.

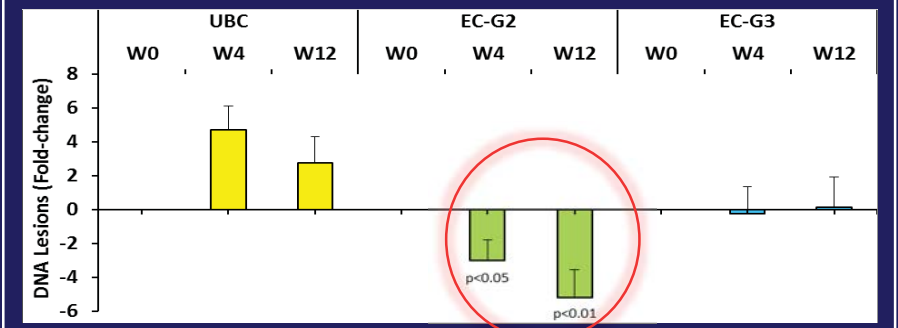

Figure 1: Fold-change in DNA damage quantified by q-PADDA in UBC, EC-G2, EC-G3 dual users over time. Dual users of EC-G2 showed a significant reduction in oral mucosa DNA damage at 4 and 12 weeks (2-6 fold). No significant reduction was observed in exclusive smokers or dual users of EC-G3. Data shown as Mean ± SEM and t test.

Conclusions

- Smokers reduced the number of combustible cigarettes when they are provided with EC devices.
- Our preliminary data show that EC-G2 users significantly reduced the oral mucosa DNA damage.
- These data suggest that EC-G2 are an effective harm reduction tool.

OCCURRENCE AND TIMING OF ADVANCED CARE DISCUSSIONS IN RECURRENT OVARIAN CANCER PATIENTS PARTICIPATING IN CLINICAL TRIALS REMAIN TO BE OPTIMIZED

Anjalika Gandhi MD, Blaire Scott, Spencer Hall, Sara Vesely PhD, Debra Richardson MD
Department of Gynecologic Oncology, Stephenson Cancer Center of OU Health

Objectives: In women with recurrent ovarian cancer (ROC), advanced care planning (ACP) such as advanced directives (AD), code status, and timely hospice referral should be addressed. In the clinical trial (CT) focused Stephenson Cancer Center (SCC), treatment with novel potentially life-prolonging therapies may alter timing of discussions. Our study compares patterns of ACP between CT and non-CT ROC patients.

Methods: All patients ≥18 years who had ROC and were ever treated at SCC for during the year of 2015 were reviewed. Patients who ever (n=84) versus never (n=41) participated in a therapeutic CT were compared. Chi-square or Fisher's exact tests and two sided t-tests or Wilcoxon Rank-Sum tests compared demographic data and ACP variables using an $\alpha=0.05$. Multivariable logistic regression estimated adjusted odds ratios (aOR) adjusted for CT participation, age, and Charlson comorbidity index.

Results: 125 patients were identified, 67% participated in CTs. Cohorts were similar in most demographic and histopathologic characteristics. Caucasian patients comprised 95% of the CT cohort vs 80% of non-CT patients ($p=0.0205$). Median duration of follow up after first recurrence was 856 days in trial patients vs 308 days in non-trial patients ($p<0.0001$). In unadjusted analyses, CT participants more frequently discussed AD (36% vs 17% non-trial patients, $p=0.0321$). Rates medical power of attorney (MPOA) discussion (54% in both), code status discussion (43% vs 27% in non-CT patients), and palliative care referral (49% vs 37% in non-CT patients) were similar. Median time between first recurrence and code status discussion was significantly longer in CT versus non-CT participants (731 days (IQR 102-1376) versus 57 days ((IQR 38-565), $p=.0379$). Of 81 deceased patients, though rates of hospice enrollment were similar (74% CT versus 71% non-trial), CT patients more frequently died in the hospital (22.8% vs 8.7%) or a care facility (14% vs 0%) ($p=0.0311$). ACP discussions and palliative care referrals tended to occur either during or after CT. In adjusted analyses, palliative care referral was the only significant predictor of discussions of code status (aOR 3.69, 95% CI 1.67-8.152), AD (aOR 14.46, 95% CI 5.04-41.49), and MPOA (aOR 8.71, 95% CI 3.66-20.73). Participation in neither late phase nor phase 1 trials significantly predicted the odds of ACP.

Conclusions: The time between the recurrence and code status discussions was significantly longer in CT participants, and ACP discussions occurred typically during or after a trial. ACP occurred more frequently when patients were referred to palliative care, independent of participation in either late phase or phase 1 CT. Prioritizing ACP and supportive care referral, especially in CT participants, may improve these rates and optimize end of life care.

Occurrence and Timing of Advanced Care Discussions in Recurrent Ovarian Cancer Patients Participating in Clinical Trials Remain to be Optimized

Authors: Anjalika Gandhi, MD MS; Blaire Scott; Spencer Hall; Sara Vesely, PhD; Debra Richardson, MD

Background:
- Ovarian cancer is the deadliest GYN cancer
- ROC is incurable
- Aggressive care still toward the end of life
- Timely palliative care services improve QOL and survival and reduce ICU admissions and hospital death
- CT participation may divert resources from ACP
- Phase 1 trial patients may have the biggest gap

Objectives:
To compare patterns of ACP between trial and non-trial ROC patients

Methods
- **Design:** retrospective cohort study
- **Patients:** ≥18 years who were treated at SCC for the diagnosis of OC during the year of 2015 and had ever recurred. Categorized based on ever participating in CT
- **Outcomes of interest:** MPOA, AD, and code status discussions and/or paperwork
- **Data sources:** EMR and Meditech
- **Statistics:** Chi-square or Fisher's exact tests and two sided t-tests or Wilcoxon Rank-Sum tests compared demographic data and ACP variables of interest using an α=0.05. Multivariable logistic regression estimated adjusted odds ratios (aOR) adjusted by CT participation, age, and CCI

RESULTS
- N=125, 67% participated in CTs
- Demographics similar except race: CT 95% Caucasian vs 80% in non-CT (p=0.0205)
- All ACP discussions, including code status, tended to occur during or after CT (Figure 1)
- Univariate outcomes in Table 1
- aOR for code status discussion in Table 2
- In all logistic models, palliative care referral was the only predictor of discussions of code status (table 2); AD (aOR 14.46, 95% CI 5.04-41.49), and MPOA (aOR 8.71, 95% CI 3.66-20.73)

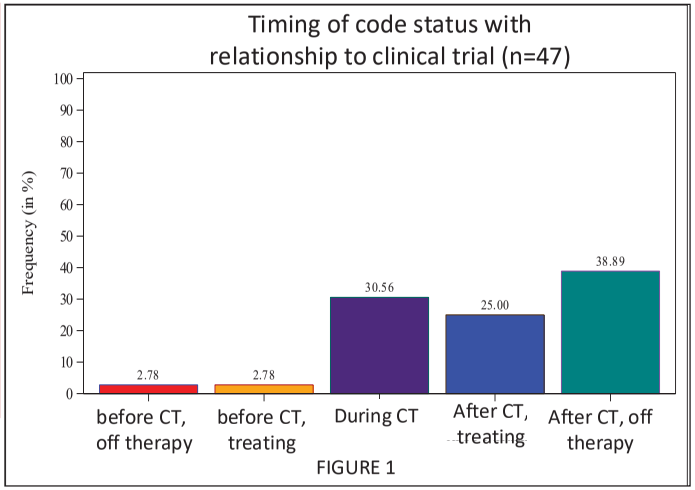

FIGURE 1

Recurrent ovarian cancer patients who participate in clinical trials tend to have longer intervals between diagnosis of recurrence and advanced care planning discussions. **Palliative care referral is the only significant predictor of advanced care planning. Early referral to palliative care, especially in clinical trial patients,** may optimize end of life care

Results

Table 1

Count (%) Or Median (IQR)	Non-CT (n=41)	CT (n=84)	p-value
Code status discussion	11 (27)	36 (43)	0.0824
MPOA discussion	22 (54)	45 (54)	0.9927
AD discussion	7 (17)	30 (36)	0.0321
Supportive or palliative care referral	15 (37)	41 (49)	0.197
Duration (days) of follow up after first recurrence	308 (91.5 - 640.0)	857.5 (437-1538)	<0.0001
Time (days) between first recurrence and code status discussion	57 (38-565)	731 (102-1376)	0.0379
Deceased	24 (56)	57 (68)	
Enrolled in hospice	17 (71)	42(74)	0.0384

Table 2 - aOR and Wald Cis for Code status discussion

	aOR	95% CI	
CT participant - only late phase (ref=non-CT)	1.833	0.651	5.16
CT participant - ever with history of phase 1 (ref=non-CT)	1.267	0.529	3.04
Referral to palliative care	3.686	1.666	8.15
Age at diagnosis	0.997	0.964	1.03
CCI	0.919	0.697	1.21

Abbreviations: GYN gynecologic, ROC recurrent ovarian cancer, QOL quality of life, ICU intensive care unit, CT clinical trial, ACP advanced care planning, MPOA medical power of attorney, AD advanced directive, CCI Charlson comorbidity index, aOR adjusted odds ratio, IQR interquartile range, CI confidence interval

OU Health | Stephenson Cancer Center

REGULATION OF HISTONE DEMETHYLASE JMJD2A BY SET7/9-MEDIATED METHYLATION

Ruicai Gu[1], Tae-Dong Kim[1], Hoogeun Song[1], Sangphil Oh[1,2], Sook Shin[1,2] and Ralf Janknecht[1,2,3]
Presenting Author's Email Address：Ruicai-Gu@ouhsc.edu
[1]Department of Cell Biology, University of Oklahoma Health Sciences Center, Oklahoma City; [2]Stephenson Cancer Center, Oklahoma City; [3]Department of Pathology, University of Oklahoma Health Sciences Center, Oklahoma City

Jumonji C domain-containing 2A (JMJD2A) is a histone H3 demethylase and its overexpression aids prostate tumorigenesis. However, how JMJD2A is regulated in its activity is unknown. We found that JMJD2A is directly methylated by SET7/9 in LNCaP prostate cancer cells. SET7/9 methylates JMJD2A on up to six lysine residues (K505, K506, K507, K563, K564, K594). In LNCaP cells, JMJD2A cooperated with its interaction partner, the ETS transcription factor ETV1, in enhancing the activity of the MMP1 promoter. However, mutation of K505/506/507 (3xR mutant) or of all six methylation sites (6xR mutant) decreased the transcriptional synergy between JMJD2A and ETV1 at the MMP1 promoter. Further, mutation of JMJD2A methylation sites reduced the physical interaction of JMJD2A and ETV1. The JMJD2A 6xR or 3xR mutants also caused reduced invasion in LNCaP cells and diminished proliferation and invasion in DU145 prostate cancer cells. Meanwhile, normal RWPE-1 prostate cells were not affected upon mutation of JMJD2A methylation sites, suggesting that JMJD2A methylation is specifically modulating cancer cells. Altogether, our data indicate that JMJD2A methylation by SET7/9 affects JMJD2A function in prostate cancer cells and thereby promotes tumorigenesis. This implies that blocking JMJD2A methylation may have therapeutic value.

Acknowledgement of funding: This work was in part funded by grant R03 CA223615 from the National Institutes of Health/National Cancer Institute.

Regulation of Histone Demethylase JMJD2A by SET7/9-Mediated Methylation

Ruicai Gu[1], Tae-Dong Kim[1], Hoogeun Song[1], Sangphil Oh[1,2], Sook Shin[1,2] and Ralf Janknecht[1,2,3]

[1] Department of Cell Biology, OUHSC, Oklahoma City; [2] Stephenson Cancer Center, Oklahoma City; [3] Department of Pathology, OUHSC, Oklahoma City

ABSTRACT Jumonji C domain-containing 2A (JMJD2A) is a histone H3 demethylase and its overexpression aids prostate tumorigenesis. However, how JMJD2A is regulated in its activity is unknown. We found that JMJD2A is directly methylated by SET7/9 in vitro and in vivo on up to six lysine residues. In LNCaP prostate cancer cells, JMJD2A cooperated with its interaction partner, the ETS transcription factor ETV1, in enhancing the activity of the MMP1 promoter, which was decreased upon mutation of JMJD2A lysines K505/506/507 (3xR mutant) or of all six methylation sites (6xR mutant). Further, mutation of JMJD2A methylation sites impaired the physical interaction of JMJD2A and ETV1. The JMJD2A 6xR or 3xR mutants also caused reduced invasion in LNCaP cells and diminished proliferation and invasion in DU145 prostate cancer cells. Altogether, our data indicate that methylation by SET7/9 affects JMJD2A function in prostate cancer cells and thereby promotes tumorigenesis.

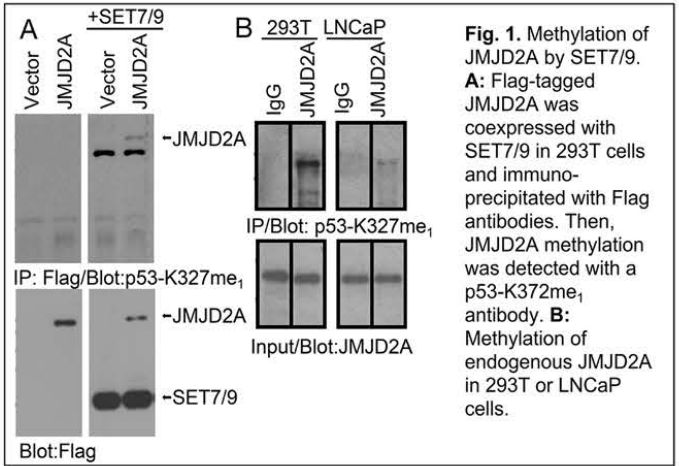

Fig. 1. Methylation of JMJD2A by SET7/9. **A:** Flag-tagged JMJD2A was coexpressed with SET7/9 in 293T cells and immuno-precipitated with Flag antibodies. Then, JMJD2A methylation was detected with a p53-K372me$_1$ antibody. **B:** Methylation of endogenous JMJD2A in 293T or LNCaP cells.

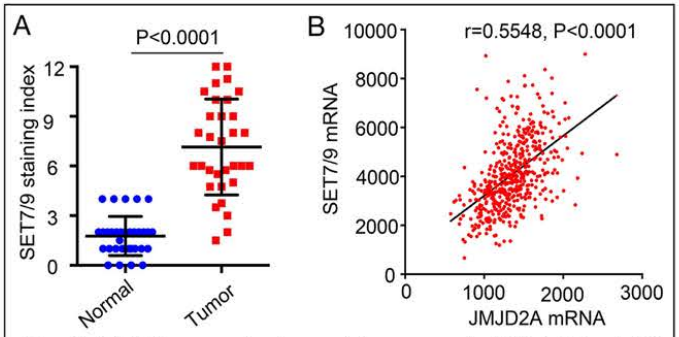

Fig. 2. SET7/9 expression in prostate cancer. **A:** IHC staining in 32 matching normal and tumor prostate specimens. **B:** Correlation of SET7/9 and JMJD2A mRNA levels in 493 human adenocarcinomas.

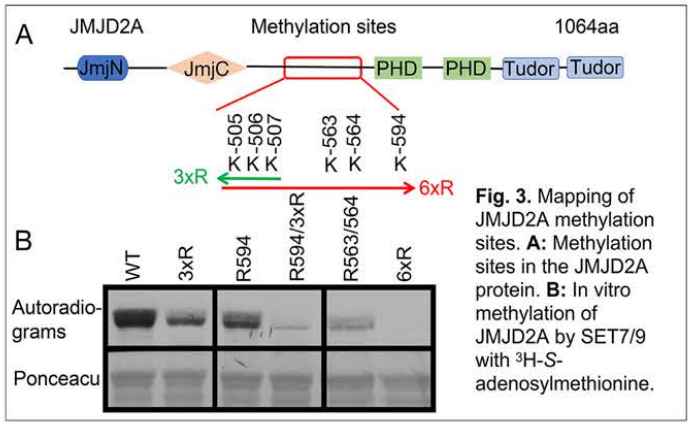

Fig. 3. Mapping of JMJD2A methylation sites. **A:** Methylation sites in the JMJD2A protein. **B:** In vitro methylation of JMJD2A by SET7/9 with ^{3}H-*S*-adenosylmethionine.

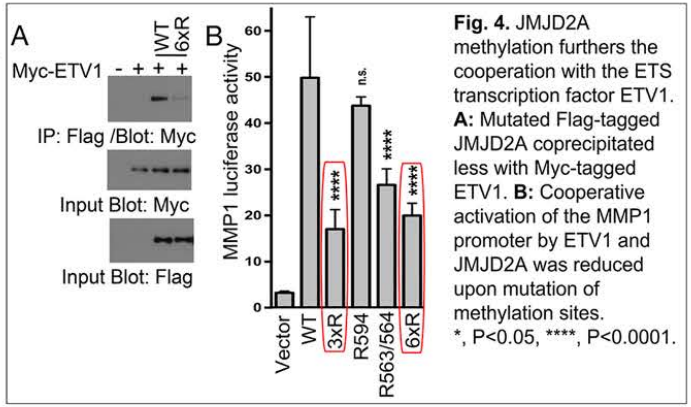

Fig. 4. JMJD2A methylation furthers the cooperation with the ETS transcription factor ETV1. **A:** Mutated Flag-tagged JMJD2A coprecipitated less with Myc-tagged ETV1. **B:** Cooperative activation of the MMP1 promoter by ETV1 and JMJD2A was reduced upon mutation of methylation sites. *, P<0.05, ****, P<0.0001.

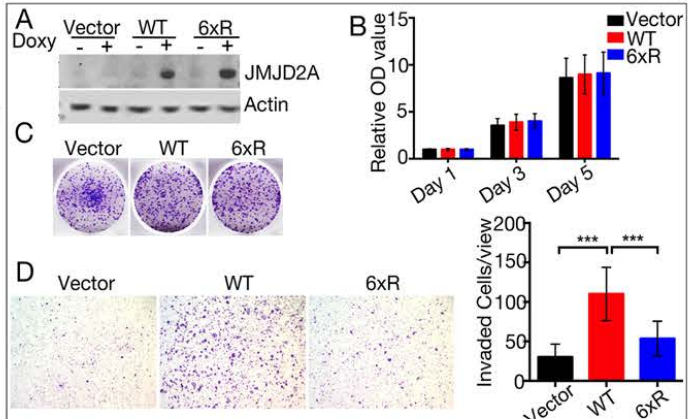

Fig. 5. Mutation of JMJD2A methylation sites reduced invasion of LNCaP cells. **A:** Western blots of doxycycline(Doxy)-inducible cells. **B, C:** No change of growth (MTT and clonogenic assay). **D:** Invasion assay. ***, P<0.005.

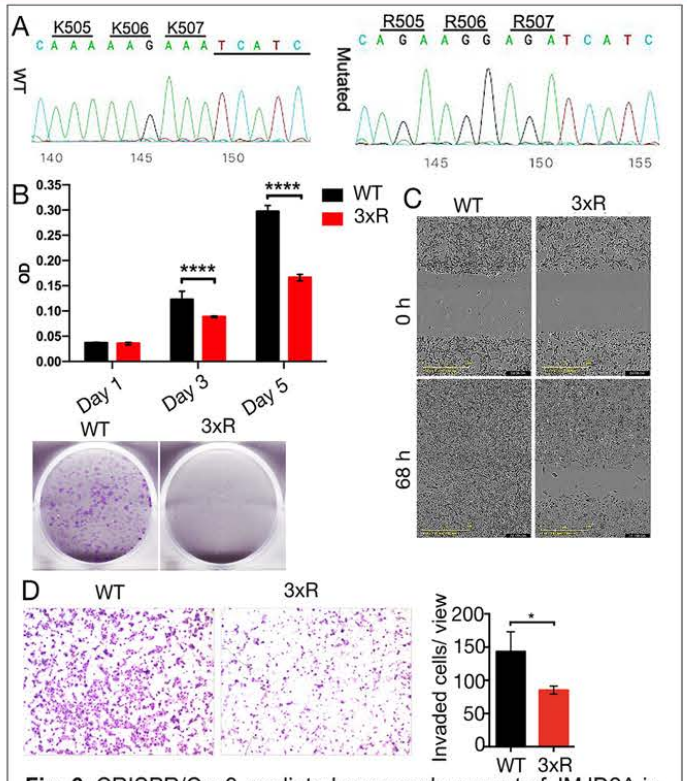

Fig. 6. CRISPR/Cas9-mediated gene replacement of JMJD2A in DU145 prostate cancer cells. **A:** Seqencing of genomic DNA (WT and 3xR). **B:** 3xR mutant is impaired in cell growth (MTT and clonogenic assay). **C, D:** 3xR mutant migrates and invades less. * , P<0.05.

CONCLUSIONS

- JMJD2A is directly methylated by SET7/9, which is overexpressed in prostate tumors similar to JMJD2A.
- SET7/9 methylates JMJD2A on up to six lysine residues (K505, K506, K507, K563, K564, K594).
- Mutation of three (3xR) or six (6xR) methylation sites decreased interaction and transcriptional synergy between JMJD2A and ETV1.
- Blocking JMJD2A methylation also caused reduced invasion in LNCaP and DU145 cells and additionally diminished proliferation and invasion in DU145 prostate cancer cells.

Acknowledgement: This work was in part funded by grant R03 CA223615 from the NIH/NCI.

IL-1B PRODUCTION VIA STING SIGNALING ENHANCES ANTITUMOR MEMORY FORMATION

Ashley R. Hoover[1,2], Kaili Liu[1], Xiao-Hong Sun[2], Wei R. Chen[1]
[1]University of Oklahoma, [2]Oklahoma Medical Research Foundation

To treat metastatic tumors, our lab has developed a unique approach that combines tumor ablative therapy with immunotherapy. We have termed this approach laser immunotherapy (LIT). LIT uses the combination of local laser ablation and local administration of an immunostimulant directly into the tumor to induce tumor-specific immune responses. Our pre-clinical studies and preliminary clinical trials demonstrated that the synergy of tumor ablative therapy and immunotherapy could not only destroy the treated primary tumors but also eradicate untreated metastases, leading to long-term survival and tumor resistance. Through single cell RNA sequencing (scRNAseq) on the tumor infiltrating leukocytes, we discovered that type I IFNs and the proinflammatory cytokine IL-1β are the dominant cytokines produced following LIT treatment. Further *in vivo* and *in vitro* analysis revealed that glycated chitosan (GC), the immune stimulating component of LIT, stimulates the production of type I IFN and IL-1β through STING signaling in dendritic cells (DCs). Furthermore, we discovered that the synergy of type I IFN and IL-1β production via STING signaling in DCs is crucial for the development of T cell memory following LIT and preventing tumor growth upon re-challenge of LIT cured survivors. The data presented within will reveal the role of IL-1β in enhancing anti-tumor memory responses generated via GC making it more suitable for immunotherapy than currently approved adjuvants.
Funding: R01CA205248-01A1 NIH

IL-1β Production via STING Signaling Enhances Antitumor Memory Formation Following LIT

Ashley R. Hoover[1,2], Kaili Liu[1], Xiao-Hong Sun[2], and Wei R. Chen[1]

[1]Stephenson School of Biomedical Engineering, University of Oklahoma, Norman, OK 73019
[2]Department of Arthritis and Clinical Immunology, Oklahoma Medical Research Foundation, Oklahoma City, Oklahoma 73104

Introduction

Laser immunotherapy (LIT) combines photothermal therapy (PTT) and an immunostimulant, N-dihydrogalactochitosan (GC) to generate effective antitumor immunity. LIT-induced immune responses can clear the treated tumor, its metastases, and prevent cancer relapse in human patients and animal models. The goal of the current study is to understand how LIT activates antitumor T cell immunity in order to eliminate poorly immunogenic metastatic tumors and prevent cancer relapse. GC induces a strong type I IFN and IL-1β response and type I IFNs are critical for the success of LIT as animals lacking the IFNaR1 are no longer responsive to LIT. In dendritic cells (DCs), GC requires STING signaling to produce type I IFN and IL-1β as DCs lacking STING no longer produce these cytokines. *In vivo*, there is no difference in survival between LIT-treated STING heterozygotes and STING deficient animals bearing B16-F10 tumors. However, while LIT-cured wild type animals rejected tumor re-challenges, when the LIT-cured STING deficient animals were re-challenged with B16-F10 tumor cells, the tumor growth was comparable to the untreated controls. This suggests that there is a memory defect in the STING deficient animals. Interestingly, STING heterozygous animals also have an immune memory defect upon B16-F10 tumor rechallenge. While type I IFN production between wild type and STING heterozygous bone marrow derived dendritic cells (BMDCs) stimulated with GC is comparable, IL-1β is dramatically reduced in the STING heterozygous BMDCs. IL-1β is a critical pro-inflammatory cytokine that enhances T cell activation, memory formation, migration, and effector function. To determine whether LIT STING heterozygous animals have a reduction in tumor specific CD8⁺ T cell development following LIT or in the development of CD8+ T cell memory formation, we assessed tumor specific CD8⁺ T cell responses via ELISPOT. In collaboration with Dr. William Hildebrand's group, we have identified several B16-F10 tumor specific peptides, a few of which initiate CD8⁺ T cell responses. LIT-cured tumor-rechallenged animals, that remain tumor free, have a strong response to 5 tumor specific peptides. Eight days post LIT treatment, both wild type and STING heterozygous animals have comparable splenic CD8⁺ T cell responses. However, both wild type and STING heterozygous animals, that were LIT cured and then rechallenged with B16-F10 tumors, failed to produce these same T cell responses. It is important to note, all LIT-cured STING heterozygous animals succumb to tumor growth while only 50% of LIT-cured re-tumor challenged wild type animals grow tumors. This posits that IL-1β plays a role in memory CD8+ T cell formation and will be further investigated using IL1R1 deficient animals. However, this does not explain why half of the LIT-cured tumor-challenged wild type animals, regrow tumors. This will be explored further by comparing the expression levels of these peptides on the B16-F10 tumors *in vivo*.

Results

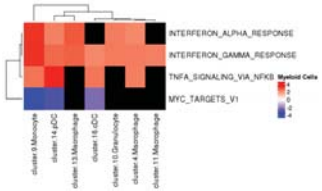

Figure 1. : Heat map of pathway enrichment for myeloid cell clusters induced by LIT. Single-cell RNA sequencing of PyMT breast tumors reveals dramatic upregulation pro-inflammatory pathways in LIT treated tumors compared to untreated tumors.

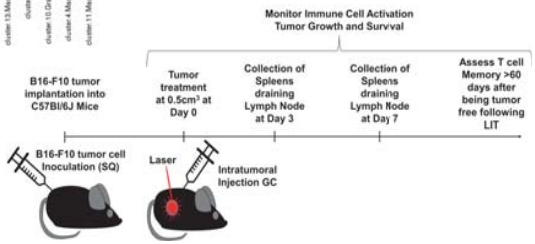

Figure 2. Schematic of LIT procedure and subsequent analysis.

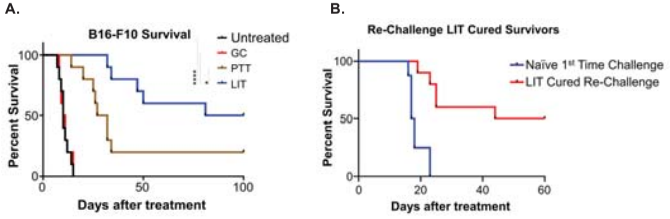

Figure 3. LIT successfully treats B1-F10 tumors. (A) Wild type C57Bl/6 mice were inoculated with B16-F10 highly metastatic tumors and then treated with GC, PTT, or PTT+GC (LIT) once the tumors reached 0.5cm³. After treatment, the animals were monitored for tumor growth and sacrificed when they reached ethical time points. (B) LIT cured animals that had been tumor free for >60 days were rechallenged on the opposite flank and monitored for tumor growth and were sacrificed once the animals reached ethical time points.

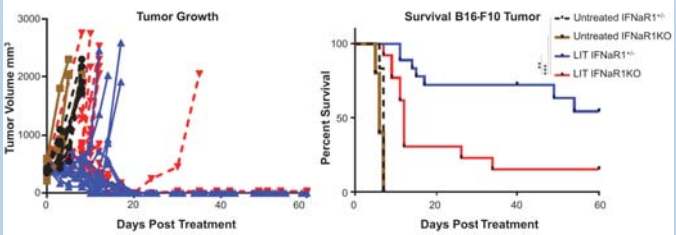

Figure 4. Type I IFNs are critical for the therapeutic effect of LIT. IFNaR1 heterozygous and deficient mice were inoculated with B16-F10 tumors. Once the tumors reached 0.5cm³ tumors were treated with LIT or left untreated. Tumor growth and survival was monitored for 60 days following treatment.

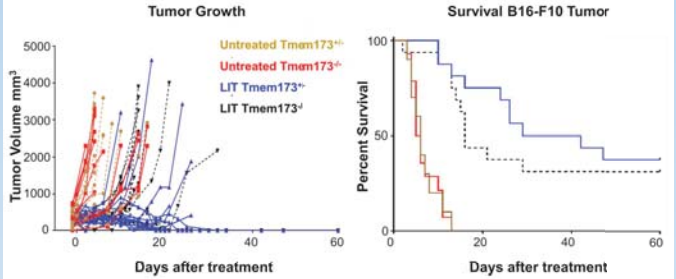

Figure 5. STING is dispensable for the successful treatment of B16-F10 tumors following LIT. Tmem173 heterozygous and deficient mice were inoculated with B16-F10 tumors. Once the tumors reached 0.5cm³ tumors were treated with LIT or left untreated. Tumor growth and survival was monitored for 60 days following treatment.

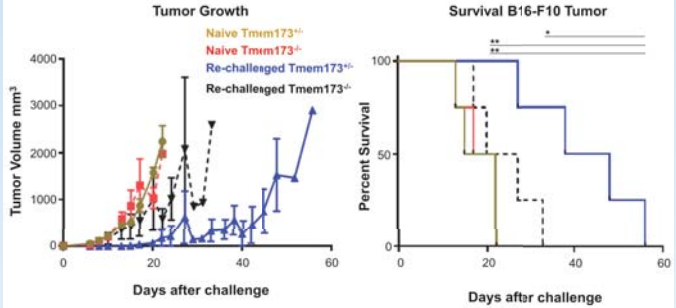

Figure 6. STING is required for the generation of immunological memory. LIT-cured STING heterozygous and deficient mice were re-challenged with B16-F10 tumors on the opposite flank. Naïve STING heterozygous and STING deficient animals (1st challenge) were used as positive controls for tumor growth. STING deficient re-challenged animals grew tumors at a similar rate as the untreated controls suggesting a memory defect.

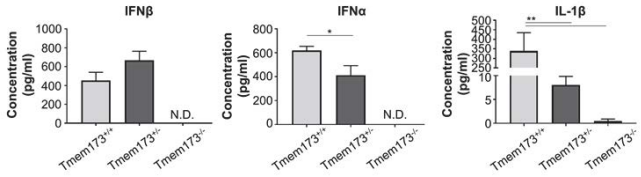

Figure 7. GC induces the production of type I IFN and IL-1β in bone marrow derived dendritic cells. BMDCs were stimulated for 24 hours with GC prior to harvesting of the supernatant for ELISA. Type I IFN production is nearly equivalent in Wild type and STING heterozygous BMDCs. IL-1β is dramatically reduced in the STING heterozygous mice.

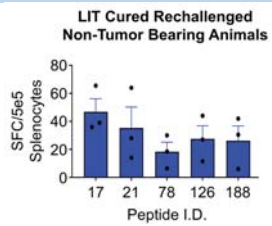

Figure 8. LIT-cured, tumor-rechallenged animals that remained tumor free develop a tumor specific CD8⁺ T cell response. LIT-cured wild type animals were rechallenged on the opposite flank with B16-F10 tumors. Tumor growth was monitored for 60 days. By the 60-day mark these animals (n=3) remained tumor free and the spleen was harvested for ELISPOTs using peptides that are expressed by specifically by B16-F10 tumor cells and not healthy mouse tissues (in collaboration with Dr. William Hildebrand's group).

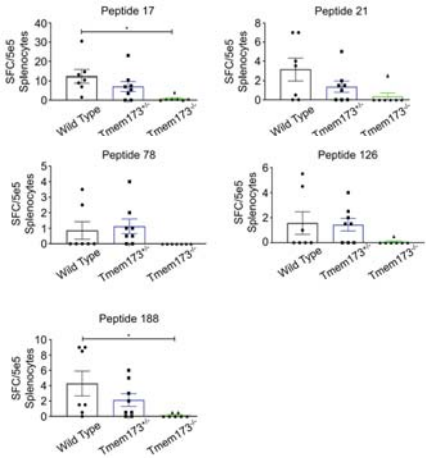

Figure 9. STING heterozygous animals develop tumor specific CD8⁺ T cells similar to wild type 8 days post LIT treatment. Animals were inoculated with B16-F10 tumor cells. Once the tumors reached 0.5cm³ they were treated with LIT. 8 days post treatment, spleens were isolated and used for ELISPOTs.

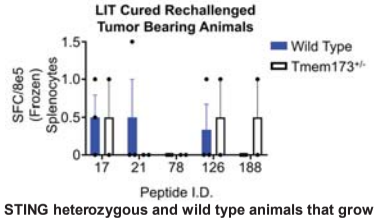

Figure 10. LIT-cured STING heterozygous and wild type animals that grow tumors upon rechallenge do not develop a CD8+ T cell specific antitumor response. After tumor challenge the animals were monitored for tumor growth. Once the tumor reached ethical endpoints, splenocytes were isolated and preserved for later use for ELISPOT.

Conclusion

- Type I IFNs are critical for the therapeutic effect of LIT as animals deficient in a type I IFN response are no longer protected from tumor progression.
- GC induces DC production of type I IFN and IL-1β through STING signaling.
- STING mediated IL-1β is involved in the generation of immunological memory following LIT.
- Current experiments are focusing specifically on IL-1β function in LIT antitumor immunity and tumor peptide expression levels.

Acknowledgements

This study was supported in part by grants from the U.S. National Institutes of Health (RO1 CA205348), and the Oklahoma Center for Advancement of Science and Technology (HR16-085).

SOCIAL DETERMINANTS OF HEALTH AND PROSTATE CANCER SCREENING

Tram Q. Le, Kelly L. Stratton, MD
tram-le-1@ouhsc.edu | (832) 221-4793
Dept. of Urology, University of Oklahoma Health Sciences Center, Oklahoma City, OK, United States

Introduction/Background: Prostate cancer is the leading cancer type and the second leading cause of death due to cancer in men in the United States. Cancer screening discussions in a clinical setting represent only one component of a broader health promotion strategy to increase cancer screening and improve cancer outcomes. Prior studies have found that social determinants of health (SDoH) are associated with an increased risk of a variety of diseases, including cancer. While the relationship between economic and educational factors and prostate cancer health screenings is well-established in the literature, less is known about other SDoH, such as health access, food access, and physical environment. This study evaluates the relationship between several SDoH and prostate cancer screening.

Methods/Materials: This study utilized publicly available data from the 2012, 2014, 2016, and 2018 Behavioral Risk Factor Surveillance System (BRFSS) of Oklahoma, a state-based telephone survey that measures the impact of health behaviors on the risk of disease, injury, and death. From the data, we obtained crosstabs of SDoH of male patients 40 years old and above in relation to receiving a prostate-specific antigen (PSA) test within the last 2 years. Factors examined include education level, income level, receiving a flu vaccine within the last year, having a dental visit within the last year, home type (single-family vs. multi-family), and food access and security. Frequencies, percentages, and confidence intervals were generated from the results. The data was subsequently analyzed via chi-square tests with α-level = 0.05 to assess the correlation between the variables of interest and PSA testing.

Results: The chi-square tests demonstrate a statistically significant positive relationship between education level and receiving a PSA test, income level and receiving a PSA test, having a dental visit and receiving a PSA test, and receiving a flu vaccine and receiving a PSA test. The chi-square test also demonstrates a significant relationship between patients' home type and their likelihood of receiving a PSA test: those who live in a single-family home are more likely to receive a test than those who live in multi-family homes. There is a statistically significant relationship between food security and receiving a PSA test; notably, patients who have never worried about being able to afford food were over 15% more likely to receive a PSA test than those who have ever worried about food affordability. There is no statistically significant relationship between perceived access to healthy foods and receiving a PSA test.

Conclusions: Given the risk of prostate cancer in American men, findings from this study can be used to prompt further research efforts to identify potential drivers of prostate cancer health disparities. Developing strategies to address these social barriers to health may help to increase prostate cancer screening rates and improve men's health.

Social Determinants of Health and Prostate Cancer Screening

Tram Q. Le, Kelly L. Stratton, MD

University of Oklahoma Health Sciences Center, Department of Urology, Oklahoma City, Oklahoma

Introduction

- Prostate cancer is the leading cancer type and the second leading cause of death due to cancer in men in the United States.
- Prior studies have found that social determinants of health (SDoH) are associated with an increased risk of a variety of diseases, including cancer.
- Cancer screenings are integral in reducing the risk of cancer and improving cancer outcomes and can be influenced by SDoH.
- This study evaluates the particular relationship between several SDoH and prostate-specific antigen (PSA) testing in Oklahoma.

Methods

The Behavioral Risk Factor Surveillance System (BRFSS), provided by the OK2SHARE database, is a state-based telephone survey that the impact of health behaviors on the risk of disease, injury, and death. From the database, crosstabs of several health factors and activities of male patients aged 40 years and above in relation to having received a PSA test within the last 2 years were obtained. Data was collected for the survey years 2012, 2014, 2016, and 2018. Factors examined include:

- income level
- home type
- education level
- food security
- receiving a flu vaccine within the last year
- having a dental visit within the last year

Frequencies, percentages, and confidence intervals were generated by the BRFSS results. These were analyzed via chi-square tests α-level = 0.05 to assess the correlation between the variables of interest and PSA testing.

Data Analysis & Results

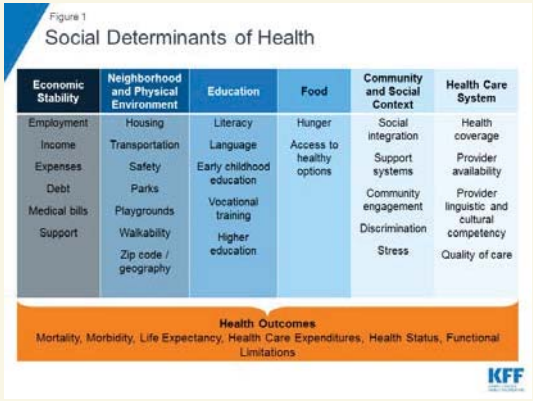

P-Values Between SDoH and PSA Testing

	2012	2014	2016	2018
Income Level	3.08227E-08	1.06459E-14	2.29073E-10	1.22529E-10
Single-Family vs. Multi-Family Home†	-	0.01698546	-	-
Education Level	8.99017E-06	1.503E-10	2.1646E-09	8.0665E-09
Easy to Purchase Healthy Foods	0.82066139	0.95874574	0.07646178	0.77999058
Worried About $ to Buy Food	1.0762E-07	-	-	-
Dental Visit in Past Year	5.1276E-16	1.7227E-16	7.138E-20	2.4223E-17
Flu Vaccine	1.6732E-28	8.1362E-27	4.1741E-25	7.9419E-18

†Survey data for patients' home type (single-family vs. multi-family) was available only for 2014.
‡Survey data for patients' anxiety about being able to afford food was available only for 2012.

With α = 0.05, the chi-square tests demonstrate:

- A statistically significant positive relationship between both education level and income level and receiving a PSA test.
- A statistically significant positive relationship between having a dental visit or receiving a flu vaccine and receiving a PSA test.
- A statistically significant relationship between food security and receiving a PSA test; notably, patients who have never had to worry about being able to afford food were over 15% more likely to receive a PSA test than those who have ever had stress over being able to afford food.
- No statistically significant relationship between access to healthy foods PSA testing.
- A significant relationship between patients' home type and their likelihood of receiving a PSA test; those who live in a single-family home are more likely to receive a test than those who live in multi-family homes.

Conclusion

- While the relationship between economic and educational factors and prostate cancer health screenings has been well-established in the literature, less is known about the other SDoH, such as social and community support, food access, and physical environment.
- The results demonstrate a potential link between various other SDoH and prostate cancer screening.
- Findings from this study can be used to prompt further research efforts to identify potentially unique drivers of prostate cancer health disparities.
- Developing strategies to address these social barriers to health may help to increase prostate cancer screening rates and improve men's health.

References

Oklahoma State Department of Health (OSDH), Center for Health Statistics, Health Care Information, Behavioral Risk Factor Surveillance System 2018 to 2019, on Oklahoma Statistics on Health Available for Everyone (OK2SHARE). Accessed at http://www.health.ok.gov/ok2share on 28DEC2020:18:35:30.

Samantha Artiga and Elizabeth Hinton Published: May 10, 2. (2019, July 09). Beyond Health Care: The Role of Social Determinants in Promoting Health and Health Equity. Retrieved January 03, 2021, from https://www.kff.org/racial-equity-and-health-policy/issue-brief/beyond-health-care-the-role-of-social-determinants-in-promoting-health-and-health-equity/

MASS SPECTROMETRY METABOLOMICS STUDIES OF SINGLE CELL IN MULTICELLULAR SPHEROIDS

Zongkai Peng; Advisor: Dr. Zhibo Yang

Multicellular spheroids are regarded as vivid models to represent the microenvironment of heterogeneous cells in *in vivo* tumors. As tumor grows, cancer cells far from the capillary supply lack nutrients and oxygen, and they possess different characteristics, such as with altered cell cycle distribution and reduced metabolite consumption, compared with others. Similar gradients of nutrients and oxygen have been found in spheroids. The conditions used to culture spheroids can be precisely controlled, while the metabolites in the microenvironment inside the spheroid can reflect these changes, making them a suitable study model to mimic the actual situation in tumors. Although metabolomics studies of spheroid models have been previously performed using traditional HPLC-MS (liquid chromatography–mass spectrometry) methods, cell heterogeneity that presents in different regions of spheroids cannot be studied using these conventional techniques. To further understand the activities of heterogeneous cells in spheroids, single-cell metabolomics analysis is an inevitable choice. The Single-probe, a microscale sampling and ionization device developed in our group can be coupled to mass spectrometer for versatile experiments such as single cell metabolomics studies.

In our studies, spheroids were cultured using HCT-116 cell line following the modified protocols. Cells at each layer were detached by incubating spheroids in trypsin solution assisted by an orbital shaker. The Single-probe was coupled to mass spectrometer to analyze these single cells. The metabolomics profiles of intracellular metabolites were visualized using principal component analysis (PCA), and analysis of variance (ANOVA) was used to determine the metabolites with significantly different abundances from cells at different layers. Our preliminary results indicate that cells in three different regions of spheroids show significantly different metabolomic profiles in PCA plots. To determine the metabolites with significantly different abundances in these regions, we performed ANOVA and tentatively labeled these species. Our results indicate a large number of lipids, including PC, DG, and MG, have different abundances in cells from different layers.

Single cell analysis of metabolites in tumor spheroids

Zongkai Peng, Mei Sun, Zhibo Yang*
Department of Chemistry and Biochemistry, University of Oklahoma, Norman, Oklahoma, 73019, USA
Corresponding author email: Zhibo.Yang@ou.edu

Introduction

1) Metabolites of cancer cells

- Intracellular metabolites reflect the cancer cell activities in different regions
- Extracellular metabolites are critical for cell-cell communication, tumor growth, and cancer cell migration

2) Spheroids obtained from 3D cell structure can be used for metabolites studies

- Better models of *in vivo* tumors compared with traditional 2D-culture cells
- Spheroids possess heterogenous cell populations in different regions
- Spheroids possess different intracellular metabolites in different regions due to the gradients of oxygen, nutrients, and energy

3) Single cell mass spectrometry (SCMS)

- A powerful tool to study cell heterogeneity
- Suitable for studies of rare cells
- Provide molecular compositions (e.g., metabolites and proteins) of cells

4) The Single-probe

- A microscale sampling and ionization device
- Allows for versatile experimental designs
- Can be coupled with MS for extracellular analysis of spheroids, SCMS, and MS imaging (MSI)

Experiments

1) Single-probe fabrication[1]

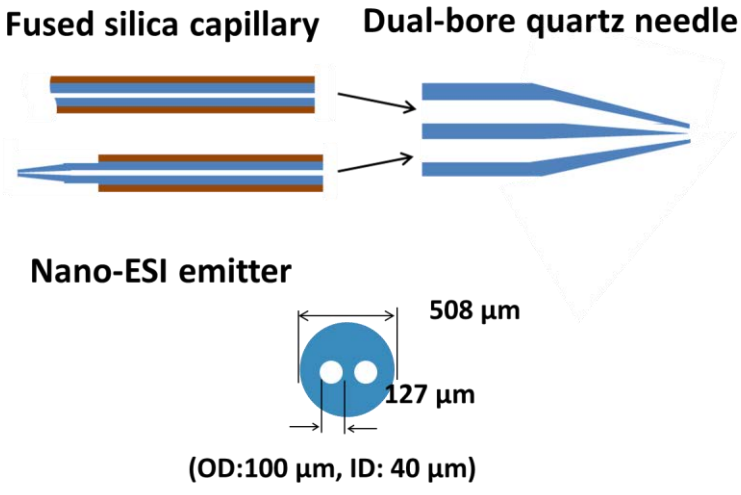

2) Single-probe SCMS setup

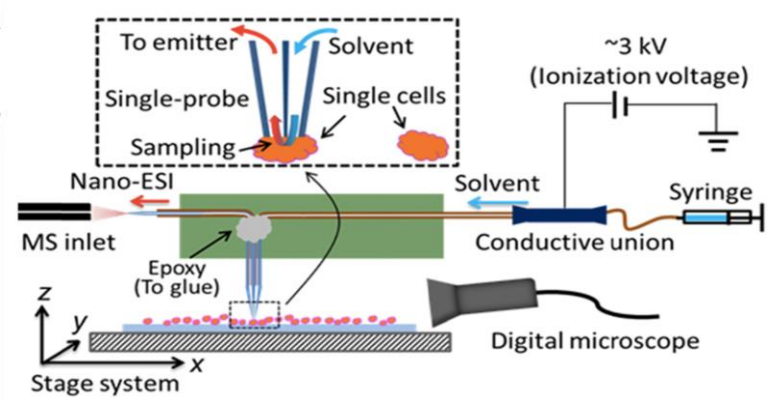

Results

1) Principal component analysis (PCA) results form different layer of spheroids

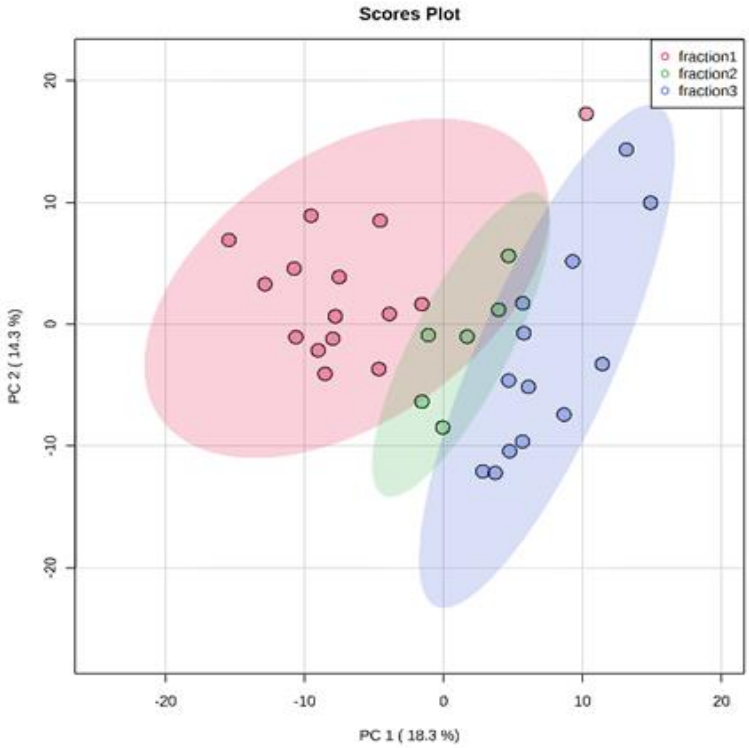

Conclusion

- Metabolites with significantly different abundances were observed in different layers of tumor spheroids
- By analyzing the metabolites results in these different regions, many fact acids are found changed significantly

([1]Mei Sun, et al., *Anal. Chem.* 2017, (89), 9069−9076.)

TICRR/TRESLIN PROTEIN EXPRESSION IS CELL CYCLE REGULATED BY THE CUL4-DDB1-DTL E3 UBIQUITIN LIGASE

Kimberlie A. Wittig[1,2*], Courtney G. Sansam[2], Tyler D. Noble[1,2], Duane Goins[2], Christopher L. Sansam[1,2*]

Presenter's e-mail address: kimberlie-wittig@ouhsc.edu

[1] Department of Cell Biology, University of Oklahoma Health Sciences Center, Oklahoma City, Oklahoma 73104, USA; [2] Cell Cycle and Cancer Biology Research Program, Oklahoma Medical Research Foundation, Oklahoma City, Oklahoma 73104, USA

DNA replication is the process of duplicating two identical copies of the genome to be equally divided during every cell division. Deregulation of DNA replication is a leading contributor to genomic instability and tumorigenesis. Therefore, tight regulation of the number of active replisomes is crucial to prevent replication stress-induced DNA damage. TICRR/TRESLIN is essential for DNA replication initiation in yeast, *Xenopus*, zebrafish, and higher eukaryotes including humans. The expression level of TICRR and its phosphorylation status determine the number of replication origins that initiate simultaneously during S-phase. However, the mechanisms regulating TICRR protein expression throughout the cell cycle are unknown.
In this study, we aimed to evaluate TICRR protein dynamics around the G1/S-phase transition. To do this, we tagged the endogenous C-terminus of TICRR with mClover in HCT-116 human colon cancer cells using CRISPR/Cas9 and applied an established flow cytometry assay to detect how levels of both insoluble and total TICRR change.

We find total TICRR expression is highest in G2/M, decreases with cell division when cells re-enter G1, and further decreases at the G1/S-phase transition. However, insoluble TICRR levels are highest in G1 and sharply decrease with S-phase entry. Although total TICRR expression decreases between G2/M and G1, insoluble TICRR levels increase demonstrating that insoluble TICRR accumulation in G1 is not due to changes in its expression. In contrast, both total and insoluble TICRR levels decrease with S-phase entry demonstrating this decrease is at least in part due to the degradation of TICRR protein. Utilizing proteasomal and neddylation inhibitors, we show that degradation of TICRR depends on cullin E3 ubiquitin ligases and is specific to S-phase. Additionally, through two targeted siRNA screens, we have identified CUL4-DDB1-DTL as the cullin complex necessary for TICRR degradation.

Collectively, our results demonstrate how total and insoluble levels of TICRR change in distinct ways throughout the cell cycle, and we have elucidated a mechanism for TICRR degradation at the G1/S transition affecting the levels of protein available for DNA replication initiation during S-phase. These results suggest a mechanism to control the rate of replication origin firing to prevent replication stress and DNA damage.

Funding: This work was supported by the National Institutes of Health [R01GM121703] and the Oklahoma Center for Adult Stem Cell Research. K.A.W. received support from the Drs. Patricia H. and J. Donald Capra Scholarship Fund.

TICRR/TRESLIN Protein Expression is Cell Cycle Regulated by the CUL4-DDB1-DTL E3 Ubiquitin Ligase

Kimberlie A. Wittig[1,2], Courtney G. Sansam[1], Tyler D. Noble[1,2], Duane Goins[1], Christopher L. Sansam[1,2]

[1]Cell Cycle and Cancer Biology Research Program, Oklahoma Medical Research Foundation, Oklahoma City, OK, USA
[2]Department of Cell Biology, University of Oklahoma Health Sciences Center, Oklahoma City, OK, USA

Introduction

DNA replication is the process of duplicating two identical copies of the genome to be equally divided during every cell division. Deregulation of DNA replication is a leading contributor to genomic instability and tumorigenesis. Tight regulation of the number of active replisomes in S-phase is crucial to prevent replication stress-induced DNA damage. TICRR/TRESLIN is an essential factor for DNA replication initiation in yeast, *Xenopus*, and higher eukaryotes including humans. The expression level of TICRR/TRESLIN and its phosphorylation status determine the number of origins that initiate simultaneously during S-phase. However, the mechanisms regulating TICRR/TRESLIN protein expression are unknown. Our hypothesis is that TICRR is "pruned" at the G1//S-phase transition in order to control the rate of origin firing preventing replication stress and DNA damage.

Methods

We tagged the endogenous C-terminus of TICRR in HCT-116 cells using CRISPR/Cas9 such that all expressed protein is tagged and applied an established flow cytometry assay to detect insoluble and total TICRR levels throughout the cell cycle. For insoluble protein detection, cells are permeabilized in CSK buffer and fixed in 4% paraformaldehyde (PFA). For total protein detection, cells are directly fixed in 4% PFA. Finally, proteins are labeled with primary and secondary antibodies and DNA is stained with propidium iodide for cell cycle analysis. siRNA screens were performed with individual siRNA (Figure 3) or siRNA pools (Figure 4) against the respective targets. Samples were collected 24 and 48 hours after transfection.

Results

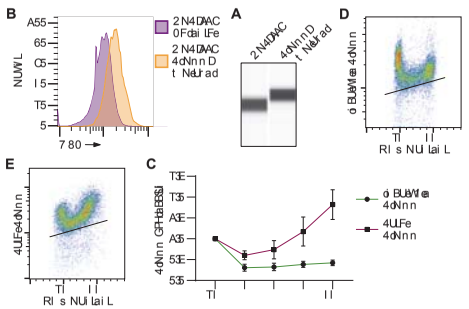

Figure 1. Successful generation of HCT-116 TICRR-mClover knock-in cell line. (A) Live cell GFP flow cytometry demonstrates a positive shift in fluorescence. (B) Capillary electrophoresis demonstrates all expressed TICRR protein is tagged. (C) Insoluble TICRR is highest in 2N cells and decreases with S-phase entry. (D) Total TICRR expression is highest in 4N cells, decreases with cell division, and is lowest in S-phase.
(E) Quantification of cells from C and D (n=6).

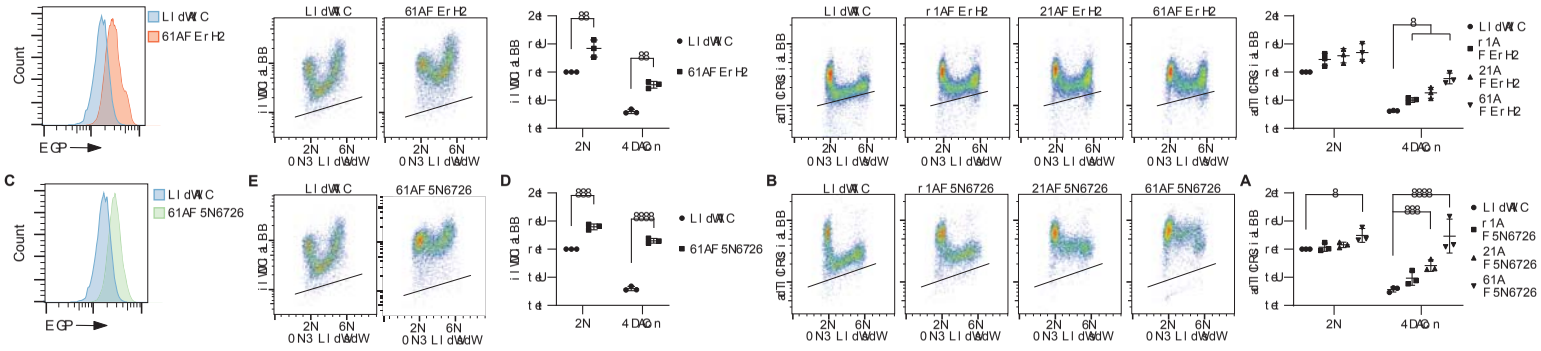

Figure 2. TICRR protein expression is regulated via cullin E3 ubiquitin ligases. (A) Live cell GFP flow cytometry demonstrates an increase in TICRR protein after treatment. (B) Total TICRR (anti-GFP) flow cytometry. (C) Quantification from B (n=3). (D) Insoluble TICRR (anti-GFP) flow cytometry. (E) Quantification from D (n=3). (F) Live cell GFP flow cytometry demonstrates an increase in TICRR protein after treatment. (G) Total TICRR (anti-GFP) flow cytometry. (H) Quantification from G (n=3). (I) Insoluble TICRR (anti-GFP) flow cytometry. (J) Quantification from I (n=3). * p<0.05, ** p<0.01, *** p<0.001, **** p<0.0001

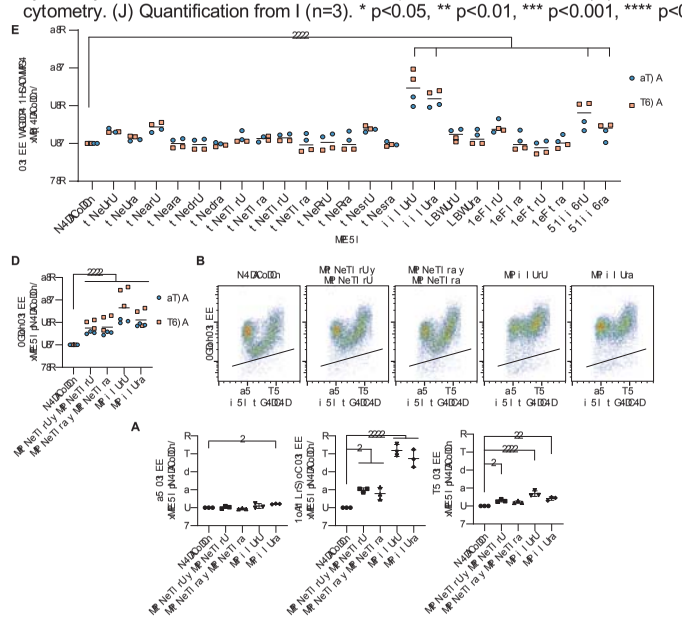

Figure 3. CUL4+B and DDB1 knockdown increase TICRR levels during S-phase. HCT-116 TICRR-mClover cells were transfected with (A) single or (B) double siRNA and collected after 24 or 48 hours for live cell flow cytometry. Values represent median GFP intensity and are normalized to untreated control. Black line indicates grand median. (C) Total protein flow cytometry 24 hours after siRNA transfection. Black line indicates upper limit of the negative control sample. (D) Quantification of 2N, early S-phase, or 4N cells from C (n=3). Data represented as mean ± SD. * p<0.05, ** p<0.01, *** p<0.001, **** p<0.0001

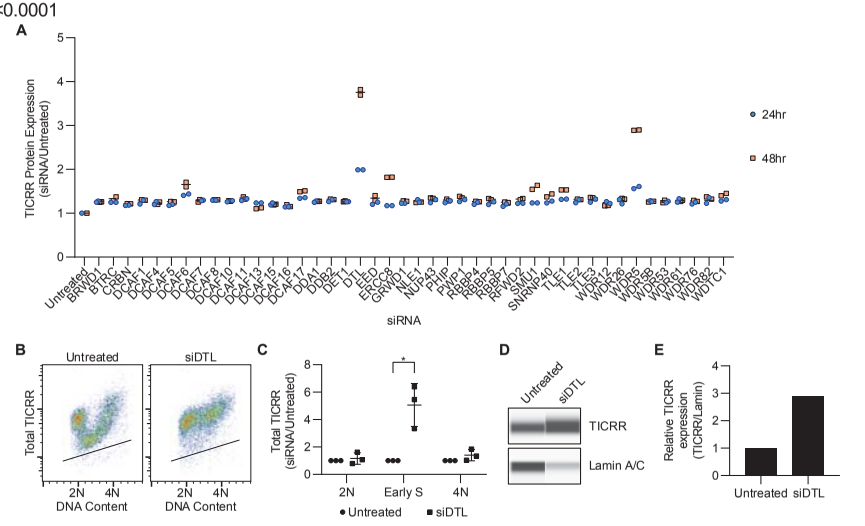

Figure 4. DTL knockdown increases TICRR levels during S-phase. (A) HCT-116 TICRR-mClover cells were transfected with a siRNA pool and collected after 24 or 48 hours for live cell flow cytometry. Values represent median GFP intensity and are normalized to untreated control. (B) Total protein flow cytometry 24 hours after siRNA transfection. Black line indicates upper limit of the negative control sample. (D) Quantification of 2N, early S-phase, or 4N cells from B (n=3). Data represented as mean ± SD. * p<0.05. (D) Capillary electrophoresis of whole cell lysates 24 hours after siRNA transfection for TICRR (anti-GFP) and Lamin A/C (anti-Lamin A/C). (E) Quantification from D. Values are normalized to the untreated control.

Conclusions

We have elucidated a mechanism for TICRR degradation at the G1/S transition. These results suggest a mechanism to control the rate of replication origin firing to prevent replication stress and DNA damage.

Funding National Institutes of Health [R01GM121703], Oklahoma Center for Adult Stem Cell Research, and the Drs. Patricia H. and J. Donald Capra Scholarship Fund

Poster Presentations

Cancer Biology

CANCER BIOLOGY POSTERS

POSTER PRESENTATION LIST
(Listed A-Z by Presenter Last Name)
*Presenting

SINGLE CELL SEQUENCING REVEALS KEY TRANSCRIPTIONAL VARIATIONS IN CONFINED MIGRATING GBM TUMOR CELLS: AN INSIGHT INTO CHOLESTEROL BIOSYNTHESIS PATHWAY ALTERATION(S)*
Anish Babu

EXPOSURE TO E-CIGARETTE AEROSOL EXTRACTS DECREASES THE EXPRESSION OF KEY PROTEINS OF THE INNATE IMMUNE RESPONSE IN LUNG EPITHELIAL CELLS
Daniel Brobst

SINGLE CELL MASS SPECTROMETRY METABOLOMICS STUDIES OF CELL-CELL INTERACTIONS BETWEEN DRUG-RESISTANT CELLS AND DRUG-SENSITIVE CELLS IN CO-CULTURE SYSTEMS*
Xingxiu Chen

AN-DISE: A POTENTIAL RNA INTERFERENCE-BASED THERAPY FOR PROSTATE CANCER*
Joshua M. Corbin

ELUCIDATING THE ROLE OF XRN2 IN DNA REPAIR AND MOTILITY PROGRAMS
Tuyen T. Dang

CHROMOSOMAL INSTABILITY OF INDUCED PLURIPOTENT STEM CELLS IN CULTURE*
Casey O DuBose

E-CIGARETTE AEROSOL ALTERS ANTIOXIDANT MASTER REGULATOR AND MODULATES INFLAMMATORY RESPONSES IN ORAL EPITHELIAL CELLS*
Vengatesh Ganapathy

BLOCKING NECROPTOSIS REDUCES INFLAMMATION AND TUMOR INCIDENCE IN A MOUSE MODEL OF DIET-INDUCED HEPATOCELLULAR CARCINOMA*
Sabira Mohammed Jazir

NOVEL AMINOISOQUINOLINE AND AMINONAPHTHYRIDINE DERIVATIVES AS NEXT-GENERATION OF RET PROTEIN TYROSINE KINASE INHIBITORS*
Ujjwol Khatri

BREAST CANCER SPECIFIC CHROMATIN REGULATOR NETWORK PREDICTS ANTHRACYCLINE RESPONSE
Jacob G Kirkland

CANCER BIOLOGY POSTERS

COMBINATION OF SINGLE CELL METABOLOMICS AND TRANSCRIPTOMICS ANALYSIS OF PRIMARY AND DRUG RESISTANT MELANOMA CANCER CELLS BY USING SINGLE-PROBE AND RNA SEQUENCE*
Yunpeng Lan

DUAL ROLES OF XRN2 IN NHEJ AND HR REPAIR
Julio C. Morales

KRCC1: A NOVEL REGULATOR OF THE DNA DAMAGE RESPONSE
Fiifi Neizer-Ashun

SINGLE CELL MASS SPECTROMETRY METABOLOMIC STUDIES OF CELL HETEROGENEITY IN PRIMARY AND METASTATIC MELANOMA*
Tra D. Nguyen

MECHANISMS OF DNA REPLICATION REGULATION DURING EARLY EMBRYONIC DEVELOPMENT*
Tyler Noble

ESTABLISHMENT OF A *DROSOPHILA MELANOGASTER* MODEL OF HIGH-RISK HUMAN PAPILLOMAVIRUS 16-INDUCED CELLULAR ABNORMALITIES*
Mojgan Padash-Barmchi

TARGETING CELL SENESCENCE REDUCED TUMOR INCIDENCE IN A MOUSE MODEL OF HEPATOCELLULAR CARCINOMA
Deepa Sathyaseelan

PROGNOSTIC SIGNIFICANCE OF APLN/APJ IN NEUROBLASTOMA*
Santny Shanmugarama

REGULATION OF CSC LINEAGE AND STEMNESS MAINTENANCE IN PROGRESSIVE NEUROBLASTOMA: RD3, A MVP IN THE LEAGUE*
Dinesh Babu Somasundaram

OPPOSITE ROLES OF THE JMJD1A INTERACTION PARTNERS MDFI AND MDFIC IN COLORECTAL CANCER*
Yuan Sui

DYNAMIC COMPLEXITY OF MITOTIC SPINDLE MICROTUBULES
Aaron R. Tipton

BREAST CANCER ENDOCRINE THERAPY EXHAUSTS ADIPOCYTE PROGENITORS PROMOTING WEIGHT GAIN AND GLUCOSE INTOLERANCE
Elizabeth A. Wellberg

CANCER BIOLOGY POSTERS

TICRR/TRESLIN PROTEIN EXPRESSION IS CELL CYCLE REGULATED BY THE CUL4-DDB1-DTL E3 UBIQUITIN LIGASE*
Kimberlie A. Wittig

SINGLE-PROBE MASS SPECTROMETRY IMAGING STUDIES OF METABOLITES RELEVANT TO BLOOD VESSEL GROWTHS*
Zhu Zou

SINGLE CELL SEQUENCING REVEALS KEY TRANSCRIPTIONAL VARIATIONS IN CONFINED MIGRATING GBM TUMOR CELLS: AN INSIGHT INTO CHOLESTEROL BIOSYNTHESIS PATHWAY ALTERATION(S)

Anish Babu[1,2], Rachel Sharp[1,4], Sydney Scott[1,2], Kenneth Jones[1,3,4], James Battiste[1,2]
[1]Stephenson Cancer Center, Depts. [2]Neurosurgery, [3]Cell Biology, [4]Harold Hamm Diabetes Center, University of Oklahoma Health Sciences Center

Confined migration is a key feature of Glioblastoma multiforme (GBM) tumor cells. Using microfluidic channels that mimic the physical confinement of brain white matter tract, we have recently shown that the cells migrate in these linear confined spaces (LCSM) are resistant to chemotherapy drugs. In this study, we leverage the single cell-sequencing (sc-Seq) analysis platform and bulk RNAseq to investigate the transcriptome profile of LCSM cells compared to standard monolayer culture (SMC) and post-migrated cells (PMC) with the aim to reveal key molecular regulators in therapy resistance. We performed sc-Seq of 8398 cells (SMC: n=2631, LCSM: n=3200, PMC: n=2567) from two established GBM cell lines (G55, LN229) and a patient derived cell line (Case#34). For sc-Seq analysis, single-cell reads were mapped to the human genome and assigned to genes using the 10X CellRanger pipeline. Normalized gene expression was then used to produce a UMAP plot providing cell clusters based on similarity of gene expression. Once cells were assigned to a cluster, custom scripts in R and Python were used to statistically derive the gene expression differences within and between cell clusters. From this, pathway analysis was performed using Ingenuity Pathway Analysis (IPA) on the differential transcriptional profiles seen in the cell clusters. We identified 7 distinct cell clusters based on cell migration states. Majority of the cells with LCSM status fall in the clusters 0, 4 and 6, and IPA analysis of differentially expressed (DE) genes in each clusters revealed that the pathways related to cholesterol biosynthesis were significantly altered in LCSM cells compared to SMC and PMC cells. Validation of key cholesterol metabolism regulator genes using qPCR assay indicates *hmgcr*, *sqle* and *mvd* are elevated in LCSM cells. Moreover cell cycle progression appears to delay in LCSM, might indicate the influence of cholesterol metabolism in cell cycle regulation. We are validating additional linked pathways and targets using qPCR, western and viability assays to make further comparisons and generate testable hypotheses. In conclusion, our sc-Seq analysis has provided important insights of molecular changes highlighting cholesterol metabolism in confined migrating GBM tumor cells that may be useful for identifying key molecular targets for GBM treatment.

Funding source: NIH COBRE (# P20GM103639 from NIGMS), Stephenson Cancer Center, OUHSC

Single cell Sequencing reveals key transcriptional variations in confined migrating GBM tumor cells: An insight into cholesterol biosynthesis pathway alteration(s)

Anish Babu[1,2], Rachel Sharp[1,4], Sydney Scott[1,2], Qionghua Shen,[5] Young-Tae Kim,[5] Kenneth Jones[1,3,4], James Battiste[1,2]

[1]Stephenson Cancer Center, Depts. [2]Neurosurgery, [3]Cell Biology, [4]Harold Hamm Diabetes Center, University of Oklahoma Health Sciences Center, [5]College of Bioengineering, University of Texas, Arlington

ABSTRACT

Confined migration is a key feature of Glioblastoma multiforme (GBM) tumor cells. Using microfluidic channels that mimic the physical confinement of brain white matter tract, we have recently shown that the cells migrate in these linear confined spaces (LCSM) are resistant to chemotherapy drugs. In this study, we leverage the single cell-sequencing (sc-Seq) analysis platform and bulk RNAseq to investigate the transcriptome profile of LCSM cells compared to standard monolayer culture (SMC) and post-migrated cells (PMC) with the aim to reveal key molecular regulators in therapy resistance.

Glioma cells diffusely infiltrate into brain parenchyma

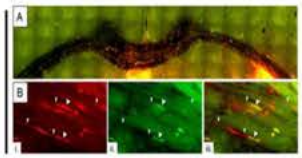

Figure 1: Invasion of GBM cells (indicated by white arrows) into brain parenchyma after xenograft implantation into mouse brain. (A) coronal section of mouse brain.. (B) magnified slice from (A) demonstrating cells in the corpus callosum as they adopt a morphology with an elongated cytoplasm and nucleus.

We performed sc-Seq of 8398 cells (SMC: n=2631, LCSM: n=3200, PMC: n=2567) from two established GBM cell lines (G55, LN229) and a patient derived cell line (Case#34). For sc-Seq analysis, single-cell reads were mapped to the human genome and assigned to genes using the 10X CellRanger pipeline.Normalized gene expression was then used to produce a UMAP plot providing cell clusters based on similarity of gene expression. Once cells were assigned to a cluster, custom scripts in R and Python were used to statistically derive the gene expression differences within and between cell clusters. From this, pathway analysis was performed using Ingenuity Pathway Analysis (IPA) on the differential transcriptional profiles seen in the cell clusters.

We identified 7 distinct cell clusters based on cell migration states. Majority of the cells with LCSM status fall in the clusters 0, 4 and 6, and IPA analysis of differentially expressed (DE) genes in each clusters revealed that the pathways related to cholesterol biosynthesis were significantly altered in LCSM cells compared to SMC and PMC cells. Validation of key cholesterol metabolism regulator genes using qPCR assay indicates *hmgcr*, *sqle* and *mvd* are elevated in LCSM cells. Moreover cell cycle progression appears to delay in LCSM, might indicate the influence of cholesterol metabolism in cell cycle regulation. We are validating additional linked pathways and targets using qPCR, western and viability assays to make further comparisons and generate testable hypotheses. In conclusion, our sc-Seq analysis has provided important insights of molecular changes highlighting cholesterol metabolism in confined migrating GBM tumor cells that may be useful for identifying key molecular targets for GBM treatment.

METHODOLOGY

Schematic showing the experimental workflow

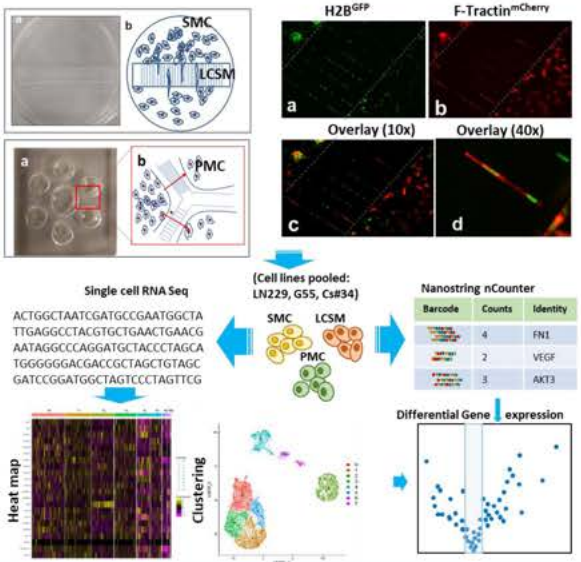

RESULTS

GBM cells in LCSM showed increased drug resistance than in SMC

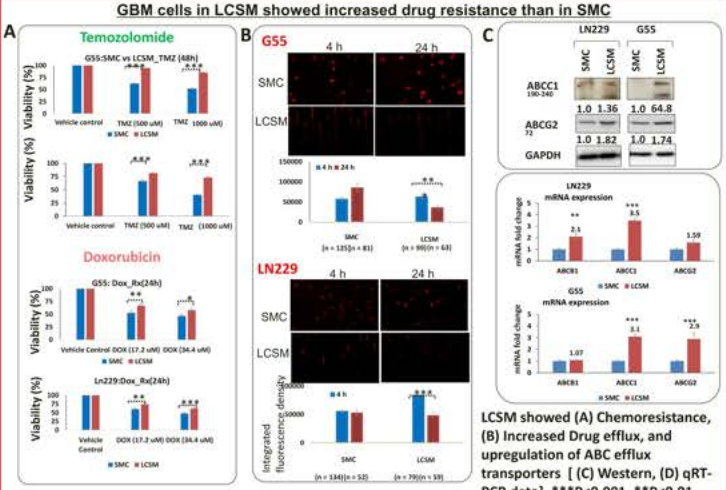

LCSM showed (A) Chemoresistance, (B) Increased Drug efflux, and upregulation of ABC efflux transporters [(C) Western, (D) qRT-PCR data], ***P<0.001, **P<0.01

Inhibition of gene or protein expression effectively reduced migration velocity of GBM cells

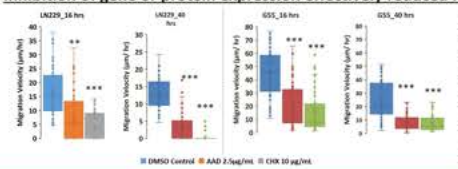

Box & Whisker plots showing the migration velocity of LN229 and G55 LCSM cells with or without Actinomycin D (AAD; transcription blocker) or Cycloheximide (CHX; translation blocker) treatment compared to untreated group at 16 hrs and 48 hrs time points. ***P<0.001, **P<0.01

scSeq analysis reveal cholesterol biosynthesis pathway upregulation in LCSM

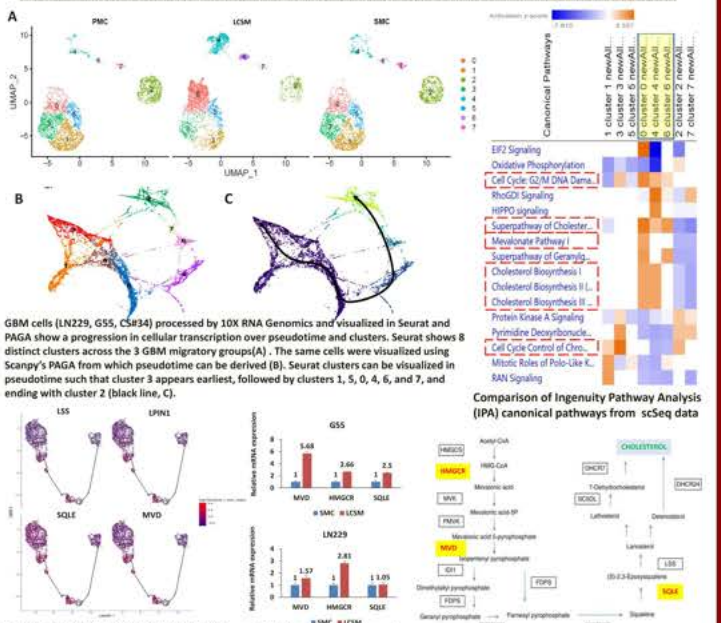

GBM cells (LN229, G55, CS#34) processed by 10X RNA Genomics and visualized in Seurat and PAGA show a progression in cellular transcription over pseudotime and clusters. Seurat shows 8 distinct clusters across the 3 GBM migratory groups(A) . The same cells were visualized using Scanpy's PAGA from which pseudotime can be derived (B). Seurat clusters can be visualized in pseudotime such that cluster 3 appears earliest, followed by clusters 1, 5, 0, 4, 6, and 7, and ending with cluster 2 (black line, C).

Comparison of Ingenuity Pathway Analysis (IPA) canonical pathways from scSeq data

Monocle identifies changes in cholesterol synthesis pathway genes in LCSM as a function of pseudo time.

qPCR data showing increased cholesterol biosynthesis pathway genes in LCSM

Overview of cholesterol biosynthesis pathway

RESULTS

Cell cycle progression is delayed in LCSM

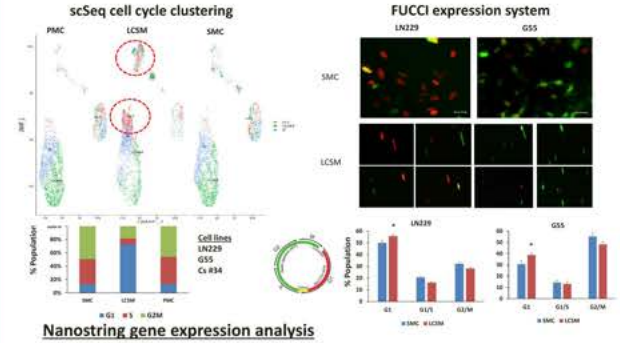

Nanostring gene expression analysis

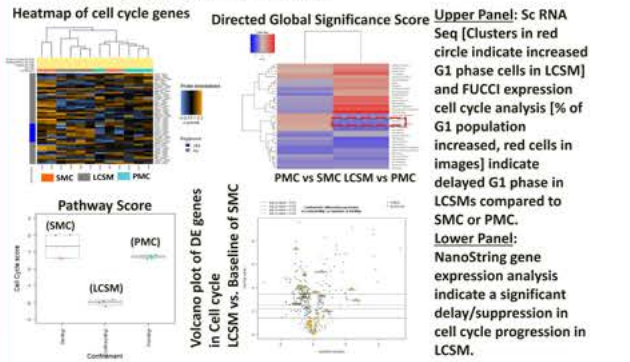

Upper Panel: Sc RNA Seq [Clusters in red circle indicate increased G1 phase cells in LCSM] and FUCCI expression cell cycle analysis [% of G1 population increased, red cells in images] indicate delayed G1 phase in LCSMs compared to SMC or PMC.

Lower Panel: NanoString gene expression analysis indicate a significant delay/suppression in cell cycle progression in LCSM.

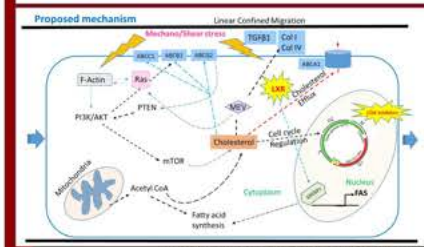

Schematic showing proposed mechanism of how cholesterol metabolism in cells in linear confined space migration influence ABC transporter based drug efflux, regulation of cell cycle and thereby induce chemoresistance. Intervention of cholesterol pathway by Liver X Receptor (LXR) inhibitor and/or cell cycle check point inhibitor may overcome chemo resistance in GBM, importantly migrating cells.

CONCLUSION and FUTURE DIRECTIONS

- GBM cells migrating along linear confined spaces show chemo resistance and gene and protein expression changes
- Single cell sequencing showed that GBM cells form 8 distinct clusters across the 3 migratory groups based on gene expression patterns and 0, 4, and 6 clusters mainly represent LCSMs.
- Cells in SMC, LCSM and PMC showed distinct gene expression (differential) changes as a function of pseudo time
- IPA canonical pathway analysis reveal significant alteration in cholesterol biosynthesis pathway(s), and cell cycle regulation, in addition to other pathways
- Cholesterol Pathway is known to regulate ABC transporter expression and thereby chemo resistance mechanisms
- We propose that Inhibition of cholesterol metabolism may directly or indirectly reduce chemoresistance by drug efflux through ABC transporter mechanisms or related mechanisms in GBM, especially in migrating cells
- Delay in cell cycle response also indicate that LCSM cells may be targetable to cell cycle check point inhibitors
- Studies on targeting cholesterol pathway using Liver X receptor (LXR) agonists and other combination therapy are in process

REFERENCES

1) Huang & Song (2020) Nat Metabol, 2:132-141, 2) Telbisz et al (2007) Biochim Biophys Acta Biomembr, 1768:2698-2713, 3) Patel et al (2019), Sci Rep, 9:15458, 4) Darmanis et al (2017), Cell Rep. 21:1399-1410

Acknowledgments

The authors would like to acknowledge the funding sources from NIH COBRE (# P20GM103639 from NIGMS), University of Oklahoma Health Sciences Center. The authors also thank technical support and assistance from Dr. Kim's lab at University of Texas Arlington, and Cancer Functional Genomics, Pathology [SCC] and Laboratory of Molecular Biology and Cytometry Research [OUHSC] core facilities.

EXPOSURE TO E-CIGARETTE AEROSOL EXTRACTS DECREASES THE EXPRESSION OF KEY PROTEINS OF THE INNATE IMMUNE RESPONSE IN LUNG EPITHELIAL CELLS

Daniel Brobst[1], Jimmy Manyanga[1,2], Constantin Georgescu[4], Jonathan Wren[4], and Lurdes Queimado[1-3]

Departments of [1]Otolaryngology Head and Neck Surgery and [2]Cell Biology; [3]TSET Health Promotion Research Center, Stephenson Cancer Center, The University of Oklahoma Health Sciences Center, Oklahoma. [4]The Oklahoma Medical Research Foundation, Oklahoma.

Conventional cigarette use is the leading cause of preventable morbidity and mortality. Electronic cigarettes (EC) have been shown to yield plasma nicotine levels similar to that seen in traditional cigarette users. ECs have been touted as a healthier alternative to traditional cigarettes and as a smoking cessation tool with mixed results. The increasing use of ECs by youth is concerning with 27.5% of high school students and 10.5% of middle school students reported using ECs in 2019. Use among young adults (18-24) is increasing with 7.6% in reporting use in 2018. Although, the public is aware of the potential acute effects of EC use, little is still known about the potential long-term health effects of EC use. Here, we used a transcriptomic approach to investigate the potential mechanisms by which EC use might contribute to human disease. E-cigarette aerosol extracts were prepared from two brands of e-cigarettes, as previously described. Mainstream tobacco smoke (MS) extract was used as a positive control. Normal lung epithelial cells were exposed to e-cigarette aerosol extracts at nicotine doses comparable to those observed in e-cigarette users for 2 weeks. Whole-cell RNA and protein was isolated. Gene expression was assessed by RNA-sequencing and western blot. Data were analyzed by Student's t-test. Exposure of epithelial cells to e-cigarette aerosols significantly altered the cellular transcriptome. One of the main pathways altered following exposure to either e-cigarette aerosol is the innate immune response. We observed that exposure to e-cigarette aerosol decreased ($p<0.0001$) the mRNA expression levels of Toll-like receptor 3 (*TLR3*). A significant reduction in TLR3 downstream target *IRF7* ($p<0.0001$) was also observed. The reduction in gene expression was similar to that observed after exposure to traditional cigarette smoke extracts. Our study suggests that exposure to e-cigarette aerosol can decrease the expression of key genes involved in innate immune response. TLR3 has also been shown to be involved in apoptosis signaling in cancer cells. A decrease in TLR3 expression could allow tumors to evade immune surveillance and apoptosis. These data suggest that the use of ECs can potentially decrease viral and anti-tumoral innate immune response, increasing health risks.

Grant support: NIH/NCI (R01CA242168, LQ) and Presbyterian Health Foundation. Dr. Queimado holds a Presbyterian Health Foundation Endowed Chair in Otolaryngology.

Exposure to E-cigarette Aerosol Extracts Decreases the Expression of Key Proteins of the Innate Immune Response in Lung Epithelial Cells

Daniel Brobst[1], Jimmy Manyanga[1,2], Constantin Georgescu[4], Jonathan Wren[4], and Lurdes Queimado[1-3]

Departments of [1]Otolaryngology Head and Neck Surgery and [2]Cell Biology; [3]TSET Health Promotion Research Center, Stephenson Cancer Center, The University of Oklahoma Health Sciences Center, Oklahoma. [4]The Oklahoma Medical Research Foundation, Oklahoma.

Background

Conventional cigarette use is a preventable health problem and the leading cause of preventable morbidity and mortality. Electronic cigarettes (EC) have been shown to produce plasma nicotine levels similar to that seen in traditional cigarette users. ECs have been touted as a healthier alternative to traditional cigarettes and as a smoking cessation tool with mixed results. The increasing use of ECs by youth is concerning with 27.5% of high school students and 10.5% of middle school students reported using ECs in 2019. Use among young adults (18-24) is increasing with 7.6% in reporting use in 2018. Although, the multi-state outbreak of severe lung illness first identified in August 2019 (EVALI) called the public attention to the potential acute effects of EC use, little is still known about the potential long-term health effects of EC use.

Aim

To evaluate changes in the transcriptome of normal human lung epithelial cells following exposure to electronic cigarette aerosol extract

Methods

Normal human lung epithelial cells (Nuli1) were exposed to extracts of two different electronic cigarette aerosol extracts. Extracts were prepared as previously published.[1] Extracts from conventional cigarette smoke were included as a control. The dose (10 puffs/5L) exposed the cells to nicotine levels seen in the plasma of EC and conventional cigarette users. Following a 2-week exposure, whole cell RNA and protein were isolated. RNA sequencing was performed to identify changes in the transcriptome and Western blots were performed to verify the RNA results.

Conclusions

- RNA sequencing data showed decreased innate immunity as one of the pathways changed the most following exposure to EC aerosol and decreases in expression of *TLR3*, *RIG1* and *ILR7* were detected. These changes were confirmed with protein expression. These decreases may lead to increased risks of viral respiratory infection in EC users.
- *TLR3* has been shown to directly trigger apoptosis in cancer cells. A decrease in *TLR3* expression may prevent this.
- Interestingly, cigarette smoke exposure has also been shown to decrease *TLR3*, *RIG1* and *ILR7* expression and lead to increased risks of viral respiratory infections.

Funding

•NIH/NCI (R01CA242168, LQ) and Presbyterian Health Foundation. Dr. Queimado holds a Presbyterian Health Foundation Endowed Chair in Otolaryngology.

Results

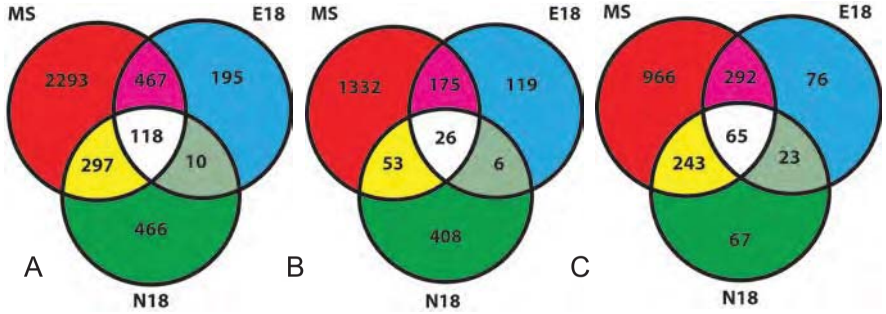

Figure 1. (A) Total number of genes detected as changed in Nuli1 cells following EC and MS exposure, (B) Number of genes increased and (C) genes decreased following exposure

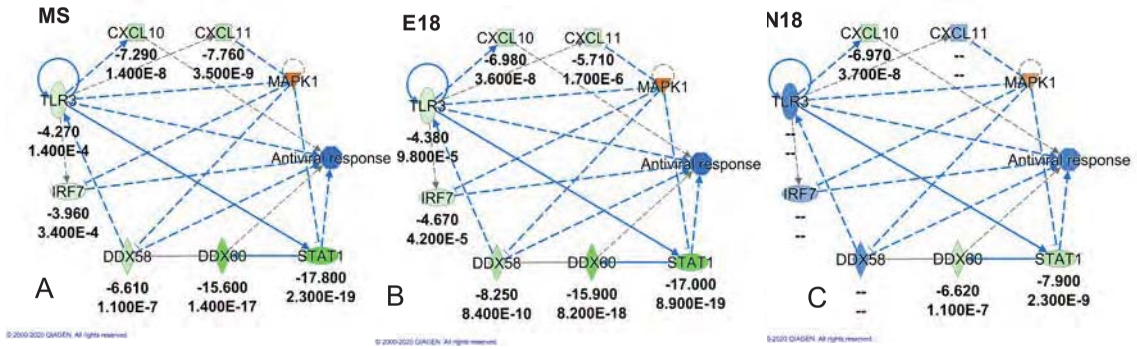

Figure 2. Innate immune response genes changed in Nuli1 cells following exposure to (A) MS, (B) E18 EC and (C)N18 EC

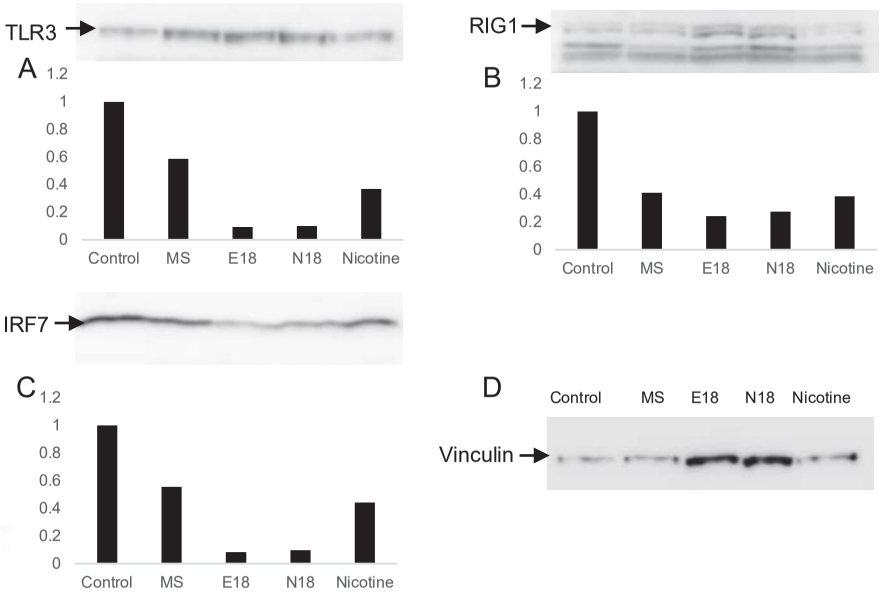

Figure 3. Western blots of innate immunity proteins in Nuli1 cells. (A) TLR3, (B) RIG1 and (C) IRF7 shown to be changed at the mRNA level following RNA sequencing. (D) Vinculin was used as a loading control and used in densitometry quantification of the Western blots

References

1.) Rubenstein et. al. *Circulation* 109: 78-83, 2004.

SINGLE CELL MASS SPECTROMETRY METABOLOMICS STUDIES OF CELL-CELL INTERACTIONS BETWEEN DRUG-RESISTANT CELLS AND DRUG-SENSITIVE CELLS IN CO-CULTURE SYSTEMS

Xingxiu Chen, Zhibo Yang
Department of chemistry and biochemistry, University of Oklahoma

Drug resistance is a major reason responsible for the failure in clinical cancer chemotherapy. The molecular mechanisms of drug resistance are of the great interest to researchers. It is believed that interactions between drug-resistant and drug-sensitive cells are relevant to the development of drug resistance in tumors. There are two major approaches for molecular exchange in cell-cell communication: secreting soluble molecules and transferring extracellular vesicles. A variety of *in vitro* co-culture systems, either with or without cell-cell contact, have been developed to study the mechanisms of cell-cell interactions. However, the systems without physical cell-cell contact cannot vividly mimic the actual physiological environment. Although a few techniques have been developed to study cell-cell contact, it is a great challenge to comprehensively analyze metabolomic profiles of individual cells among heterogeneous populations in such *in vitro* co-culture systems.

Mass spectrometry (MS) is a powerful tool for the analysis of cellular metabolites, which directly reflect the genetic and environmental changes of cells. To study the cell-cell interactions among different types of cells, single cell MS (SCMS) metabolomics analysis is needed. The Single-probe developed by our group is a miniaturized multifunctional device that can be coupled with MS to characterize cellular metabolites in live single cell. In this work, the Single-probe MS technique has been utilized for metabolomics studies of interactions between drug-resistant and drug-sensitive cells in co-culture systems.

Irinotecan-resistant (IRI-resistant) cells and drug-sensitive HCT 116 cells were used as models to construct the co-culture systems. MTT assay results indicate the levels of irinotecan resistance in drug-sensitive HCT 116 cells were significantly increased due to the presence of IRI-resistant cells in co-culture systems (without cell contact). To differentiate these two types of cells, HCT 116 cells with stable GFP expression (HCT 116-GFP) were used to represent the drug-sensitive cells. The SCMS studies illustrate that GFP labeling has no significant influence on cell metabolites. In the co-culture system with cell contact, metabolic profiles of HCT 116-GFP cells were significantly changed by the IRI-resistant cells. Interestingly, both types of cells tend to exhibit increased similarities of metabolomic profiles after co-culture. Investigation of cell metabolites altered by co-culture shows that a series of monosaturated lipids were significantly upregulated in HCT 116-GFP cells. We hypothesize SteaoylCoA desaturase-1 is responsible for the enhanced drug resistance of drug-sensitive cells in co-culture conditions. More experiments need to be carried out to test this hypothesis.

Single Cell Mass Spectrometry Metabolomics Studies of Cell-Cell Interactions Between Drug-resistant Cells and Drug-sensitive Cells in Co-culture Systems

Xingxiu Chen, Zhibo Yang*

Department of Chemistry & Biochemistry, University of Oklahoma

Introduction

- Drug resistance to chemotherapy medicine is a major reason for clinical cancer treatment failure.
- It is believed that interactions between drug-resistant and drug-sensitive cells are relevant to the development of drug resistance in tumors.
- A variety of *in vitro* co-culture systems, either with or without cell-cell contact, have been developed to study the mechanisms of cell-cell interactions. However, the systems without physical cell-cell contact cannot vividly mimic the actual physiological environment. Although a number of techniques have been developed to study cell-cell contact, it is a great challenge to comprehensively analyze metabolomic profiles of individual cells among heterogeneous populations in such *in vitro* co-culture systems.
- Mass spectrometry (MS) is a powerful tool for the analysis of cellular metabolites, which directly reflect the genetic and environmental changes of cells. To study the cell-cell interactions among different types of cells, single cell MS (SCMS) metabolomics analysis is needed.
- **In this work, the Single-probe MS technique has been utilized to study cell-cell interactions in a co-culture system with cells possessing different levels of anticancer drug resistance.**

Methods

- **Single-probe Mass Spectrometry**:

The Single-probe is a miniaturized multifunctional device that can be coupled with MS to characterize cellular metabolites in live single cell. The Single-probe composes of three major parts: Nano-ESI emitter, dual-bore quartz tip, and fused silica capillary.

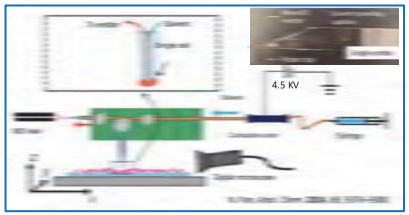

- **MTT assay for cell viability measurement:**

Drug treatments were carried out for IRI-resistant cells in 96-well plates.

MTT was added into 96-well plates for absorbance measurement (570 nm) using a microplate reader.

Methods

- **Workflow of SCMS study on Co-culture system:**

Irinotecan-resistant (IRI-resistant) cells and drug-sensitive HCT-116 cells were used as models to study the cross-communication.

Step 1: Establish co-culture system with cell contact. Stable HCT-116 cells with GFP expression (HCT-116-GFP) were used to represent the drug-sensitive cells. Both types of cells were seeded in the same well of 6-well plates, allowing for cell attachment onto gridded glass coverslips.

Step 2: Capture florescence image. To identify the two types of cells in co-culture system, fluorescence images were taken using a Nikon Eclipse Ti fluorescence microscope.

Step 3: SCMS study. The Single-probe SCMS technique was used to analyze single IRI-sensitive and resistant cells.

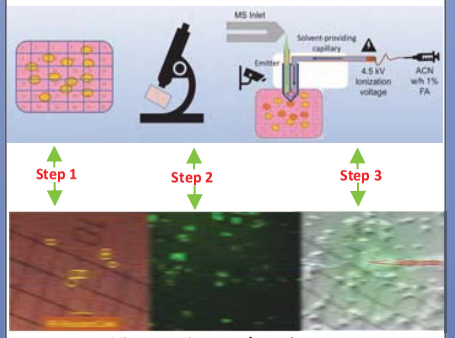

Microscopy images of co-culture system

Results

Elevated IRI-resistance of HCT 116 cells after Co-culture.

MTT assay results indicate that the levels of irinotecan resistance of regular HCT-116 cells were significantly increased due to the presence of IRI-resistant cells in the co-culture systems without cell contact (porous membrane). The drug resistance level increased along with the increase of co-culture time and the density of IRI-resistant cells .

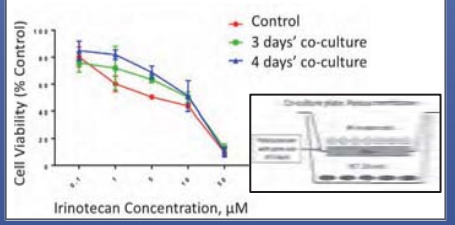

Results

GFP labeling has no significant influence on the metabolic profiles of cells.

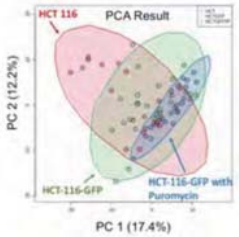

HCT 116-GFP were used to represent the drug-sensitive cells in the co-culture system with contact. The SCMS studies were carried out for HCT 116, HCT 116-GFP, and HCT 116-GFP cultured with puromycin (to maintain HCT116-GFP populations). The results illustrate that GFP labeling has no significant influence on cell metabolites.

Metabolic profiles of HCT116-GPF cells are significantly changed in co-culture system.

In the co-culture system with cell contact, metabolic profiles of HCT-116-GFP cells were significantly changed by the IRI-resistant cells. Interestingly, both types of cells tend to exhibit increased similarities of metabolomic profiles after co-culture.

PCA plot

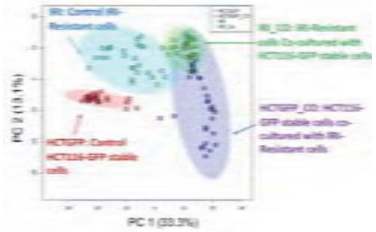

Results from student's t-test show that a series of monosaturated lipids (e.g., SM and PC) were significantly upregulated in HCT 116-GFP cells.

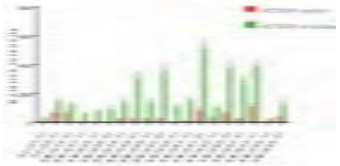

Pathway Mechanism

We hypothesize that Steaoyl-CoA desaturase-1 (SCD-1), a key enzyme in charge of producing monosaturated fatty acids from unsaturated fatty acids, is responsible for the enhanced drug resistance of drug-sensitive cells in the co-culture conditions. Yet, more experiments need to be carried out to test this hypothesis.

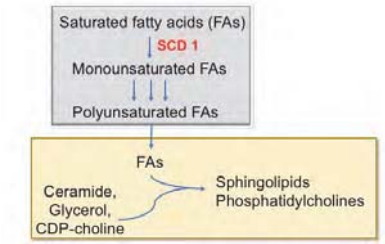

Conclusion

1. The Single-probe SCMS was successfully applied to studying cell-cell interaction in mixed co-culture systems.
2. Advantages of our biological model system: allows for cell-cell physical contact, avoids the usage of extra material in cell growth medium and the requirement of complete seal between different cell types, and more importantly, offers to analyze the individual responses of single cells in heterogenous systems.
3. The level of irinotecan resistance in regular HCT-116 cells was significantly increased due to the presence of IRI-resistant cells in the co-culture systems without cell contact. The metabolic profiles of HCT-116-GFP stable cells were significantly changed by the IRI-resistant cells in co-culture system with contact.

Acknowledgement

Dr. Yang's group members: Yanlin Zhu, Zhu Zou, Zongkai Peng, Yunpeng Lan, Tra Nguyen, Dan Chen, Zhihao Ma. Drs. Paul Sims (OU) and Chuanbin Mao (OU).
Funding: NIH (R01GM116116, R21CA204706).

AN-DISE: A POTENTIAL RNA INTERFERENCE-BASED THERAPY FOR PROSTATE CANCER

Joshua M. Corbin[1,2], Constantin Georgescu[3], Jonathan D. Wren[3], Chao Xu[1,4], Adam S. Asch[1,5], Maria J. Ruiz-Echevarría[1,2,5]
Presenting author's email: joshua-corbin@ouhsc.edu
[1]Stephenson Cancer Center, Oklahoma City, OK, [2]Department of Pathology, Oklahoma University Health Sciences Center, Oklahoma City, OK, [3]Genes and Human Disease Research Program, Division of Genomics and Data Sciences, Oklahoma Medical Research Foundation, Oklahoma City, OK, [4]Department of Biostatistics and Epidemiology, Oklahoma University Health Sciences Center, Oklahoma City, OK, [5]Department of Medicine, Oklahoma University Health Sciences Center, Oklahoma City, OK.

Androgen receptor (AR) signaling is a critical driver of therapeutic response in patients with advanced prostate cancer (PCa). First- and second-generation therapies targeting AR signaling are initially effective, but the benefits are short lived, and most patients relapse with castration resistant prostate cancer (CRPC) which is lethal. Therapeutic resistance and disease progression develop, in most cases, because of molecular adaptation of the AR, AR-coregulators and oncogenic pathways, resulting in persistent AR signaling activation. Therefore, development of effective therapies against advanced PCa remains a critical unmet clinical need.

We have identified specific small RNAs (sh/si RNAs) that trigger potent androgen signaling inhibition and prostate cancer cell death. Transcriptomic and sh/siRNA seed sequence analyses indicate that expression of these toxic shRNAs lead to downregulation of androgen receptor-coregulatory genes thru mRNA 3'-UTR sequence complementarity to the seed sequence of the toxic shRNAs. These findings reveal a specialized form of the "Death Induced by Survival gene Elimination --DISE" mechanism in prostate cancer cells, that we have termed Androgen Network (AN)-DISE. Here we present mechanistic details of AN-DISE, and discuss its therapeutic potential for rapid translation into clinical trials.

Funding Sources: OCAST HR18-037(M.J.R.E.), INBRE C3145217(M.J.R.E), Stephenson Cancer Center/NCI/NIH (P20 GM103639, P30 CA225520), NIH 5U54GM104938 (J.D.W.).

AN-DISE: A potential RNA interference-based therapy for prostate cancer

Joshua M. Corbin[1,2], Constantin Georgescu[3], Jonathan D. Wren[3], Chao Xu[1,4], Adam S. Asch[1,5], Maria J. Ruiz-Echevarría[1,2,5]

1. Stephenson Cancer Center, Oklahoma City, OK.
2. Department of Pathology, Oklahoma University Health Sciences Center, Oklahoma City, OK.
3. Genes and Human Disease Research Program, Division of Genomics and Data Sciences, Oklahoma Medical Research Foundation, Oklahoma City, OK.
4. Department of Biostatistics and Epidemiology, Oklahoma University Health Sciences Center, Oklahoma City, OK.
5. Department of Medicine, Oklahoma University Health Sciences Center, Oklahoma City, OK.

Funding Acknowledgements

OCAST HR18-037 (M.J.R.E)
OK-INBRE P20 GM103447
Stephenson Cancer Center/NCI/NIH P20 GM103639, P30 CA225520, NIH 5U54GM104938 (J.D.W)

Abstract

Androgen receptor (AR) signaling is a critical driver of therapeutic response in patients with advanced prostate cancer (PCa). First- and second-generation therapies targeting AR signaling are initially effective, but the benefits are short lived, and most patients relapse with castration resistant prostate cancer (CRPC) which is lethal. Therapeutic resistance and disease progression develop, in most cases, because of molecular adaptation of the AR, AR-coregulators and oncogenic pathways, resulting in persistent AR signaling activation. Therefore, development of effective therapies against advanced PCa remains a critical unmet clinical need.

We have identified specific small RNAs (sh/si RNAs) that trigger potent androgen signaling inhibition and prostate cancer cell death. Transcriptomic and sh/siRNA seed sequence analyses indicate that expression of these toxic shRNAs lead to downregulation of androgen receptor-coregulatory genes thru mRNA 3'-UTR sequence complementarity to the seed sequence of the toxic shRNAs. These findings reveal a specialized form of the "Death Induced by Survival gene Elimination --DISE" mechanism in prostate cancer cells, that we have termed Androgen Network (AN)-DISE. Here we present mechanistic details of AN-DISE, and discuss its therapeutic potential for rapid translation into clinical trials.

Background: DISE Model

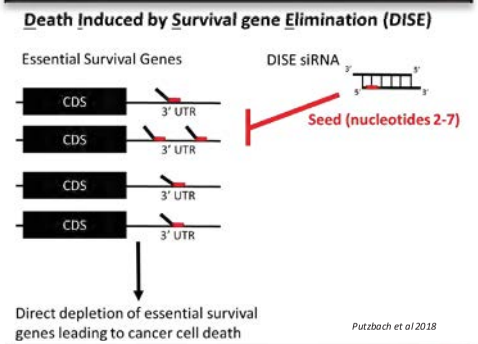

AN-DISE Model

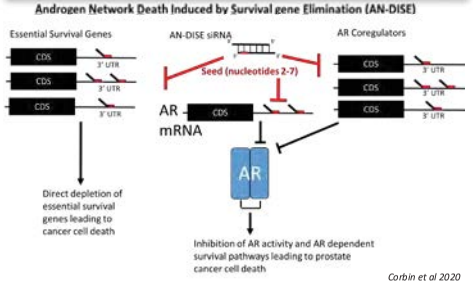

References

Hu, T., et al., Genome-wide CRISPR screen identifies HNRNPL as a prostate cancer dependency regulating RNA splicing. Proc Natl Acad Sci U S A, 2017. 114(26): p. E5207-E5215.
DePriest A.D., et al., Regulators of Androgen Action Resource: a one-stop shop for the comprehensive study of androgen receptor action. Database (Oford), 2016. 2016.
Putzbach, W., et al., DISE: A Seed-Dependent RNAi Off-Target Effect That Kills Cancer Cells. Trends Cancer, 2018. 4(1): p. 10-13.
Corbin JM, et al (2020). Seed-mediated RNA interference of androgen signaling and survival networks induces cell death in prostate cancer cells. BioRxiv. https://doi.org/10.1101/2020.07.17.209379.

Results

FIGURE 1: TMEFF2 TARGETED shRNA REDUCE VIABILITY IN CANCER CELL LINES INDEPENDENT OF TMEFF2 LEVELS

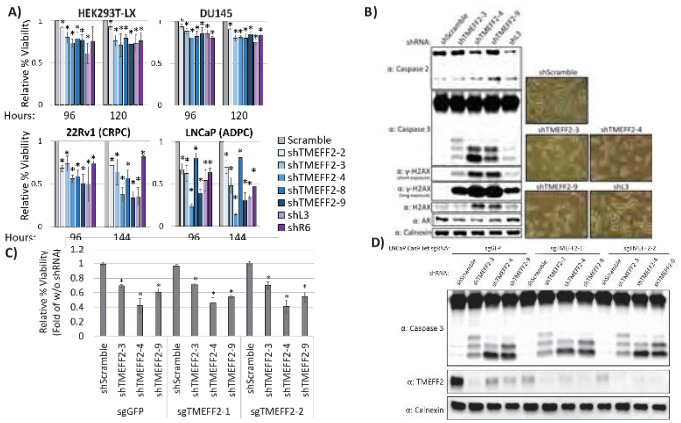

Figure 1: (A) Viability of HEK293T-LX, DU145, 22Rv1 and LNCaP cells transduced with plasmids expressing TMEFF2-targeted shRNAs (shTMEFF2-2, -3, -4, -8, -9), CD95L and CD95 targeted shRNAs (shL3, shR6; known to induce DISE) or shScramble control. Viability was determined by trypan blue and is presented as percent viability relative to shScramble. N=4, error bars ±SD, * p<.05 determined by t-test. **(B)** Western blot analysis (left panel) showing Caspase 2 and Caspase 3 cleavage, γ-H2AX and H2AX protein expression in lysates obtained from LNCaP cells expressing shTMEFF2-3, shTMEFF2-4, shTMEFF2-9, shL3 or shScramble control shRNA 96 hours after transduction. Pictures (right panel) were taken 96 hours after transduction. Calnexin was used as a loading control. **(C)** Relative percent viability and **(D)** western blot analysis showing TMEFF2 expression and caspase 3 cleavage in lysates from LNCaP Cas9 sgGFP, sgTMEFF2-1 and sgTMEFF2-2 cell grown in 500 ng/ml dox (to induce TMEFF2 knockout) and subsequently transduced with plasmids expressing TMEFF2-targeted shRNAs or shScramble control. Viability was measured by trypan blue 96 hours after transductions, and presented as percent viability relative to the viability of cells without shRNA expression. N=3, error bars ±SD, * p<.05 determined by t-test. Lysates for western blot were also obtained 96 hours after shRNA transductions, and Calnexin was used as a loading control.

FIGURE 2: TARGET shRNAs INHIBIT ANDROGEN SIGNALING AND DOWNREGULATE ESSENTIAL AND AR COREGULATORY GENES

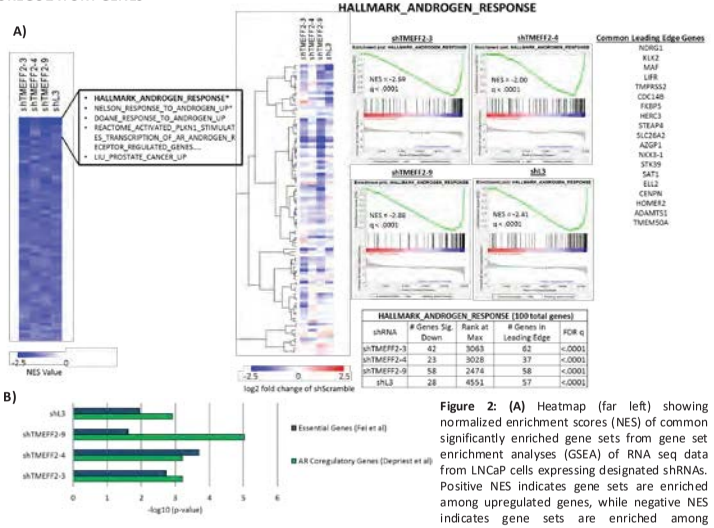

Figure 2: (A) Heatmap (far left) showing normalized enrichment scores (NES) of common significantly enriched gene sets from gene set enrichment analyses (GSEA) of RNA seq data from LNCaP cells expressing designated shRNAs. Positive NES indicates gene sets are enriched among upregulated genes, while negative NES indicates gene sets are enriched among downregulated genes, relative to shScramble control cells. Heatmap (middle) and GSEA plots show gene expression from the Hallmark Androgen Response gene set relative to shScramble control cells. **(B)** Bar graph showing –log10 p-value for enrichment of AR coregulatory genes (green) and LNCaP essential genes (dark blue) among significantly downregulated genes relative to shScramble control LNCaP cells.

FIGURE 3: REDUCTION IN VIABILITY AND ANDROGEN SIGNALING INHIBITION ARE MEDIATED THROUGH THE SEED SEQUENCE OF shRNAs/siRNAs

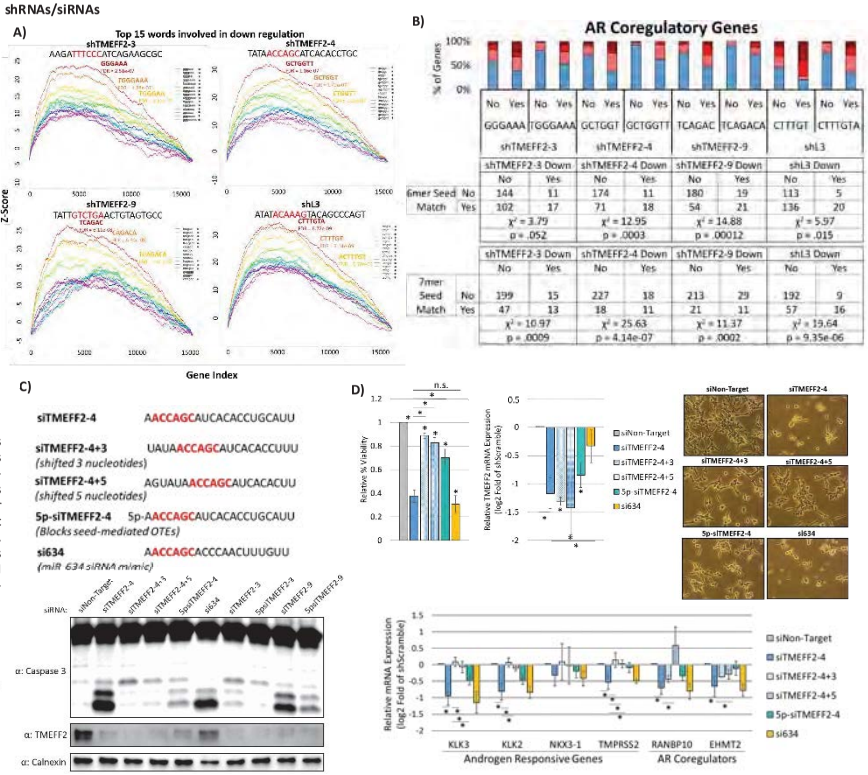

Figure 3: (A) cWords enrichment plots showing the top 15 enriched 6mer, 7mer and 8mer in the 3' UTR of genes downregulated by designated shRNAs according to RNA-seq analyses. Y-axis shows Z-score enrichment values. X-axis contains rank ordered genes from the most downregulated to upregulated expression. The top 3 enriched 3' UTR sequences and FDR values are labeled (red: most enriched, orange: second most enriched, yellow: third most enriched). Unprocessed shRNA guide strand sequences are above each plot, and the potential 6mer seed sequence complementary to the most enriched 6mer 3' UTR sequence associated with gene downregulation is in red. * indicates enriched sequences that are complementary to potential shRNA seed motifs. **(B)** AR coregulatory gene set (Depriest et al) stratified by downregulation (yes or no) and by the presence in their 3'-UTR of single, 2, or more, 6mer or 7mer sequences identified by cWords analyses . Only the most significantly associated with gene downregulation by each shRNA (potential 3' UTR seed matches) were used. Contingency tables are located below each stacked bar graph. P-values were calculated by chi square test of independence, and are labeled on the bottom of each contingency table. **(C)** Top: Guide strand sequences for siRNAs based on the seed sequence identified in cWords analysis for shTMEFF2-4. siTMEFF2-4 seed sequences are in red. 5p designates an ON-Target-Plus modification (Dharmacon) that blocks seed mediated gene downregulation. 4+3 and 4+5 are shifted target sequences. Bottom: Western blot analysis showing Caspase 3 cleavage and TMEFF2 protein expression in lysates from LNCaP cells transfected with the designated siRNAs. Lysates were obtained 72 hours after siRNA transfections. Calnexin was used as a loading control. **(D)** Top: Relative percent viability and TMEFF2 mRNA expression in LNCaP cells transfected with siTMEFF2-4 and control siRNAs. Cell viability was determined by trypan blue. mRNA expression was determined by RT qPCR. Bottom: Relative androgen responsive, AR coregulator and AR mRNA expression in LNCaP cells transfected with siTMEFF2-4 and control siRNAs. RNA was extracted 72 hours after siRNA transfections. mRNA expression was determined by RT qPCR using RPL8, RPL38, PSMA1 and PPP2CA housekeeping genes for normalization. N=4, error bars ±SD, * p<.05 compared to siNon-target. Bars with * designate significant differences relative to siTMEFF2-4. Significance was determined by t-test.

FIGURE 4: AN-DISE INHIBITS TUMOR GROWTH IN CASTRATION-RESISTANT PROSTATE CANCER XENOGRAFT

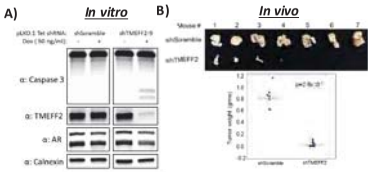

Figure 4: (A) Western blot analysis of Caspase 3 cleavage, TMEFF2 and AR protein (lower band: AR-V7) expression in lysates from 22Rv1 shScramble and shTMEFF2-9 cell lines grown in the presence and absence of 50 ng/ml doxycycline for 5 days to induce shRNA expression. Calnexin was used as a loading control. **(B)** Pictures of tumors (top panel) and dehydrated tumor weight (bottom panel) of xenograft tumors formed by 22Rv1 cells expressing dox-inducible shScramble and shTMEFF2-9 shRNAs after being injected subcutaneously into opposite flanks of NSG mice fed on doxycycline chow to induce shRNA expression. Mice were sacrificed and tumors were excised after four to five weeks of tumor growth. N=7, significance was determined by t-test for the means indicated by pink bar.

ELUCIDATING THE ROLE OF XRN2 IN DNA REPAIR AND MOTILITY PROGRAMS

Tuyen T. Dang, PhD. and Julio C. Morales, PhD.
University of Oklahoma Health Science Center, Neurosurgery Department, Stephenson Cancer Center
tuyen-dang@ouhsc.edu

Glioblastoma multiforme (GBM) is a highly aggressive brain cancer. The standard course of treatment is a combination of radiation and chemotherapy. Even with the dual treatment, the 5-year survival rate of patients with GBM is between 4-7%. Therefore, there is an urgent need to develop novel therapies to increase the survivorship. A possible cause of the low survival rate for GBM patients is the presence of motile neoplastic cells with efficient DNA repair abilities. These motile cells have been shown to be resilient against chemotherapy and radiation. They often continue to grow unchecked leading to lethal secondary tumor disease.

XRN2 is upregulated in GBMs as compared to normal and other brain cancer types. XRN2 is a 5'-3' exonuclease that resolve DNA:RNA hybrids (R loops) that arise during transcription, especially at the 3' end of genes. R-loop biology can affect gene expression by modulating the access of genes to transcription factors, miRNA transcription, and methylation status of genes. Our preliminary data have shown that loss of XRN2 sensitizes to a variety of DNA damaging agents but in particular ionizing radiation. In addition, XRN2 is required for DNA repair in specifically DNA double stranded break repair and cell motility.

To understand how XRN2 modulates DNA repair and cell motility, we conducted RNA-Seq analyses of two GBM cell lines with and without XRN2 expression and found that XRN2 can regulate genes involved in DNA repair pathway and cell motility. We have conducted a mini-cherry picked screen of the XRN2 targets and found at least 6 genes to be required for DNA double stranded break repair. A subset of the 6 genes were also found to be sensitive to DNA damage agents such as ionizing radiation, etoposide, and Parp-1 inhibition. In addition, some of these XRN2-mediated targets are required for cell motility. A number of these XRN2-regulated genes have inhibitors. The next phase of the project is to determine if the XRN2-target inhibitors can synergize with DNA damaging agents such as ionizing radiation to increase the death of neoplastic cells.

Our goal is to develop a patient signature that can better predict patient outcome and if possible a new synergetic treatment plan to increase the efficacy of radio-therapies.

Acknowledgement of funding: P20GM103639 (to JCM).

Elucidating the role of XRN2 in cell motility and DNA repair programs

Tuyen T. Dang, PhD., Julio C. Morales, PhD.
The University of Oklahoma Health Science Center
Stephenson Cancer Center
Department of Neurosurgery, Oklahoma City, OK, USA
tuyen-dang@ouhsc.edu, julio-morales@ouhsc.edu

Introduction: Glioblastoma multiforme (GBM) is a highly aggressive brain cancer. The standard course of treatment is a combination of radiation and chemotherapy. Even with the dual treatment, the 5-year survival rate of patients with GBM is between 4-7%. Therefore, there is an urgent need to develop novel therapies to increase the survivorship. A possible cause of the low survival rate for GBM patients is the presence of motile neoplastic cells with efficient DNA repair abilities. These motile cells have been shown to be resilient against chemotherapy and radiation. They often continue to grow unchecked leading to lethal secondary tumor disease.

XRN2 is upregulated in GBMs as compared to normal and other brain cancer types. XRN2 is a 5'-3' exonuclease that resolve DNA:RNA hybrids (R loops) that arise during transcription, especially at the 3' end of genes. R-loop biology can affect gene expression by modulating the access of genes to transcription factors, miRNA transcription, and methylation status of genes. Our preliminary data have shown that loss of XRN2 sensitizes to a variety of DNA damaging agents but in particular ionizing radiation (IR). In addition, XRN2 is required for DNA repair in specifically DNA double stranded break repair and cell motility.

To understand how XRN2 modulates DNA repair and cell motility, we conducted RNA-Seq analyses of two GBM cell lines with and without XRN2 expression and found that XRN2 can regulate genes involved in DNA repair pathway and cell motility. We have conducted a mini-cherry picked screen of the XRN2 targets and found at least 6 genes to be required for DNA double stranded break repair. Some of these targets were found to be sensitive to DNA damaging agents such as IR, etoposide and Parp-1 inhibition.

In addition, some of these XRN2-mediated targets are required for cell motility. A number of these XRN2-regulated genes have inhibitors. The next phase of the project is to determine if the XRN2-target inhibitors can synergize with DNA damaging agents such as ionizing radiation to increase the death of neoplastic cells.

Hypothesis: Based on these observations, we hypothesized that XRN2 contributes to glioma disease progression by acting as a radiation protectant and driver of neoplastic cell motility and/or invasion.

Impact: Findings from these studies would impact on radiation treatment of cancer patients by identifying who would best benefit from conventional radiation and possibly new drug targets to work in concert with radiation to increase efficacy.

XRN2 expression correlates with disease and poor patient outcome

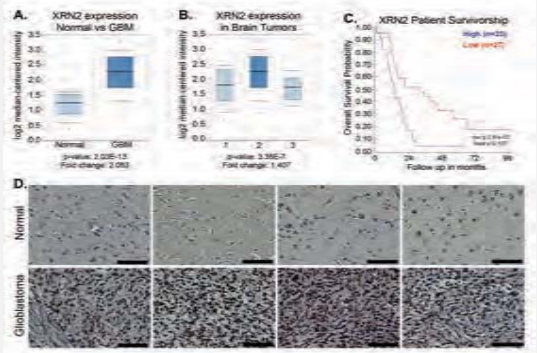

Analyses from the Sun Brain database (Oncomine) show increase XRN2 mRNA levels in GBM as compared to **A.** Normal, **B.** Astrocytoma (1), GBM (2), and Oligodendroglial tumors (3). **C.** Kaplan-Meier graph of XRN2 expression shows a poorer outcome in XRN2 high (blue) compared to XRN2 low (red) patients. Graph from R2: Genomics Analysis . **D.** IHC of XRN2 (brown) in patient tumor tissues. Counterstained with hematoxylin (nuclei, blue). Scale bar is 200 micron.

Loss of XRN2 sensitizes cells to DNA damaging agents

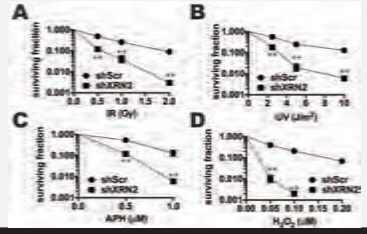

Knockdown of XRN2 expression through shRNA (shXRN2) sensitizes the cells to the following DNA damaging agents: **A.** Ionizing radiation, **B.** Ultraviolet, **C.** Aphidicolin, and **D.** Hydrogen Perioxide as compared to a scramble shRNA (shScr) control.

XRN2 is required for GBM cell motility

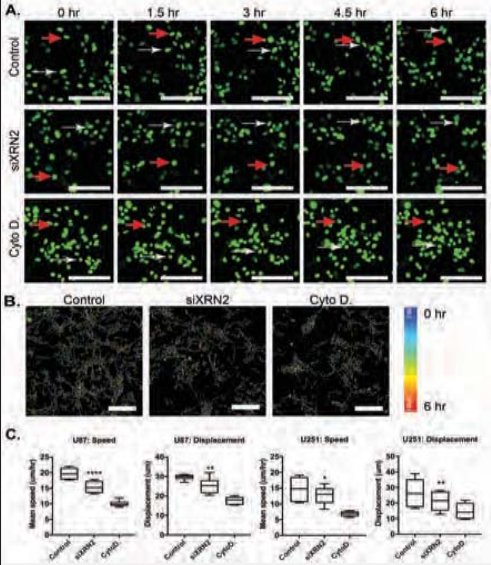

A. Subconfluent imaging of U87 H2B-GFP transfected for 72 hrs or treated with 0.2 uM of cytochlasin D (non-motile control). Images were taken with LSM710 confocal microscope with an environmental chamber. Images were taken every 30 minutes. Tracking duration 6 hours. Arrows are representative tracking over time. Scale bars are 100 um. **B.** Tracks of cell movement over time. Scale bars are 100 micron. **C.** Quantification of live cell imaging of U87 and U251 GBM cells using TrackMate. * represents significant p-value based on t-test.

XRN2 regulates genes involved in DNA damage repair and cell

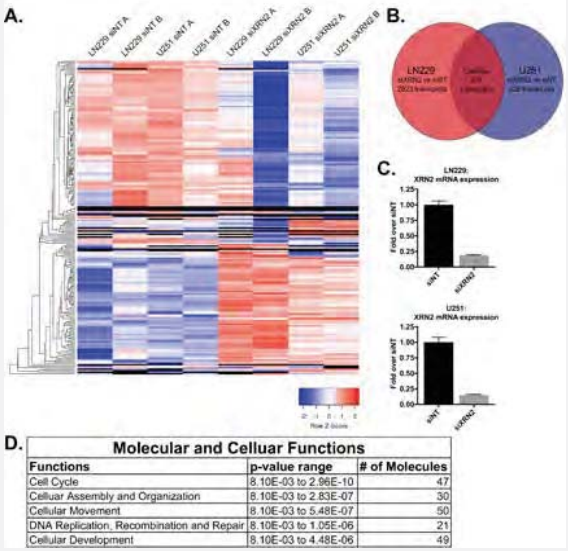

D.

Molecular and Cellular Functions		
Functions	**p-value range**	**# of Molecules**
Cell Cycle	8.10E-03 to 2.96E-10	47
Cellular Assembly and Organization	8.10E-03 to 2.83E-07	30
Cellular Movement	8.10E-03 to 5.48E-07	50
DNA Replication, Recombination and Repair	8.10E-03 to 1.05E-06	21
Cellular Development	8.10E-03 to 4.48E-06	49

MiSeq on GBM cell lines transfected with corresponding siRNAs. **A.** Expression heatmap of the 209 transcripts in B. **B.** Venn-diagram of transcription landscape in LN229 and U251 from A. **C.** qPCR of XRN2 mRNA expression in samples transfected with the corresponding siRNAs. **D.** Cellular programs for which XRN2 targets are involved in.

XRN2-targets are required for DNA double stranded break repair

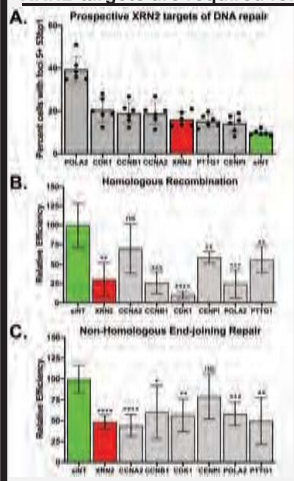

A. Quantification of 53bp1 5+ foci formation of LN229 cells transfect with siRNAs targeting listed genes. After 72hrs of transfection cells were harvested for immunofluorescence and stained with a 53bp1 antibody. Cells were imaged on a Cytation 5 (BioTek) and foci detection was done with Gen5 spot counting add-on (BioTek). **B.** Quantification of homologous recombination repair efficiency utilizing U2OS reporter cell line from Dr. Jeremy Stark lab. Cells were transfected with siRNAs targeting the listed genes. **C.** Quantification of non-homologous end-joining repair efficiency utilizing U2OS reporter cell line from Dr. Jeremy Stark lab. Cells were transfected with siRNAs targeting the listed genes. SiNT is our non-targeting siRNA control. * represents significant p-value based on t-test.

XRN2-targets are required for cell motlity

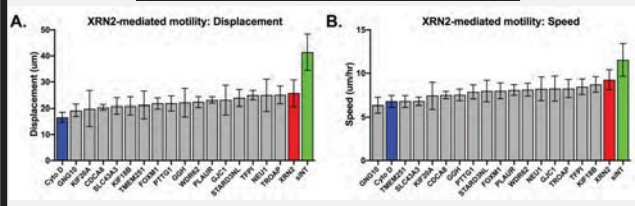

Quantification of live-cell imaging of U251 cells transfected with siRNAs targeting listed genes. Subconfluent tracking of 72 hrs siRNA transfection or treated with 0.2 uM of cytochlasin D (non-motile control). Images were taken with LSM710 confocal microscope with an environmental chamber. Images were taken every 30 minutes. Tracking duration 6 hours. **A.** Displacement quantification **B.** Speed quantification. TrackMate (Fiji) was used to track and measure the movement of the cells.

XRN2 is required for GBM tumor establishment

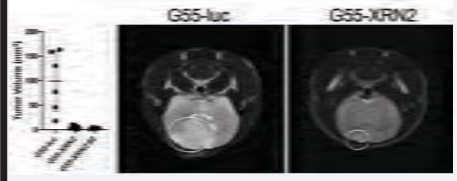

Tumor volume and representative MRI images of mouse brain xenografts using G55 GBM patient cell line. Cells expressed a shRNA targeting either luciferase (luc) or XRN2 and were orthotopically injected into the brain

Future directions:

1. Elucidate XRN2-mediated DNA repair of double stranded DNA breaks induced by ionizing radiation and chemotherapy.
2. Determine if XRN2-targets are required for GBM motility/invasion.
3. Determine if XRN2-targets are required for GBM tumor establishment

Acknowledgments:
I would like to thank the OMRF imaging core facility for the usage of their LSM710 microscope and OUHSC Laboratory for Molecular Biology and Cytometer Research for their assistance with the MiSeq. I would like to express my appreciation to Dr. Jeremy Stark for gifting us the U2OS DNA repair reporter cell lines and to Dr. Rheal Towner's group for their collaboration on the mouse xenograft experiments. Funding source: P20GM103639 (to JCM).

CHROMOSOMAL INSTABILITY OF INDUCED PLURIPOTENT STEM CELLS IN CULTURE

Casey O DuBose[1], Christopher L Sansam[1], Gary J Gorbsky[1]
[1]Oklahoma Medical Research Foundation, Department of Cell Cycle and Cancer Biology

Since their creation in 2007, induced pluripotent stem cells (iPSCs) have offered great promise in the field of regenerative medicine. By reprogramming a patient's own cells, immunological rejection can be avoided during transplantation. Though iPSCs have much promise, they are still fraught with pitfalls which must be overcome, namely the accumulation of genetic aberrations that can occur in culture. During development and expansion iPSCs must be grown in artificial culture conditions for extend periods of time, which has the potential to introduce many types of genetic abnormalities. In addition to point mutations, these genomic alterations can range from aneuploidy to subchromosomal aberrations, characteristics often associated with cancer cells. To gain new insight into the nature of these chromosomal aberrations, iPSCs were grown and examined periodically over the course of 50 passages. While the iPSCs were being cultured, their genomic integrity was examined periodically using optical mapping technology. This technology can identify structural variations across the entire genome ranging from 500 base pairs to megabase pairs in length. Compared to next generation sequencing, optical mapping produces longer read lengths capable of better detecting large structural variants. Notably, inversions and balanced translocations, which do not produce copy number changes, can be distinguished.

Optical mapping of IPSCs detected hundreds of structural variations, comprised of insertions, deletions, duplications, and inversions, not present in the general population. Multiple gene groups, such as those involved in cell differentiation and chromosomal rearrangement, were disproportionately affected by coding sequence variation caused by the detected structural variants. Also analyzed was the colocalization of structural variations with repetitious elements in the genome, which may enhance certain types of structural variation. In addition to subchromosomal changes, a third copy of chromosome 12 was detected in one line. This trisomy was confirmed via chromosome spreads, which indicated that the aberration entered the cell population at approximately passage 22 and became the dominant genotype within four additional passages. These studies draw new light on the potential danger of genome instabilities that evolve during culture of iPSCs. Supported by a grant from The Oklahoma Center for Adult Stem Cell Research to GJG and grants 5R35GM126980 to GJG and 1R01GM121703 to CLS from the National Institute of General Medical Sciences.

Investigating the Genomic Stability of Induced Pluripotent Stem Cells in Long Term Culture

Casey O DuBose, Christopher L Sansam, PhD, Gary J Gorbsky, PhD
Oklahoma Medical Research Foundation

Introduction:
Induced pluripotent stem cells (iPSCs) offer great promise in the field of regenerative medicine. A product of reprogramming a patient's own cells, iPSCs avoid the issue of immunological rejection during transplantation, a distinct advantage over the use of embryonic stem cells. During development and expansion iPSCs must be grown in artificial culture conditions, which can allow the development of genetic abnormalities. Some of these genetic changes may lead to the development of malignant cells which, if reintroduced into a patient, could lead to cancer. We grew two iPSC lines and periodically tested them using the Bionano Saphyr, an optical mapping instrument able to identify structural variations across the entire genome. These studies provide evidence for genetic changes that may occur with culture of iPSC's. These effects must be considered in use of iPSCs for regenerative therapy.

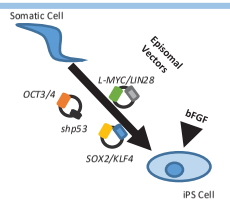

Figure 1: Somatic cells are reprogrammed to produce iPSCs. There are many methods to induce pluripotency in somatic cells. The cell line for this experiment was created using episomal vectors containing a modified cocktail of the original Yamanaka factors.

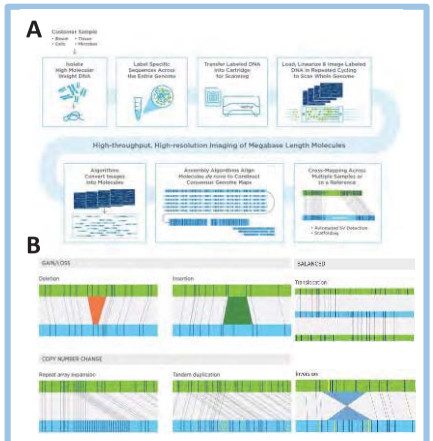

Figure 3: The Bionano Saphyr generates de novo genome maps by labeling DNA molecules and optically imaging them.[1] **A)** High molecular weight DNA is isolated, labeled through a direct labeling reaction, linearized and imaged by thea sample DNA molecule corresponds to variations in label density. The green molecules Saphyr instrument. **B)** This figure illustrates how variations in represent a reference map, while the blue molecules represent the sample consensus genome map.

Figure 4: The Variant Annotation Pipeline process enables users to filter structural variants based on frequency in the general population. By comparing user generated gene maps to a control database, we are able to identify structural variants unique to our samples and eliminate potential false positives.

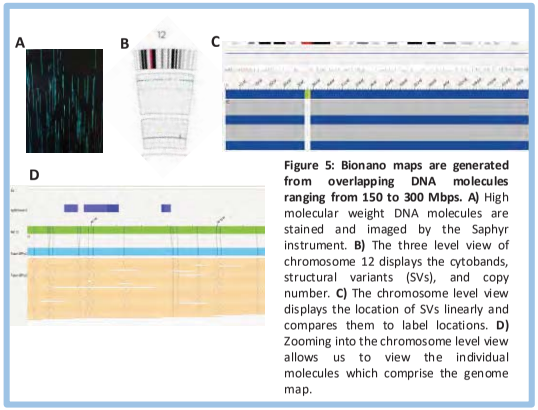

Figure 5: Bionano maps are generated from overlapping DNA molecules ranging from 150 to 300 Mbps. A) High molecular weight DNA molecules are stained and imaged by the Saphyr instrument. **B)** The three level view of chromosome 12 displays the cytobands, structural variants (SVs), and copy number. **C)** The chromosome level view displays the location of SVs linearly and compares them to label locations. **D)** Zooming into the chromosome level view allows us to view the individual molecules which comprise the genome map.

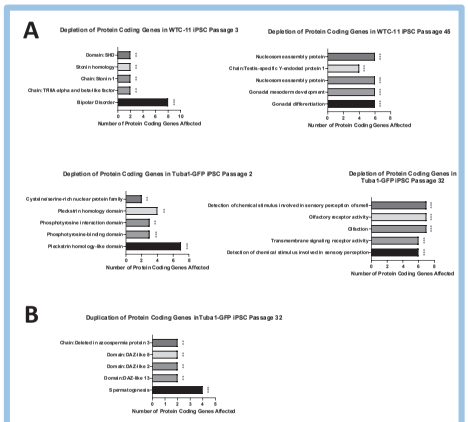

Figure 6: Many gene ontology groups are disproportionately affected by SVs. A) Many gene ontology groups were depleted as a consequence of a deletion, insertion, or inversion interfering with the coding sequence of a gene. In WTC-11 Passage 45, many Gonadal development gene groups were affected by a single deletion more than affected by duplication SVs, which can lead to overexpression of the gene product. three million base pairs in length, which is depicted in figure 5A. The five lowest p values for each sample are shown (* = $P \leq 0.05$, ** = $P \leq 0.01$, *** = $P \leq 0.001$). **B)** Only the late passage sample of the Tuba1-GFP iPSC line displayed a significant enrichment of gene ontology groups

Conclusions:

- **We detected the gain of an additional chromosome 12 in one iPSC line, which became the dominant genotype in approximately 5 passages.**
- **We found no significant change in the doubling time of both iPSC lines over the course of 50 passages.**
- **We identified hundreds of structural variants not found in the general population, and examined their size and distribution between early and late passage samples.**
- **We identified several gene ontology groups which were disproportionately affected by structural variant depletion or duplication.**
- **We found no correlation between structural variant incidence and genomic repeat density.**

Support:
Supported by a grant from the Oklahoma Center for Adult Stem Cell Research to GJG and grants from the National Institute of General Medical Sciences to CLS and GJG.

Citations:
1. Figures 3A/B taken from Bionano Genomics Resources at bionanogenomics.com

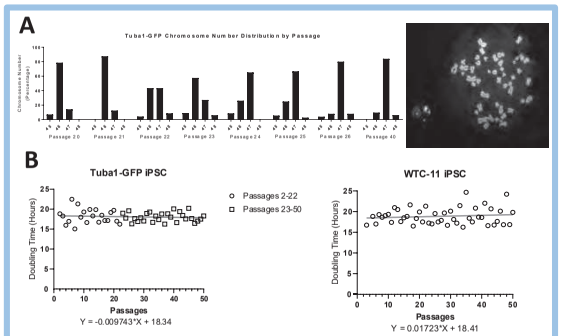

Figure 2: iPSCs were monitored over the course of 50 passages. A) Chromosome spreads were prepared for the Tuba1-GFP iPSC line at various passages. Between passages 22 and 24 the mitotic chromosome number for this line shifted from 46 to 47, indicating the gain of an additional chromosome. **B)** The doubling time was calculated at each passage for both iPS cell lines. Neither cell line experienced significant changes in doubling time with additional passages.

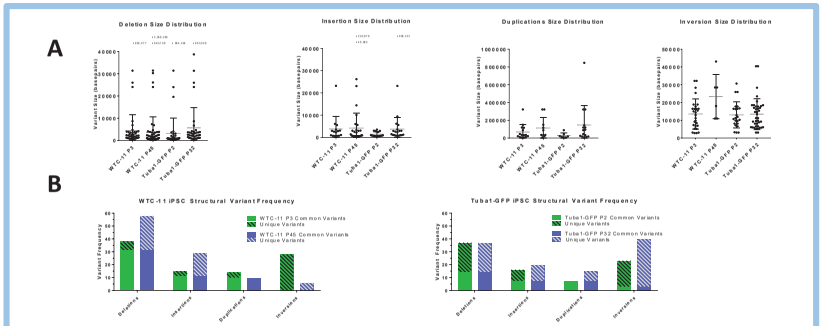

Figure 5: Structural variant size distribution and frequency changes over time. A) Structural variant distribution varies by variant type and between early and late samples of each cell line. The passage number from which the sample was collected is indicated after the cell line (P3=passage three). Particularly large variants are depicted as dots above their sample. The average structural variant size increased from the early to late passage sample in both cell lines. This can be seen in the size distributions of both deletions and insertions, where the largest variants are accrued in the late passage samples. **B)** The total number of variants is shown by variant type and sample. Variants were designated unique if they were not detected in the other sample from the same cell line. The Tuba1-GFP cell line accrued additional structural variants of every type except deletions, which held constant. By contrast, the WTC-11 cell line experienced a decrease in duplications and inversions, potentially due to the proportion of cells with these variants lowering to a point below detection.

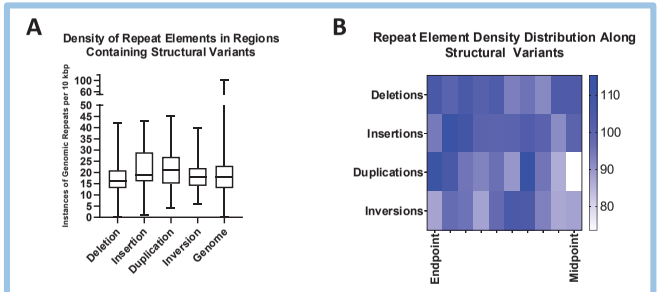

Figure 7: The distribution of repeat elements surrounding structural variants. A) The BNG sequencing results from all four samples were divided into 10kbp windows. Repeat elements were totaled in windows containing SVs, then compared to the repeat element density in the human genome. **B)** Each SV was divided into windows corresponding to five percent of the SVs total length, then the number of base pairs which overlapped with known genomic repeats was totaled. After determining the average number of base pairs per window for a given SV, the percent difference from the average for each window was calculated. The heat map shown is an average of all detected SVs from both iPSC lines. No window was enriched with repeats higher than 120% of the average, indicating that there was no disproportionate localization of repeats along the length of any variant type.

E-CIGARETTE AEROSOL ALTERS ANTIOXIDANT MASTER REGULATOR AND MODULATES INFLAMMATORY RESPONSES IN ORAL EPITHELIAL CELLS

Vengatesh Ganapathy[1], Jimmy Manyanga[1,2], Daniel Brobst[1], Constantin Georgescu[4], Jonathan Wren[4], and Lurdes Queimado[1-3]

Departments of [1]Otorhinolaryngology, and [2]Cell Biology; [3]TSET Health Promotion Research Center, Stephenson Cancer Center, The University of Oklahoma Health Sciences Center, Oklahoma. [4]The Oklahoma Medical Research Foundation, Oklahoma.

Background and Aims: The use of electronic cigarette (e-cig) has skyrocketed among the youths, in part because e-cigs are perceived as a safe substitute to conventional cigarettes. Yet, the resulting health effects of e-cig use remain unclear. E-cig aerosols contain harmful and potentially harmful substances, such as flavoring agents, carbonyl compounds, heavy metals, carcinogens and reactive oxygen species (ROS). A recent *in-vitro* study from our laboratory showed that e-cig aerosols can also increase cellular ROS and suppress the cellular antioxidant capacity. Here, we investigate the effect of exposure to e-cig aerosols on the expression of antioxidant regulators and downstream inflammatory responses in oral epithelial cells.

Methods: Human oral epithelial cancer (UM-SCC-1) cells were exposed for 48 h, or every other day for 2 weeks, to e-cig aerosol extracts (18 mg/ml of nicotine; tobacco flavor) prepared from two distinct e-cig brands. Standard tobacco extracts were used as positive control. Whole-cell RNA was isolated and processed for RNA-sequencing. The expression of altered genes was further validated by RT-PCR, western blotting and ELISA. Data were analyzed by Student's t-test.

Results: RNA-sequencing data showed that exposure of oral epithelial cells to e-cig aerosol extracts for 48 h or 2 weeks led to alterations in several major cellular pathways, including inflammatory and immune response, cell death and survival, cell migration and proliferation, and aryl-hydrocarbon receptor signaling. Within the oxidative stress pathway, we observed decreased levels of master regulator NRF2 and its downstream targets, e.g. glutathione peroxidases (GPX2 and GPX7) and glutathione-S-transferases (GSTA4 and GSTK1), and increased expression of nuclear factor-κB (NF-κB). At the protein level, after 2 weeks of exposure, we observed a decrease in NRF2 and SOD2 and an increase in CD54, IL-1Ra, IL-1a, and IL-10.

Conclusion: E-cig aerosol exposure decreases the expression of NRF2, a major regulator of the antioxidant response, and increases the expression of NFKB and inflammatory markers in oral epithelial cells. The unbalance between NRF2 and NFKB pathways might put the cells under additional oxidative stress, which can have major biological implications. Overall, our study suggests that e-cig aerosols not only carry high levels of ROS but also alter the cellular antioxidant and inflammatory responses which can worsening the oral health of e-cig users.

Grant support: This work was supported by the National Institutes of Health, National Cancer Institute (R01CA242168, LQ) and the Presbyterian Health Foundation (LQ). Dr. Queimado holds a Presbyterian Health Foundation Endowed Chair in Otorhinolaryngology.

E-CIGARETTE AEROSOL ALTERS ANTIOXIDANT MASTER REGULATOR AND MODULATES INFLAMMATORY RESPONSES IN ORAL EPITHELIAL CELLS

Vengatesh Ganapathy[1], Jimmy Manyanga[1,2], Daniel Brobst[1], Constantin Georgescu[4], Jonathan Wren[4], and Lurdes Queimado[1-3]

Departments of [1]Otorhinolaryngology, and [2]Cell Biology; [3]TSET Health Promotion Research Center, Stephenson Cancer Center, The University of Oklahoma Health Sciences Center, [4] The Oklahoma Medical Research Foundation, Oklahoma.

Background

The use of electronic cigarette (e-cig) has skyrocketed among the youths. Yet, the resulting health effects of e-cig use remain unclear. E-cig aerosols contain harmful and potentially harmful substances, such as flavorings, heavy metals, carcinogens and reactive oxygen species (ROS). We have shown that e-cig aerosols can also increase cellular ROS and suppress the cellular antioxidant capacity.

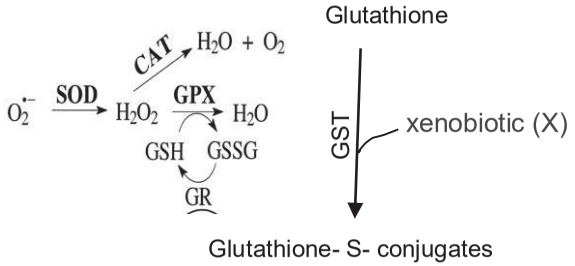

Figure 1. The superoxide dismutase (SOD) enzyme converts superoxide radical into hydrogen peroxide. The catalase (CAT) and glutathione peroxide (GPX) enzymes convert hydrogen peroxide into water. Glutathione conjugation to a xenobiotic (X) via glutathione-S-transferase (GST) results in the formation of a glutathione-S conjugate. The expression of these enzymes is regulated by NRF2.

Aim

To investigate the effect of exposure to e-cig aerosols on the expression of antioxidant regulators and downstream inflammatory responses in oral epithelial cells.

Methods

Human oral epithelial cancer (UM-SCC-1) cells were exposed for 48 h (acute exposure), or every other day for 2 weeks (chronic exposure), to e-cig aerosol extracts (E18, N18) or mainstream tobacco smoke (MS) extract. Whole-cell RNA was isolated and processed for RNA-sequencing. The expression of altered genes was further validated by RT-PCR, western blotting and ELISA. Data were analyzed by Student's t-test.

Results

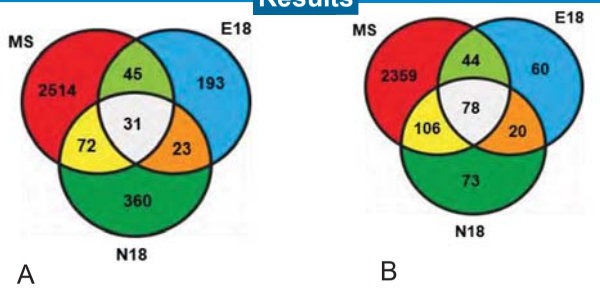

Figure 2. Acute or chronic exposure to e-cig aerosol increased (A) or decreased (B) number of genes. Only chronic is shown, similar pattern was observed in acute exposure.

Group	Gene	Expr Log Ratio	Expr p-value
48h_C vs E18	GPX2	-5.05	0.000013
48h_C vs N18	NFE2L2	-5.45	0.0000038
48h_C vs N18	RELA	4.71	0.000037
2W_C vs E18	GSTA4	-6.67	0.000000092
2W_C vs E18	GSTK1	-6.48	0.00000016
2W_C vs N18	GPX7	-4.53	0.000063

Table 1. Exposure to e-cig aerosol alters the antioxidant master regulator NRF2 (NFE2L2) and its downstream targets, and increased expression of RELA (NF-kB subunit)

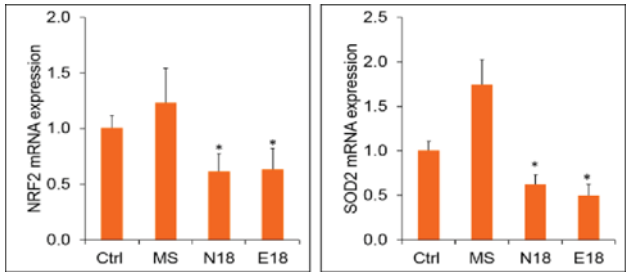

Figure 3. chronic exposure to e-cig aerosol (E18, N18), but not to MS smoke, led to a decrease in *NRF2* and *SOD2* mRNA expression in UM-SCC-1 cells. *NRF2* and *SOD2* mRNA were quantified by RT-PCR. * p<0.01

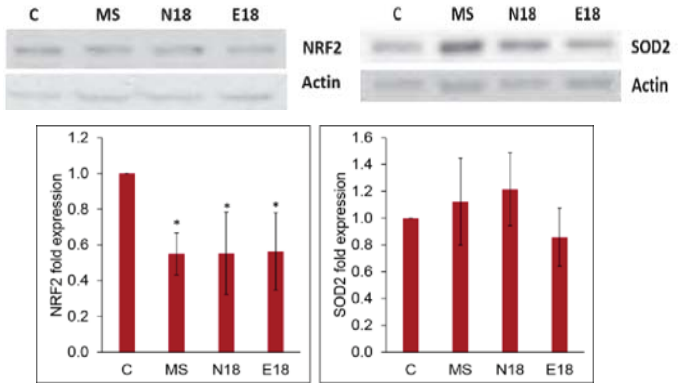

Figure 4. Chronic exposure to e-cig aerosol significantly decreases NRF2 protein. NRF2 and SOD2 protein as measured by Western blotting. * p<0.01

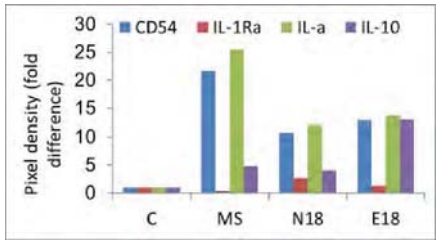

Figure 5. Chronic exposure to e-cig (N18, E18) aerosol or MS smoke extracts significantly increases inflammatory markers.

Conclusions

- E-cig aerosol exposure decreases the expression of NRF2, a major regulator of the antioxidant response, and increases the expression of NFKB and inflammatory markers in oral epithelial cells.
- The unbalance between NRF2 and NFKB pathways might put the cells under additional oxidative stress, which can have major biological implications.
- Our study suggests that e-cig aerosols not only carry high levels of ROS but also alter the cellular antioxidant and inflammatory responses which can worsening the oral health of e-cig users.

Funding

NIH/NCI (R01CA242168, LQ) and PHF (LQ).

BLOCKING NECROPTOSIS REDUCES INFLAMMATION AND TUMOR INCIDENCE IN A MOUSE MODEL OF DIET-INDUCED HEPATOCELLULAR CARCINOMA

Sabira Mohammed Jazir[1], Evan Nicklas[2], Ramasamy Selvarani[2], Dawei Wang[2], Arlan Richardson[1, 2, 3] and Deepa Sathyaseelan[1, 2]

[1]Stephenson Cancer Center, [2]Department of Biochemistry & Molecular Biology, The University of Oklahoma Health Sciences Center, and [3]Oklahoma City VA medical Center

Hepatocellular carcinoma (HCC) ranks as the fourth cancer-related cause of death worldwide. Non-resolving chronic inflammation is proposed to be a major contributor in the development and progression of HCC. Necroptosis is a novel programmed cell death pathway that plays a major role in inflammation through the release of damage-associated molecular patterns (DAMPs). Necroptosis is initiated when necroptotic stimuli sequentially activate receptor-interacting serine/threonine-protein kinase (RIPK1), RIPK3, and mixed lineage kinase domain like pseudokinase (MLKL) through phosphorylation leading to membrane disruption and release of DAMPs. DAMPs in turn activate immune cells to produce proinflammatory cytokines (e.g. TNFα) leading to a positive feedback loop resulting in chronic non-resolving inflammation. Obesity is considered a major risk factor for HCC development. In obesity, nonalcoholic fatty liver disease (NAFLD) progresses to nonalcoholic steatohepatitis (NASH), fibrosis, and ultimately to HCC. Based on this, we hypothesized that inflammation arising from hepatic necroptosis plays a major role in the progression of NAFLD to HCC and that preventing necroptosis will reduce inflammation and thereby the progression of NAFLD to HCC.

To test our hypothesis, we used *Ripk3*$^{-/-}$ and *Mlkl*$^{-/-}$ mice which are deficient in the key necroptotic proteins. Mice were fed either a normal chow diet as control or choline-deficient L-amino acid-defined high fat (60%) diet (CD-HFD) which induces HCC in 6-months. After 6-months of CD-HFD feeding, 100% of control mice developed liver tumors, whereas *Ripk3*$^{-/-}$ and *Mlkl*$^{-/-}$ mice showed a significant reduction in tumor incidence. As immune cells contribute to inflammation, we assessed changes in immune cell population in liver by flow cytometry. A significant increase in immune cell infiltration (CD45 positive cells), total monocyte and macrophage (F4/80 positive cells) and inflammatory monocytic (Ly6C^{hi} CCR2^{+} cells) populations were observed in the livers of control mice fed CD-HFD. Blocking necroptosis significantly reduced immune cell infiltration and expression of proinflammatory cytokines (TNFα and IL-6) associated with HCC progression in the livers of *Ripk3*$^{-/-}$ *and Mlkl*$^{-/-}$ mice fed CD-HFD. Thus, our findings show for the first time that blocking necroptosis could reduce immune cell infiltration, inflammation and tumor incidence in a mouse model of diet-induced HCC.

Funding: NIH/NIA grant, OCAST, and PHF seed grant.

BLOCKING NECROPTOSIS REDUCES INFLAMMATION AND TUMOR INCIDENCE IN A MOUSE MODEL OF DIET-INDUCED HEPATOCELLULAR CARCINOMA

Sabira Mohammed Jazir[1], Evan Nicklas[2], Ramasamy Selvarani[2], Dawei Wang[2], Arlan Richardson[1,2,3], and Deepa Sathyaseelan[1,2]

[1]Stephenson Cancer Center, [2]Department of Biochemistry & Molecular Biology, The University of Oklahoma Health Sciences Center and [3]Oklahoma City VA medical Center

Background of the study

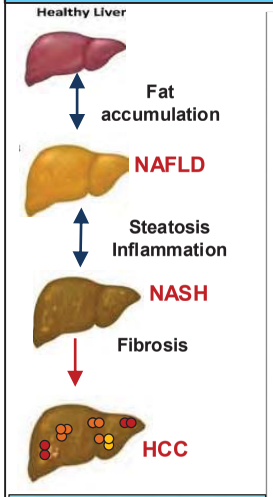

LIVER CANCER IN THE U.S.

Liver cancer is currently the...

4 most common cause of cancer death in men.

8 most common cause of cancer death in women.

Necroptosis – Inflammatory cell death pathway

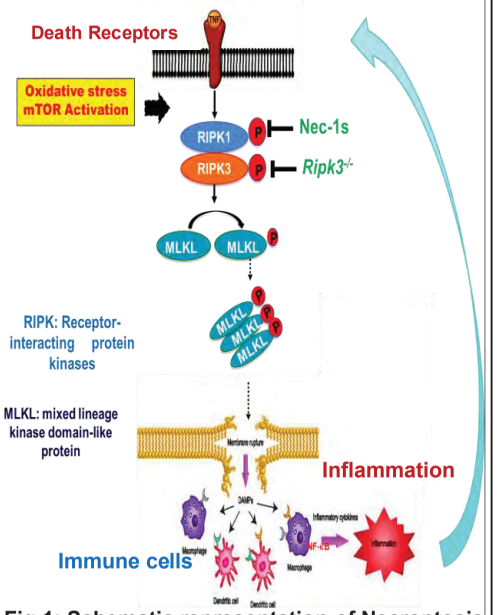

Fig.1: Schematic representation of Necroptosis

Hypothesis

Inflammation arising from hepatic necroptosis plays a major role in the progression of NAFLD (Non alcoholic Fatty liver disease) to HCC and preventing necroptosis will reduce inflammation and the progression of NAFLD to HCC.

Experimental Design

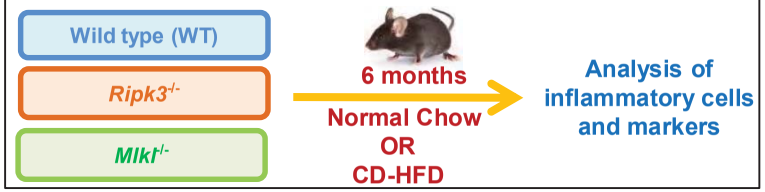

CD-HFD: Choline deficient amino acid defined – High Fat diet (60%))
NAFLD: Non alcoholic Fatty Liver Disease
NASH: Non alcoholic SteatoHepatitis

Results

CD-HFD induces hepatic necroptosis

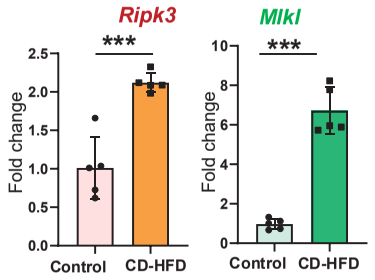

Fig.2: Transcript levels of the necroptotic markers in the liver of WT mice fed with normal chow as Control diet or CD-HFD for 6 months. Fold change is expressed after normalizing with house keeping gene expression. ***p<0.0005, Student's t test

Blocking necroptosis reduces tumor incidence in diet-induced HCC model

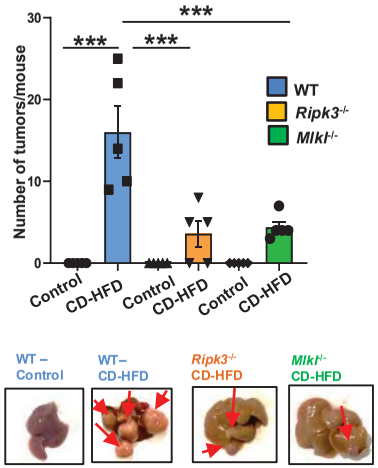

Fig.3: Tumour incidence in WT, *Ripk3*$^{-/-}$ and *Mlkl*$^{-/-}$ fed with normal chow as control diet or CD-HFD for 6 months. ***p<0.0005, One way ANOVA

Blocking necroptosis reduces inflammatory markers in the liver of diet-induced HCC model mice

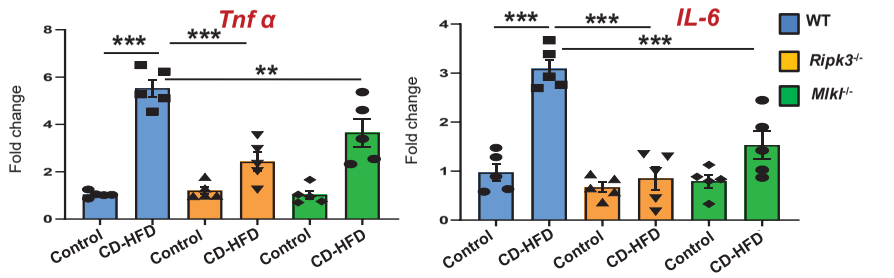

Fig.4: Transcript levels of inflammatory markers in the livers of WT, *Ripk3*$^{-/-}$ and *Mlkl*$^{-/-}$ fed with normal chow as control diet or CD-HFD for 6 months. Fold change is expressed after normalizing with house keeping gene expression. ***p<0.0005, **p<0.005 , One way ANOVA

Blocking necroptosis reduces hepatic immune cell infiltration in response to CD-HFD

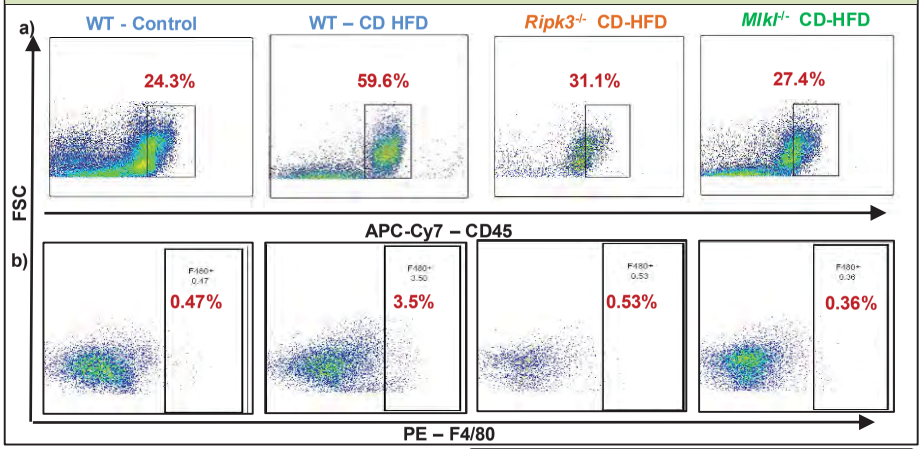

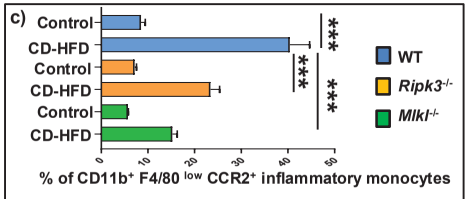

Fig.5: Flow cytometric analysis of immune cells a) CD45+ cells, b) F4/80+ cells , c) inflammatory monocytes in the livers of WT, *Ripk3*$^{-/-}$ and *Mlkl*$^{-/-}$ fed with control diet or CD-HFD for 6 months. ***p<0.0005, One way ANOVA

Relevance of the study

- First report which shows that blocking necroptosis reduces tumor burden in a murine model of diet induced HCC.
- Blocking necroptosis reduces the infiltration of inflammatory immune cells into the liver in response to CD-HFD.
- Blocking necroptosis reduces inflammation, which is a potential contributor to the development of HCC.

FUNDING : This work was supported by NIH/NIA R01 AG059718, Oklahoma Center for the Advancement of Science and Technology research grant (HR18-053) and Presbyterian Health Foundation (OUHSC) Seed grant to DS.

NOVEL AMINOISOQUINOLINE AND AMINONAPHTHYRIDINE DERIVATIVES AS NEXT-GENERATION OF RET PROTEIN TYROSINE KINASE INHIBITORS

Ujjwol Khatri[1, 2], Tao Shen[1, 2], Xuan Liu[1, 2], Xueqing Hu[1, 2], Herman Sintim[3], and Jie Wu[1, 2]
[1]Department of Pathology, [2]Peggy and Charles Stephenson Cancer Center, University of Oklahoma Health Sciences Center, Oklahoma City, OK 73104, [3]Department of Chemistry and Center for Drug Discovery, Purdue University, West Lafayette, IN 47907

Aberrantly activated rearranged during transfection (RET) by gene fusions or oncogenic mutations causes several malignancies including medullary thyroid carcinoma (MTC), and non-small cell lung cancer (NSCLC). Recently, two potent and selective RET protein tyrosine kinase inhibitors (TKIs), selpercatinib (LOXO-292) and pralsetinib (BLU-667), were approved for treating RET-altered cancers, which are effective on the V804M/L gatekeeper mutants but unable to inhibit the acquired G810C/S/R mutations at the solvent front of the RET ATP binding site. The objective of our investigation is to develop the 3rd generation of RET TKIs capable of inhibiting both solvent-front and gatekeeper mutants of oncogenic RET kinase. Using a panel of KIF5B-RET (KR) fusion-dependent BaF3 cell lines with and without V804M or G810C/S/R mutants, we screened 54 compounds, mostly of aminoisoquinoline and aminonaphthyridine derivatives, for inhibition of KR and its solvent-front and gatekeeper mutants. Selpercatinib, pralsetinib, and ponatinib were used as controls. Ten potent compounds were selected for detailed IC50 analysis. Four compounds, HSL476, HSND 17, HSND18, and HSN608 with good calculated partition coefficient (cLogP: 2.0 to 3.2) were identified as the most potent inhibitors of KR (IC_{50}s <4 nM) and its gatekeeper and solvent-front mutants (IC_{50}s <30 nM) in the BaF3 cell model. Immunoblotting analyses showed that these compounds potently inhibited kinase activity as well as induced apoptosis in both KR and its mutant dependent cells. Thus, we have identified potent lead compounds with excellent aqueous solubility for inhibiting both gatekeeper and solvent-front mutants of the oncogenic RET kinase.

This work was supported by research grants R41CA250707 and R01CA242845.

NOVEL AMINOISOQUINOLINE AND AMINONAPHTHYRIDINE DERIVATIVES AS NEXT-GENERATION OF RET PROTEIN TYROSINE KINASE INHIBITORS

Ujjwol Khatri[1, 2], Tao Shen[1,2], Xuan Liu[1,2], Xueqing Hu[1,2], Herman Sintim[3], and Jie Wu[1,2]

[1]Department of Pathology, [2]Peggy and Charles Stephenson Cancer Center, University of Oklahoma Health Sciences Center, Oklahoma City, OK 73104 [3]Department of Chemistry and Center for Drug Discovery, Purdue University, West Lafayette, IN 47907

Abstract

Aberrantly activated rearranged during transfection (RET) by gene fusions or oncogenic mutations causes several malignancies including medullary thyroid carcinoma (MTC), and non-small cell lung cancer (NSCLC). Recently, two potent and selective RET protein tyrosine kinase inhibitors (TKIs), selpercatinib (LOXO-292) and pralsetinib (BLU-667), were approved for treating RET-altered cancers, which are effective on the V804M/L gatekeeper mutants but unable to inhibit the acquired G810C/S/R mutations at the solvent front of the RET ATP binding site. The objective of our investigation is to develop the 3rd generation of RET TKIs capable of inhibiting both solvent-front and gatekeeper mutants of oncogenic RET kinase. Using a panel of KIF5B-RET (KR) fusion-dependent BaF3 cell lines with and without V804M or G810C/S/R mutants, we screened 54 compounds, mostly of aminoisoquinoline and aminonaphthyridine derivatives, for inhibition of KR and its solvent-front and gatekeeper mutants. Selpercatinib, pralsetinib, and ponatinib were used as controls. Ten potent compounds were selected for detailed IC50 analysis. Four compounds, HSL476, HSND 17, HSND18, and HSN608 with good calculated partition coefficient (cLogP: 2.0 to 3.2) were identified as the most potent inhibitors of KR (IC_{50}s <4 nM) and its gatekeeper and solvent-front mutants (IC_{50}s <30 nM) in the BaF3 cell model. Immunoblotting analyses showed that these compounds potently inhibited kinase activity as well as induced apoptosis in both KR and its mutant dependent cells. Thus, we have identified potent lead compounds with excellent aqueous solubility for inhibiting both gatekeeper and solvent-front mutants of the oncogenic RET kinase.

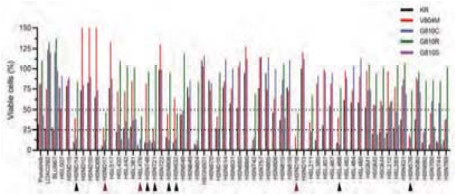

Fig. 1. Screening of aminoisoquinoline and aminonaphthyridine derivatives for inhibition of KR and its solvent-front and gatekeeper mutants. BaF3/KR(WT), and V804M, G810C, G810R, and G810S mutant cell lines were used to screen for the viability at 20nM concentration for each compound. Ponatinib, LOXO292, and Blu667 were used as control. Ten compounds (arrow heads) were selected for IC50 determination. Red arrow heads indicate compounds with estimated IC_{50}s <20 nM for all mutants.

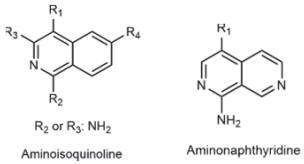

Fig. 2. General structure of aminoisoquinoline and aminonaphthyridine compounds. Variation of R groups leads to different chemical properties of these compounds.

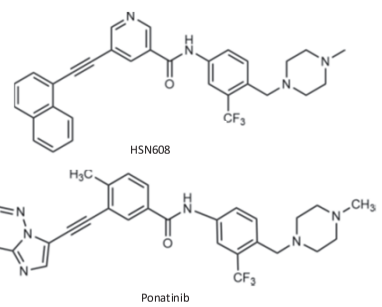

Fig. 3. Structure of HSN608, an aminonaphthyridine compound and Ponatinib. Changing a benzamide unit found in ponatinib into a nicotinamide group improves aqueous solubility, kinase inhibition potency and general drug-likeness.

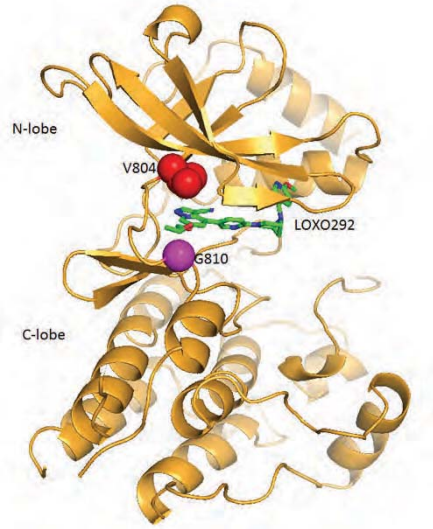

Fig.4.. Crystal structure of LOXO292 bound RET (PDB: 7JU6). The gatekeeper V804 residue is shown in red and the G810 solvent front residue is shown in magenta.

Compounds	IC_{50} (nM) RET mutant			
	WT	V804M	G810C	G810R
HSND17	1.698	14.08	11.46	24.53
HSN721	2.983	11.92	16.51	73.28
HSN576	4.251	20.43	18.24	43.75
HSND14	4.02	19.98	15.93	32.96
HSND18	1.59	14.73	11.26	17.91
HSN748	5.297	88.22	57	54.92
HSN721	2.694	10.32	16.51	86.82
HSN608	3.886	18.96	18.64	28.84
HSN632	2.858	34.89	34.81	14.05
HSL468	3.492	33.53	12.36	46.75
HSL476	1.756	10.17	11.62	17.99
Ponatinib	10.32	95.59	43.63	76.79
BLU667	16.59	18.5	627.1	7363
LOXO292	12.07	29.14	818.6	2623

Fig.5. IC_{50} of lead compounds and known RET inhibitors drugs. IC_{50} values of selected compounds along with the controls.

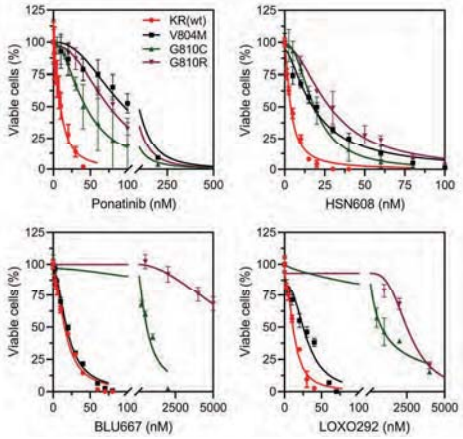

Fig.6. Cell viability curves for the controls compared to highly potent HSN compound HSN608. Ponatinib, BLU667, and LOXO292 are used as controls. IC_{50} was calculated using Cell Titer Glo assay after treatment of each cell lines for 72 hours. Experiment was performed in six technical and two biological replicates.

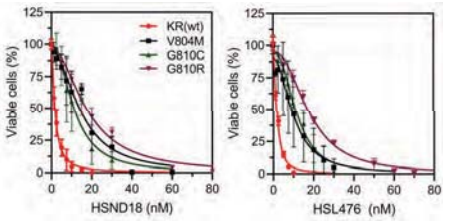

Fig. 7. Cell viability curves HSND18 and HSL476. IC_{50} were determined using cell titer glo assay after treatment of each cell lines for 72 hours. Experiment was performed in six technical and two biological replicates.

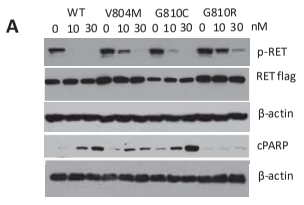

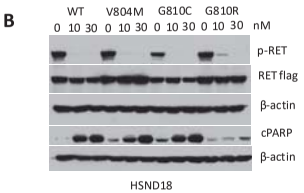

Fig.8. Immunoblotting analysis of RET kinase inhibition and apoptosis in BaF3 derived cells. HSN608 and HSND18 were treated with indicated compounds. Cell lysates were analyzed by immunoblotting of indicated antibodies.

Conclusion

- We have identified aminoisoquinoline and aminonaphthyridine derivatives as potent lead compounds with excellent aqueous solubility for inhibiting both gatekeeper and solvent-front mutants of the oncogenic RET kinase.
- These novel compounds are very effective compared to the existing RET inhibitors Ponatinib, BLU667 and LOXO292 with the most potent inhibitors of KR (IC_{50}s <4 nM) and its gatekeeper and solvent-front mutants (IC_{50}s <30 nM) in the BaF3 cell model.

BREAST CANCER SPECIFIC CHROMATIN REGULATOR NETWORK PREDICTS ANTHRACYCLINE RESPONSE

Jacob G Kirkland[1,2,6] Jose A Seoane[1,3,4] Jennifer L. Caswell-Jin[3] Christina N Curtis[1,3,4] Gerald R Crabtree[1,2,5]

[1]Department of Genetics, Stanford University School of Medicine, Stanford CA, USA, [2]Department of Pathology, Stanford University School of Medicine, Stanford CA, USA, [3]Department of Medicine (Oncology), Stanford University School of Medicine, Stanford CA, USA, [4]Stanford Cancer Institute, Stanford University School of Medicine, Stanford CA, USA, [5]Howard Hughes Medical Institute Stanford University, Stanford, CA, USA, [6]Future Address (2021): Cell Cycle and Cancer Biology Program, Oklahoma Medical Research Institute, Oklahoma City, OK, USA

The accessibility of the genome to regulatory, recombination and repair proteins is controlled in part by the opposition between *trithorax* and *polycomb* genes that fine-tune accessibility, histone modifications and gene activity. Breast cancer is largely driven by copy-number variation (CNV) and altered gene dosage. Our results indicate that Chromatin Regulatory genes (CRGs) operate within a breast cancer specific co-variance transcriptional network that includes members of the classic *polycomb* and *trithorax* genes but broadly extends to over 100 chromatin regulators. To validate the extensive chromatin regulatory network, we used a systems biology approach with the aim of achieving a better understanding of chromatin regulator modulation of anthracycline response in breast cancer patients. Since anthracyclines work in part via inhibition of topoisomerase-II (TOP2) on accessible DNA, we hypothesized that CRGs that mediate DNA accessibility might predict anthracycline response. Using cell line datasets and evaluating the interaction between CRG expression and treatment in predicting survival in a metacohort of early-stage breast cancer patients, we identify CRGs whose expression levels dictate anthracycline benefit across the clinical subgroups. Consistent with our hypothesis, CRGs that promote DNA accessibility, including *trithorax* complex members, were associated with anthracycline sensitivity when highly expressed, whereas CRGs that reduce accessibility, were associated with decreased anthracycline sensitivity. Using molecular biology approaches we validated that expression levels of a Chromatin Regulator, *KDM4B,* modulates TOP2 accessibility to chromatin, elucidating a new pathway of anthracycline resistance. Our novel data-driven methodology identifies a collection of chromatin regulatory genes that form a cancer specific covariate network, parts of which predict response to TOP2 inhibitors likely through alteration of chromatin accessibility. This chromatin regulatory network will inform a robust signature of anthracycline (TOP2i) response that is broadly applicable and provides insight for novel therapeutic targeting and with implications for breast cancer patient stratification and treatment decisions.

A chromatin regulatory network predicts response to TopII inhibitors in breast cancer

Jacob G. Kirkland[1,2,7*], Jose A. Seoane[1,3,4*], Jennifer L. Caswell-Jin[3], Gerald R. Crabtree[2,5,6] and Christina Curtis[1,2,4]

Stanford University School of Medicine Departments of Genetics[1], Pathology[2], Medicine (Oncology)[3], Stanford Cancer Institute[4], Developmental Biology[5], HHMI[6]

Future Address (2021): Cell Cycle and Cancer Biology Program, Oklahoma Medical Research Institute, Oklahoma City, OK, USA[7]

Howard Hughes Medical Institute

Abstract

The accessibility of the genome to regulatory, recombination and repair proteins is controlled in part by the opposition between trithorax and polycomb genes that fine-tune accessibility, histone modifications and gene activity. Breast cancer is largely driven by copy-number variation (CNV) and altered gene dosage. What leads to CNV in breast cancer is largely unknown, but CNV may result from structural and organizational changes in the nucleus as a result of altered chromatin regulation. To determine chromatin regulators that may contribute to this phenomenon we examined the expression levels of a near complete group of chromatin regulators in about 1100 primary breast cancer samples[1]. Our results indicate that these genes operate within a breast cancer specific co-variance transcriptional network that includes members of the classic polycomb and trithorax genes but broadly extends to over 100 chromatin regulators. To validate the extensive chromatin regulatory network, we asked if it actually modulates accessibility by assessing the responses of breast cancer patients to inhibitors of Topoisomerase-II (TOP2) activity, which are highly sensitive to DNA accessibility[2,3]. Indeed, 54 of the genes within the chromatin regulatory network predicted clinical responses to inhibitors of TOP2 and appear to directly modulate chromatin accessibility. The cancer-specific nature of the chromatin regulatory network suggests that it might be a new target for therapeutic development.

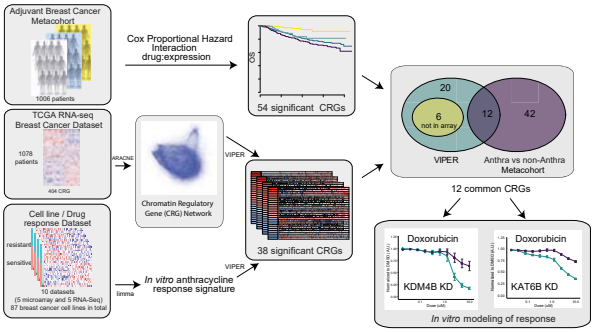

A Breast Cancer Specific Chromatin Regulatory Network

Chromatin Regulator Gene Expression Predicts TOP2 Inhibitor Response

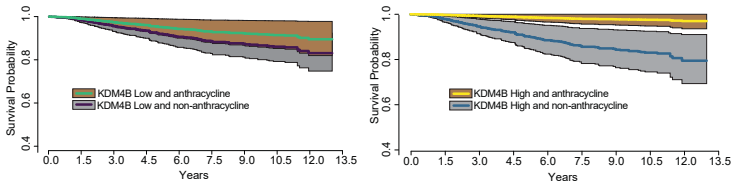

KDM4B Modulates TOP2 Inhibitor Response

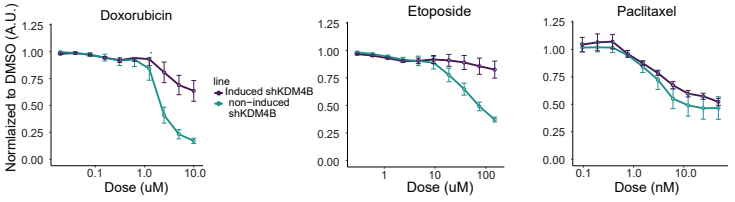

KDM4B Modulates Chromatin TOP2 Accessibility Not Inhibitor Targets

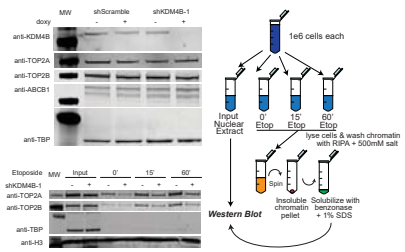

Model

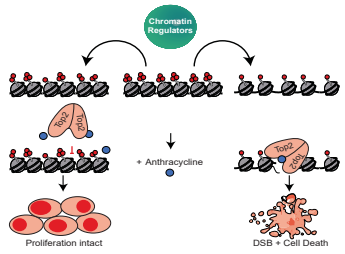

FIRE-dCas9[4] Recruitment of KDM4B

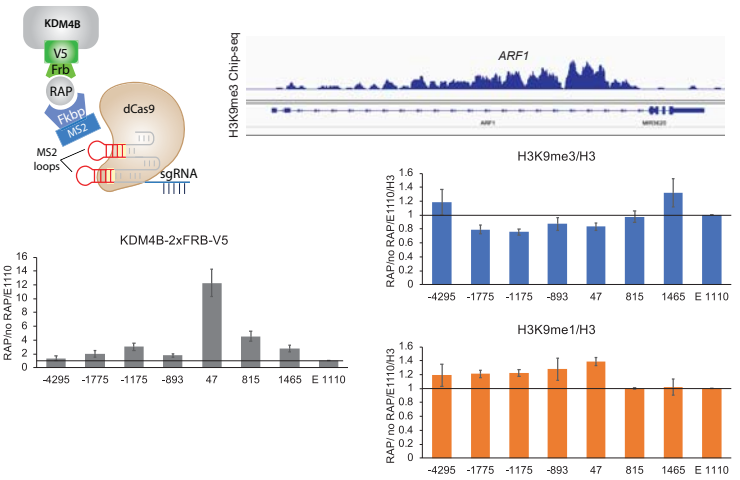

Conclusions

Our novel data-driven methodology identifies a collection of chromatin regulatory genes that form a cancer specific co-variate network, parts of which predict response to TOP2 inhibitors likely through alteration of chromatin accessibility. This chromatin regulatory network will inform a robust signature of anthracycline (TOP2i) response that is broadly applicable and provides insight for novel therapeutic targeting.

References

1. Cancer Genome Atlas, N. Comprehensive molecular portraits of human breast tumours. Nature 490, 61-70 (2012)
2. Dykhuizen, E.C.*, and Hargreaves D.* et al. BAF complexes facilitate decatenation of DNA by topoisomerase-IIalpha. Nature 497, 624-627 (2013).
3. Miller, E.L., et al. TOP2 synergizes with BAF chromatin remodeling for both resolution and formation of facultative heterochromatin. Nat Struct Mol Biol 24, 344-352 (2017).
4. Braun SMG*, Kirkland JG*, Chory EJ, Husmann D, Calarco JP, and Crabtree GR. 2017. "Rapid and Reversible Epigenome Editing by Endogenous Chromatin Regulators." Nature Communications 8 (1): 560.

Funding

Stanford Medicine
The V Foundation for Cancer Research
CDMRP Department of Defense
hhmi Howard Hughes Medical Institute
National Cancer Institute
Susan G. Komen for the cure
BCRF Breast Cancer Research Foundation

COMBINATION OF SINGLE CELL METABOLOMICS AND TRANSCRIPTOMICS ANALYSIS OF PRIMARY AND DRUG RESISTANT MELANOMA CANCER CELLS BY USING SINGLE-PROBE AND RNA SEQUENCE

Yunpeng Lan, Tra Nguyen, Zhibo Yang*
University of Oklahoma, College of art and science, Department of Chemistry and Biochemistry

Melanoma is a type of skin cancer turning into a major public health problem in many countries. The survival rate has improved substantially with the current therapy including surgery of localized tumour and chemotherapy. However, surgery cases a lot of pain for the patience. At the same time, it is hard to effect a radical cure of Melanoma because of the metastatic melanoma and the unclear boundary of tumour and health tissue. Surgery always is followed by relapse causing more pain. Hence, chemotherapy is used as another option or adjuvant therapy for melanoma. The most advanced drug for melanoma chemotherapy is BRAF inhibitor, such as vemurafenib, dabrafenib and encorafenib.

Recently, researcher revealed an appearance of drug resistant melanoma cancer cells. Many bulk analysis were used to understand the mechanism, but it is not be able to reveal difference between individual cells. Hence, single-cell analysis was applied to understand the cell heterogeneity of melanoma cancer cells. Testing the same type of cells by different single-cell -omics technique provides a deeper understandings and cross validation. However, none of them could test the same contents in one cell. In this case, we would like to design a device that allows us to do transcriptomics and metabolomics analysis for the same cell. Mass spectrometry (MS) has become the most effective tools for metabolomics studies for both targeted and untargeted metabolomics studies and single-cell RNA sequence (scRNA-seq) is a genomic approach for massager RNA molecules in biological samples. One of the techniques named micropipette needle showed the potential to obtain a cell content for both metabolomics analysis and transcriptomics analysis in our previous studies. A glass capillary tube was pulled by a pipet puller to form a sharp tip on one side (around 15 μm). UV epoxy was used to connect the micropipette needle to a fused silica capillary. The other side of the capillary was connected with a syringe. By using an Eppendorf cell manipulation system and a syringe pump, the micropipette was be able to suck the target cells into the micropipette. The cell lysis formed in the organic solution in syringe. The lysis could be used by connecting with ionization voltage and form electrospray ionization (ESI) for MS as well as for the further scRNA-seq. Based on our previous studies, the requirement of sample quantity for both tests matches the volume we obtain from the micropipette needle.

Funding support: National Institutes of Health (R01GM116116).

Combination of Single Cell Metabolomics and Transcriptomics Analysis of Primary and Drug Resistant Melanoma Cancer Cells by Using Single-probe and RNA Sequence

Yunpeng Lan, Tra D. Nguyen, Dr. Zhibo Yang*

Department of Chemistry and Biochemistry

Abstract

Melanoma is a type of skin cancer turning into a major public health problem in many countries. Recently, researcher revealed an appearance of drug resistant melanoma cancer cells. Many bulk analyses were used to understand the mechanism, but it is not be able to reveal difference between individual cells. Hence, single-cell analyses were applied to understand the cell heterogeneity of melanoma cancer cells. However, none of them could test the same contents in one cell. In this case, we would like to design a device that allows us to do transcriptomics and metabolomics analysis for the same cell. Mass spectrometry (MS) has become the most effective tools for metabolomics studies for both targeted and untargeted metabolomics studies and single-cell RNA sequence (scRNA-seq) is a genomic approach for massager RNA molecules in biological samples.

Introduction

Melanoma is a type of skin cancer turning into a major public health problem in many countries. The efforts were put on understanding of this disease and great advances have been made, such as predisposition genes BRAF mutation, which was developed into therapeutic management. However, it is hard to effect a radical cure of Melanoma because of the metastatic melanoma and the unclear boundary of tumour and health tissue. In order to review the effect of therapeutic processes, genomics, transcriptomics protein omics and metabolomic studies were applied. Single-cell analysis is one of the directions to understand the cell heterogeneity which become more and more popular in research. However, there is not a Single-cell tool could review two or more omics studies through one cell.

Mass spectrometry (MS) has become the most effective tools for metabolomics studies. Especially for single cell analysis, many techniques have been developed based on MS, such as Matrix-assisted laser desorption/ionization (MALDI). RNA sequence (RNA-seq) is a genomic approach for massager RNA molecules in biological samples. In 2009, the first single-cell RNA-sequencing (scRNA-seq) study was published. Up until right now, the commercial availability of scRNA-seq has been developed. More and more exciting discoveries were announced by scRNA-seq including biomedical researcher or clinician. In here, we would like to combine the two technique for one cell analysis to review a deep understanding of drug impact and for other disease studies.

One of the techniques named micropipette needle showed the potential to obtain a cell content for both metabolomics analysis and transcriptomics analysis. A glass capillary tube was pulled to form a sharp tip on one side (around 15 µm). UV epoxy was used to connect the micropipette needle to a fused silica capillary. The other side of the capillary was connected with a syringe. By using an Eppendorf cell manipulation system and a syringe pump, the micropipette was be able to suck the target cells into the micropipette. The cell lysis formed in the organic solution in syringe. Then signal of cell for MS could last more than 5 min. Specially, the signal could continue after stop the pump and ionization voltage and restart it. This gives us confidence for capturing cells and save the cell contents for the other analysis. We plan to run MS metabolomics analysis for 1 min which could obtain enough data based on our pervious study then run transcriptomics analysis by using the result contents.

Method

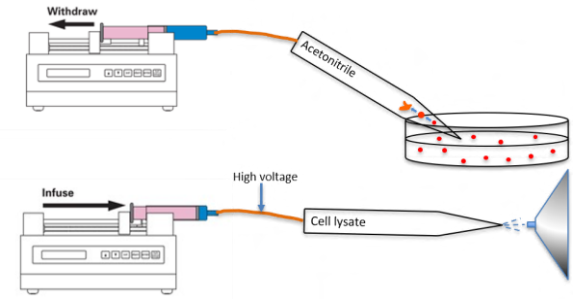

Figure 1. The sketch of micropipette processing. Up: extract cells from the medium; Down: MS analysis

Results

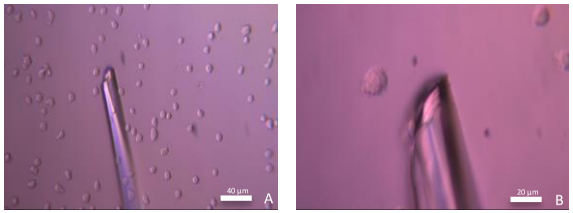

Figure 2. Micropipettes with cells under microscope

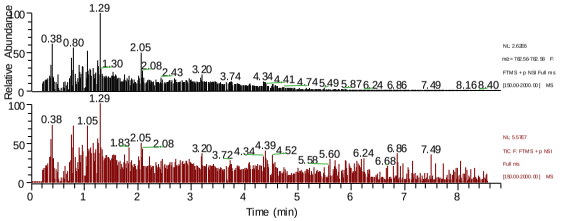

Figure 3. Micropipette duration signals' duration of cells

	WM114	WM266-4
Cell number	10	5

Table 1. Numbers of each type of cells

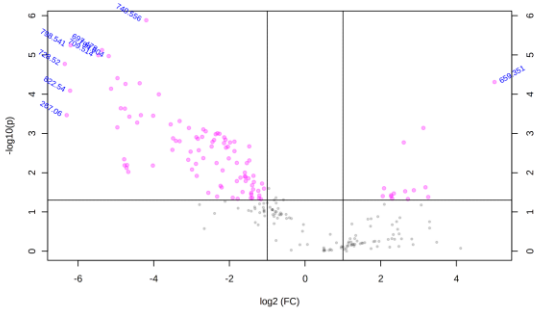

Figure 4. Volcano plot (color points: m/z with p-value lower than 0.05)

Figure 5. Principal components analysis

Discussion

Figure 1. is the sketch of the device. As we mentioned earlier, we will run MS analysis for 1 min and save results of the sample for scRNA-seq. Figure 2. A is the picture of cell and micropipette under microscope. B is enlargement from A. The size of the micropipette is similar comparing with single cell. Figure 3. shows the duration of each cell. The top is a common lipid for cells. We believe with the signal, there are cell contents running over the MS. The signal for a single cell could last 5 minutes and for the first 4 minutes the signal did not reduce significantly. In our experiment, 10 WM114 and 5 WM266-4 cells were detected showed by Table 1. Figure 4. is the statistical analysis which is called as Volcano plot which could review the significant points from the data file. In here, over 100 m/z were identified as highly significant (p value lower than 0.05). First 5. is principal components analysis (PCA). The two types of cells are separated completely which means their metabolic profiles have the significant different.

Conclusion

- The micropipette usefully captured single cell from the cell medium.
- The signal for a single cell was more than 5 min which means after 1 min the cell contents still enough for other analysis.
- The micropipette showed ability of differentiating different types of cells.

Acknowledgement

This project was assisted by Dr. Inna Smalley at moffitt cancer center.
Funding support: National Institutes of Health (R01GM116116).

DUAL ROLES OF XRN2 IN NHEJ AND HR REPAIR

Julio C. Morales and Tuyen T. Dang
Julio-Morales@ouhsc.edu
University of Oklahoma Health Science Center, Department of Neurosurgery and Stephenson Cancer Center

There is a growing body of evidence that demonstrates a connection between factors traditionally associated with transcription and the double strand break (DSB) repair pathways. During the process of normal transcription RNA:DNA hybrids (R loops) are formed and resolved, causing no harm to the cell. However, unresolved R loops have been associated with DSB formation, genetic instability, and chromosomal translocations. This genetic instability primarily occurs in S-phase, where the replication machinery collides with unresolved R loops. These collisions lead to DSB formation, chromosomal translocations, and eventually tumors; due to the inherent oncogenic potential of free DNA ends. Interestingly, it has been demonstrated that R loops are required to be made and resolved in a timely manner at the break site for DNA repair to be completed effectively. How the cell deals with these R loops made in response to DSB formation is not known. One factor that bridges the DNA repair and transcription fields is the 5'-3' exoribonuclease XRN2. We have gathered data implicating XRN2 in the response and repair of DSBs. We found that loss of XRN2 leads to increased DSB formation, sensitivity to ionizing radiation, replication stress and R-loop formation. We also found that there is an accumulation of DSB repair factors at the poly-A region of genes that undergo R-loop dependent transcription termination. Using a plasmid based non-homologous end-joining (NHEJ) assay, we found that loss of XRN2 abrogates the cells ability to repair DNA via the NHEJ pathway. Yet, the mechanistic function of XRN2 in the NHEJ repair pathway is not known. Loss of XRN2 leads to an increase in R loops at the poly-A region of the □-actin gene. We can demonstrate that H2AX is phosphorylated at this region of the genome with XRN2, suggesting the loss of XRN2 is leading to DSB formation. Interestingly, loss of XRN2 also leads to a decrease Ku70 accumulation at the poly-A region of the □-actin gene. Also, we have found that over-expression of human RNaseH1, an enzyme that specifically degrades RNA moieties from RNA:DNA hybrids, restores Ku70 binding to the poly-A region of the □-actin gene after loss of XRN2. These data suggest that the mechanistic function of XRN2 in NHEJ to aid in resolving R loops formed at the DSB site, allowing Ku70 binding and NHEJ repair pathway progression.

Funding: P20GM103639

Dual roles of XRN2 in NHEJ and HR repair

Tuyen T. Dang, PhD and **Julio C. Morales, PhD.**
The University of Oklahoma Health Science Center
Stephenson Cancer Center
Department of Neurosurgery, Oklahoma City, OK, USA

Abstract: XRN2 is a 5'-3' exonuclease and have been shown to resolve RNA: DNA hybrids, R loops, during transcription termination. Increasing amount of evidence support a role of R loops in DNA damage response, DDR. We have found that XRN2 is required for resolving R loops generated in response to DNA damage, and this act is required for Ku70 binding at the break site. In addition, we have found that XERN2 is required for limiting DNA end resectioning during homologous recombination.

Impact: Findings from these studies would impact on radiation treatment of cancer patients by identifying who would best benefit from conventional radiation and possibly new drug targets to work in concert with radiation to increase efficacy.

Introduction: There is a growing body of evidence that demonstrates a connection between factors traditionally associated with transcription and the DSB repair pathways. This is due to the fact that evidence has been gathered demonstrating the association between transcription, double strand breaks, genetic instability, and most recently chromosomal translocations. During the process of normal transcription RNA:DNA hybrids (R loops) are formed and resolved, causing no harm to the cell. However, unresolved R loops have been associated with DSB formation, genetic instability, and chromosomal translocations. This genetic instability primarily occurs in S-phase where the replication machinery collides with unresolved R loops. These collisions lead to DSB formation, chromosomal translocations, and eventually tumors due to the inherent oncogenic potential of free DNA ends. Although, we are beginning to understand how DSBs are formed by unresolved R loops, little is known about how the cell repairs these types of lesions. It has been published that factors involved primarily in transcription are also associated with DNA repair pathways. We have gathered data implicating the transcription termination factor XRN2 in the response and repair of DSBs.

XRN2 is a 5'-3' RNA endonuclease that degrades RNA and resolves R loops. We found that loss of XRN2 leads to increased DSB formation, sensitivity to ionizing radiation, replication stress, R-loop formation and increased PARP1 activity. We also found that there is an accumulation of DSB repair factors at the 3' end of genes that undergo R-loop dependent transcription termination. Although increased DSBs are consistent with increased R-loop formation increased ionizing radiation and chemotherapy sensitivity is not. Interestingly, we have also observed that the increased chemo-sensitivity demonstrated in XRN2 deficient cells is directly related to whether R loops are present. We also find that XRN2 functions in both the non-homologous end-joining (NHEJ) and homologous recombination (HR) DSB repair pathways. XRN2 is required to resolve R loops created at the break site, allowing for Ku70 binding and completion of DSB repair through NHEJ. In HR repair, our data suggest that XRN2 required for limiting DNA end resectioning. This suggest that mediating R-loop formation may be consideration when treating cancer patients with radiation of any chemo-therapy that induces DSB.

XRN2 is required for Ku70 binding at DSB sites

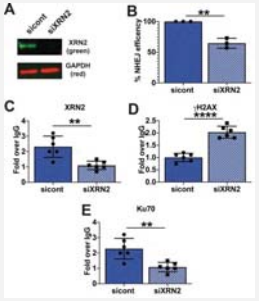

(A) Steady state levels of XRN2 in LN229 cells were determined western blot. (B) Relative NHEJ repair was determined in U2OS-EJ5 cells exposed to control and XRN2 siRNA. immunofluorescence. Chromatin Immunoprecipitation/qRT-PCR experiments were performed in LN229 cells transfected with control and XRN2 siRNA to examine the accumulation of (C) XRN2, (D) H2AX and (E) Ku70 at DSB site.

RNaseH1 expression restores Ku70 binding at DSB site

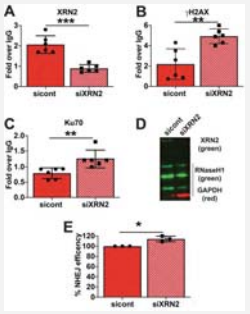

Chromatin Immunoprecipitation/qRT-PCR reactions were performed in LN229 RNaseH1 expressing cell lines exposed to control and XRN2 siRNA to examine the accumulation of (A) XRN2, (B) H2AX and (C) Ku70 at DSB site. (D) Steady state levels of XRN2 was measured by western blot in U2OS-EJ5 RNaseH1 expressing cells. (E) NHEJ efficiency was measured in U2OS-EJ5 RNaseH1 expressing cells exposed to control and XRN2 siRNA.

Loss of XRN2 abrogates HR repair

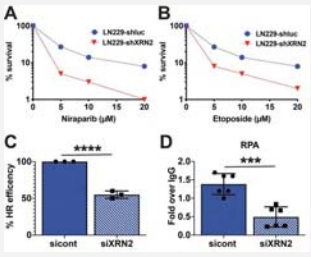

Cellular survival in XRN2 positive (LN229-luc) and LN229 negative (LN229-shXRN2) cells was determined by colony forming assay after exposure to (A) Niraparib and (B) Etoposide. (C) Homologous repair efficiency was measured in U2OS-DR cells exposed to control and XRN2 siRNA. (D) Chromatin immunoprecipitation/qRT-PCR was used to examine the accumulation of RPA32 at DSB site.

XRN2 limits DNA end resectioning

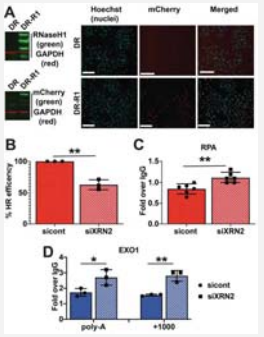

(A) Steady state levels of RNaseH1 was examined in U2OS-DR cells by western blot and immunofluorescence. (B) HR repair was examined in U2OS-DR RNaseH1 expressing cells exposed to control and XRN2 siRNA. Chromatin immunoprecipitation/qRT-PCR experiments were performed to examine the accumulation of (C) RPA32 and (D) EXO1 at DBS sites.

Model of XRN2 function in DSB repair

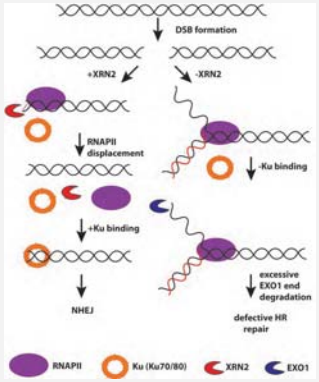

Future directions:

1) Perform ChIP experiments in parental and RNasesH1 over expressing cells to determine how R-loops affect recruitment of DNA damage repair proteins to sites of double strand breaks.

2) Determine if R loops ca dictate DNA repair pathway choice in response to double strand breaks

Funding:

NIGMS: P20GM103639
COMAA: C5112501

KRCC1: A NOVEL REGULATOR OF THE DNA DAMAGE RESPONSE

Fiifi Neizer-Ashun[1], Shailendra Dwivedi[2,3], Resham Bhattacharya[1,2,3]
[1]Department of Cell Biology, University of Oklahoma Health Sciences Center, [2]Department of Obstetrics and Gynecology, University of Oklahoma Health Sciences Center, [3]Peggy and Charles Stephenson Cancer Center, University of Oklahoma Health Sciences Center.

The primary objective of every life form is to deliver its genetic material to the next generation intact and unchanged. This is difficult to achieve because cells are daily bombarded with endogenous and exogenous damaging agents that introduce breaks in the DNA and threaten genomic integrity if left unrepaired. To counter this threat, the cell has developed mechanisms to detect DNA damage, initiate checkpoint and mediate repair; collectively known as the DNA damage response (DDR). The checkpoint kinases 1 and 2 (CHK1 and CHK2) play important roles in regulating DDR.

Recently, our lab demonstrated that the lysine-rich coiled coil 1 (KRCC1), a protein with unknown biology is overexpressed in ovarian cancer. Silencing KRCC1 induces DNA damage, decreases clonal growth, and potentiates apoptosis resulting in reduced tumor growth.

Current studies in our lab show that KRCC1 associates with CHK1, 14-3-3 and the catalytic subunit of the DNA-dependent protein kinase (DNA-PKc). Silencing KRCC1 increased phosphorylation of histone3 (H3S10) and H2AX (γH2AX), a mitotic and DNA damage marker respectively. Interestingly, CHK1 phosphorylation increased at S345 and decreased at S296. Concurrently, CHK1 activity was inhibited, evidenced by stabilization of CDC25A, a substrate of CHK1. Additionally, DNA repair via non-homologous end joining (NHEJ) and homologous recombination (HR) was significantly decreased, corroborating decrease in total levels of the catalytic subunit of the DNA-dependent protein kinase (DNA-PKc) and decreased RAD51 foci in KRCC1 silenced cells.

Altogether, these results suggest that KRCC1 may play a critical role in DDR via CHK1 regulation and DNA-PKc stabilization.

Funding: Work was supported by OCASCR, 2020 award to RB.

KRCC1: a novel regulator of the DNA damage response.

Fiifi Neizer-Ashun[1], Shailendra Dwivedi[2,3], Resham Bhattacharya[1,2,3]

[1]Department of Cell Biology, [2]Department of Obstetrics and Gynecology, [3]Peggy and Charles Stephenson Cancer Center, University of Oklahoma Health Sciences Center.

ABSTRACT

The primary objective of every life form is to deliver its genetic material to the next generation intact and unchanged. This is difficult to achieve because cells are daily bombarded with endogenous and exogenous damaging agents that introduce breaks in the DNA and threaten genomic integrity if left unrepaired. To counter this threat, the cell has developed mechanisms to detect DNA damage, initiate checkpoint and mediate repair; collectively known as the DNA damage response (DDR). The checkpoint kinases 1 and 2 (CHK1 and CHK2) play important roles in regulating DDR. Recently, our lab demonstrated that the lysine-rich coiled coil 1 (KRCC1), a protein with unknown biology is overexpressed in ovarian cancer. Silencing KRCC1 induces DNA damage, decreases clonal growth, and potentiates apoptosis resulting in reduced tumor growth. Current studies in our lab show that KRCC1 associates with CHK1, 14-3-3 and the catalytic subunit of the DNA-dependent protein kinase (DNA-PKc). Silencing KRCC1 increased phosphorylation of histone3 (H3S10) and H2AX (γH2AX), a mitotic and DNA damage marker respectively. Interestingly, CHK1 phosphorylation increased at S345 and decreased at S296. Concurrently, CHK1 activity was inhibited, evidenced by stabilization of CDC25A, a substrate of CHK1. Additionally, DNA repair via non-homologous end joining (NHEJ) and homologous recombination (HR) was significantly decreased, corroborating decrease in total levels of the catalytic subunit of the DNA-dependent protein kinase (DNA-PKc) and decreased RAD51 foci in KRCC1 silenced cells. Altogether, these results suggest that KRCC1 may play a critical role in DDR via CHK1 regulation and DNA-PKc stabilization.

RESULTS

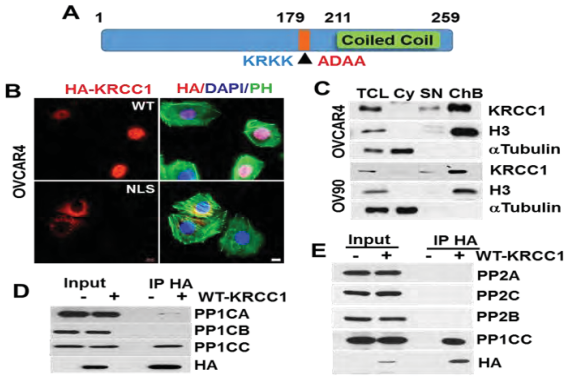

Figure 1- Localization and interactions of KRCC1.
A. Schematic representation of KRCC1 with nuclear localization signal sequence (NLS, blue mutated to red). **B.** OVCAR4 cells were transfected with HA-tagged WT or NLS mutant KRCC1 and KRCC1 localization determined by immunofluorescence with phalloidin (PH) and DAPI. (Bar=20 μm) **C.** Subcellular fractionation was performed in OVCAR4 and OV90 cells to detect endogenous KRCC1, total cell lysate (TCL), cytoplasm (Cy), soluble nuclear (SN), chromatin bound fraction (ChB). Fraction purity determined by respective markers. **D, E.** OV90 cells were transfected with HA-tagged WT-KRCC1 for 30h. Association of KRCC1 with various catalytic subunits of protein phosphoatase 1 and 2 (PP1 and PP2) were determined by immunoprecipitation.

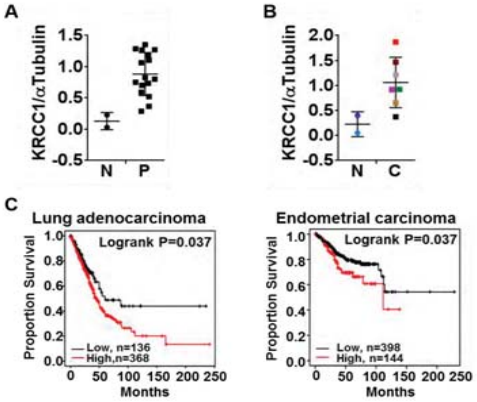

Figure 2- Expression of KRCC1 correlates with poor prognosis in cancer.
A. Relative quantitation of KRCC1 expression in normal fallopian tissue (N) and ovarian tumors (P) **B.** Relative quantitation of KRCC1 expression in respective normal (N) and ovarian cancer (C) cell lines. **C.** Kaplan-Meier curves evaluated by log-rank test to determine association between expression of KRCC1 with overall survival in lung adenocarcinoma and endometrial carcinoma.

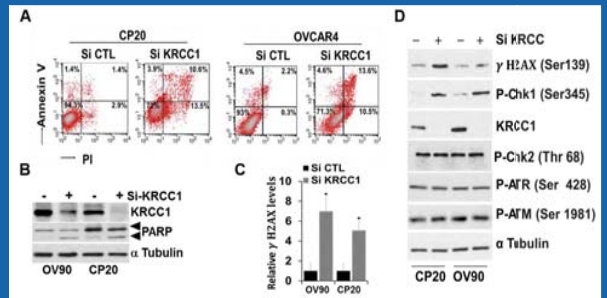

Figure 3- Silencing KRCC1 induces apoptosis.
A. CP20 and OVCAR4 cells were transfected with either scrambled (siCTL) or KRCC1 siRNA (siKRCC1) for 72h, stained with AnnexinV/PI and analyzed by flow cytometry. **B.** OV90 and CP20 cells were transfected with either scrambled (siCTL) or KRCC1 siRNA (siKRCC1) for 72h and immunoblotted for cleaved PARP. **C.** Relative quantitation of phosphorylated histone H2AX (γH2AX) in OV90 and CP20 cells after KRCC1 silencing evaluated by immunofluorescence. **D.** CP20 and OV90 cells were transfected with either scrambled (siCTL) or KRCC1 siRNA (siKRCC1) for 72h. Expression of checkpoint and DNA damage response markers was determined by immunoblotting.

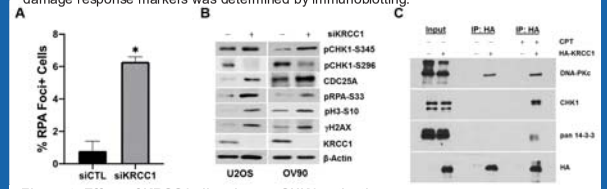

Figure 4- Effect of KRCC1 silencing on CHK1 activation.
A. OV90 cells were transfected with either scrambled (siCTL) or KRCC1 siRNA (siKRCC1) for 72h and evaluated for replication protein A 32 (RPA32) foci positivity by immunofluorescence, an indication of replication stress. **B.** U2OS and OV90 cells were transfected with either scrambled (siCTL) or KRCC1 siRNA (siKRCC1) for 72h. Markers of CHK1 activation and expression of CHK1-dependent DDR markers were determined by immunoblotting. **C.** OV90 cells were transected with empty vector (EV) or HA tagged KRCC1 (HA-KRCC1) for 30h and treated with camptothecin (CPT, 3μM for 2h) to induce damage. Association of KRCC1 with critical regulators of DDR were determined by immunoprecipitation in the presence or absence of damage (CPT, 3μM for 2h).

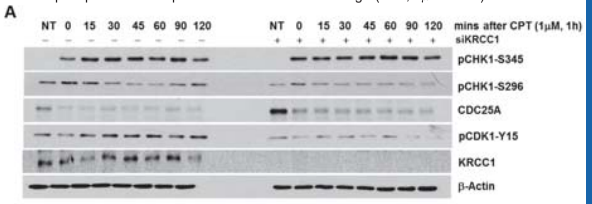

Figure 5- Effect of KRCC1 silencing on CHK1-mediated DDR.
A. OV90 cells were transfected with either scrambled (siCTL) or KRCC1 siRNA (siKRCC1) for 70h and treated with camptothecin (CPT,1μM for 1h). One plate was left without treatment (NT). Cells were collected immediately following treatment (0h) or washed and allowed to recover in fresh warm media for 2h and collected at indicated time points and immunoblotted for respective CHK1-mediated DDR markers.

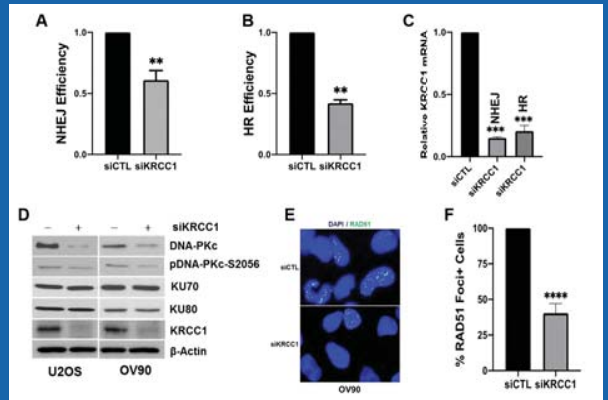

Figure 6- Effect of KRCC1 silencing on DNA repair.
A, B. U2OS cells with integrated GFP repair cassettes for non-homologous end joining (NHEJ) and homologous recombination (HR) were transfected with either scrambled (siCTL) or KRCC1 siRNA (siKRCC1) for 24h followed by transfection with the rare cutting I-SceI endonuclease for 48h. GFP expression, indicative of efficient repair by either NHEJ or HR was evaluated by live cell imaging. **C.** Relative KRCC1 mRNA expression in U2OS-NHEJ and U2OS-HR cells after KRCC1 silencing. **D.** To elucidate the mechanism for KRCC1-mediated NHEJ, U2OS and OV90 cells were transfected with either scrambled (siCTL) or KRCC1 siRNA (siKRCC1) for 72h. Critical NHEJ markers were evaluated by immunoblotting. **E, F.** To elucidate the mechanism for KRCC1-mediated HR, OV90 cells were transfected with either scrambled (siCTL) or KRCC1 siRNA (siKRCC1) for 70h and treated with camptothecin (CPT,1μM for 1h). Cells were washed and allowed to recover in fresh warm media for 2h and evaluated for RAD51 foci positivity by immunofluorescence (2h recovery time point is where RAD51 foci is most prominent in control cells).

PROPOSED MODEL & CONCLUSION

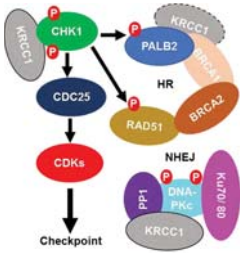

Conclusion
Here we investigated the novel role of KRCC1 as a regulator in CHK1-mediated DNA damage response. We report that KRCC1 is overexpressed in cancer and overexpression correlates with poor overall survival. KRCC1 associates with PP1CC, CHK1, DNA-PKc, and 14-3-3. Silencing KRCC1 induces DNA damage, impairs CHK1 activation resulting in a defective checkpoint. Additionally, silencing KRCC1 decreases total levels of DNA-Pkc and RAD51 foci formation leading to decreased DNA repair via NHEJ and HR respectively, and potentiates apoptosis.
The propensity of KRCC1 silencing to impinge on two obligate mechanisms of cancer cell survival presents a unique avenue for future therapeutic consideration.

ACKNOWLEDGEMENT

This study was supported by OCASCR, 2020 award to Dr. Resham Bhattacharya.

SINGLE CELL MASS SPECTROMETRY METABOLOMIC STUDIES OF CELL HETEROGENEITY IN PRIMARY AND METASTATIC MELANOMA

Tra D. Nguyen, Zhibo Yang*
Department of Chemistry and Biochemistry, University of Oklahoma, Norman, OK 73019

Introduction: Melanoma has four developing stages where the cancer begins in the outermost layer of skin and continue spreading to lymphatic system. It eventually metastasizes to other body organs. Four cell line models (IGR 39 and IGR 37, WM 115 and WM 266-4) are chosen to study their intracellular metabolomic profiles using Single-probe single cell mass spectrometry. The differences in metabolomic profiles in primary and metastatic melanoma at single cell level are studied for the first time.

Methods: IGR 39 and WM 115 are classified as primary melanoma from primary tumor in the patients. IGR 37 and WM 266-4 (so called metastatic melanoma cells) are found in the metastatic lymph node after the primary tumor spread to the lymphatic system. The difference in their intracellular metabolites can be unveiled by studying cell heterogeneity in melanoma cells using single-probe single cell mass spectrometry (SCMS). Single probe is a miniature device that is coupled to a mass spectrometer. This technique determines the difference in the metabolomic profiles between cell-to-cell as well as identify novel metabolites that can differentiate between primary and metastatic melanoma.

Results: Four cell models (IGR 39 and IGR 37, WM 115 and WM 266-4) are analyzed with an amount of 50 cells for each cell model. Approximately 200 cells in total would be detected and generated mass spectrometry data for further analysis. The data pretreatment is composed of background removal, peaks alignment and statistical analysis. Results will be visualized using Principal Component Analysis (PCA) and Partial Least Squares Discriminant analysis (PLSDA). Random Forest, P-value and T-test will be performed as statistical tools. Significant metabolites will be identified and provide more insights to the development from primary to metastatic melanoma.

Conclusions: The cellular heterogeneity between IGR 39, 37 and WM 115, 266-4 (primary and metastatic melanoma cells) can be revealed under single-probe single cell analysis and identify the similarities and differences in their metabolomic profiles.

Future Directions: Primary and metastatic cells will be treated with Vemurafenib which is an FDA-approved drug for melanoma. The influence of drug can be investigated between control cells (with no drug treatment) and treated cells (with Vemurafenib treatment) to have a better understanding of the development from primary to metastatic melanoma.

Acknowledgement: Funded by National Institutes of Health (R01GM116116).

The UNIVERSITY of OKLAHOMA

Department of Chemistry and Biochemistry

Single Cell Mass Spectrometry Metabolomic Studies of Cell Heterogeneity in Primary and Metastatic Melanoma

Tra D. Nguyen, Yunpeng Lan, Zhibo Yang*

Abstract

Four melanoma cell line models (IGR 39 and IGR 37, WM 115 and WM 266-4) are chosen to study their intracellular metabolomic profiles using Single-probe single cell mass spectrometry. The differences in metabolomic profiles in primary and metastatic melanoma at single cell level are studied for the first time. The difference in their intracellular metabolites can be unveiled by studying cell heterogeneity in melanoma cells using single-probe single cell mass spectrometry (SCMS). Four cell models (IGR 39 and IGR 37, WM 115 and WM 266-4) are analyzed with approximately 40-50 cells each. Principal Component Analysis (PCA) and Volcano plots are used to visualize the metabolomic profiles of cells. Random Forest, P-value and T-test will be performed as statistical tools. Significant metabolites will be identified and provide more insights to the development from primary to metastatic melanoma. The cellular heterogeneity between IGR 39, 37 and WM 115, 266-4 (primary and metastatic melanoma cells) have successfully demonstrated a clear distinction using single-probe single cell analysis and highlight the differences in their metabolomic profiles.

Introduction

Melanoma is one of the most serious types of cancer when the mutation occurs in the pigment producing cells in the skin which are also known as melanocytes. The skin cancer started spreading when melanocytes are divided uncontrollably. Melanoma has usually developed in the skin with a few areas which are at high risk such as chest, back, leg, and face. Melanoma has been confirmed to have four developing stages where the cancer begins in the outermost layer of skin and continue spreading to lymphatic system. It eventually metastasizes to other body organs which include lungs, liver and brain. Hence, four cell line models (IGR 39 and IGR 37, WM 115 and WM 266-4) are chosen to study the difference in their intracellular metabolomic profiles using Single-probe single cell mass spectrometry technique to have a comprehensive understanding in the development of melanoma from early stage to later stage.

IGR 39 and WM 115 are primary melanoma since they were derived from primary tumor or lesion in the patients. IGR 37 and WM 266-4 (metastatic melanoma) are found in the metastatic lymph node after the primary tumor spread to the lymphatic system. Cell heterogeneity has derived from the study of cell-to-cell variation because the population of "seemingly identical" cells are actually heterogenous. The phenotypic differences among subpopulation of cells would provide more insights to the understanding of cell-to-cell variation as well as melanoma progression from primary to metastatic form and contribute to a more effective treatment of skin cancer therapy.

Single probe single cell mass spectrometry (SCMS) has been applied to reveal the difference in metabolomic profiles between primary and metastatic cells. Single probe is a miniature device that was designed to be coupled with the mass spectrometer. Besides, data pretreatment is composed of background removal, peaks alignment and statistical analysis. The four cell models' single-probe SCMS data will be visualized using Principal Component Analysis (PCA). Other statistical tools which provide more comprehensive understanding of this study is Random Forest which reveal the class errors of each cell model during data acquisition. P-value and T-test will be performed among IGR 39 and 37, WM 115 and 266-4 to study the similarities and differences metabolites that were detected in their cells.

Methods

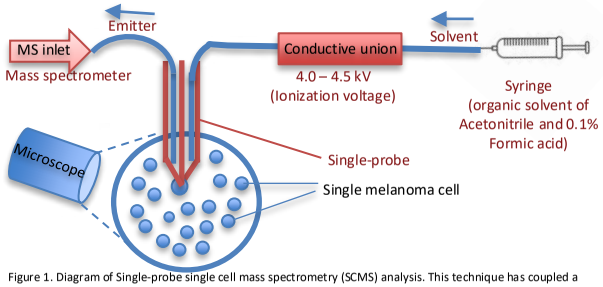

Figure 1. Diagram of Single-probe single cell mass spectrometry (SCMS) analysis. This technique has coupled a single probe to the mass spectrometer and generated mass spectra. They will detect intracellular metabolites and provide more insights to this metabolomics study.

Results

Table 1. Number of detected single cells using Single-probe single cells mass spectrometry technique

	WM 115 (primary cells)	WM 266-4 (metastatic cells)	IGR 39 (primary cells)	IGR 37 (metastatic cells)
Number of single cells	44	43	41	39

Statistical analysis

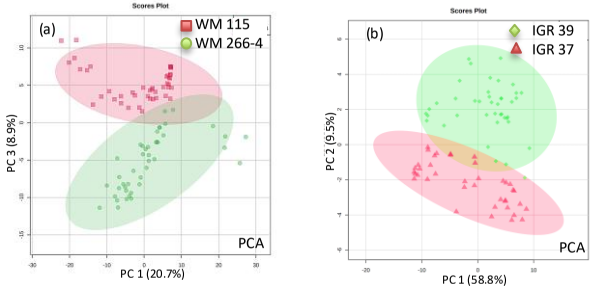

Figure 2: Principal Component Analysis (PCA) plots between different group of cells. The primary cells (IGR 39 and WM 115) shares little to almost no overlap in comparison to metastatic cells (IGR 37 and WM 266-4) respectively. P-values for the PCA results are 0.01.

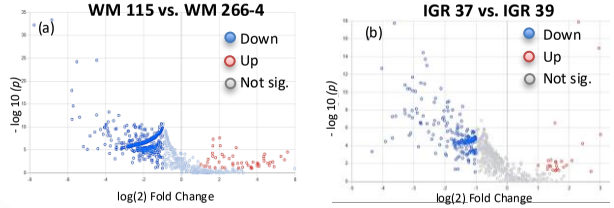

Figure 3: Volcano plots between WM 115 vs. 266-4 (fig. 3a) and IGR 37 vs. IGR 39 (fig. 3b). The fold change (FC) threshold is 2.0 and p-value threshold is 0.1.

m/z	p-values
742.566	4.51E-34
766.568	5.69E-33
683.485	2.79E-25
768.583	5.86E-25
720.587	1.09E-18
709.512	2.51E-15
226.951	5.39E-14
746.602	2.34E-13
794.599	2.90E-13
815.744	7.23E-13

Figure 4a. Top 10 most significant m/z list (WM 115 vs. 266-4) and their p-values. Blue text = sig. down in fig. 3a.

m/z	p-values
493.254	1.27E-18
778.532	1.73E-18
772.521	9.38E-17
407.217	1.12E-15
756.548	3.50E-15
734.567	1.93E-14
784.581	9.60E-14
820.52	2.01E-13
770.505	1.99E-12
697.475	8.68E-12

Figure 4b. Top 10 most significant m/z list (IGR 37 vs. IGR 39) and their p-values. Red text = sig. up in fig. 3b.

Results

Table 2. Random Forest tables highlighted that the class errors for each type of cells are extremely low (<5%). Almost all cells have been distinctly detected and identified so the number of misclassified cells is only within 1-2 cells.

	WM 115	WM 266-4	Class error	% error
WM 115	44	0	0.0	0%
WM 266-4	1	42	0.0233	2.33%

	IGR 39	IGR 37	Class error	% error
IGR 39	39	2	0.0488	4.88%
IGR 37	0	39	0.0	0%

Conclusions

- Cell heterogeneity in both primary and metastatic melanoma cells have successfully investigated using Single-probe single cell mass spectrometry.
- Primary cells (IGR 39 and WM 115) and Metastatic cells (IGR 37 and WM 266-4) have demonstrated a clear distinction in their intracellular metabolomic profiles.

=> The metabolism of primary cells has been altered when melanoma spreads or metastasizes to other organs in the body. The metabolism of metastatic cells must adapt to form new tumor and survive throughout the body.

- Statistical analysis (such as PCA, Volcano plots, Random Forest classification, p-value, etc.) are great tools to illustrate differences in their intracellular metabolomic profiles of both primary and metastatic melanoma cells.
- Having a more comprehensive understanding of the metabolites that are detected from primary and metastatic cells definitely provide more insights into the spread of melanoma in general and contribute the development of melanoma therapy.

Future directions

- MS/MS Mass spectrometry for metabolites identification.
- Conducting the cell viability of our four cells model using Vemurafenib and determining the IC_{50} of this drug compound are my next step to study their drug resistance.
- The influence of drug can be investigated between control cells (with no drug treatment) and treated cells (with Vemurafenib treatment) to have a better understanding of the development from primary to metastatic melanoma.

Acknowledgement

- OU MS Core Facility
- Dr. Yang and all group members in Yang lab: Zhu Zou, Xingxiu Chen, Zongkai Peng, Dan Chen
- Funding: Funded by National Institutes of Health (R01GM116116).

MECHANISMS OF DNA REPLICATION REGULATION DURING EARLY EMBRYONIC DEVELOPMENT

Tyler Noble[1,2], Emily Clowdus[1,2], Joseph Siefert[1,2], Duane Goins[2], Christopher Sansam[1,2]
Tyler-Noble@ouhsc.edu
[1] University of Oklahoma Health Sciences Center, Department of Cell Biology, Oklahoma City, OK, [2] Oklahoma Medical Research Foundation, Cell Cycle and Cancer Biology Research Program, Oklahoma City, OK

Deregulated DNA replication causes human developmental disorders and cancer, but we know little about how DNA replication is coordinated with changes in transcription and chromatin structure. The initiation of replication forks follows a spatiotemporal pattern called the replication timing program. We have developed the zebrafish into a model system to study the mechanisms by which the replication timing program changes during the extensive changes in the cell cycle, transcription, chromatin organization, and nuclear structure that occur during development.

Our previous studies identified changes in DNA replication timing patterns occurring from the onset of zygotic transcription through gastrulation in zebrafish embryos. We are currently probing the mechanisms by which those changes occur. Rif1 has previously been shown to regulate DNA replication timing by suppressing activation of late-replicating origins in cultured mammalian cells and yeast. Recently, the Rif1 gene in drosophila was shown to be integral for developmental remodeling of the drosophila cell cycle through its replication timing function. In mammals, Rif1 has also been linked to heterochromatin organization and gene silencing. The broader role of Rif1 in establishing the replication timing program and chromatin structure during early vertebrate development remains unknown. We have generated Rif1 mutant zebrafish, and have performed RNA sequencing and whole-genome replication timing analyses on multiple developmental stages. Surprisingly, Rif1 loss predominantly impacts DNA replication after gastrulation, while it has a stronger effect on transcription during zygotic genome activation. Our results indicate that Rif1 has distinct roles in DNA replication and transcription control that manifest at different stages of development.

This work was supported by National Institutes of Health National Institute of General Medical Sciences grant 1R01GM121703 and by the Oklahoma Center for Adult Stem Cell Research.

Mechanisms of DNA Replication Regulation During Early Embryonic Development

Emily Clowdus[1,2], Tyler Noble[1,2], Joseph Siefert[1,2], Duane Goins[2], Christopher Sansam[1,2]

[1]University of Oklahoma Health Sciences Center, Department of Cell Biology, Oklahoma City, OK
[2]Oklahoma Medical Research Foundation, Cell Cycle and Cancer Biology Research Program, Oklahoma City, OK

Introduction: Eukaryotic DNA replication origins follow a specific pattern of initiation termed the replication-timing program (RT). Clusters of origins within large genomic domains activate together and each domain follows a temporal order of initiation throughout S phase. Recent analyses of replication-timing patterns in early- and late-replicating segments of the genome reveal that replication timing correlates with chromatin organization and gene activity. The extensive nuclear changes that occur with cellular differentiation have been well studied, but it remains undetermined if there is a causal relationship between transcriptional activity and replication timing, or if they are maintained independently by epigenetic modifications. Rif1 has previously been shown to mediate DNA replication timing by suppressing activation of late-replicating origins; in addition, Rif1 has been linked to heterochromatin organization and gene silencing. The role of Rif1 in establishing the replication timing program and chromatin structure during early development remains unknown.

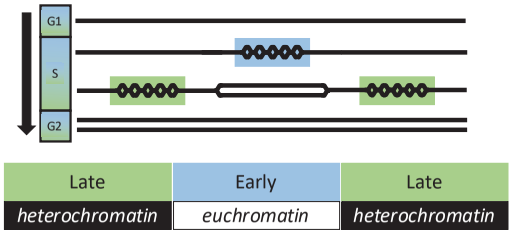

Leading Questions for Replication Timing

1. When is it established?
2. In what ways does it change during development?
3. What are the mechanisms of its initiation, maintenance, and change?
4. Does loss of Rif1 impact establishment and changes of RT in an embryonic model? If so, is this related to transcriptional changes?

Hypothesis: Rif1 controls gene expression through its role in DNA replication timing, ***OR*** Rif1 affects gene expression and replication timing independent of one another.

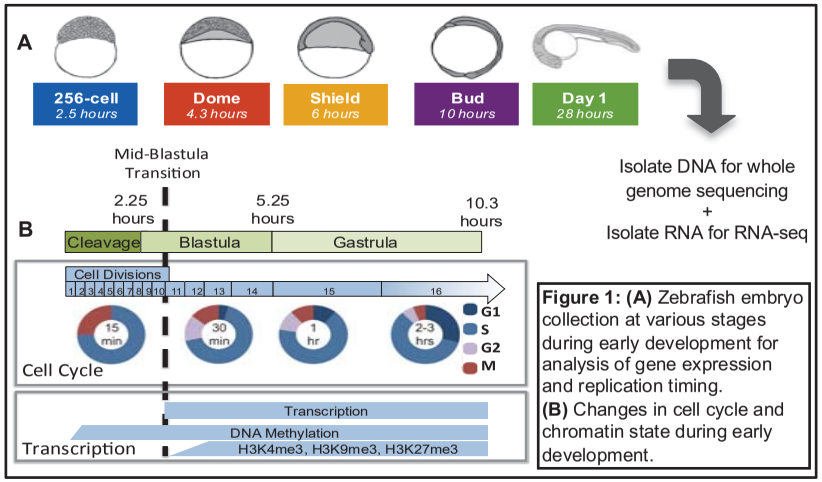

Figure 1: (A) Zebrafish embryo collection at various stages during early development for analysis of gene expression and replication timing. **(B)** Changes in cell cycle and chromatin state during early development.

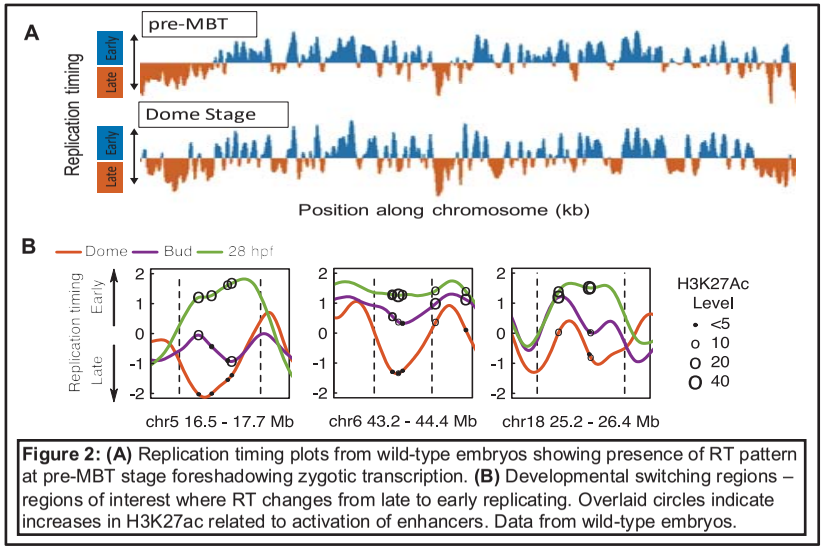

Figure 2: (A) Replication timing plots from wild-type embryos showing presence of RT pattern at pre-MBT stage foreshadowing zygotic transcription. **(B)** Developmental switching regions – regions of interest where RT changes from late to early replicating. Overlaid circles indicate increases in H3K27ac related to activation of enhancers. Data from wild-type embryos.

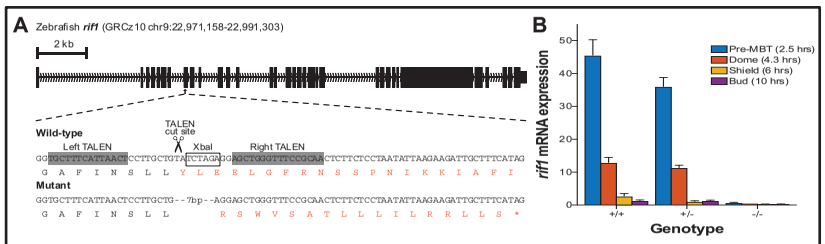

Figure 3: (A) Generating *rif1* mutant zebrafish using TALENs. **(B)** *rif1* mRNA expression established by qRT-PCR.

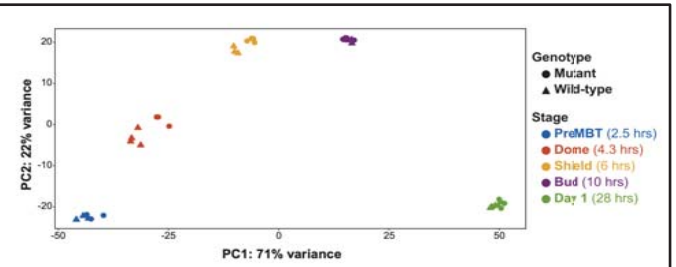

Figure 4: Comparison of RNA-seq data. PCA plot of RNA-seq samples for pools of wild-type and *rif1* mutant conditions at time points 2.5hpf-28hpf; the most difference is seen at the early stages dome and shield.

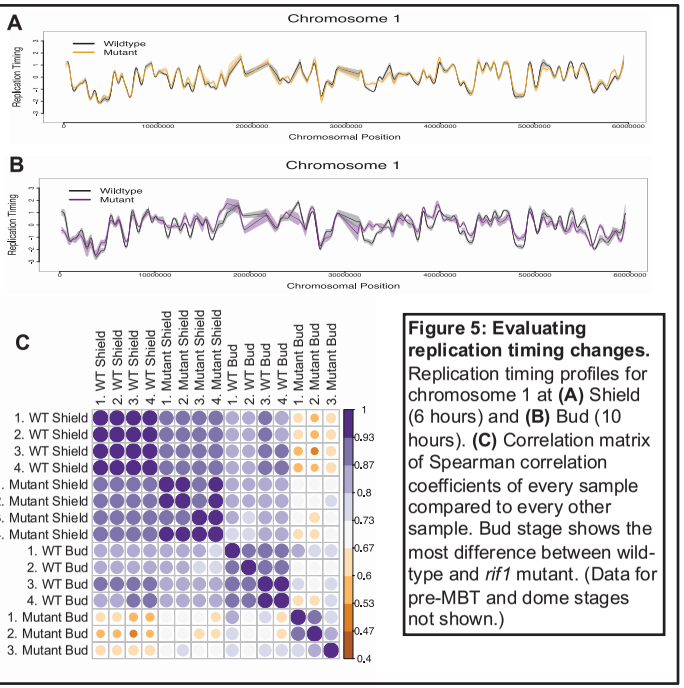

Figure 5: Evaluating replication timing changes. Replication timing profiles for chromosome 1 at **(A)** Shield (6 hours) and **(B)** Bud (10 hours). **(C)** Correlation matrix of Spearman correlation coefficients of every sample compared to every other sample. Bud stage shows the most difference between wild-type and *rif1* mutant. (Data for pre-MBT and dome stages not shown.)

Key Observations:

- Rif1 affects gene expression during early development, before the onset of gastrulation.
- Rif1 has an effect on replication timing at the end of gastrulation.

Conclusion:

- Rif1 plays a role in DNA replication timing and gene expression independent of one another. The effect on gene expression could be a result of the number of origins that fire rather than replication timing.

Funding provided by OCASCR and NIH NIGMS grant 1R01GM121703

ESTABLISHMENT OF A *DROSOPHILA MELANOGASTER* MODEL OF HIGH-RISK HUMAN PAPILLOMAVIRUS 16-INDUCED CELLULAR ABNORMALITIES

Mojgan Padash-Barmchi, McKenzi E. Ormsbee, Prashant J. Patel, Lydia Hashemi, Jacquelyn A. Nielson
mojgan.padash@ou.edu
Department of Biology, University of Oklahoma, Norman, OK

High-risk human papillomaviruses (HPV) lead to many forms of cancer including cervical, vulvar, vaginal, anal, penile and oropharyngeal cancers, most of which do not yet have a known cure. HPV16 is present in a majority of these cases and induces cancer through the expression of its oncogenes, E5, E6 and E7. With the aid of the human ubiquitin protein-ligase E6AP/UBE3A, these oncoproteins target several key cellular proteins for degradation, including PDZ domain proteins that are necessary for tumor suppression and the maintenance of cell polarity and epithelial integrity. Although previous *in vivo* models have been beneficial for understanding the cellular and molecular mechanism of the disease, they face many limitations when performing large-scale genetic and drug screening. Given the conservation of many genes and signaling pathways between flies and mammals, establishment of a fruit fly model of HPV16 can overcome these challenges and provide a better understanding of the disease mechanism. We have previously established a *Drosophila* model of HPV18-induced cellular abnormalities and demonstrated that the model serves as an excellent complementary model to mouse models of HPV18.

Here in this study, Gal4/UAS system was used to express HPV16 oncogenes E5, E6, and E7 with human UBE3A exclusively in the eye epithelial cells of *Drosophila melanogaster*. This expression resulted in significant cellular abnormalities that prevented development beyond the pupal stage. Further analysis of the eye epithelia using immunolabeling techniques revealed excessive apoptosis during the third instar larval stage followed by over proliferation during the pupal stage. These results suggest that not all E5, E6, E7 + hUBE3A-expressing cells undergo apoptosis in response to HPV16 oncogenes and that the excessive overgrowth is triggered during early pupal stage, which could in part be due to persistent expression of E5, E6, E7 and hUBE3A. Additionally, several proteins targeted for degradation by HPV 16 oncoproteins in human cells were also degraded in the *Drosophila* epithelial cells and that the cell polarity and junction were compromised. These results suggest that the *Drosophila* HPV16 E5, E6, E7+hUBE3A model could serve as an excellent *in vivo* model for understanding the mechanism and development of novel therapeutics for HPV16-induced cancers.

ESTABLISHMENT OF A *DROSOPHILA MELANOGASTER* MODEL OF HIGH-RISK HUMAN PAPILLOMAVIRUS 16-INDUCED CELLULAR ABNORMALITIES

McKenzi E. Ormsbee, Prashant J. Patel, Lydia Hashemi, Jacquelyn A. Nielson, Mojgan Padash-Barmchi
Department of Biology, University of Oklahoma, Norman, OK

INTRODUCTION

- Human Papillomavirus (HPV) is the leading cause of cervical cancer.
- No effective therapeutic is available for HPV cancers primarily due to lack of sufficient knowledge of disease mechanism.
- Mouse models are beneficial for understanding the disease mechanism but face limitations when performing large-scale genetic and drug screening.
- *Drosophila* has proven to be an excellent model system to model human diseases including cancers due to conservation of many genes and signaling pathways.
- The aim of this study is to establish a *Drosophila* model of HPV16-induced cancer to overcome the limitations of mouse models of the disease.

RESEARCH QUESTION

Can *Drosophila melanogaster* be used to model HPV16-induced cancer?

METHODS

Gal4-UAS binary expression system

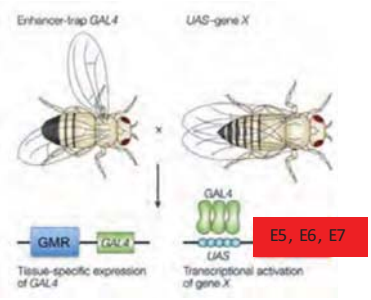

Adapted from Nature review/Genetics

RESULTS

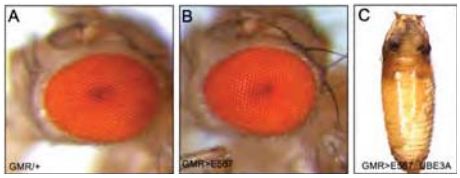

Fig 1. Co-expression of HPV16 E5, E6, E7 and hUBE3A in *Drosophila* eyes results in lethality at pupal stage.

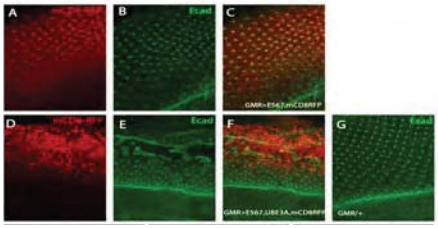

Fig 2. Co-expression of HPV16 E5, E6, E7 and hUBE3A in *Drosophila* eye epithelia results in loss of epithelial integrity in larval stage (D-F) compared to controls (A-C, G).

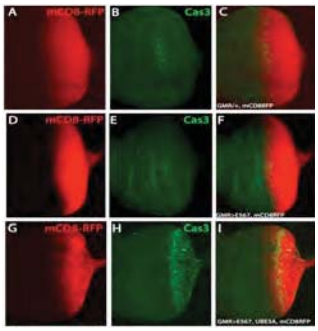

Fig 3. Loss of epithelial integrity caused by expression of HPV16 E5, E6, E7+hUBE3A in larval stage is due to apoptosis (G-I).

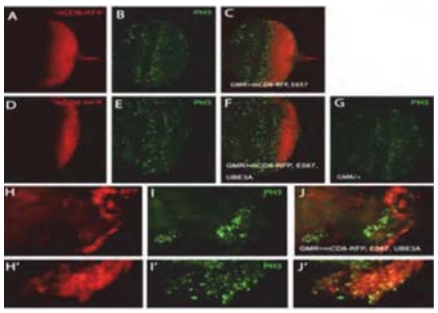

Fig 4. Co-expression of E5, E6, E7 and hUBE3A leads to overproliferation of eye epithelia in pupal stage (H-J'). No Overproliferation is seen in larval stage (D-F).

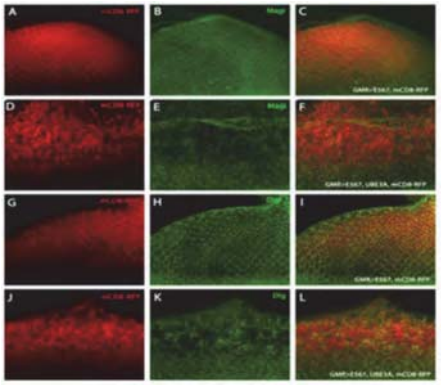

Fig 5. HPV16 E5, E6, and E7 with the assistance of hUBE3A degrade *Drosophila* homologs of human PDZ domain proteins Magi (D-F) and Dlg (J-L).

CONCLUSIONS

- HPV16 oncogenes E5, E6, E7 cause cellular abnormalities in *Drosophila* epithelia and their action requires the assistance of human UBE3A.
- PDZ domain proteins targeted for degradation by HPV16 oncogenes in human cells are similarly degraded in *Drosophila* epithelial cells.

ONGOING STUDIES

- Examining the level and localization of p53
- Blocking apoptosis in HPV16E5, E6, E7-expressing cells to examine their morphology and behavior
- Examining the functional interaction between oncogenic Ras and E5/E6/E7

TARGETING CELL SENESCENCE REDUCES TUMOR INCIDENCE IN A MOUSE MODEL OF HEPATOCELLULAR CARCINOMA

Deepa Sathyaseelan[1, 2,4,] Sabira Mohammed Jazir[1], Evan Nicklas[2], Jacob Brown[5], Maria Kamal[3], Wenyi Luo[3], Arlan Richardson[1,2,4,6], Holly Van Remmen[5,6]

[1]Stephenson Cancer Center, [2]Department of Biochemistry & Molecular Biology, [3]Department of Pathology, 4Center for Geroscience and Healthy Brain Aging, The University of Oklahoma Health Sciences Center, [5]Aging and Metabolism Research Program, Oklahoma Medical Research Foundation, and [6]Oklahoma City VA medical Center.

Hepatocellular carcinoma (HCC), the primary form of liver cancer, is the second cancer-related cause of death worldwide, and the ninth leading cause of cancer-related deaths in the US. The major risk factors for HCC are chronic hepatitis viral infection and excess alcohol consumption. Recently, non-alcoholic fatty liver disease (NAFLD) and non-alcoholic steatohepatitis (NASH) that are associated with obesity and metabolic syndrome are emerging as new risk factors for HCC development. HCC is predicted to be the third leading cause of cancer-related deaths in the US by 2030 due to the obesity epidemic.

Chronic inflammation is a key driver of HCC initiation and progression, and we found that inflammation and pathways associated with inflammation (cell senescence and necroptosis) are elevated in the livers of mice deficient in the anti-oxidant enzyme Cu/Zn-superoxide dismutase (*Sod1*$^{-/-}$ or Sod1KO mice). Sod1KO mice are a novel mouse model of HCC that develops spontaneous NAFLD/NASH and progresses to fibrosis and HCC with age, stages similar to obesity associated HCC in humans. Sod1KO have ~30% reduction in lifespan and more than 70% of Sod1KO mice develop spontaneous HCC with age. Because senescent cells are known to secrete proinflammatory and pro-tumorigenic factors (senescence-associated secretory phenotype, SASP) that support tumor growth, here we tested whether targeting cell senescence have an effect on hepatic inflammation in Sod1KO mice. Sod1KO mice were treated with the senolytics, dasatinib and quercetin (D+Q), which have been shown to target senescent cells. Four groups of 6-month-old female mice were used for the study and were treated with vehicle or D+Q for 7 months: (1) wild type mice (littermates) treated with vehicle, (2) wild type mice treated with D+Q, (3) Sod1KO mice treated with vehicle, (4) Sod1KO mice treated with D+Q. Senolytics treatment reduced expression of cell senescence marker (p16), immune cells, and proinflammatory cytokines in the livers of Sod1KO mice compared to vehicle treated Sod1KO mice. Importantly, senolytic treatment reduced tumor incidence in Sod1KO mice by nearly 87%. In addition, marker of necroptosis (phosphorylated MLKL) was reduced in the livers of Sod1KO mice by senolytic treatment. Thus, our findings show that senolytics, D+Q, dramatically reduced HCC in the Sod1KO mice and this appears to be due to the reduction in cell senescence and necroptosis, which lead to chronic inflammation.

TARGETING CELL SENESCENCE REDUCES TUMOR INCIDENCE IN A MOUSE MODEL OF HEPATOCELLULAR CARCINOMA

Sabira Mohammed Jazir[1], Evan Nicklas[2], Jacob Brown[5], Maria Kamal[3], Wenyi Luo[3], Arlan Richardson[1,2,4,6], Holly Van Remmen[5,6] and Deepa Sathyaseelan[1,2,4]

[1]Stephenson Cancer Center, [2]Department of Biochemistry & Molecular Biology, [3]Department of Pathology,

[4]Center for Geroscience and Healthy Brain Aging, The University of Oklahoma Health Sciences Center,

[5]Aging and Metabolism Research Program, Oklahoma Medical Research Foundation, and [6]Oklahoma City VA medical Center

Abstract

Chronic inflammation is a key driver of hepatocellular carcinoma (HCC) initiation and progression. Inflammation and pathways mediating inflammation (cell senescence and necroptosis) are elevated in the livers of mice deficient in the anti-oxidant enzyme Cu/Zn-superoxide dismutase (*Sod1*KO mice). *Sod1*KO mice are a novel mouse model of HCC that develops spontaneous NAFLD/NASH and progresses to fibrosis and HCC with age. *Sod1*KO have ~30% reduction in lifespan and more than 70% of *Sod1*KO mice develop spontaneous HCC with age. Sod1KO mice were treated with the senolytics, dasatinib and quercetin (D+Q), which have been shown to target senescent cells. Senolytics treatment reduced expression of cell senescence marker (p16), immune cells, and proinflammatory cytokines in the livers of *Sod1*KO mice compared to vehicle treated *Sod1*KO mice. Importantly, senolytic treatment reduced tumor incidence in *Sod1*KO mice by nearly 87%. In addition, marker of necroptosis (phosphorylated MLKL) was reduced in the livers of *Sod1*KO mice by senolytic treatment. Thus, our findings show that senolytics, D+Q, dramatically reduces HCC in the *Sod1*KO mice and this appears to be due to the reduction in cell senescence and necroptosis, which lead to chronic inflammation.

Background of the study

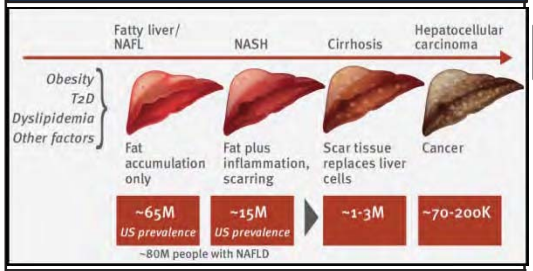

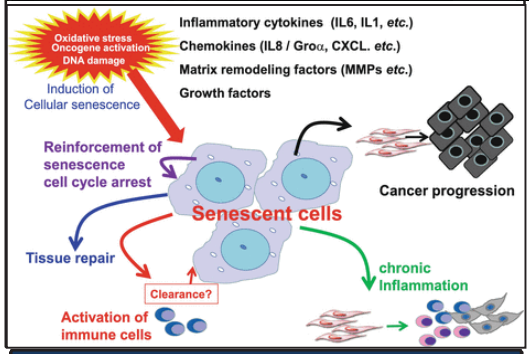

Experimental Design

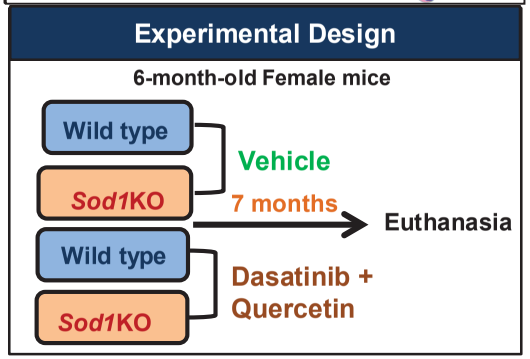

Results

Senolytic treatment reduced inflammation and associated pathways in *Sod1*KO mice

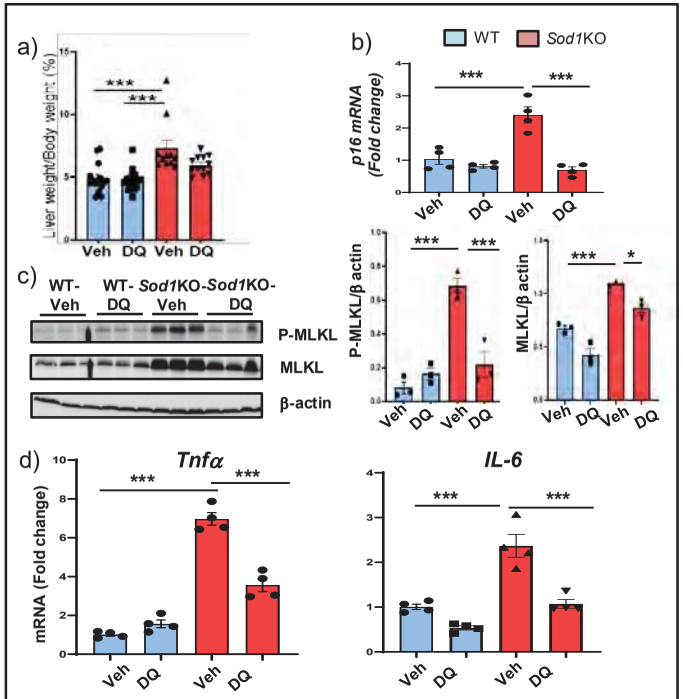

Fig. 1. (a) Comparison of liver weights of WT and *Sod1*KO mice treated either with Veh or DQ for 7 months, **(b)** Transcript levels of p16, **(c)** Western blot of phosphor MLKL and MLKL, **(d)** Transcript levels of TNF alpha and IL6 in the livers of WT and *Sod1*KO mice treated either with Veh or DQ for 7 months. *** p< 0.0005. One Way ANOVA.

Funding: OCAST (DS), OMRF research funds (HVR), VA merit grant (AR)

Senolytic treatment reduces immune cell cluster formation in *Sod1*KO mice

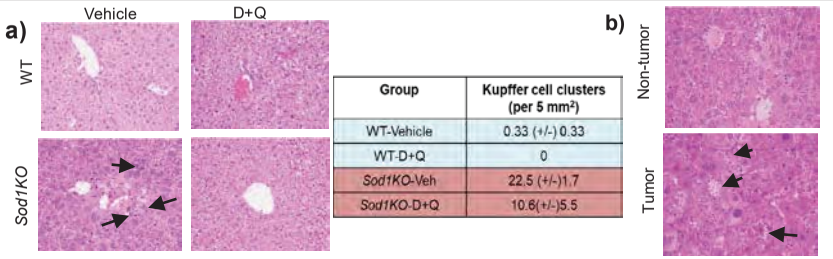

Group	Kupffer cell clusters (per 5 mm²)
WT-Vehicle	0.33 (+/-) 0.33
WT-D+Q	0
*Sod1*KO-Veh	22.5 (+/-)1.7
*Sod1*KO-D+Q	10.6(+/-)5.5

Fig. 2. (a) Images showing H&E staining of liver sections from WT and *Sod1KO* mice treated with vehicle or D+Q. Black arrows indicate Kupffer cell clusters. Quantification of Kupffer cell clusters are shown in the table. **(b)** Images showing H&E staining of liver sections from non-tumor and tumor region of *Sod1*KO mice. Arrows indicate fat droplets (steatosis) in tumor. Magnification: 40x.

Senolytic treatment reduced HCC tumor burden in *Sod1*KO mice

a)

Group	Tumor incidence/ mice (%)
WT-Veh	0/15 (0)
WT-D+Q	0/16 (0)
Sod1KO-Veh	7/11 (63.6%)
Sod1KO-D+Q	1/13 (7.7%)

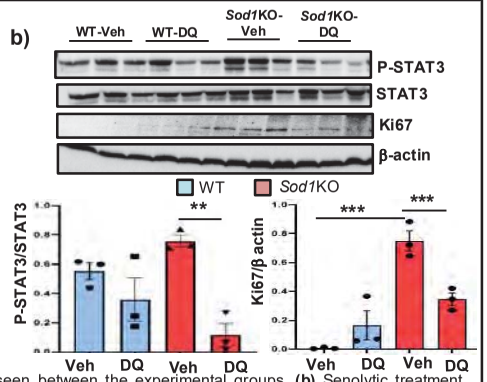

Fig. 3. (a) Table represents the tumor incidence seen between the experimental groups. **(b)** Senolytic treatment reduces the expression of proteins in pathways associated with cancer and cellular proliferation in the liver of Sod1KO mice. ***p<0.0005. One way ANOVA.

Conclusion

Senolytic treatment dramatically reduced HCC incidence in the *Sod1*KO mice and this appears to be due to the reduction in pathways that mediate chronic inflammation, i.e. cell senescence and necroptosis.

PROGNOSTIC SIGNIFICANCE OF APLN/APJ IN NEUROBLASTOMA

Santny Shanmugarama[1,2], Dinesh Babu Somasundaram[1] and Natarajan Aravindan[1,2,3]
Departments of [1]Radiation Oncology, [2]Pathology and [3]Anesthesiology, University of Oklahoma Health Sciences Center, Oklahoma City, OK, USA

Apelin and its receptor APJ are constitutively expressed in human tissues, and are instrumental in the regulation of blood pressure, cardiac function, apoptosis, angiogenesis, proliferation, metabolism etc. Recent studies recognized an unparalleled abundance, and their pivotal role in the initiation, progression and resistance of multifarious cancers. However, expression levels of apelin/APJ in neuroblastoma (NB), the most common cancer in infants, and its significance in disease evolution remained unexplored. In this study, two well-characterized NB patient cohorts were used: Study cohort 1 (all stages, diagnosis/progressive; apelin/APJ protein expression/immunohistochemistry; n = 92) and; R2 validation cohorts (mRNA expression - apelin, 17 cohorts, total *n* 3010; APJ, 19 cohorts, total n = 2899). In addition, the significance of APJ in disease dissemination is validated with a well-defined mouse model of progressive disease. We observed a strong and cell line dependent transcriptional (mRNA, QPCR) and translational (immunoblotting) abundance of both Apelin and APJ in human NB cells. RNA-seq data revealed equivocal association patterns of apelin and APJ expression with patient survival. In general, while Apelin showed high-is-worse association to disease stage, MYCN status and clinical outcomes, an interesting low-is-worse association was noted with APJ. IHC analysis in our study cohort of 92 patients revealed unique and defined associations of apelin/APJ expression to disease stage, MYCN and risk status, acquired resistance with current clinical therapy and patient outcomes. *In vivo* mouse models of progressive disease affirms the modified status of APJ in metastatic tumors when compared to the non-metastatic primary xenografts. Together, the outcomes of this study clearly portray that apelin/APJ is highly expressed in NB and further imply that the high-levels of apelin/APJ associates with tumor progression and poor clinical outcomes. Unveiling the mechanism(s) of apelin/APJ in NB pathogenesis and disease evolution are warranted and, such directions could identify novel targets and/or signaling that could be exploited for better treatment strategy, particularly for high-risk NB.

Funding: This work was partially or in full, funded by Oklahoma Center for the Advancement of Science and Technology, OCAST-HR19-04; National Institutes of Health, NIH-P20GM103639 and; NIH-NCI- Cancer Center Support Grant P30CA225520

REGULATION OF CSC LINEAGE AND STEMNESS MAINTENANCE IN PROGRESSIVE NEUROBLASTOMA: RD3, A MVP IN THE LEAGUE.

[1]Dinesh Babu Somasundaram and [1,2,3] Natarajan Aravindan
Departments of [1]Radiation Oncology, [2]Pathology and [3]Anesthesiology, University of Oklahoma Health Sciences Center, Oklahoma City, OK, USA. dsomasun@ouhsc.edu

Our studies recognized that the retinal degeneration protein 3 (RD3) is constitutively expressed in human adult and fetal tissues beyond retina. Further, we showed that transcriptional/translational loss of RD3 highly associated with advanced disease stage and poor clinical outcomes in neuroblastoma (NB) patients. We identified that RD3 loss is instrumental in NB pathogenesis and, more importantly defined its acquired loss in progressive NB after intensive multimodal clinical therapy. Herein, we investigated the mechanisms, how acquired loss of RD3 orchestrates NB progression. Cell lines derived during diagnosis from stage 4 NB patients off primary (CHLA-15) or metastatic (CHLA-42, SH-SY5Y) site, those with constitutive RD3 expression was used as parental controls. Analogous clones of stable RD3 knock-outs were developed (shRNA-RNAi), validated (immunoblotting) and were assayed for whole genome transcriptomic modifications using high-throughput Illumina transcriptome RNA-Seq. Differential gene expression analysis with stringent criteria (log2 fold change) coupled with false discovery rate calculation clearly identified 575 conserved (across three independent cell-lines) genetic determinants that could translate RD3-loss associated disease progression. IPA-functional bioinformatics identified regulation of cellular-lineage directed (stem-cell pluripotency, EMT, Senescence, epithelial adherens junction etc.) signaling coupled with select tumor evolution (NFκB, GPCR, mTOR, Wnt/β-catenin, stat3 etc.) signaling. Individual gene QPCR validation of experimentally observed 13 lead (mean FDR >7.0) candidates affirmed RNA-Seq outcomes. Actuated FAM129A, HAS2, ICAM1, S100A11, TSPAN8, HLA-F, ASIC4, AXL, VCAM1, KLHDC7B, MAGEL2 and, repressed tumor suppressor FOXN4 and NB differentiation factor ROBO2 in RD3-KOs recognized diverted cell lineage (EMT, poor differentiation, stimulated CSCs, CSC stemness maintenance), drug resistance, immune modulation/evasion, and tumor progression (clonal selection and expansion, growth and malignancy, invasion and migration, angiogenesis). For the first time, these results demonstrate the RD3-loss dependent transcriptomic addiction of disease evolution drivers in NB cells. Further, the outcomes imply that RD3 directly regulates key CSC cell lineage and tumor progression / dissemination signaling events. Current investigations are appropriately directed to unveil the functional mechanism(s) that could benefit salvage therapy for progressive NB.

Funding: This work was partially or in full, funded by Oklahoma Center for the Advancement of Science and Technology, OCAST-HR19-04; National Institutes of Health, NIH-P20GM103639 and; NIH-NCI- Cancer Center Support Grant P30CA225520

Regulation of CSC lineage and stemness maintenance in progressive neuroblastoma: RD3, a MVP in the league

[1]Dinesh Babu Somasundaram and [1, 2,3] Natarajan Aravindan

Departments of [1]Radiation Oncology, [2]Pathology and [3]Anesthesiology, University of Oklahoma Health Sciences Center, Oklahoma City, OK, USA.

dsomasun@ouhsc.edu

Background

Neuroblastoma (NB) is the most common cancer of infancy and accounts for nearly one tenth of pediatric cancer deaths. High-risk NBs consist of small populations of cells with preserved stemness characteristics. These clones exhibit the ability to form highly resistant tumorospheres and have high metastatic potential. Retinal Degeneration Protein 3 (RD3) that encodes a 195-amino-acid-long is critical in the regulation of guanylate cyclase (GC) signaling and photoreceptor cell survival and constitutively expressed in human adult and fetal tissues beyond retina. Further, we showed that transcriptional/translational loss of RD3 highly associated with advanced disease stage and poor clinical outcomes in neuroblastoma (NB) patients. We identified that RD3 loss is instrumental in NB pathogenesis and, more importantly defined its acquired loss in progressive NB after intensive multimodal clinical therapy. Herein, we investigated the mechanisms, how acquired loss of RD3 orchestrates NB progression. Cell lines derived during diagnosis from stage 4 NB patients off primary or metastatic site, those with constitutive RD3 expression was used as parental controls. Analogous clones of stable RD3 knock-outs were developed (shRNA-RNAi), validated (immunoblotting) and were assayed for whole genome transcriptomic modifications using high-throughput Illumina transcriptome RNA-Seq. Differential gene expression analysis with stringent criteria (log2 fold change) coupled with false discovery rate calculation clearly identified 575 conserved (across three independent cell-lines) genetic determinants that could translate RD3-loss associated disease progression. IPA-functional bioinformatics identified regulation of cellular-lineage signaling coupled with select tumor evolution signaling. Individual gene QPCR validation for repressed tumor suppressor, NB differentiation factor were experimentally observed 13 lead (mean FDR >7.0) candidates affirmed RNA-Seq outcomes in RD3-KOs recognized diverted cell lineage, drug resistance, immune modulation/evasion, and tumor progression. For the first time, these results demonstrate the RD3-loss dependent transcriptomic addiction of disease evolution drivers in NB cells. Further, the outcomes imply that RD3 directly regulates key CSC cell lineage and tumor progression / dissemination signaling events. Current investigations are appropriately directed to unveil the functional mechanism(s) that could benefit salvage therapy for progressive NB.

Methods

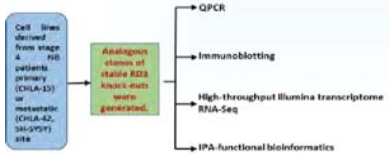

Results

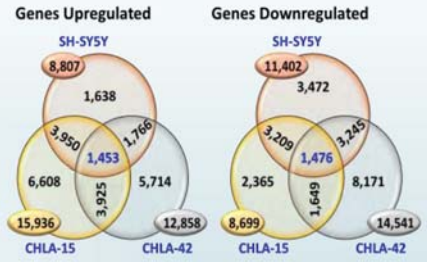

Genetic landscape of NB cells: *Venn diagrams of gene comparison analysis from whole genome gene expression profile showing genes that are upmodulated and downmodulated in cell lines derived during diagnosis from stage 4 NB patients off primary (CHLA-15) or metastatic (CHLA-42 and SH-SY5Y).*

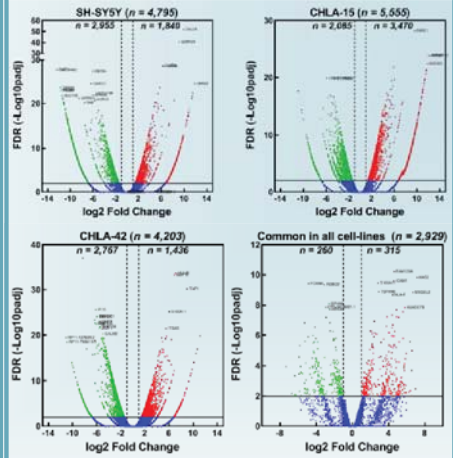

Volcano plots: *The distribution of the gene expression fold changes and corrected p-values in each subgroup (a) SH-SY5Y, (b) CHLA-15, (c) CHLA-42 and (d) common in all cell lines were shown. A total number of 4,795 genes in SH-SY5Y, 5,555 in CHLA-15, 4,203 in CHLA-42 and 2,929 common genes in all cell lines with p-value < 0.05 were used for the analysis. Genes with absolute fold change ≥ 7 are used for the individual QPCR analysis. Plots are generated using plotted with GraphPad Prism with moderated t-test and Benjamini-Hochberg testing correction*

13 lead (mean FDR >7.0) genes affirmed in RNA-Seq

RNA sequencing was done via Illumina platforms and the gene expression level is estimated by the abundance of transcripts. The threshold of differential analysis is set as FDR and the genes with the FDR above 7 has been selected for the individual QPCR analysis.

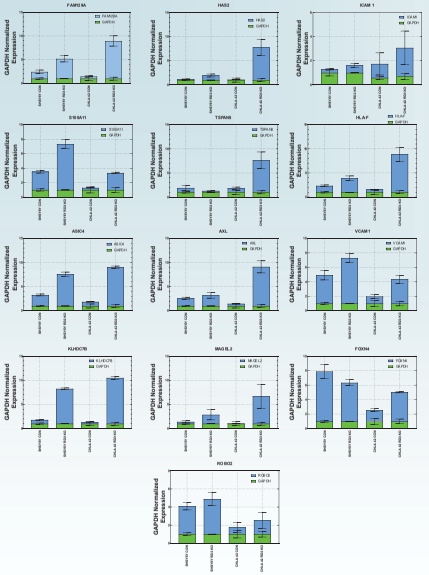

Transcriptional level of genes selected from RNA-Seq: *QPCR showing mRNA levels of genes from RNA-Seq with mean FDR >7.0 in parental and RD3 knockout clones*

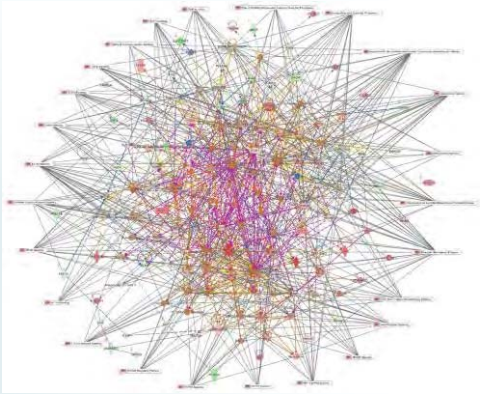

Ingenuity Pathway Analysis: *Upregulated and downregulated genes were imported into the Ingenuity Pathways Analysis (IPA) software and were subjected to functional annotations and regulatory network analysis using upstream regulator analysis (URA), downstream effects analysis (DEA) prediction algorithms. Overlay of top statistically significant canonical pathways identified by IPA analysis with direct relationship showing tightly inter-regulated signaling events that drive stem-cell pluripotency, EMT, Senescence, epithelial adherens junction and tumor evolution.*

Summary and Conclusion

The outcomes of this study demonstrate the RD3-loss dependent transcriptomic addiction of disease evolution drivers in NB cells. Further, the outcomes imply that RD3 directly regulates key CSC cell lineage and tumor progression / dissemination signaling events. Also, we integrated the power of next generation sequencing with the ingenuity pathway analysis platform to understand the NB cells with and silencing the RD3 expression and to highlight various signaling networks in NB. Current investigations are appropriately directed to unveil the functional mechanism(s) that could benefit salvage therapy for progressive NB.

Acknowledgements

This work was partially or in full, funded by Oklahoma Center for the Advancement of Science and Technology, OCAST-HR19-04; National Institutes of Health, NIH-P20GM103639 and; NIH-NCI- Cancer Center Support Grant P30CA225520

OPPOSITE ROLES OF THE JMJD1A INTERACTION PARTNERS MDFI AND MDFIC IN COLORECTAL CANCER

Yuan Sui[1], Xiaomeng Li[2,3], Sangphil Oh[3,4], Bin Zhang[2], Willard M. Freeman[4,5], Sook Shin[3,4] and Ralf Janknecht[1,3,4]

Presenting Author's Email Address：yuan-sui@ouhsc.edu

[1]Department of Pathology, University of Oklahoma Health Sciences Center, Oklahoma City, USA; [2]China-Japan Union Hospital of Jilin University, Changchun, China; [3]Department of Cell Biology, University of Oklahoma Health Sciences Center, Oklahoma City, USA; [4]Stephenson Cancer Center, Oklahoma City, USA; [5]Oklahoma Medical Research Foundation, Oklahoma City, USA

MyoD family inhibitor (MDFI) and MyoD family inhibitor domain-containing (MDFIC) are homologous proteins known to regulate myogenic transcription factors. Hitherto, their role in cancer is unknown. We discovered that *MDFI* is up- and *MDFIC* downregulated in colorectal tumors. Mirroring these different expression patterns, MDFI stimulated while MDFIC inhibited the growth of HCT116 colorectal cancer cells. Further, MDFI and MDFIC interacted with JMJD (Jumonji C domain-containing) 1A, a histone demethylase and epigenetic regulator involved in colorectal cancer. JMJD1A influenced transcription of several genes that were also regulated by MDFI or MDFIC. Notably, the *HIC1* tumor suppressor gene was stimulated by JMJD1A and MDFIC, but not MDFI, and HIC1 overexpression phenocopied the growth suppressive effects of MDFIC in HCT116 cells. Similar to colorectal cancer, *MDFI* was up- and *MDFIC* downregulated in breast, ovarian and prostate cancer, but both *MDFI* and *MDFIC* were overexpressed in brain, gastric and pancreatic tumors. This implies cancer-critical roles for MDFI and MDFIC beyond colorectal tumors and also points out that MDFIC might be a tissue-specific suppressor or promoter of tumorigenesis. Altogether, our data suggest a tumor modulating function for MDFI and MDFIC in colorectal and other cancers that may involve their interaction with JMJD1A and a MDFIC-HIC1 axis.

Acknowledgement of funding: This work was in part funded by a seed grant from the Stephenson Cancer Center (W.M.F. and R.J.).

Opposite Roles of the JMJD1A Interaction Partners MDFI and MDFIC in Colorectal Cancer

Yuan Sui[1], Xiaomeng Li[2,3], Sangphil Oh[3,4], Bin Zhang[2], Willard M. Freeman[4,5], Sook Shin[3,4] and Ralf Janknecht[1,3,4]

[1]Pathology Department, OUHSC; [2]China-Japan Union Hospital of Jilin University, China; [3]Cell Biology Department, OUHSC; [4]Stephenson Cancer Center; [5]Oklahoma Medical Research Foundation

ABSTRACT

MyoD family inhibitor (MDFI) and MyoD family inhibitor domain-containing (MDFIC) are homologous proteins known to regulate myogenic transcription factors. Hitherto, their role in cancer is unknown. We discovered that *MDFI* is up- and *MDFIC* downregulated in colorectal tumors. Mirroring these different expression patterns, MDFI stimulated and MDFIC inhibited growth of HCT116 colorectal cancer cells. Further, MDFI and MDFIC interacted with JMJD (Jumonji C domain-containing) 1A, a histone demethylase and epigenetic regulator involved in colorectal cancer. JMJD1A influenced transcription of several genes that were also regulated by MDFI or MDFIC. Notably, the *HIC1* tumor suppressor gene was stimulated by JMJD1A and MDFIC, but not MDFI, and HIC1 overexpression phenocopied the growth suppressive effects of MDFIC in HCT116 cells. Altogether, our data suggest a tumor modulating function for MDFI and MDFIC in colorectal cancer that may involve their interaction with JMJD1A and a MDFIC-HIC1 axis.

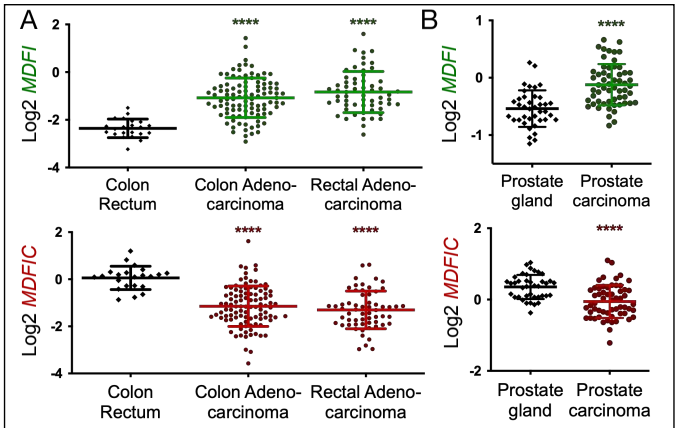

Fig. 1. Altered mRNA levels of *MDFI* and *MDFIC* in cancerous compared to healthy tissue. ****, P<0.0001. A: Colorectal tissues; B: Prostate tissues.

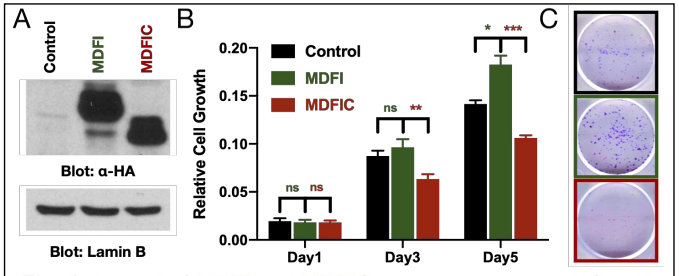

Fig. 2. Impact of MDFI and MDFIC overexpression on HCT116 cells. A: Western blot; B: Growth assay; C: Clonogenic assay.

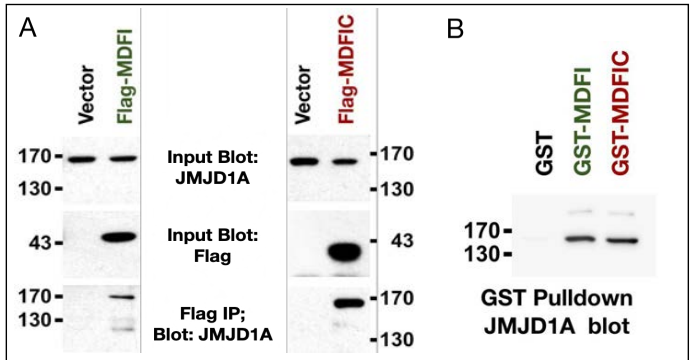

Fig. 3. Interaction of JMJD1A with MDFI and MDFIC. A: Co-immunoprecipitation of JMJD1A with MDFI and MDFIC; B: GST pull down assay with purified protein.

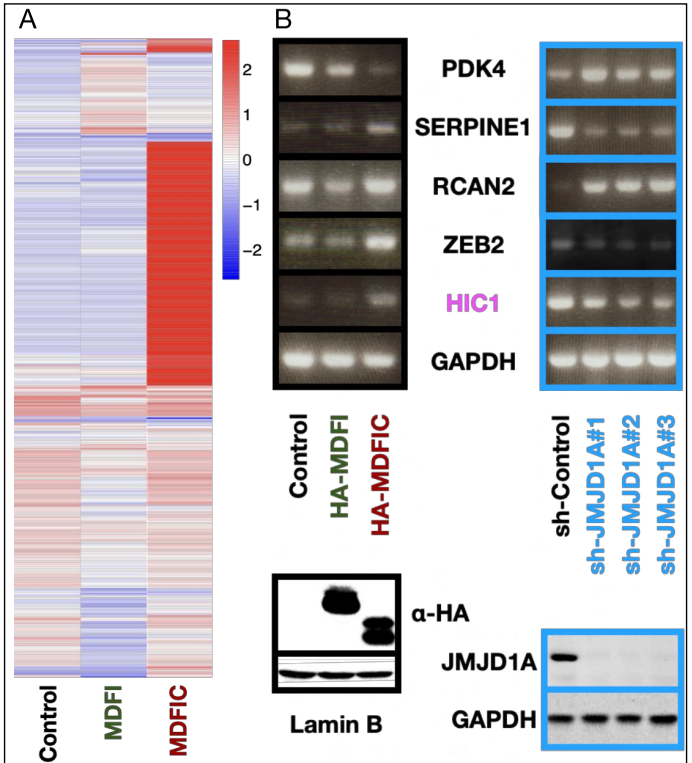

Fig. 4. Joint regulation of target genes. A: Hierarchical clustering of 525 target genes differentially regulated by MDFI and MDFIC. B: RT-PCR proving coregulation of several targets by JMJD1A.

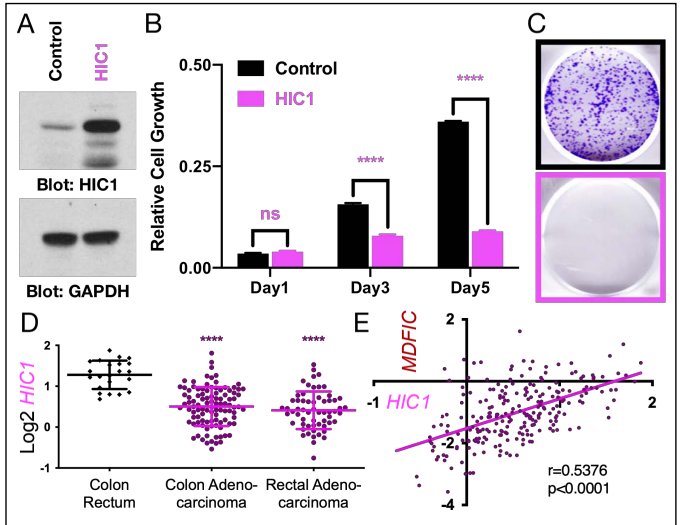

Fig. 5. Impact of HIC1 overexpression on HCT116 cancer cells. A: Western blot; B: Growth assay; C: Clonogenic assay; D: *HIC1* mRNA levels in normal and diseased colorectal tissues. E: Correlation between *HIC1* and *MDFIC* mRNA levels across all 234 samples in the TCGA data shown in panel D. ****, P<0.0001.

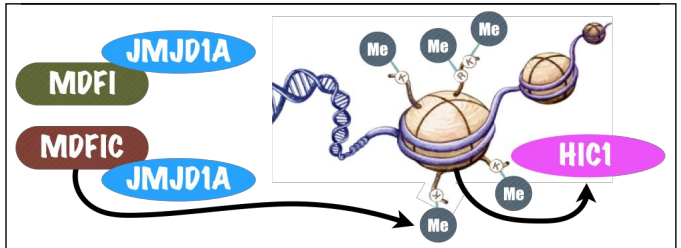

Fig. 6. Scheme of MDFI, MDFIC and JMJD1A interactions and resultant induction of HIC1 expression.

CONCLUSIONS

- First demonstration that MDFI and MDFIC are cancer-critical proteins;
- Perplexing potential opposite function of MDFI and MDFIC in colon, prostate and breast (not shown) cancer;
- MDFI and MDFIC can affect transcription through JMJD1A;
- Upregulation of HIC1 by the MDFIC/JMJD1A complex may suppress colorectal tumorigenesis.

Acknowledgement: This work was in part funded by a seed grant from the Stephenson Cancer Center.

DYNAMIC COMPLEXITY OF MITOTIC SPINDLE MICROTUBULES

Aaron R. Tipton and Gary J. Gorbsky
Aaron-tipton@omrf.org
Oklahoma Medical Research Foundation, Cell Cycle and Cancer Biology Dept.

Mitotic spindle microtubules interact with centrosomes, kinetochores, chromosome arms, each other and other cellular elements in regulating chromosome movement and cell cycle progression through M phase. Study of spindle microtubule assembly/disassembly kinetics utilizing fluorescence dissipation after photoactivation render a biphasic recovery plot distinguishing two populations, those with turnover half-time of a few minutes and those with a turnover of a few seconds. These two populations have conventionally been considered to reflect the dynamics of kinetochore versus non-kinetochore microtubules respectively. To test this and other conventions regarding mitotic spindle microtubule dynamics, we carried out photoactivation experiments while manipulating specific microtubule interactions. We first eliminated end-on microtubule kinetochore interactions by depleting the NDC80 complex in U2OS cells. In the absence of end-on interactions with kinetochores, photoactivation analyses remained biphasic with slow and fast turnover populations. Loss of kinetochores increased the percentage of fast-turnover microtubules and decreased the slow-turnover population. In addition, the half-time for recovery of the slow population was decreased. These results suggest that only a portion of slow turnover microtubules are eliminated when end-on attachment of microtubules is abrogated, leading to the conclusion that other slow turnover populations of microtubules co-exist within the spindle. We hypothesized that at least one contributor to this additional slow turnover population were interpolar microtubules. Analysis of monopolar spindles after treatment of cells with the Eg5 inhibitor, STLC, to eliminate interpolar microtubules led to a decrease in the half-time for turnover of the slow population, supporting our hypothesis. Experiments utilizing cold treatment of cells have previously shown that non-kinetochore spindle microtubules are selectively sensitive to reduced temperature. In photoactivation experiments, reduction of temperature to ~25^{o}C increased the half times of slow and fast populations when compared to controls at 37^{o}C, but resulted in only minor changes in proportions of each. Our studies indicate that the mitotic spindle is comprised of multiple microtubule sub-populations and that the conventional binary interpretation of photoactivation experiments as reflecting kinetochore and non-kinetochore microtubule dynamics is an oversimplification. More precise dissection of the dynamics of microtubule sub-classes are required for a full understanding of the role of mitotic spindle dynamics in facilitating chromosome movement and cell cycle control in M phase.

DYNAMIC COMPLEXITY OF MITOTIC SPINDLE MICROTUBULES

Aaron R. Tipton and Gary J. Gorbsky

Cell Cycle and Cancer Biology, Oklahoma Medical Research Foundation, Oklahoma City, OK 73104, USA

Abstract

Mitotic spindle microtubules interact with centrosomes, kinetochores, chromosome arms, each other and other cellular elements in regulating chromosome movement and cell cycle progression through M phase. Study of spindle microtubule assembly/disassembly kinetics utilizing fluorescence dissipation after photoactivation render a biphasic recovery plot distinguishing two populations, those with turnover half-time of a few minutes and those with a turnover of a few seconds. These two populations have conventionally been considered to reflect the dynamics of kinetochore versus non-kinetochore microtubules respectively. To test this and other conventions regarding mitotic spindle microtubule dynamics, we carried out photoactivation experiments while manipulating specific microtubule interactions. We first eliminated end-on microtubule kinetochore interactions by depleting the NDC80 complex in U2OS cells. In the absence of end-on interactions with kinetochores, photoactivation analyses remained biphasic with slow and fast turnover populations. Loss of kinetochores increased the percentage of fast-turnover microtubules and decreased the slow-turnover population. In addition, the half-time for recovery of the slow population was decreased. These results suggest that only a portion of slow turnover microtubules are eliminated when end-on attachment of microtubules is abrogated, leading to the conclusion that other slow turnover populations of microtubules co-exist within the spindle. We hypothesized that at least one contributor to this additional slow turnover population were interpolar microtubules. Analysis of monopolar spindles after treatment of cells with the Eg5 inhibitor, STLC, to eliminate interpolar microtubules led to a decrease in the half-time for turnover of the slow population, supporting our hypothesis. Experiments utilizing cold treatment of cells have previously shown that non-kinetochore spindle microtubules are selectively sensitive to reduced temperature. In photoactivation experiments, reduction of temperature to ~25oC increased the half times of slow and fast populations when compared to controls at 37oC, but resulted in only minor changes in proportions of each. Our studies indicate that the mitotic spindle is comprised of multiple microtubule sub-populations and that the conventional binary interpretation of photoactivation experiments as reflecting kinetochore and non-kinetochore microtubule dynamics is an oversimplification. More precise dissection of the dynamics of microtubule sub-classes are required for a full understanding of the role of mitotic spindle dynamics in facilitating chromosome movement and cell cycle control in M phase.

Rationale

+ Early Analysis of spindle microtubule kinetics utilizing fluorescence dissipation after photoactivation described two main populations, a slow and a fast turnover population.

+ Historically, the two microtubule populations were suggested to reflect kinetochore versus non-kinetochore microtubules respectively.

+ This two component demarcation seems likely oversimplified.

+ We tested the concept of kinetochore versus non-kinetochore microtubules by manipulation of spindle microtubules populations, revealing a complex landscape.

+ The proteosome inhibitor MG132 was added just prior to imaging to prevent mitotic exit in some experiments.

+ STLC = Eg5 inhibitor

+ Low Temp = 23-25^{O}C

+ ZM447439 = Aurora B inhibitor

+ Red numbers denote statistical significance.

Loss of Kinetochore End-On Attachment

Figure 1

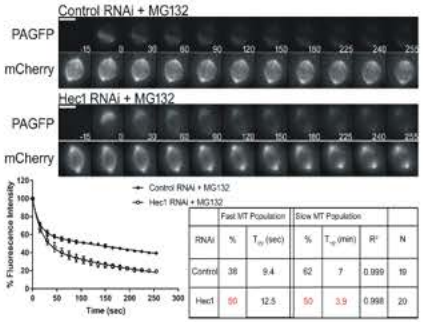

RNAi	Fast MT Population %	Fast MT Population $T_{1/2}$ (sec)	Slow MT Population %	Slow MT Population $T_{1/2}$ (min)	R^2	N
Control	38	9.4	62	7	0.999	19
Hec1	50	12.5	50	3.9	0.998	20

Loss of Interpolar MT

Figure 2

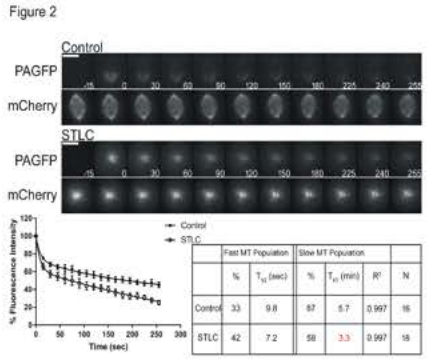

	Fast MT Population %	Fast MT Population $T_{1/2}$ (sec)	Slow MT Population %	Slow MT Population $T_{1/2}$ (min)	R^2	N
Control	33	9.8	67	5.7	0.997	16
STLC	42	7.2	58	3.3	0.997	18

Reduction of Temperature

Figure 3

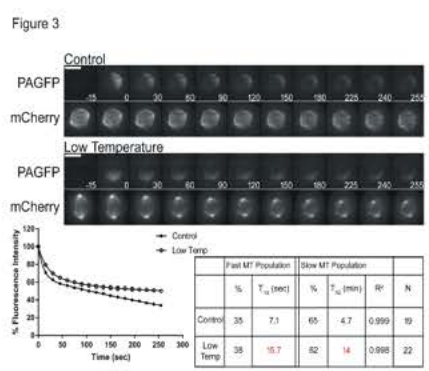

	Fast MT Population %	Fast MT Population $T_{1/2}$ (sec)	Slow MT Population %	Slow MT Population $T_{1/2}$ (min)	R^2	N
Control	35	7.1	65	4.7	0.999	19
Low Temp	38	15.7	62	14	0.998	22

Loss of Aurora B Kinase Activity

Figure 4

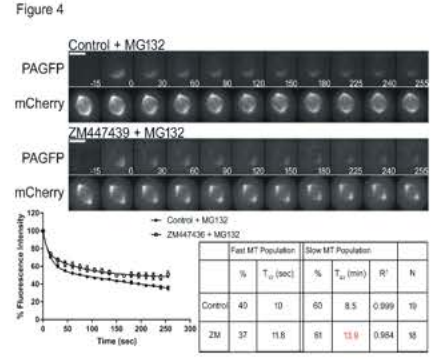

	Fast MT Population %	Fast MT Population $T_{1/2}$ (sec)	Slow MT Population %	Slow MT Population $T_{1/2}$ (min)	R^2	N
Control	40	10	60	8.5	0.999	19
ZM	37	11.8	61	13.9	0.984	18

Funded by grants R35GM126980 from the National Institute of General Medical Sciences and HR12-177 from the Oklahoma Center for Advancement of Science and Technology to GJG

Loss of Kinetochore End-On Attachment Combined with Aurora B Inhibition

Figure 5

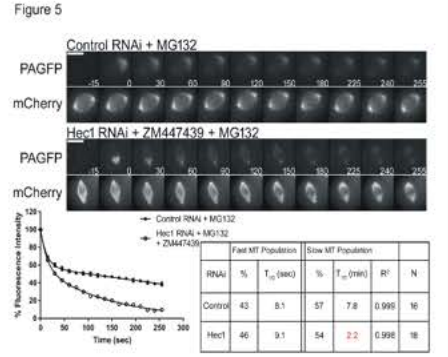

RNAi	Fast MT Population %	Fast MT Population $T_{1/2}$ (sec)	Slow MT Population %	Slow MT Population $T_{1/2}$ (min)	R^2	N
Control	43	8.1	57	7.8	0.999	16
Hec1	46	9.1	54	2.2	0.998	18

Prolonged Metaphase Arrest

Figure S1

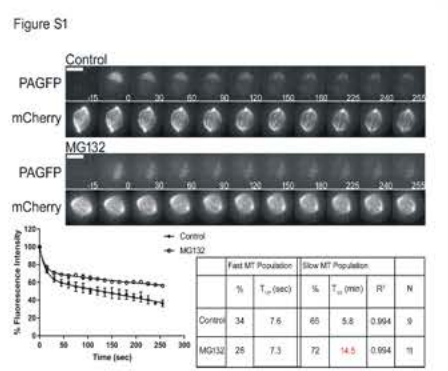

	Fast MT Population %	Fast MT Population $T_{1/2}$ (sec)	Slow MT Population %	Slow MT Population $T_{1/2}$ (min)	R^2	N
Control	34	7.6	66	5.8	0.994	9
MG132	28	7.3	72	14.5	0.994	11

Conclusions

+ Mitotic spindles in cells lacking functional kinetochores still reveal fast and slow turnover microtubule populations. (Fig. 1)

+ Slow microtubule population turnover is faster (decreased $T_{1/2}$) following the loss of spindle bipolarity. (Fig. 2)

+ Turnover of both fast and slow microtubule populations is slower (increased $T_{1/2}$) following temperature reduction. (Fig. 3)

+ Turnover of the slow microtubule population is slower (increased $T_{1/2}$) following Aurora B kinase inhibition. (Fig. 4)

+ Aurora B kinase stabilizes non end-on attached slow turnover microtubules. (Fig. 5)

+ Slow microtubule population turnover is slower (increased $T_{1/2}$) following a 3h metaphase arrest (MG132). (Fig. S1)

+ In contradiction to the established paradigm, photoactivation reveals multiple populations of mitotic spindle microtubules even in the absence of normal kinetochore attachments or spindle bipolarity.

TICRR/TRESLIN PROTEIN EXPRESSION IS CELL CYCLE REGULATED BY THE CUL4-DDB1-DTL E3 UBIQUITIN LIGASE

Kimberlie A. Wittig[1,2*], Courtney G. Sansam[2], Tyler D. Noble[1,2], Duane Goins[2], Christopher L. Sansam[1,2*]

Presenter's e-mail address: kimberlie-wittig@ouhsc.edu

[1] Department of Cell Biology, University of Oklahoma Health Sciences Center, Oklahoma City, Oklahoma 73104, USA; [2] Cell Cycle and Cancer Biology Research Program, Oklahoma Medical Research Foundation, Oklahoma City, Oklahoma 73104, USA

DNA replication is the process of duplicating two identical copies of the genome to be equally divided during every cell division. Deregulation of DNA replication is a leading contributor to genomic instability and tumorigenesis. Therefore, tight regulation of the number of active replisomes is crucial to prevent replication stress-induced DNA damage. TICRR/TRESLIN is essential for DNA replication initiation in yeast, *Xenopus*, zebrafish, and higher eukaryotes including humans. The expression level of TICRR and its phosphorylation status determine the number of replication origins that initiate simultaneously during S-phase. However, the mechanisms regulating TICRR protein expression throughout the cell cycle are unknown.

In this study, we aimed to evaluate TICRR protein dynamics around the G1/S-phase transition. To do this, we tagged the endogenous C-terminus of TICRR with mClover in HCT-116 human colon cancer cells using CRISPR/Cas9 and applied an established flow cytometry assay to detect how levels of both insoluble and total TICRR change.

We find total TICRR expression is highest in G2/M, decreases with cell division when cells re-enter G1, and further decreases at the G1/S-phase transition. However, insoluble TICRR levels are highest in G1 and sharply decrease with S-phase entry. Although total TICRR expression decreases between G2/M and G1, insoluble TICRR levels increase demonstrating that insoluble TICRR accumulation in G1 is not due to changes in its expression. In contrast, both total and insoluble TICRR levels decrease with S-phase entry demonstrating this decrease is at least in part due to the degradation of TICRR protein. Utilizing proteasomal and neddylation inhibitors, we show that degradation of TICRR depends on cullin E3 ubiquitin ligases and is specific to S-phase. Additionally, through two targeted siRNA screens, we have identified CUL4-DDB1-DTL as the cullin complex necessary for TICRR degradation.

Collectively, our results demonstrate how total and insoluble levels of TICRR change in distinct ways throughout the cell cycle, and we have elucidated a mechanism for TICRR degradation at the G1/S transition affecting the levels of protein available for DNA replication initiation during S-phase. These results suggest a mechanism to control the rate of replication origin firing to prevent replication stress and DNA damage.

Funding: This work was supported by the National Institutes of Health [R01GM121703] and the Oklahoma Center for Adult Stem Cell Research. K.A.W. received support from the Drs. Patricia H. and J. Donald Capra Scholarship Fund.

TICRR/TRESLIN Protein Expression is Cell Cycle Regulated by the CUL4-DDB1-DTL E3 Ubiquitin Ligase

Kimberlie A. Wittig[1,2], Courtney G. Sansam[1], Tyler D. Noble[1,2], Duane Goins[1], Christopher L. Sansam[1,2]

[1]Cell Cycle and Cancer Biology Research Program, Oklahoma Medical Research Foundation, Oklahoma City, OK, USA
[2]Department of Cell Biology, University of Oklahoma Health Sciences Center, Oklahoma City, OK, USA

Introduction

DNA replication is the process of duplicating two identical copies of the genome to be equally divided during every cell division. Deregulation of DNA replication is a leading contributor to genomic instability and tumorigenesis. Tight regulation of the number of active replisomes in S-phase is crucial to prevent replication stress-induced DNA damage. TICRR/TRESLIN is an essential factor for DNA replication initiation in yeast, *Xenopus*, and higher eukaryotes including humans. The expression level of TICRR/TRESLIN and its phosphorylation status determine the number of origins that initiate simultaneously during S-phase. However, the mechanisms regulating TICRR/TRESLIN protein expression are unknown. Our hypothesis is that TICRR is "pruned" at the G1//S-phase transition in order to control the rate of origin firing preventing replication stress and DNA damage.

Methods

We tagged the endogenous C-terminus of TICRR in HCT-116 cells using CRISPR/Cas9 such that all expressed protein is tagged and applied an established flow cytometry assay to detect insoluble and total TICRR levels throughout the cell cycle. For insoluble protein detection, cells are permeabilized in CSK buffer and fixed in 4% paraformaldehyde (PFA). For total protein detection, cells are directly fixed in 4% PFA. Finally, proteins are labeled with primary and secondary antibodies and DNA is stained with propidium iodide for cell cycle analysis. siRNA screens were performed with individual siRNA (Figure 3) or siRNA pools (Figure 4) against the respective targets. Samples were collected 24 and 48 hours after transfection.

Results

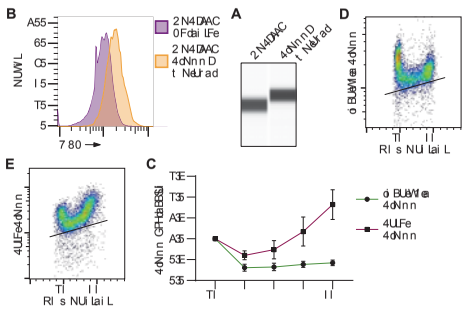

Figure 1. Successful generation of HCT-116 TICRR-mClover knock-in cell line. (A) Live cell GFP flow cytometry demonstrates a positive shift in fluorescence. (B) Capillary electrophoresis demonstrates all expressed TICRR protein is tagged. (C) Insoluble TICRR is highest in 2N cells and decreases with S-phase entry. (D) Total TICRR expression is highest in 4N cells, decreases with cell division, and is lowest in S-phase.
(E) Quantification of cells from C and D (n=6).

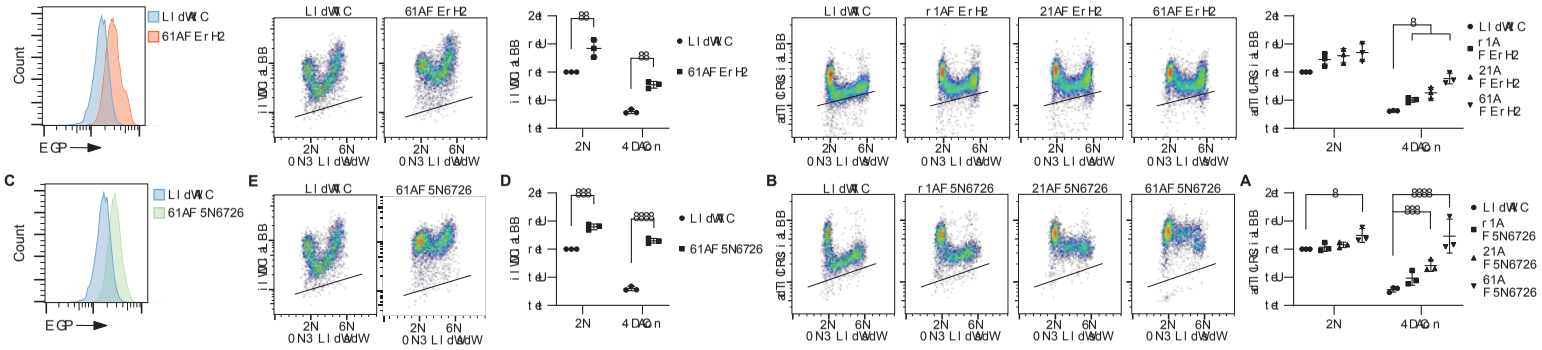

Figure 2. TICRR protein expression is regulated via cullin E3 ubiquitin ligases. (A) Live cell GFP flow cytometry demonstrates an increase in TICRR protein after treatment. (B) Total TICRR (anti-GFP) flow cytometry. (C) Quantification from B (n=3). (D) Insoluble TICRR (anti-GFP) flow cytometry. (E) Quantification from D (n=3). (F) Live cell GFP flow cytometry demonstrates an increase in TICRR protein after treatment. (G) Total TICRR (anti-GFP) flow cytometry. (H) Quantification from G (n=3). (I) Insoluble TICRR (anti-GFP) flow cytometry. (J) Quantification from I (n=3). * p<0.05, ** p<0.01, *** p<0.001, **** p<0.0001

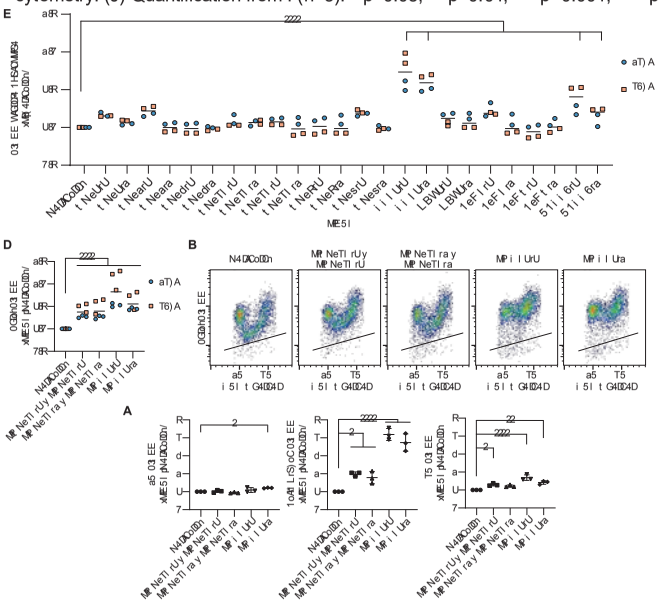

Figure 3. CUL4+B and DDB1 knockdown increase TICRR levels during S-phase. HCT-116 TICRR-mClover cells were transfected with (A) single or (B) double siRNA and collected after 24 or 48 hours for live cell flow cytometry. Values represent median GFP intensity and are normalized to untreated control. Black line indicates grand median. (C) Total protein flow cytometry 24 hours after siRNA transfection. Black line indicates upper limit of the negative control sample. (D) Quantification of 2N, early S-phase, or 4N cells from C (n=3). Data represented as mean ± SD. * p<0.05, ** p<0.01, *** p<0.001, **** p<0.0001

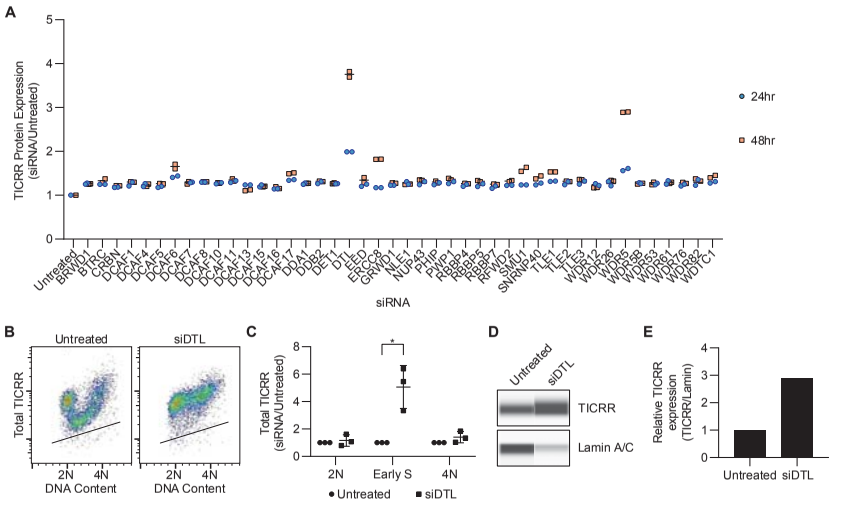

Figure 4. DTL knockdown increases TICRR levels during S-phase. (A) HCT-116 TICRR-mClover cells were transfected with a siRNA pool and collected after 24 or 48 hours for live cell flow cytometry. Values represent median GFP intensity and are normalized to untreated control. (B) Total protein flow cytometry 24 hours after siRNA transfection. Black line indicates upper limit of the negative control sample. (D) Quantification of 2N, early S-phase, or 4N cells from B (n=3). Data represented as mean ± SD. * p<0.05. (D) Capillary electrophoresis of whole cell lysates 24 hours after siRNA transfection for TICRR (anti-GFP) and Lamin A/C (anti-Lamin A/C). (E) Quantification from D. Values are normalized to the untreated control.

Conclusions

We have elucidated a mechanism for TICRR degradation at the G1/S transition. These results suggest a mechanism to control the rate of replication origin firing to prevent replication stress and DNA damage.

Funding National Institutes of Health [R01GM121703], Oklahoma Center for Adult Stem Cell Research, and the Drs. Patricia H. and J. Donald Capra Scholarship Fund

SINGLE-PROBE MASS SPECTROMETRY IMAGING STUDIES OF METABOLITES RELEVANT TO BLOOD VESSEL GROWTHS

Zhu Zou[1], Pengchun Yu[2], Xiang Tian[1], Jie Zhu[2], Zhibo Yang[1]
Presenting author's email address: zhuzou2017@ou.edu
[1]University of Oklahoma, Norman, OK, United States, [2]Oklahoma Medical Research Foundation, Oklahoma City, OK, United States

Angiogenesis is found to be related to many diseases, such as diabetic retinopathy and cancer. TABV (Tumor Associated Blood Vessel) has also been found to play an important role in the development of cancers. With the obvious severity, there has hardly been effective clinical treatment on the abnormal blood vessel growth. In our studies, we obtained spatially-resolved distribution of metabolomic profiles of blood vessels via the Single-probe mass spectrometry imaging (MSI) method. MSI data were analyzed using Matlab and Python scripts to generate mass spectrometry images (MSI) in order to compare with optical images. After the spatial information was registered from MSI image space to optical image space, we were able to select the pixels with blood vessels and analyze their metabolomic profiles. The change in the abundance of metabolites can provide molecular information for fundamental understanding of disease mechanisms and potentially design effective treatment to control or adjust blood vessel growth.

The Single-probe is a homemade device composed of a dual-bore quartz needle and two fused silica capillaries inserted into two bores of the needle. One capillary provides solvent flowing through the tip of the probe, where substances are extracted from sample surface through microscale liquid extraction, and the other capillary delivers solution containing analytes to the nano-ESI emitter for ionization followed by MS analysis using a Thermo LTQ Orbitrap XL mass spectrometer. When MS imaging scans are conducted, a pixel-to-pixel scan is done on the section of samples. With the ion intensities for all different peaks obtained from all pixels, ion images can be generated to represent the chemical profiles, including the compositions and relative abundances at designated positions. Optical images are also obtained to locate blood vessels prior to MSI measurement. Metabolites are identified through tandem MS (MS/MS), and MSI data are processed and analyzed using automated scripts. MSI images can also be fused with optical images to obtain improved spatial resolution and correlated locations of histological hallmarks and metabolites.

Funding: NIH (R01GM116116, R21CA204706), AHA (19CDA34760260)

Single-Probe Mass Spectrometry Imaging Studies of Metabolites Relevant to Blood Vessel Growths

Zhu Zou, Pengchun Yu, Xiang Tian, Zhibo Yang*
Department of Chemistry and Biochemistry
University of Oklahoma, Norman, Oklahoma, 73019, USA
Corresponding author email: Zhibo.Yang@ou.edu

Introduction

Angiogenesis is an irreversible physiological process that represents the development of new blood vessels. It is found to be related to many diseases, such as diabetic retinopathy and cancer.
Our ultimate goal is to study the chemical profile of growing blood vessels and develop treatment for angiogenesis.

Method

Single probe is a homemade device that can sample spots on surface through microscale liquid extraction. Solvent flows in from the solvent-providing channel and extracts analytes from the spot at the tip, then delivers them to MS through the emitter.
The Single-probe is held on a robotic arm and pixel-to-pixel scan is run with an xyz-translational stage.

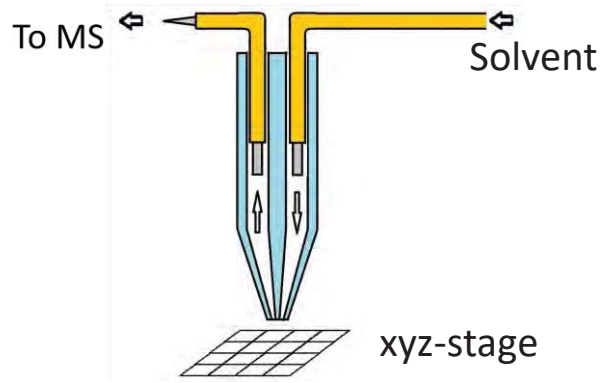

Result

Fluorescence image and MS images of mice retina are taken. Different patterns have been observed for different peaks.

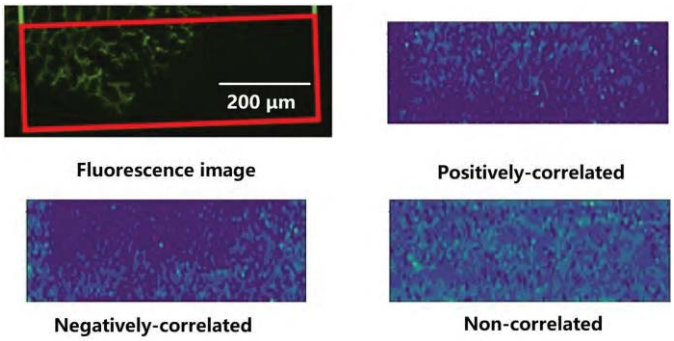

Conclusion

The method is under development. Resolution still needs improvement to better correlate substances with blood vessels.

Funding: NIH (R01GM116116, R21CA204706),AHA (19CDA34760260)
Acknowledgement: Dr. Yang's group members, Dr. Yihan Shao, Dr. Genwei Zhang

Cancer Control & Prevention

CANCER CONTROL AND PREVENTION POSTERS

POSTER PRESENTATION LIST

Listed A-Z by Presenter Last Name
Presenting*

EVERYDAY DISCRIMINATION AND STRESSFUL LIFE EVENTS ARE ASSOCIATED WITH PAST-30 DAY SUBSTANCE USE AMONG ADULTS EXPERIENCING HOMELESSNESS
Adam C. Alexander

TOBACCO USE AND TREATMENT PREFERENCES AMONG ADULTS ACCESSING SERVICES AT A DAY SHELTER*
Laili Boozary

MEASURING DNA DAMAGE TO ASSESS THE USE OF ELECTRONIC CIGARETTES AS A TOBACCO HARM REDUCTION STRATEGY*
Mayilvanan Chinnaiyan

CONFLICTING INFORMATION AGGRAVATES EMOTION-RECOGNITION DEFICITS IN TEENAGERS AT RISK FOR USE OR ABUSE OF CARCINOGENS*
Blas Espinoza-Varas

THE RELATIONSHIP BETWEEN TRAVEL BURDEN AND HPV-ASSOCIATED CANCER SURVIVAL OUTCOMES: AN ANALYSIS OF THE UNIVERSITY OF OKLAHOMA MEDICAL CENTER CANCER REGISTRY, 2005-2019*
Sameer Gopalani

CIGARETTE SMOKING AND QUIT BEHAVIORS ARE ASSOCIATED WITH SEXUAL ORIENTATION TRANSITION BETWEEN WAVES 1 AND 4 OF THE POPULATION ASSESSMENT OF TOBACCO AND HEALTH (PATH) STUDY*
Afsheen Hasan

POTENTIAL OF PHARMACEUTICAL INTERVENTION IN PLATELETS AND CANCER POSITIVE FEEDBACK LOOP*
Zitha Redempta Isingizwe

EFFECT OF CONTINUED TOBACCO USE ON HEAD AND NECK CANCER TREATMENT OUTCOMES AND PATIENT SURVIVAL*
Matthew Krutz

CANCER CONTROL AND PREVENTION POSTERS

HYPERTENSION DRUG OLMESARTAN MEDOXOMIL PROMOTES COLONIC TUMORIGENESIS IN AOM-INDUCED CRC RAT MODEL*
Nandini B Kumar

BESTATIN, A LTA4 HYDROLASE INHIBITOR PREVENTS INTESTINAL TUMORS IN THE APC MUTANT RODENT MODELS REPRESENTING FAP PATIENTS*
Venkateshwar Madka

THE IMPACT OF GUT MICROBIAL TOXINS AND PGE2 ON IL-23 PRODUCTION AND ITS ROLE IN OBESITY ASSOCIATED COLORECTAL TUMORIGENESIS*
Janani Panneerselvam

E-CIGARETTE AEROSOL ALTERS MITOCHONDRIA DNA DAMAGE AND BIOGENESIS*
Balaji Sadhasivam

BUILDING PARTNERSHIPS WITH COMMUNITY STAKEHOLDERS TO ELIMINATE CANCER-RELATED HEALTH DISPARITIES AMONG AFRICAN AMERICANS IN OKLAHOMA

Adam C. Alexander (adam-alexander@ouhsc.edu) [a,b]

[a] TSET Health Promotion Research Center, Stephenson Cancer Center, University of Oklahoma Health Sciences Center, Oklahoma City, Oklahoma, United States, [b] Department of Family and Preventive Medicine, University of Oklahoma Health Sciences Center, Oklahoma

Role of funding source: The ongoing research mentioned in this presentation is supported by funds from the Oklahoma Tobacco Settlement Endowment Trust (R21-02) and Community Outreach and Engagement Core.

The Stephenson Cancer Center (SCC) is uniquely positioned to provide statewide leadership in cancer research, treatment, education, and outreach, and its central mission is to engage communities within Oklahoma to decrease cancer burden, particularly among minority and under-represented populations. However, engagement with African Americans in Oklahoma is lacking despite significant cancer disparities. The incidence and mortality rates of cancer are generally higher among African Americans than Whites in Oklahoma. Most importantly, the 5-year cancer survival rate for African Americans living in Oklahoma is 47.1%, the lowest survival rate of all racial/ethnic groups in Oklahoma. African Americans are motivated and eager to address these significant health challenges, and there is an opportunity for SCC to renew its relationship and collaborate with community stakeholders to build lasting partnerships that will shape the direction of African Americans' health in Oklahoma for decades. This presentation will provide an overview of the planned activities in 2021 to reestablish our connection with community stakeholders and African Americans in Oklahoma. Topics will include (1) establishing a research workgroup and a community advisory board for cancer disparity research with African Americans; (2) monitoring disparities associated with the COVID-19 pandemic and race-related social unrest and their impact on modifiable lifestyle-related cancer risk factors; and (3) improving cancer screening behavior among African Americans using mobile health technology and lay health educators. These efforts will serve as the foundation for building larger community-based interventions to promote cancer prevention and care and eliminate cancer-related health disparities among African Americans in Oklahoma.

Are discrimination and stressful life events associated with current substance use among adults experiencing homelessness?

Adam C. Alexander, Joseph J.C. Waring, Oluwakemi Olurotimi, Jasmin, Kurien, Bishop Noble, Michael S. Businelle, Chaelin K. Ra, Sarah J. Ehlke, Laili K. Boozary, Amy M. Cohn, & Darla E. Kendzor

The University of Oklahoma Health Sciences Center, Stephenson Cancer Center, TSET Health Promotion Research Center

Background

- Substance use is widespread among adults experiencing homelessness.
- Many homeless adults use multiple substances, which may worsen health outcomes and reduce the likelihood of successful cessation.
- Substances use may be a maladaptive coping mechanism for accumulated trauma and stress.

Aims & Hypotheses

- **Aim:** Describe stressful life events (SLE) and experiences of discrimination among adults experiencing homelessness and determine whether SLEs and discrimination are correlated with past 30-day substance use and substance use disorder (SUD).

- **Hypothesis:** SLEs and everyday discrimination will be associated with an increased likelihood of past 30-day substance use and screening positive for a substance use disorder.

Methods

- Homeless adults (N = 501) were recruited from a day shelter in Oklahoma City, Oklahoma, using word-of-mouth and flyers posted within the shelter. Adults were eligible to complete the study survey if they had a valid shelter identification card. Eligible participants completed a series of measures on a tablet computer, and study staff in a private room assisted participants who were unable to read.
- **Measures:** Participants completed a measure of stressful life events (i.e., Life Stressor Checklist-Revised) and perceived discrimination frequency (i.e., Every-day Discrimination Scale).
- Substance use was measured by asking participants about when they had last used these substances, with the following response options: "never used," "have used, but not in the past year," "have used in the past year, but not in the past 30-days," "have used in the past 30-days," and "have used yesterday." .
  - These questions were asked for the following substances: Cannabis, alcohol, opioids, amphetamine, crack, and cocaine use
- Past 30-day cigarette use was measured by asking participants, "have you smoked cigarettes or cigarillos in the past 30-days", with a yes (1) or no (0) response option.
  - Alternative tobacco product use was measured by asking participants whether they used at least one of the following nine tobacco products in the past-30 days: (1) snus, (2) roll-your-own cigarettes, (3) hookah or waterpipe, (4) dissolvable tobacco products, (5) electronic cigarettes, (6) cigars, (7) chewing tobacco, and (8) other products.
- Multiple substance use was operationalized as the total number of substances (i.e., cannabis, alcohol, cigarettes, ATPs [n = 8], opioids, amphetamine, crack, and cocaine) used in the past 30-days (min = 0 and max =14).
- Multivariable logistic regression models were used to determine whether SLEs and discrimination were associated with current substance use and multivariable linear regressions were used to evaluate the association of SLEs and everyday discrimination with multiple substance use.

Results

- As shown in **Table 1**, most participants (74.7%, n = 374) had used cigarettes or cigarillos in the past 30-days, 40.2% (n = 201) had used at least one ATP, and just over a third had used cannabis (39.5%, n = 198) and alcohol (39.5%, n = 198) in the past 30-days. Fewer adults in the sample reported past 30-day use of opioids (5.8%, n = 29), amphetamines (14.4%, n = 72), crack (2.4%, n = 12), or cocaine (3.2%, n = 16).
- As participants reported experiencing more SLEs, they also reported more everyday discrimination ($r = 0.42$, $p < .01$).
- As shown in **Table 2**, SLEs were associated with the increased odds of current cannabis (aOR = 1.37, p < .01), ATP (aOR = 1.41, p < .01), alcohol (aOR = 1.33, p = .01), illicit substance use (aOR = 1.47, p < .01). SLEs were also associated with currently using multiple substances (B = 0.47, p < .01).
- After accounting for SLEs, everyday discrimination was only associated with current cannabis use (aOR = 1.27, p = .02).

Table 1 Sample characteristics (N=501)

Variable	Mean (SD) or N (%)
Sex (% male)	361 (72.1%)
Age (years)	45.6 (SD = 11.8)
Race (% white)[a]	205 (40.9%)
Education (years)	11.6 (SD = 2.8)
Stressful life events	10.2 (SD = 6.4)
Everyday discrimination	1.8 (SD = 1.5)
Past-30 day substance use	71 (48.6%)
Cannabis	198 (39.5%)
Alcohol	198 (39.5%)
Cigarettes or cigarillos	374 (74.7%)
Alternative tobacco products[a]	201 (40.2%)
Opioids	29 (5.8%)
Amphetamine	72 (14.4%)
Crack	12 (2.4%)
Cocaine	16 (3.2%)
Multiple substance use	2.7 (SD = 2.2)

Table 2 Results of the associations of stressful life events and everyday discrimination with past 30-day substance use and substance use disorder (odds ratio, 95% CI)

	Cannabis	Alcohol	Cigarettes or cigarillos	Alternative tobacco products	Illicit substances [b]
SLEs and everyday discrimination analyzed in separate models					
Stressful life events	**1.52** (1.25, 1.86)	**1.35** (1.10, 1.66)	**1.31** (1.04, 1.65)	**1.40** (1.14, 1.71)	**1.49** (1.17, 1.89)
Everyday discrimination	**1.44** (1.19, 1.74)	1.17 (0.96, 1.41)	**1.31** (1.05, 1.64)	1.18 (0.98, 1.43)	1.19 (0.95, 1.49
SLEs and everyday discrimination analyzed in the same models					
Stressful life events	**1.37** (1.10, 1.71)	**1.33** (1.06, 1.67)	1.20 (0.93, 1.55)	**1.37** (1.10, 1.71)	**1.47** (1.13, 1.92)
Everyday discrimination	**1.27** (1.03, 1.57)	1.04 (0.84, 1.29)	1.22 (0.95, 1.56)	1.04 (0.85, 1.29)	1.02 (0.79, 1.31)

Note: Stressful life events and everyday discrimination scores were standardized with a mean of 0 and a standard deviation of 1. All models were adjusted for sex (Males vs. Females), age (years), education (years), and race (Whites [ref] vs. Blacks vs. American Indian/Alaskan Native vs. Other), and ethnicity.

Discussion

- SLEs were associated with an increase in the odds of current cannabis, alcohol, illicit, and multiple substance use.
- However, findings related to everyday discrimination were less consistent. Although when analyzed separated everyday discrimination was associated with various substance use outcomes, including cannabis, cigarette or cigarillo, and multiple substance use, after accounting for SLEs, everyday discrimination was only associated with the past 30-day prevalence of cannabis use.
- Overall, the findings highlight the links between SLEs and discrimination with substance use, though stronger and more consistent relations were observed between SLEs and substance use relative to findings for discrimination.
- Cessation and harm reduction interventions for substance use that provide psychotherapy to help homeless adults overcome traumatic stressors, such as physical and sexual abuse, and provide real-time stress-management for chronic discrimination, may help reduce substance use.
- Using these strategies and other innovative methods to decrease the consumption of substances will improve a range of health and psychosocial outcomes among adults experiencing homelessness and reduce health disparities in this underserved and understudied population.

Funding

This research and preparation of this manuscript were supported by the Oklahoma Tobacco Settlement Endowment Trust grant R21-02.

TOBACCO USE AND TREATMENT PREFERENCES AMONG ADULTS ACCESSING SERVICES AT A DAY SHELTER

Laili Kharazi Boozary, M.S.[1,4], Adam C. Alexander, Ph.D.[3,4], Joseph J. C. Waring, BPH[4], Summer G. Frank-Pearce, Ph.D., MPH [2,4], Sarah J. Ehlke, Ph.D.[4], Michael S. Businelle, Ph.D.[3,4], Amy M. Cohn, Ph.D.[4,5], and Darla E. Kendzor, Ph.D.[3,4]

[1] Department of Psychology, Cellular and Behavioral Neurobiology, The University of Oklahoma, Norman, OK, [2]Department of Biostatistics and Epidemiology, Hudson College of Public Health, The University of Oklahoma Health Sciences Center, Oklahoma City, OK, [3] Department of Family and Preventive Medicine, The University of Oklahoma Health Sciences Center, Oklahoma City, OK, [4] TSET Health Promotion Research Center, Stephenson Cancer Center, The University of Oklahoma Health Sciences Center, Oklahoma City, OK, [5] Department of Pediatrics, The University of Oklahoma Health Sciences Center, Oklahoma City, OK

Background: Although smoking rates have declined to 14% among adults in the U.S., 70-80% adults experiencing homelessness continue to smoke. Approaches are needed to address persisting tobacco-related health disparities. The current study characterized tobacco use and treatment preferences among adults accessing day shelter services.

Methods: Adults completed a survey at the Homeless Alliance Day Shelter in Oklahoma City to assess sociodemographic characteristics, tobacco history, tobacco treatment preferences, and substance use.

Results: Of participants, 75.2% (n=406) reported current smoking, and most wanted to quit (57.2%). Current smokers reported smoking 13.9 (SD=10.0) cigarettes per day (CPD; 57.1% smoked <10 CPD) and had been smoking for 23.3 (SD=12.7) years on average. Smokers were primarily male (74.9%), 45.7 (SD=11.2) years of age on average, and largely of White (41.1%, n=167), Black (25.9%, n=105), or American Indian (12.8%, n=52) race. A total of 7.2% (n=29) were veterans. The most commonly tried cessation aids included the nicotine patch (22.9%), nicotine gum/lozenges (19.0%), e-cigarettes (ECs; 14.5%), and the Oklahoma Tobacco Helpline (10.1%). Most had not previously tried any cessation aids (51.7%). Smokers most commonly endorsed cold turkey (25.1%), nicotine replacement therapy (24.6%), money or gift cards for quitting (17.2%), prescription medications (16.5%), and switching to ECs (16.0%) as offering the best chance for quitting. Participants most commonly reported cravings (54.7%), stress/mood (39.4%), habit (38.7%), and being around other smokers (36.2%) as the most difficult aspects of quitting. A total of 55.4% of all smokers reported interest in using ECs for smoking cessation and 14.5% had used ECs in the past 30 days. Smokers who reported past 30-day EC use more often used fruit/candy/other flavored (50.9%) or menthol/mint (22.0%) ECs vs. tobacco flavored (15.3%) ECs, and more frequently perceived some (39.0%) or extreme/a lot of risk (28.8%), vs. no/little risk (32.2%) associated with EC use. Past 30-day cannabis use (51.5%), heavy drinking (58.8%), and injection drug use (12.5%) were prevalent, as were mental illnesses including Generalized Anxiety Disorder (28.1%), Posttraumatic Stress Disorder (26.9%), and Major Depressive Disorder (22.5%).

Conclusion: Findings suggest that homeless shelter guests were interested in smoking cessation, though evidence-based treatments were underutilized. Smokers may benefit from education about cessation aids along with increased access. A focus on non-traditional smoking cessation approaches including EC switching and financial incentives for quitting may be warranted, and non-tobacco substance use and mental health problems may need to be considered and potentially addressed as part of a broader treatment approach.

TOBACCO USE AND TREATMENT PREFERENCES AMONG ADULTS ACCESSING SERVICES AT A DAY SHELTER

Laili K. Boozary, Adam C. Alexander, Joseph J. C. Waring, Summer G. Frank-Pearce, Sarah J. Ehlke, Michael S. Businelle, Amy M. Cohn, & Darla E. Kendzor

The University of Oklahoma Health Sciences Center, Stephenson Cancer Center, TSET Health Promotion Research Center, Oklahoma City, OK

Health Promotion Research Center

Background

- Adults experiencing homelessness have mortality rates 3x higher than the general population.
- 70-80% of homeless adults smoke despite studies showing that many 40-70%) report that they are ready to quit.
- Alternative cessation strategies may benefit those experiencing homelessness, particularly the treatments preferred by this population.

PURPOSE

- The current study describes the personal characteristics and treatment preferences of smokers accessing day shelter services.
- **Findings will inform future smoking cessation intervention approaches for adults experiencing homelessness and/or accessing shelter service.**

Methods

Participants

Eligibility Criteria

- Adults 18+ years old
- Utilizing Homeless Alliance Day Shelter

Key Measures and Scales

- Smoking Status
- Demographics
- Tobacco Use
  - Motivation to Stop Scale (Kotz et al., 2013)
  - Heaviness of Smoking Index (Kozlowski et al., 1994)
- Mental Health
  - PHQ-Depression (Spitzer et al., 1999)
  - GAD-7 (Kroenke et al., 2007)
  - Primary Care PTSD Screen (Prins et al., 2003)
- Substance Use
  - Texas Christian University Drug Screen 5 (Research, 2020)
  - Alcohol Quantity, Frequency, and Binge Drinking Questionnaire

Procedures

- Participants were approached by study staff and asked to complete surveys
- Participants were compensated for their time

Analytic Plan

- SAS 9.4
- Descriptive statistics: mean and frequency analyses
- Comparisons: chi-square and t-tests

Funding: This study was supported by funding from Oklahoma Tobacco Settlement Endowment Trust grant R21-02.

Results

Table 1: Demographic Characteristics of Smokers

Characteristic	Overall (n = 540)	Smokers (n = 406)
Age	45.65 ± 11.65	45.67 ± 11.19
Sex, Female	29.44 (159)	25.12 (102)
Race		
White	38.03 (205)	41.23 (167)
Black or African American	26.72 (144)	25.93 (105)
American Indian/Alaska Native	15.03 (81)	12.84 (52)
Latinx	11.32 (61)	10.86 (44)
Other	8.91 (48)	9.14 (37)
Currently Homeless	91.11 (492)	92.12 (374)
Marital Status, %single	82.09 (440)	84.12 (339)
Education, mean	11.53 ± 2.80	11.51 ± 2.62
Employment, % not employed	88.15 (476)	89.66 (364)
Insurance status, % uninsured	63.89 (345)	66.01 (268)
Household income, % <$5,000	69.39 (306)	70.00 (238)

Results *(cont.)*

See Table 1. Of the total sample, 75.19% (n = 406) were Smokers…

- 56.93% (n = 230) endorsed some desire to quit smoking,
- 51.29% (n = 159) of smokers were interested in a free smoking cessation program
- 25.12% (n = 102) participants endorsed Cold Turkey as offering the best chance of cessation success
- 55.38% (n = 211) were interested in using e-cigarettes as a smoking cessation strategy.
- **Top 3 Reasons for Using E-Cigarettes**: A) I can use it in places where cigarettes are not allowed (38.98%, n = 23), B) to help me quit smoking cigarettes (37.29%, n = 22), & C) to help me cut down on smoking cigarettes (37.29% n = 22)
- 71.54% (n = 186) reported a belief that God absolutely exists & (42.02 %, n = 221) participated in religious services at least once a week or more
- 22.51% (n = 88) had PHQ diagnosis of depression, 26.85% (n = 109) screened positive for PTSD, and 28.13% (n = 110) screened positive for moderate-severe GAD
- 31.20% (n = 122) screened positive for moderate or severe *SUD*
- 51.49% (n = 208) used marijuana in the past 30 days
- 23.02% (n = 90) engaged in heavy drinking
- 12.50% (n = 49) used needles to inject drugs within the past 6 months
- Only 43.10% of smokers reported owning a cell phone
- Only 41.94 (n = 164) reported that they were Extremely Confident in filling out medical forms (i.e. health literacy).
- 45.78% (n = 179) endorsed feeling anxious or uncertain about household food supply, 65.47% (n = 256) endorsed Insufficient Food Quality, and 63.17% (n = 247) endorsed Insufficient Food Intake

Results *(cont.)*

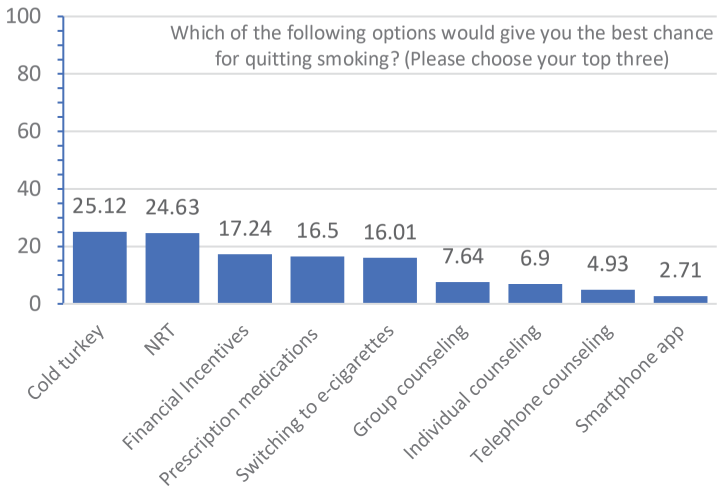

Conclusion

- Findings offer guidance about potential smoking cessation intervention strategies for adults accessing day shelter services.
- Interventions may need to provide education about effective smoking cessation treatments and incorporate alternative strategies such as financial incentives for quitting and e-cigarette switching. See Figure 1.
- Cessation intervention strategies must consider low health literacy, and high rates of mental illness, substance use, and food insecurity.

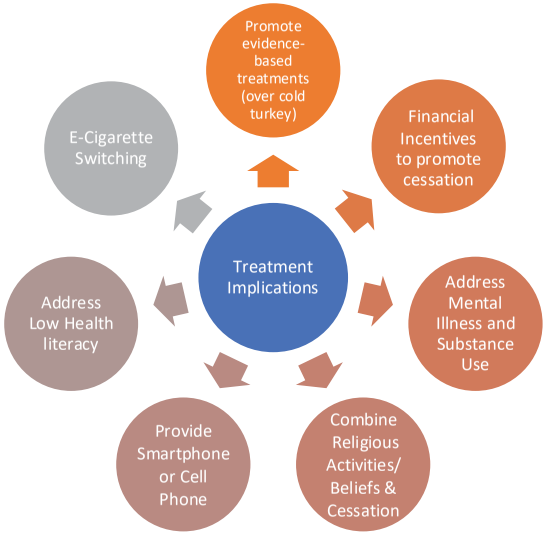

Figure 1. Implications and Recommendations for Smoking Cessation Interventions for Adults Experiencing Homelessness.

TSET

MEASURING DNA DAMAGE TO ASSESS THE USE OF ELECTRONIC CIGARETTES AS A TOBACCO HARM REDUCTION STRATEGY

Mayilvanan Chinnaiyan[1], Vengatesh Ganapathy[1], Balaji Sadhasivam[1], Yan D. Zhao[2], Theodore L. Wagener[4,5], Lurdes Queimado[1,3]

Departments of [1]Otorhinolaryngology, and [2]Biostatistics & Epidemiology; [3]TSET Health Promotion Research Center, Stephenson Cancer Center, The University of Oklahoma Health Sciences Center. [4]Center for Tobacco Research, The Ohio State University Comprehensive Cancer Center, and [5]The Ohio State University Wexner Medical Center.

Background and Aims: Millions of smokers across the U.S. struggle to quit tobacco daily. Nicotine replacement and counseling are essential tools in every smoking cessation plan. Electronic cigarettes (EC) deliver plasma nicotine levels similar to that seen in smokers, and deliver less chemicals than tobacco smoke. Thus, addressing the role of ECs in tobacco harm reduction is essential. Towards that goal, we quantified DNA damage in the oral epithelial cells of exclusive combustible tobacco users and dual users of EC devices.

Methods: Adult smokers who were not planning to quit were randomized to 3 distinct groups: "Usual Brand Cigarettes" (UBC), 2nd generation ECs (G2), or 3rd generation ECs (G3), and provided free tobacco products according to assigned group. Tobacco product use details, CO level, blood, saliva, oral mucosa and urine samples were collected at each visit. DNA was extracted from oral cells and damage was quantified by q-PADDA, at 3 time point visits (Week 0, 4, 12). Data analysis was performed using ANOVA model.

Results: Data from 93 participants (UBC=35, G2=27 and G3=31) are included in this report. At enrolment (week 0), there were no significant differences in age, sex or tobacco product use across groups. At 12 weeks, CO levels and combustible tobacco use were significantly reduced in G2 and G3 dual users (UBC=18±10, G2=6±7, G3=7±7 cig/day). A significant reduction in the levels of oral mucosa DNA damage at 4 and 12 weeks (2 to 6 fold) was observed in dual users of combustible tobacco and G2 EC devices, but not G3 devices, when compared with exclusive combustible tobacco users.

Conclusion: Our study shows that when provided with EC devices, smokers significantly reduced the number of combustible cigarettes smoked. Dual users of combustible tobacco and G2 EC devices have significantly lower the levels of DNA damage in their oral mucosa compared with exclusive combustible tobacco or G3 dual users. These data suggest that 2nd generation EC devices are an effective harm reduction tool.

Grant support: NIH/NCI (R01CA204891, Wagener; R01CA242168, Queimado) and PHF (Queimado). Dr. Queimado holds a PHF Endowed Chair in Otorhinolaryngology.

MEASURING DNA DAMAGE TO ASSESS THE USE OF ELECTRONIC CIGARETTES AS A TOBACCO HARM REDUCTION STRATEGY

Mayilvanan Chinnaiyan[1], Vengatesh Ganapathy[1], Balaji Sadhasivam[1], Yan D. Zhao[2], Theodore L. Wagener[4,5], Lurdes Queimado[1,3]

Departments of [1]Otorhinolaryngology, and [2]Biostatistics & Epidemiology; and [3]TSET Health Promotion Research Center, Stephenson Cancer Center, The University of Oklahoma Health Sciences Center. [4]Center for Tobacco Research, The Ohio State University Comprehensive Cancer Center, and [5]The Ohio State University Wexner Medical Center

Background

- Millions of smokers across the U.S. struggle to quit tobacco use daily due to nicotine addiction.
- Electronic cigarettes (EC) provide an alternative mode of nicotine delivery.
- EC use has increased since users perceive them as safe. In 2020, about 3.6 million youth nationwide reported currently using ECs.
- Besides nicotine, EC aerosol contains harmful chemicals and known carcinogens.
- Studies reported that EC aerosol causes DNA damage and suppresses DNA repair proteins.

Aims

- To determine whether ECs can reduce tobacco harm, we quantified DNA damage in oral epithelial cells of exclusive combustible tobacco users and dual users of 2nd and 3rd generation ECs.

Methods

- Adult smokers who were not planning to quit in the next three months were randomized into 3 distinct groups.

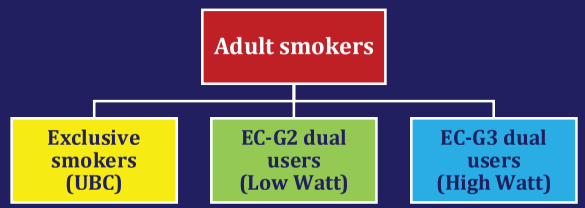

Methods

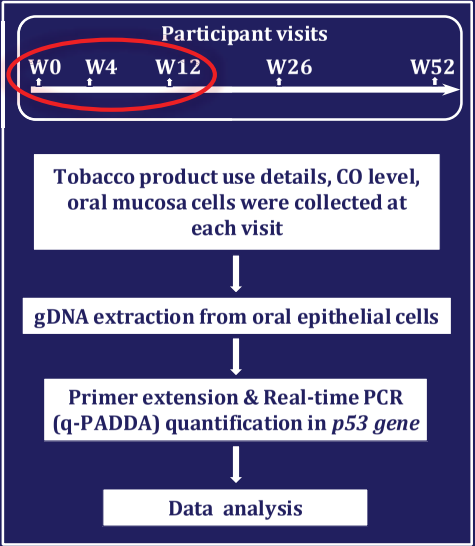

Results

	Exclusive smokers (UBC)	EC-G2 dual users	EC-G3 dual users
Cases (#)	35	27	31
Age (y)	42±12	42±13	43±14
Sex (M:F)	12:13	7:20	11:20

Table 1: Participants demographic details. There was no difference observed in age across the groups. Data shown as Mean ± SD.

Grant Support

NIH/NCI (R01CA204891, Wagener; R01CA242168, Queimado) and the PHF (Queimado). Dr. Queimado holds a PHF Endowed Chair in ORL.

Results

	Exclusive smokers (UBC)			EC-G2 dual users			EC-G3 dual users		
Weeks	W0	W4	W12	W0	W4	W12	W0	W4	W12
Tob. cigs/day	17 ± 10	18 ± 10	18 ± 10	16 ± 8	8 ± 7	9 ± 8	17 ± 7	9 ± 7	8 ± 7
E-cig puffs /day	0	0	0	0	65 ± 140	89 ± 198	0	57 ± 67	52 ± 57
Watts	-	-	-	-	7.7 ± 1.1	8.2 ± 1.0	-	26 ± 12	28 ± 16
CO (ppm)	24 ± 16	22 ± 17	23 ± 21	26 ± 14	20 ± 19	16 ± 16	26 ± 16	18 ± 12	19 ± 16

Table 2: Tobacco product use over time and markers of exposure. There was a reduction in the number of tobacco cigarettes and CO levels observed at 4 & 12 weeks in dual users of tobacco and electronic cigarette. Data shown as Mean ± SD.

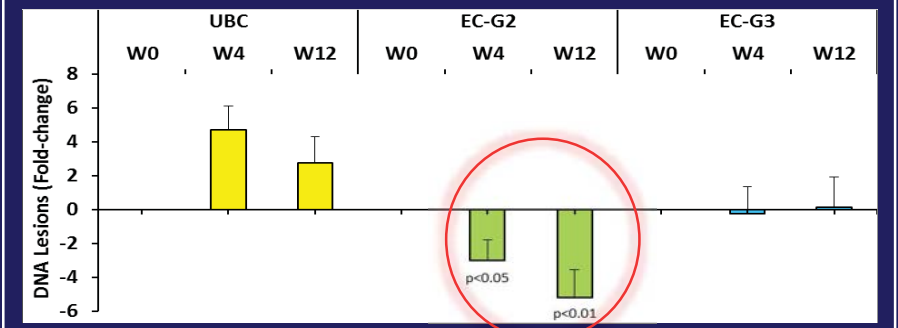

Figure 1: Fold-change in DNA damage quantified by q-PADDA in UBC, EC-G2, EC-G3 dual users over time. Dual users of EC-G2 showed a significant reduction in oral mucosa DNA damage at 4 and 12 weeks (2-6 fold). No significant reduction was observed in exclusive smokers or dual users of EC-G3. Data shown as Mean ± SEM and t test.

Conclusions

- Smokers reduced the number of combustible cigarettes when they are provided with EC devices.
- Our preliminary data show that EC-G2 users significantly reduced the oral mucosa DNA damage.
- These data suggest that EC-G2 are an effective harm reduction tool.

CONFLICTING INFORMATION EXACERBATES EMOTION-RECOGNITION DEFICITS IN TEENAGERS AT RISK FOR CARCINOGEN SUBSTANCE USE OR ABUSE

B. Espinoza-Varas
Communication Sciences & Disorders, OU Health Sciences Center

Among teenagers, an early marker of risk for carcinogen substance use or abuse (CSUA) is failure to comply with role-model verbal directives such as “quit smoking, say no to alcohol,” the compulsory nature of which is conveyed by emotional voice tones (lenient, stern, angry, etc.); understanding the causes of this failure is critical for preventing and rehabilitating CSUA. Among other things, complying requires sensitivity to and correct recognition of the voice-tone emotion, especially in information- or response-conflict conditions that impose executive-function demands (e.g., engaging inhibitory control upon hearing “quit smoking”). In addition to activating automatic, bottom-up as well as voluntary, top-down attention mechanisms, the emotional voice tone elicits negative affect, and feedback from emotion neural activity (e.g., amygdala) could help activate and sustain neural activity necessary for behavioral control (e.g., prefrontal cortex). Here, the effects of imposing information or response conflict (i.e., executive-functions demands) on the ability to discern the voice tone (lenient versus stern) of impeding (e.g., quit!) or instigating (e.g., do it!) verbal directives were measured in three conditions: 1) in the absence of information conflict; 2) while attempting to inhibit potent but inappropriate responses prompted by conflicting ear-laterality information (inhibitory-control demands); and 3) while having to switch between incompatible response-mapping rules from trial to trial (cognitive-flexibility demands). Participants included two non-CSUA teenager samples, one with positive (FH+) the other with negative (FH−) family history of alcohol-use disorder, but matched in intelligence, depression, anxiety, handedness, socioeconomic status, and Child Behavior Check List scores. In all conditions, the percent voice-tone recognition errors were significantly larger in FH+ than in FH− teenagers, and larger with instigating than with impeding verbal directives. The between-sample differences were small in the absence of conflict but grew larger with laterality and more so with set-shifting conflict, suggesting that emotion recognition deficits of FH+ teenagers are more pronounced when dealing with information and /or response conflict (e.g., complying with parental versus peers verbal directives). Deficits in the recognition of voice-tone emotions could account in part for the increased risk of CSUA in FH+ teenagers. Research funded by the Alcohol Beverage Medical Research Foundation.

CONFLICTING INFORMATION EXACERBATES EMOTION-RECOGNITION DEFICITS IN TEENAGERS AT RISK FOR CARCINOGEN SUBSTANCE USE OR ABUSE

B. Espinoza-Varas (Communication Sciences & Disorders, OU Health Sciences Center)

METHOD

Participants. Alcohol-abstinent healthy teenagers (mean age=17.5 years). Family History of alcohol abuse: positive (FH+) in 20 of them, negative (FH-) in the other 21. **Verbal directives spoken in lenient or stern voice-tone (VT)** by Native-English talker, four impeding (quit, halt, stop, back off) and four instigating (do it, start, begin, go). **Task.** On the left or right earphone, each trial presented the cue word "left" or "right" spoken in neutral **VT** followed by an impeding or an instigating target voice directive, spoken in stern or lenient **VT** (e.g., left→quit). The cue matched the ear side to reinforce the laterality information effect. Participants identified the target **VT** tone as lenient or stern by pressing a left- or right-hand key. **Stimulus-Response Mapping**. For Impeding directives, lenient or stern **VT** mapped onto left- or right-hand responses, and this mapping was reversed for instigating directives. **No-conflict VT recognition (NC)**. Assessed the ability to identify the **VT** in the absence of information or response conflict, presenting only impeding or only instigating directives. On each trial, the cue and target were presented in both ears and perceived at the center of the head instead of lateralized to the left or right ear.

CONFLICTING INFORMATION

Laterality and loudness conflict (LC). Assessed effects of information and response conflict on **VT** recognition; trials presented only impeding or only instigating directives and the cue and ear side could be incongruent (in conflict), or congruent (no conflict) with the correct response side. **Example:** in a conflict trial, the cue word "left" followed by the directive "quit" uttered in stern **VT** were presented on the left ear; the cue and ear side prompted a "left" response, but its **VT** called for an incongruent "right" response. Being correct required ignoring the cue and ear side, suppressing a "left" key response, attending selectively to the target **VT**, and pressing the "right" key. Owing to the tendency to respond with the hand matching the ear side, these condition assessed inhibitory control for potent responses prompted by laterality cues that were in conflict with the voluntary mapping of responses to **VT**. **Set-switching conflict (SS)**, Presented both impeding and instigating directives within each trial block, and being correct required adhering to the respective mapping of **VT** to response side. That is, on each trial participants had to discern the target **VT** (lenient or stern) and its voice directive set (impeding or instigating). Across trials, they had to switch mapping rules depending on the directive, impeding or instigating.

RESULTS

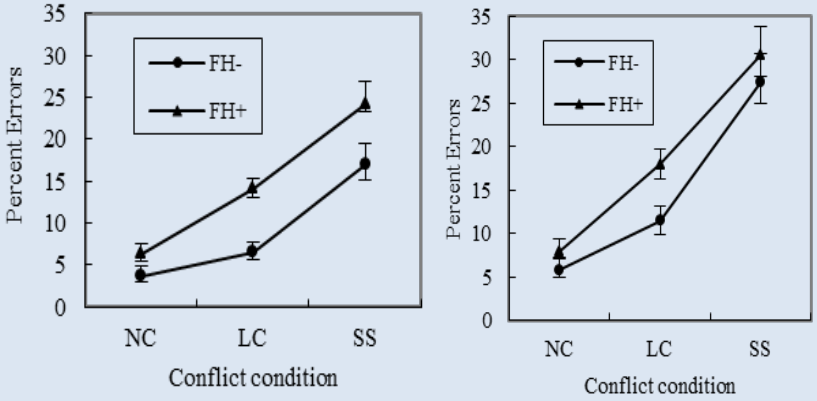

Percent VT recognition errors for impeding (left) and instigating (right) directives in FH- and FH+ teenagers. Three conditions (X-axis): no-conflict (NC), laterality-loudness (LC), set-switching conflict (SC.). In all conditions, percent errors were higher in participants with positive (FH+) rather than negative (FH-) family history, and this trend is largest in laterality-loudness and switching conditions than in no-conflict conditions.

CONCLUSIONS

FH+ participants seem to have a deficit in the ability to discern lenient from stern **VT**, especially in the midst of information or response conflict. Recognizing accurately the **VT** of regulatory directives is important to regulate behavior (e.g., underage drinking). A **VT** recognition deficit could increase the risk of engaging in underage drinking. The present tasks seem to have high sensitivity at detecting cognitive deficits associated with family history, especially since the samples sizes are quite small.

Funded by Alcohol Beverage Medical Research Foundation

THE RELATIONSHIP BETWEEN TRAVEL BURDEN AND HPV-ASSOCIATED CANCER SURVIVAL OUTCOMES: AN ANALYSIS OF THE UNIVERSITY OF OKLAHOMA MEDICAL CENTER CANCER REGISTRY, 2005-2019

Sameer V. Gopalani[1] (Sameer-Gopalani@ouhsc.edu), Lance Ford[1], Hanh Dung Dao[1], Nancy Etzold[2], Janis E. Campbell[1], Amanda E. Janitz[1]

[1] Department of Biostatistics and Epidemiology, Hudson College of Public Health, [2] University of Oklahoma Medicine Cancer Registry

Introduction: Travel burden for cancer can impact diagnosis, treatment, and patient outcomes. However, the relationship between travel burden from HPV-associated cancer (cervical, vulvar, vaginal, penile, anal, and oropharyngeal cancers) and survival outcomes remains poorly understood. Therefore, we 1) estimated the 5-year survival rates and 2) assessed the association between travel distance to a cancer center and overall survival for patients with HPV-associated cancers.

Methods: Patients included in this study (*N*=3,407) received care for HPV-associated cancers at the University of Oklahoma Medical Center (OUMC) from January 1, 2005 to December 31, 2019. Network analysis was conducted in ArcGIS (v10.8) to individually calculate the unidirectional distance from each patient's geocoded residential address at diagnosis to OUMC. Patients were categorized based on short (<25 miles), intermediate (25-74.9 miles), and long (75+ miles) travel distances to define our study exposure. The outcome of interest was overall survival and defined as the time from the date of initial diagnosis to the date of last contact. Survival analyses were undertaken in SAS (v9.4) using Kaplan-Meier estimation and Cox proportional hazard models to evaluate the association between travel distance and overall survival.

Results: Of the 3,407 patients who received treatment for an HPV-associated cancer at OUMC, 1,547 (45.4%) traveled a short distance to OUMC, while 773 (22.7%) and 1,087 (31.9%) traveled intermediate and long distances, respectively. The proportion of deaths were 33.2% (513/1547), 41.5% (321/773), and 36.0% (391/1087) among the short, intermediate, and long travel distance groups, respectively. Furthermore, the 5-year survival rates were 66%, 60%, and 63% for the short, intermediate, and long travel distance groups, respectively. In univariate analysis, travel distance to treatment was associated with overall survival (*p*=0.003). The hazard of death was 1.26 (unadjusted hazard ratio [HR]; 95% confidence interval [CI]: 1.10, 1.45) times greater among patients in the intermediate travel group compared to those in the short distance group. We observed no difference in the hazard of death among patients in the long distance group compared to those in the short distance group (unadjusted HR=1.14; 95% CI: 1.0, 1.3). The findings of this study are limited by the moderately high percentage of censored observations (64%).

Conclusions: Initial findings from our analysis indicate that patients in the intermediate distance group had a higher hazard of death than those who traveled the shortest distance to OUMC. Future analyses will consider the association between travel distance and overall survival in the presence of confounders and effect modifiers.

Acknowledgement of Funding: LF, HDD, and SG are supported by the Hudson Fellows in Public Health program through the University of Oklahoma Health Sciences Center.

CIGARETTE SMOKING AND QUIT BEHAVIORS ARE ASSOCIATED WITH SEXUAL ORIENTATION TRANSITION BETWEEN WAVES 1 AND 4 OF THE POPULATION ASSESSMENT OF TOBACCO AND HEALTH (PATH) STUDY

Afsheen Hasan, Sydney A. Martinez
Presenting author's email: Afsheen-Hasan@ouhsc.edu
Department of Biostatistics and Epidemiology

Funding: No funding

Introduction: Sexual and gender minority (SGM) populations experience poorer health outcomes compared to their non-SGM counterparts. Studies suggest individuals who change sexual orientation over time report increased substance use. We examined sexual orientation transition and the association between that transition and smoking prevalence and quit behaviors.

Methods: Data from Waves 1 and 4 of PATH were used to examine transition of sexual orientation among adults age 18 years and older and the association between sexual orientation transition and cigarette use. We calculated weighted proportions and performed chi-square tests to examine if the transition in sexual orientation was associated with smoking prevalence and quit behaviors from Wave 1 to Wave 4.

Results: Overall, 21,285 adults participated in both waves. Based on weighted proportions, 5.2% of US adults identified as Lesbian, Gay, Bisexual or something else (LGB) at Wave 1, of whom 34.7% (n=426) transitioned to straight by Wave 4. Among individuals who identified as straight in Wave 1, 1.8% (n=494) transitioned to LGB by Wave 4. Current smoking status remained similar among individuals who were LGB in both waves (30.9% in 1 and 31.4% in 4), straight in both waves (17.6% in 1 and 17.9% in 4), and LGB in Wave 1 and straight in Wave 4 (21.9% in 1 and 22.1% in 4). Current smoking prevalence significantly increased between waves for individuals who identified themselves as straight in Wave 1 and LGB in Wave 4 (18.9% in 1 and 22.9% in 4). Individuals who transitioned from straight to LGB were significantly less likely to quit smoking. Among this group, only 14.8% of Wave 1 current smokers were no longer smoking at Wave 4 compared to 16.7% for those who remained LGB, 17.9% for those who remained straight, and 19.8% for those who were LGB and then straight.

Conclusion: Although smoking prevalence is highest among LGB individuals, the burden of increasing smoking and unsuccessful quitting is higher among individuals who transition from straight to LGB status. Examining smoking patterns among individuals experiencing transition in SGM identity is essential to address disparities in these unique populations.

Cigarette smoking and quit behaviors are associated with sexual orientation transition between Waves 1 and 4 of the Population Assessment of Tobacco and Health (PATH) Study

Afsheen Hasan, Sydney Martinez
Department of Biostatistics and Epidemiology, Hudson College of Public Health

BACKGROUND

•Sexual and gender minority (SGM) populations experience poorer health outcomes compared to their non-SGM counterparts. Individuals who change sexual orientation over time report increased substance use.

•We examined sexual orientation transition and the association between that transition and smoking prevalence and quit behaviors.

METHODS

•Data from Waves 1 and 4 of PATH were used to examine transition of sexual orientation among adults age 18 years and older and the association between sexual orientation transition and cigarette use.

•We calculated weighted proportions and performed chi-square tests to examine if the transition in sexual orientation was associated with smoking prevalence and quit behaviors from Wave 1 to Wave 4.

RESULTS

•Overall, 21,285 adults participated in both waves.
•Based on weighted proportions, 5.2% of US adults identified as Lesbian, Gay, Bisexual or something else (LGB) at Wave 1.
•Table 1 displays number and percentages of LGB at Wave 1 and their transition by Wave 4.

Figure 1: : Slopegraph showing effect of change in sexual orientation identity among adults age 18 and over between Wave 1 and Wave 4

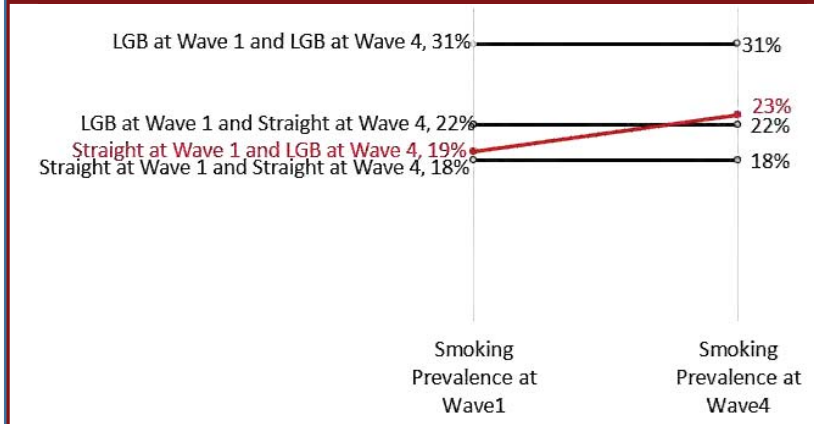

Table 1: Number and percentages of LGB at Wave 1 and their transition by Wave 4, n=20,702

		LGB in wave 4, n (%)		
		Yes	No	Total
LGB in Wave 1, n (%)	Yes	1082 (3.4)	426 (1.8)	1508 (5.2)
	No	494 (1.7)	18700 (93.2)	19194 (94.9)
	Total	1576 (5.1)	19126 (95)	20,702

Quit Behaviors

Individuals who transitioned from straight to LGB from Wave 1 to Wave 4 were significantly less likely to quit smoking
- 14.8% of Wave 1 current smokers were no longer smoking at Wave 4

Compared to:
- 16.7% for those who remained LGB
- 17.9% for those who remained straight
- 19.8% for those who were LGB and then straight

CONCLUSION

Although smoking prevalence is highest among LGB individuals, the burden of increasing smoking and unsuccessful quitting is higher among individuals who transition from straight to LGB status. Examining smoking patterns among individuals experiencing transition in SGM identity is essential to address disparities in these unique populations.

HUDSON COLLEGE OF PUBLIC HEALTH
The UNIVERSITY of OKLAHOMA HEALTH SCIENCES CENTER

POTENTIAL OF PHARMACEUTICAL INTERVENTION IN PLATELETS AND CANCER POSITIVE FEEDBACK LOOP

Zitha Redempta Isingizwe[1] and Doris M. Benbrook, PhD[1,2]

[1]Department of Pharmaceutical Sciences [2]Stephenson's Cancer Center, University of Oklahoma Health Sciences Center, Oklahoma City, 73104

Significance: High platelet counts and advanced stage of ovarian cancer go hand-in-hand in promoting each other in a feed-forward loop that results in coagulation and chemotherapy resistance.

Objective and Hypothesis We sought to develop an experimental model of the positive interactions between platelets and cancer cells and test the hypothesis that interference with platelet clotting will inhibit this interaction.

Approach: The contribution of platelets to cancer or normal epithelial cell spheroid's size and density were evaluated using a magnetic 3D cancer spheroids assay. Viability of these spheres was evaluated using MTT and SRB cytotoxicity assays and H&E staining. The shear-free platelet aggregation assay was performed in the presence of cancer cells to evaluate their contribution to platelets stimulation. Furthermore, we evaluated possible interruption of this feed-forward loop using antiplatelet agents: aspirin—a cyclooxygenase (COX)-1 and -2 inhibitor, celecoxib—a selective COX-2 inhibitor, clopidogrel—an ADP binding inhibitor, dipyridamole—an ADP uptake inhibitor, eptifibatide—a platelet's GP IIb/IIIa inhibitor, and prostacyclin—a platelet aggregation inhibitor.

Results: Incubation of platelets with cancer spheroids as they are forming decreased the size and density of the spheres within 15 minutes of exposure. Cytotoxity assays and H&E staining indicated that these spheres were live and viable. Western blot analysis suggested that the process was independent of E-Cadherin, N-cadherin or occluding expression. Incubation of cancer cells with platelets caused clumping of platelets in a cancer cells number-dependent manner. Pre-treating platelets with up to 1mM of aspirin, clopidogrel, dipyridamole, and prostacyclin did not prevent cancer cell-induced aggregation, unlike celecoxib, which prevented aggregation at high concentrations, and eptifibatide, which was able to prevent aggregation at low concentrations as 0.1 μM.

Conclusions: The positive interaction between platelets and cancer cells can be mimicked in co-culture conditions. This interaction appears to involve platelets GPIIb/IIIa binding, but not prostaglandins, E- and N-cadherin or occludin.
This project was funded by NCI R01 CA196200

POTENTIAL OF PHARMACEUTICAL INTERVENTION IN PLATELETS AND CANCER POSITIVE FEEDBACK LOOP

Zitha Redempta Isingizwe[1] (zitha-isingizwe@ouhsc.edu) and Doris M. Benbrook, Ph.D. [1,2]

[1]Departement of Pharmaceutical Sciences [2]Departement of Obstetrics and Gynecology, Gynecologic Cancer Program, Stephenson Cancer Center, University of Oklahoma Health Sciences Center, Oklahoma City, OK, USA

INTRODUCTION

Cancer is the second leading cause of deaths worldwide after cardiovascular diseases. A commonality between cancer and cardiovascular diseases is dysregulation of platelets. Ovarian cancer patients present with thrombocytosis (a platelet count ≥450 000/µL), which correlates with chemoresistance and poor prognosis. The ovarian clear cell carcinoma histology has the highest incidence of blood coagulation and platelet aggregation, chemoresistance, and venous thromboembolisms (VTE), and VTE as a cause of death. Platelets and cancer are known to promote each other in a feedforward mechanism that is poorly understood. In the current study, we aimed to develop an experimental model to study interventions that could disrupt the cancer/platelets loop by using antiplatelet agents.

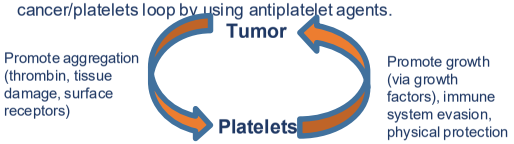

OBJECTIVES

The objectives of this study were to:

1. Evaluate reciprocal effects of cancer cells and platelets on each other

2. Evaluate loop disruption using anti platelet agents: aspirin—a cyclooxygenase (COX)-1 and -2 inhibitor, celecoxib—a selective COX-2 inhibitor, clopidogrel—an ADP binding inhibitor, dipyridamole—an ADP uptake inhibitor, eptifibatide—a platelet's GP IIb/IIIa inhibitor, and prostacyclin—a platelet aggregation inhibitor.

RESULTS

I : Incubation of platelets with cancer spheroids as they are forming decreased the size and density of the spheres within 15 minutes of exposure

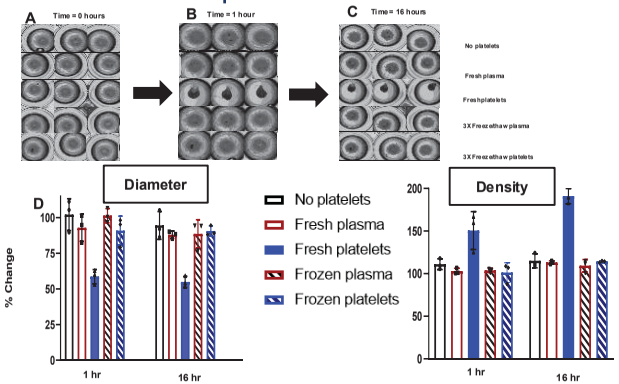

Figure 1. 60% confluent cells were magnetic sensitized by co-incubating with NanoShuttle™ Biocompatible nanoparticles 24 hours prior to forming the spheres. Once cells were confluent, extra nanoparticles were washed off and cells were cultured on a 96 wells plate on top of magnetic spheroid drive holder to facilitate the formation of cell aggregates for 1- 4 hours. The magnet were removed and the resulting spheroids are imaged using Optronix GelCount colony counter **(A)** Before treatment with either control culture media, fresh plasma, fresh platelets, plasma or platelets after 3 cycle of freeze-thaw at -80 and 37°C **(B)** One hour post treatment **(C)** 16 hours posttreatment **(D)** Quantified cancer spheroids density and diameter.

II. Exposure of magnetic spheroids to platelets did not induce cell death

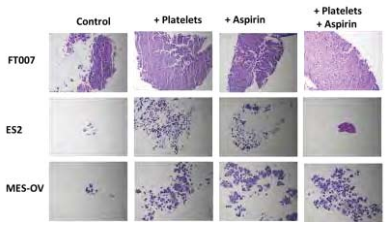

Figure 2 60% confluent cells were magnetic sensitized by co-incubating with NanoShuttle™ Biocompatible nanoparticles 24 hours prior to forming the spheres. Once cells were confluent, extra nanoparticles were washed off and 10^5healthy fallopian tube (FT007), ovarian clear cell carcinoma cells (ES2) or high grade serous ovarian cancer cells were cultured resuspend in culture media and plated on a 96 wells plate on top of magnetic spheroid drive holder to facilitate the formation of cell aggregates for 1- 4 hours. Wells were pretreated with either control culture media or 100 µM aspirin prior to addition of 10^7 platelets. Spheres were incubated for 72 hours, fixed in formalin and an H&E staining was performed.

III. Platelets did not alter the viability of the cells in the spheroids

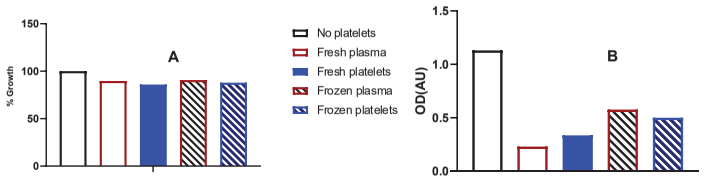

C

Treatment	Live %	Cell size (µM)
Control (No platelets)	8	15.17
With fresh plasma	6	18.33
With fresh platelets	13	17.45

Figure 3 Magnet sensitized 10^5 cancer cells were cultured in 150 µl of culture media and plated on a 96 wells plate on top of magnetic spheroid drive holder to facilitate the formation of cell aggregates for 1- 4 hours. Wells were treated with either control culture media, fresh plasma, fresh platelets, plasma or platelets after 3 cycle of freeze-thaw at -80 and 37°C. (A) Quantified MTT viability assay after overnight incubation (B) Quantified SRB protein assay after overnight incubation (C) live cells % and size after 72 hours incubation

IV. Eptifibatide inhibits shear free tumor cell induced platelet aggregation at low concentration

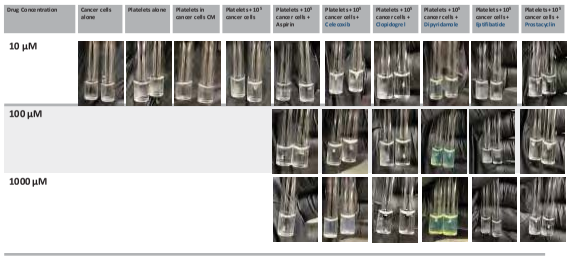

Figure 4. 2.10^8 platelets in 250 µl of phenol red free DMEM/F-12 media) were incubated with 10^5 cancer cells or 250 µl of overnight conditioned media (CM). Cancer cells alone, plasma without platelets alone or platelets alone were used as controls. Cells were resuspended in phenol red free DMEM/F-12 prior to use, and the dilutions with the same media were utilized so that all wells end up with the same amount of liquids. Cancer cells/platelets mixtures were immediately treated with 10, 1000 or 1000 µM of one of the antiplatelet agents in duplicates : aspirin, celecoxib, clopidogrel, dipyridamole, eptifibatide or prostacyclin.

V. Incubation of cancer cells with platelets caused clumping of platelets in a cancer cells number dependent manner

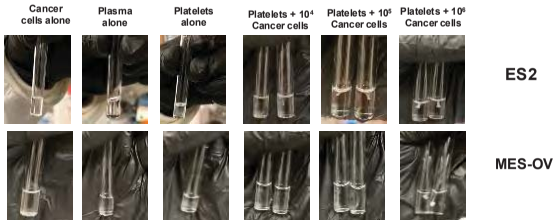

Figure 5. 2.10^8 platelets in 250 µl of phenol red free DMEM/F-12 media were incubated with either, plama with no platelets, media control or with ES2 or MESOV cancer cells : 10^4 ,10^5 , or 10^6cancer cells. Cancer cells alone in the absence of platelets or plasma were used as control.

VI. Healthy cells conditioned media failed to induce aggregation

Figure 6. 2.10^8 platelets were incubated with 250 µl of overnight conditioned phenol red free DMEM/F-12 media from healthy fallopian tube primary cultures (FT100) or clear cell carcinoma cells (ES2)

CONCLUSIONS

- The positive interaction between platelets and cancer cells can be mimicked in co-culture conditions.
- Platelets increase cancer spheres density and decrease spheres size while cancer cells induce platelets aggregation.
- Platelet/cancer cells interaction appears to involve platelets GPIIb/IIIa binding, but not, cox-1 or cox-2, prostaglandins,
- The exact mechanism of this feed-forward loop remains an active area of investigation in our lab.

FUTURE DIRECTIONS

1. Identify components in cancer cell conditioned mead responsible for inducing platelet aggregation
2. Quantified platelets aggregation assays in the presence of shear stress
3. Conduct receptor/ligand binding and interaction studies with the GPIIb/IIIa platelet receptor
4. *In vivo* assays using animal models
5. Healthy and cancer patients' derived platelet studies

ACKNOWLEDGMENTS

- This project was funded by NCI R01 CA196200 and the University of Arizona Lauder Alberts Gift.
- H&E staining was performed by the Stephenson Cancer Center Tissue Pathology Core facility.

EFFECT OF CONTINUED TOBACCO USE ON HEAD AND NECK CANCER TREATMENT OUTCOMES AND PATIENT SURVIVAL

Matthew Krutz[1], Rachad Mhawej[1], Vijay Raj[1], Lane Driskill[1], Geraldine Chissoe[1], Pawan Acharya[4], Daniel Zhao[3,4], Lurdes Queimado[1-3]

Departments of [1]Otorhinolaryngology, [2]Cell Biology, and [4]Biostatistics & Epidemiology; [3]TSET Health Promotion Research Center, Stephenson Cancer Center, The University of Oklahoma Health Sciences Center, Oklahoma.

Background and Aims: Resistance to chemo and/or radiation therapy presents a major obstacle in the long-term effectiveness of cancer treatment. Following an initial head and neck cancer diagnosis, continued tobacco use is causally related to both all-cause and cancer-specific mortality. Here, we evaluate the impact of smoking cessation in therapy response and survival outcomes among patients with head and neck cancer who presented as smokers at diagnosis.

Methods: Patients diagnosed with oral or oropharyngeal squamous cell carcinoma who were treated with intent to cure (n=324) at the OU Medical Center between 2006 and 2018 were included in this study. Clinical and demographic data was retrospectively collected. Patients were grouped by smoking status at diagnosis: never smoker, former smoker, or current smoker. Current smokers were further separated into two groups based on whether they quit smoking before treatment initiation or not. Primary outcomes included response to first line of therapy and overall survival. Categorical and continuous variables were analyzed by chi-square and t-test, respectively. Difference in survival between groups was estimated by cox proportional-hazards model.

Results: 106 patients were never-smokers, 82 were former smokers, and 136 were current smokers. There were no differences in age and sex across groups. Within the current smoker group, 56 (41%) stopped smoking before initiating cancer therapy. Current smokers who quit before initiating cancer treatment achieve higher rates of complete response to first line therapy than those who continue to smoke (86 % versus 72.5%). Current smokers who quit before cancer therapy had significantly higher overall survival (p=0.02) than current smokers who continued to smoke during cancer therapy.

Conclusions: Our study shows that patients who continue smoking during chemo-radiation have decreased response to cancer therapy and lower overall survival compared to patients who stopped smoking before cancer treatment. Thus, patients who quit smoking at diagnosis of head and neck cancer can obtain a survival benefit.

Grant support: Presbyterian Health Foundation (PHF) and NIH/NCI (R01CA242168, LQ). Dr. Queimado holds a PHF Endowed Chair in Otorhinolaryngology.

EFFECT OF CONTINUED TOBACCO USE ON HEAD AND NECK CANCER TREATMENT OUTCOMES AND PATIENT SURVIVAL

Matthew Krutz[1], Rachad Mhawej[1], Vijay Raj[1], Lane Driskill[1], Geraldine Chissoe[1], Pawan Acharya[4], Daniel Zhao[3,4], Lurdes Queimado[1-3]

Departments of [1]Otorhinolaryngology, [2]Cell Biology, and [4]Biostatistics & Epidemiology; [3]TSET Health Promotion Research Center, Stephenson Cancer Center, The University of Oklahoma Health Sciences Center, Oklahoma.

Introduction

- Resistance to chemo and/or radiation therapy presents a major obstacle in the long-term effectiveness of cancer treatment.
- Following an initial head and neck cancer diagnosis, continued tobacco use is causally related to both all-cause and cancer-specific mortality.
- We hypothesize that cessation of tobacco use at cancer diagnosis will improve response to therapy and survival outcomes.

Specific Aims

1. To evaluate the impact of smoking cessation on response to first-line therapy among patients who presented as smokers at diagnosis.
2. To evaluate the impact of smoking cessation on survival outcomes among patients who presented as smokers at diagnosis.

Materials & Methods

- Patients with oral or oropharyngeal squamous cell carcinoma who were treated with intent to cure at the OU medical center between 2006 and 2018 were included.
- Clinical and demographic data was retrospectively collected.
- Patients were grouped based on smoking status at diagnosis: never smokers, previous smokers, current smokers who quit, and current smokers who continued smoking.
- Primary outcomes included response to first line of therapy and overall survival

Results

		Never Smokers	Previous Smokers	Current smokers who quit at diagnosis	Current smokers who didn't quit at diagnosis	P-value
Age		59.7 ± 12.1	63.4 ± 10	56.1 ± 9.4	55.8 ± 9.9	
Sex	Male	80 (75%)	60 (73%)	41 (73%)	69 (86%)	0.1606
	Female	26 (25%)	22 (27%)	15 (27%)	11 (14%)	
Treatment Group	Chemo & Radiation	44 (42%)	33 (40%)	20 (36%)	41 (51%	0.2411
	Surgery + Chemo & Radiation	38 (36%)	22 (27%)	16 (29%)	21 (26%)	
	Radiation + Surgery	24 (23%)	27 (33%)	20 (36%)	18 (23%)	
Primary Site	Oral Cavity	44 (42%)	40 (49%)	31 (55%)	24 (30%)	0.0168
	Oropharynx	62 (58%)	42 (51%)	25 (45%)	56 (70%)	
Stage	1	5 (5%)	3 (4%)	1 (2%)	2 (3%)	0.2231
	2	6 (6%)	14 (17%)	2 (4%)	7 (9%)	
	3	28 (26%)	11 (13%)	12 (21%)	21 (26%)	
	4A	62 (58%)	50 (61%)	38 (68%)	46 (58%)	
	4B	5 (5%)	4 (5%)	3 (5%)	4 (5%)	

Table 1. Population Characteristics Across Smoking Status Groups.

	Current smokers who didn't quit at diagnosis	Current smokers who quit at diagnosis	P-value
No/Partial Response	22 (28%)	8 (14%)	0.0674
Complete Response	58 (73%)	48 (86%)	

Table 2. Response to treatment in different smoking status groups. Data was analyzed using a Chi-square test.

	Current smokers who didn't quit at diagnosis	Current smokers who quit at diagnosis	P-value
Deceased	27 (34%)	9 (16%)	0.0215
Alive	53 (66%)	47 (84%)	

Table 3. Vital Status in different smoking status groups. Data was analyzed using a chi-square test.

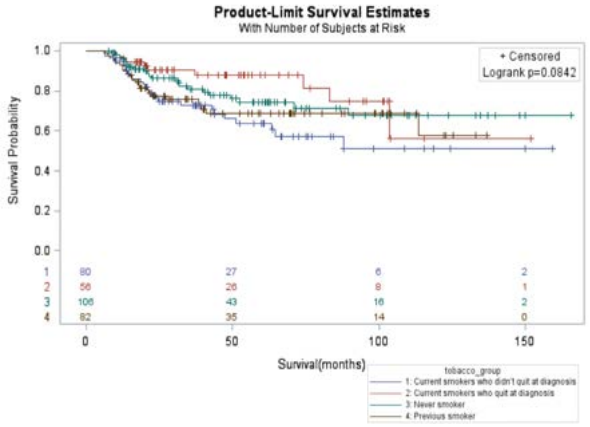

Figure 1: Overall Survival, Kaplan-Meier Survival Curve.

Parameter	Pr>ChiSq	Hazard Ratio	95% CI
Current smokers who quit at diagnosis	0.0249	0.421	0.198-0.897
Never smokers	0.0726	0.600	0.344-1.048
Previous smokers	0.4128	0.794	0.458-1.378

Table 4: Analysis of Maximum Likelihood Estimates. Current smokers who didn't quit smoking at diagnosis were used as the reference group.

Conclusions & Future Directions

- Current smokers at time of head and neck cancer diagnosis who quit smoking before therapy may respond better to chemo and/or radiation therapy.
- Current smokers at time of head and neck cancer diagnosis who quit smoking before therapy have higher overall survival compared to patients who continued smoking during treatment.
- Our data suggests that patients who quit smoking at diagnosis of head and neck squamous cell carcinoma respond better to therapy and can obtain a survival benefit.
- A prospective study would further validate these findings.

Funding

- Presbyterian Health Foundation (PHF) and NIH/NCI (R01CA242168, LQ and NCI/SCC P30CA225520). Dr. Queimado holds a PHF Endowed Chair in Otorhinolaryngology

HYPERTENSION DRUG OLMESARTAN MEDOXOMIL PROMOTES COLONIC TUMORIGENESIS IN AOM-INDUCED CRC RAT MODEL

Nandini B Kumar, Venkateshwar Madka, Yuting Zhang, Gopal Pathuri, Janani Panneerselvam, Nicole Stratton, Anil Singh, Chinthalapally V Rao
cv-rao@ouhsc.edu
Center for Cancer Prevention and Drug Development, Hem-Onc Section, Department of Medicine, Stephenson Cancer Center, University of Oklahoma Health Sciences Center, Oklahoma City, OK

Some retrospective studies suggest an inverse risk-association between the use of angiotensin signaling inhibitors and colorectal cancer (CRC). The angiotensin receptor blocker olmesartan medoxomil (OLM) is commonly prescribed for hypertension treatment. Here we sought to determine the chemopreventive efficacy of OLM using the azoxymethane (AOM)-induced CRC rat model. Male and female F344 rats (n=6/gender/group) were randomized and subcutaneously injected with 20 mg/kg of AOM once weekly for two weeks. One week later, AIN76-A diets containing OLM (0 ppm to 480 ppm) were fed to rats. Six weeks after treatment, rats were euthanized and evaluated for toxicity and aberrant crypt foci (ACF) inhibition. OLM-fed rats, particularly at ≥160 ppm, showed signs of toxicity. There was a modest decrease in the total ACFs without any change multicrypt ACFs in male rats; however in females there was an increase in multicrypt ACFs as compared to the control diet group. For tumor efficacy evaluation, 5-week-old F344 rats were randomized (n=30/gender/group) and CRC was induced as above. At the adenoma stage (12-weeks after AOM-treatment), rats were administered OLM (0, 20 and 40 ppm) in the diet for 33 weeks, and colonic tumors were evaluated. In the control group, there was a huge disparity in colonic tumor incidence and multiplicity between genders with ~3-fold less tumors in female rats. Surprisingly, colon tumor incidence was significantly increased (3-fold; $P<0.0002$) in the OLM-treated female rats (77% OLM vs 24% control). Colon tumor multiplicity analysis also showed tumor promoting effects. In the 20 ppm OLM-treated male and female rats, colonic adenocarcinoma multiplicities were increased by ~91% ($p<0.01$) and ~362% ($p<0.0001$), respectively, when compared with their respective controls. Although there was no dose response, similar tumor promoting effects were found in 40 ppm OLM-treated rats. To understand male vs female colon tumor disparities and OLM tumor promoting effects, we carried out RNA-Seq analysis of colonic tumors. Reflecting tumor data, gene expression analysis also showed significant differences between male and female rats with respect to type II-interferon, PI3K-AKT, cholesterol, lipid droplet, mucin, IL-3, cell-cycle and nucleotide GPCR signaling pathways. OLM treatment significantly upregulated 586 and 740 genes, and downregulated 648 and 564 genes in male and female rat tumors, respectively. Of the 293 common genes identified, Irx5, Lrrn1, Ly6g6e, Sccpdh, Hoxd12, Igfbp1, Krt81 and DSC3 were upregulated up to 245-fold; and Rfxapl1, Serpinb3a, REg3b, Bnc1 and Ak4 were down-regulated 10 - 200-fold with OLM treatment. In conclusion, chronic administration of OLM did not provide any chemopreventive benefit against colonic tumors in the AOM-induced F344 rat CRC model. Further studies are warranted to assess the risk of colon cancer associated with long-term OLM use, particularly in females. (*Supported by NCI* HHSN261201500038I)

Hypertension drug Olmesartan Medoxomil promotes colonic tumorigenesis in AOM-induced CRC rat model

Nandini Kumar[1], Venkateshwar Madka[1], Yuting Zhang[1], Gopal Pathuri[1], Janani Panneerselvam[1], Nicole Stratton[1], Anil Singh[1], Chinthalapally V Rao[1,2]

[1]Center for Cancer Prevention and Drug Development, Hem-Onc Section, Department of Medicine, Stephenson Cancer Center, University of Oklahoma Health Sciences Center, and [2]VA Medical Center, Oklahoma City, OK

Email: vmadka@ouhsc.edu / cv-rao@ouhsc.edu

BACKGROUND

- Colorectal cancer (CRC) is a commonly diagnosed cancer in men and women.
- Retrospective studies suggest an inverse risk-association between the use of angiotensin signaling inhibitors and CRC.
- The angiotensin receptor blocker Olmesartan medoxomil (OLM) is commonly prescribed for hypertension treatment.
- Here we sought to determine the chemopreventive efficacy of OLM using the azoxymethane (AOM)-induced CRC rat model.

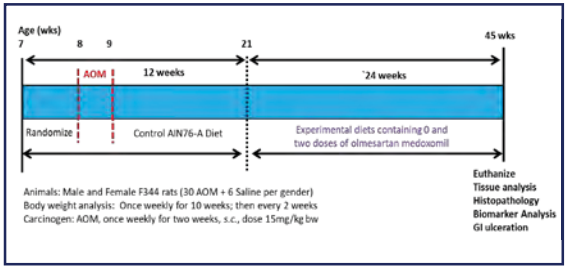

METHODS

- ❑ *For dose selection & ACF study*: Male and female F344 rats (n=6/gender/group) were randomized and given AOM injection s.c. (20 mg/kg) once weekly for two weeks.
- One week later, AIN76-A diets containing OLM (0 ppm to 480 ppm) were fed to rats.
- After six weeks of OLM treatment, rats were euthanized and evaluated for toxicity and aberrant crypt foci (ACF) inhibition.

- ❑ *For tumor efficacy evaluation*, 5-week-old F344 rats were randomized (n=30/gender/group) and AOM was injected to induced CRC as described above .
- At the adenoma stage (12-weeks after AOM-treatment), rats were administered OLM (0, 20 and 40 ppm) in the diet for 33 weeks.
- At 45 weeks age, rats were euthanized and colonic tumors were evaluated.

- ❑ *Transcriptome analysis*: RNA extracted from control and OLM treated colonic tumors was evaluated for gene expression changes using Illumina RNA seq analysis.

Fig 2. Effect of OLM on AOM induce rat colonic ACF.

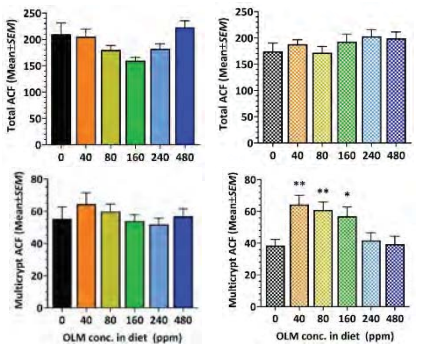

Fig 3. Effect of OLM on body weigh gain in rats.

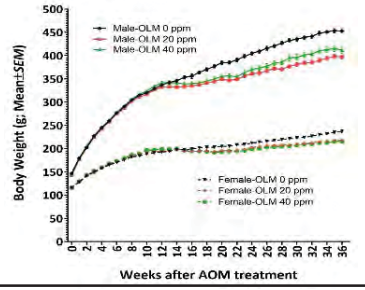

Fig 4. Effect of OLM treatment on AOM induce colonic tumors incidence & multiplicity in male (blue) and female (pink) rats.

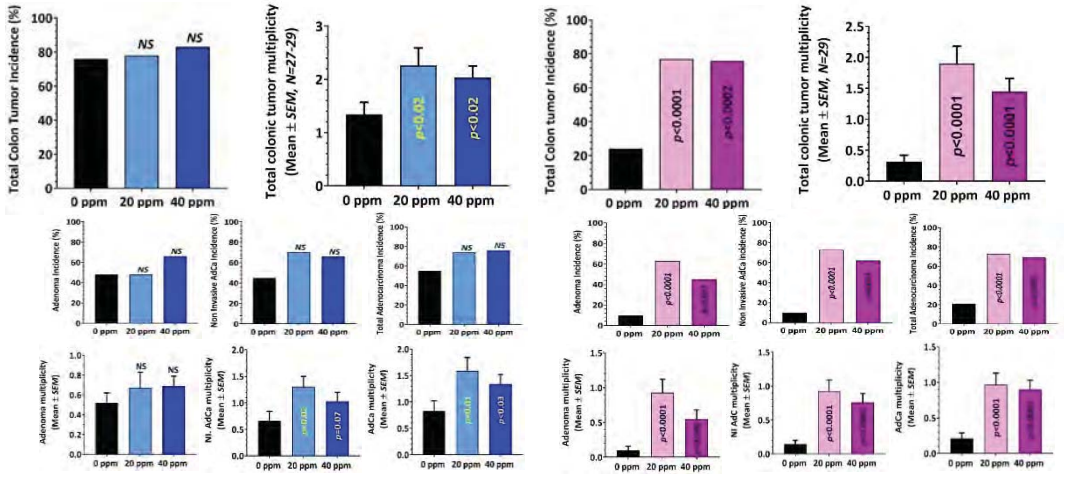

Fig 5. Effect of OLM on rat colonic tumors gene expressions.

	Male	Female
UP	197	187
DOWN	96	106
Total	293	293

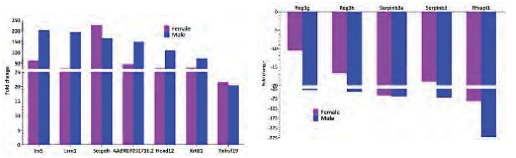

RESULTS & CONCLUSIONS

- OLM-fed rats, particularly at ≥160 ppm, delayed body weight gain. With similar body weight delay was observed with lower doses in long term efficacy study.
- There was no significant changes in multicrypt ACFs formation in male rats. In females there was an increase in multicrypt ACFs as compared to the control diet group.
- There was a huge disparity in colonic tumor incidence and multiplicity between genders. Female rats had ~3-fold less tumors compared to male rats on control diet.
- OLM treatment led to significant increase of colon tumor incidence (3-fold; P<0.0002) in female rats, when compared to its control (77% OLM vs 24% control).
- Colon tumor multiplicity data clearly suggested tumor promoting effects of OLM. In the 20 ppm OLM-treated male and female rats, adenocarcinoma multiplicities were increased by ~91% (p<0.01) and ~362% (p<0.0001), respectively, when compared with their respective controls.
- OLM treatment significantly upregulated 586 and 740 genes, and downregulated 648 and 564 genes in male and female rat tumors, respectively. Of the 293 common genes identified, Irx5, Lrrn1, Ly6g6e, Sccpdh, Hoxd12, Igfbp1, and Krt81 were upregulated up to 245-fold; and Rfxapl1, Serpinb3a, REg3b, Bnc1 and Ak4 were down-regulated 10 - 200-fold with OLM.
- Pathway analysis of RNA-Seq data also showed significant differences between male and female rats with respect to type II-interferon, PI3K-AKT, cholesterol, lipid droplet, mucin, IL-3, cell-cycle and nucleotide GPCR signaling pathways.
- In conclusion, chronic administration of OLM did not provide any chemopreventive benefit against colonic tumors in the AOM-induced F344 rat CRC model. Further studies are warranted to assess the risk of colon cancer associated with long-term OLM use, particularly in females.

(Supported by NCI HHSN261201500038I and VA Merit Award)

BESTATIN, A LTA4 HYDROLASE INHIBITOR PREVENTS INTESTINAL TUMORS IN THE APC MUTANT RODENT MODELS REPRESENTING FAP PATIENTS

Venkateshwar Madka, Gopal Pathuri, Hari Prasad Gali[1], Nandini Kumar, Nagendra Sastry Yarla, Anh Bao, Adam S Asch[2], CV Rao

Presenting author's email: vmadka@ouhsc.edu, cv-rao@ouhsc.edu

Center for Cancer Prevention and Drug Development, [1]College of Pharmacy, University of Oklahoma HSC, Oklahoma City, OK, [2]Stephenson Cancer Center, Department of Medicine

Colorectal cancer (CRC) is the third most common cancer in the United States with an estimated 145,600 new cases and 51,020 deaths in 2019. Studies suggest leukotriene B4 (LTB4) synthesized by leukotriene A4 hydrolase (LTA4H) enzyme plays a role in carcinogenesis. LTA4H over expression and increased LTB4 levels were found in CRC tissues that correlated with stage and poor survival. Hence we investigated repurposing bestatin (Ubenimex), an orally active potent reversible small molecule inhibitor of LTA4H to prevent CRC in high-risk FAP patients using APC mutant preclinical rodent models. Six week old *Apc*$^{min/+}$ male and female mice (n≥15) were assigned to control and treatment groups. After administering bestatin (0 ppm or 1000 ppm) in diet for 14 weeks, mice were euthanized and intestines were evaluated for tumors.

Control diet fed *Apc*$^{min/+}$ mice developed colonic tumor with multiplicity at 1.35±0.16 (Mean±*SEM*) in males and 0.86±0.13 in females. Colonic tumor incidence was 91% and 73% in the male and female mice respectively. Additionally, *Apc*$^{min/+}$ mice developed 30.52±1.66 (male) and 29.57±2.74 (female) small intestinal polyps (SIP). Dietary bestatin led to strong suppression of intestinal tumor development. While bestatin treated male mice had 55% less colonic tumors (0.60±0.21; $p<0.01$), the female mice had 59% less colon tumors (0.35±0.12; $p<0.008$) as compared to their respective controls. Importantly colonic tumor incidence was inhibited by >50% in both genders. Bestatin administration was reduced colonic tumor incidence by 56% ($p<0.001$) in male and 52% ($p<0.026$) in female mice. Small intestinal polyps (SIPs) were also significantly less in the treated mice compared to untreated. Male mice developed 29% less SIP (21.67±2.32; $p<0.006$) while female had showed 46% fewer SIP (16.00±1.98; $p<0.0005$) in comparison to control diet fed group.

PIRC (polyposis in rat coli) rats model that replicates CRC in FAP patients. PIRC rats (n=6) at 8 weeks age were randomized by polyp number after colonoscopy, and assigned to control and bestatin (1000 ppm) groups for 8 weeks. Colonic polyp development in each rat was evaluated by colonoscopy after treatment. Bestatin treatment led to strong suppression of colonic polyps. In the post-treatment period significantly lower (~72% less; $p<0.005$) colonic polyps were observed in PIRC rats. Pharmacokinetic analysis suggested dietary bestatin yielded substantial levels of agent in serum (15µg/mL) and colon content (up to 250 µg/g). LTB4 levels in the plasma and colon tumors were also significantly lowered by ~70% ($p<0.004$) and ~26% ($p<0.01$). Colonic tumors from the treated animals also showed an increase in NK and NKT cells suggesting immune-modulatory effects of the agent. In summary bestatin demonstrated excellent safety profile, pharmacokinetics, and chemopreventive effects against CRC in preclinical models and warrants further validation clinically.

Bestatin, a LTA4 hydrolase inhibitor prevents intestinal tumors in the APC mutant rodent models representing FAP patients

Venkateshwar Madka, Gopal Pathuri, Hariprasad Gali, Nandini Kumar, Nagendra S. Yarla, Anh Bao, Adam S Asch, Chinthalapally .V. Rao

Center for Cancer Prevention and Drug Development, Hem-Onc Section, Department of Medicine, Stephenson Cancer Center, University of Oklahoma Health Sciences Center, Oklahoma City, OK

Email: vmadka@ouhsc.edu / cv-rao@ouhsc.edu

Background

- Colorectal cancer (CRC) is the third most common cancer in the US with an estimated 145,600 new cases and 51,020 deaths in 2020.
- Studies suggest leukotriene B_4 (LTB_4) synthesized by leukotriene A_4 hydrolase (LTA_4H) enzyme plays a role in colon tumorigenesis.
- LTA_4H over-expression and increased LTB_4 levels are found in CRC that correlates with stage and poor survival .
- Bestatin (Ubenimex), an orally active potent reversible small molecule inhibitor of LTA_4H and enhancer of immune function
- Hence we investigated repurposing bestatin to prevent CRC in high-risk FAP patients using APC mutant preclinical rodent (mice and rats) models.

Objectives

1. *To determine the chemopreventive efficacy of bestatin against intestinal tumors in Apc $^{min/+}$ mouse model.*
2. *Effect of bestatin treatment on colonic polyposis in APC-mutant (PIRC) rats.*
3. *Evaluate the biomarkers of efficacy of bestatin.*

Methodology

- Six week old Apc $^{min/+}$ male and female mice (n≥15) were assigned to control and treatment groups. After administering bestatin (0 ppm or 1000 ppm) in diet for 14 weeks, mice were euthanized and intestines were evaluated for tumors.
- PIRC (polyposis in rat coli) rats model that replicates CRC in FAP patients. PIRC rats (n=6) at 8 weeks age were randomized by polyp number after colonoscopy, and assigned to control and bestatin (1000 ppm) groups for 8 weeks. Colonic polyp development in each rat was evaluated by colonoscopy after treatment.
- Colonic tumors and serum from each group was analyzed for pharmacodynamics biomarkers of efficacy.

(Supported by Kerley-Cade Endowed Chair & SCC funds)

Intestinal tumors prevention by bestatin in Apc $^{min/+}$ mice

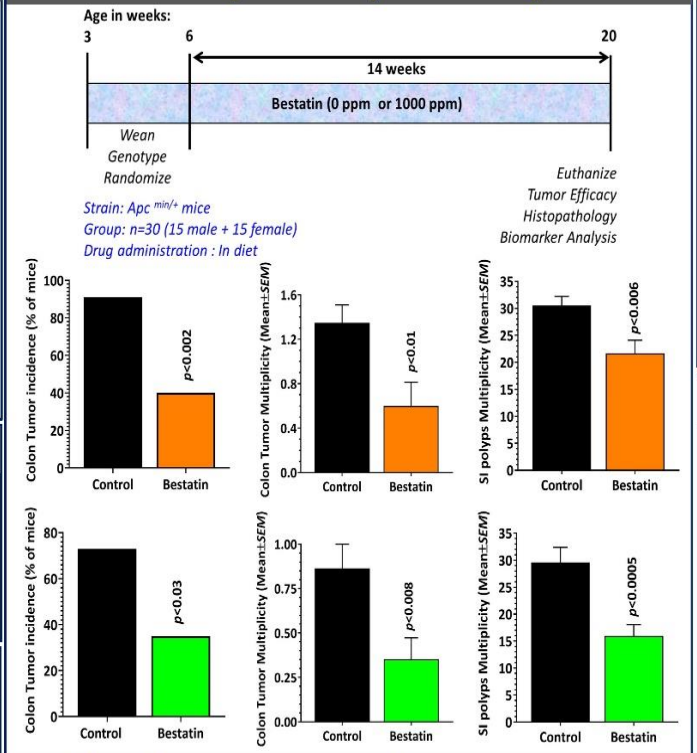

Effect of bestatin on tumor infiltrating immune cells

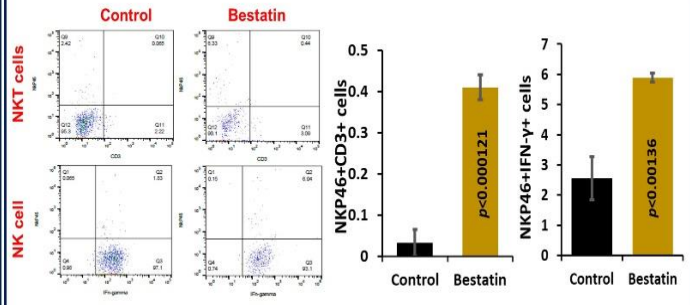

Effect of bestatin on colonic polyps & LTB4 levels in PIRC rat

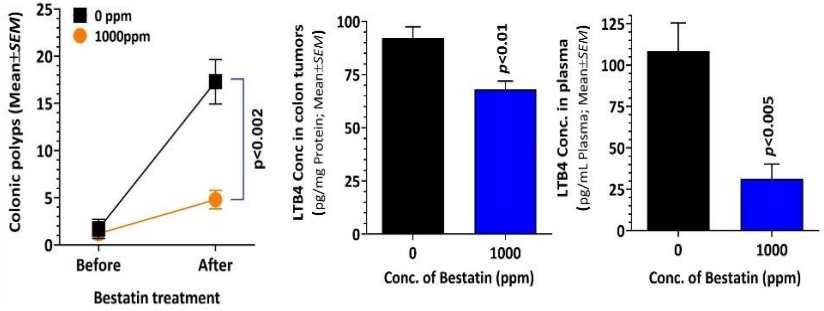

Principle findings & Conclusion

- Control diet fed *Apc $^{min/+}$* mice developed colonic tumor with multiplicity at 1.35±0.16 (Mean±SEM) in males and 0,.86±0.13 in females. Colonic tumor (CT) incidence was 91% and 73% in the male and female mice respectively.
- Control mice also developed 30.52±1.66 (male) & 29.57±2.74 (female) small intestinal polyps.
- Dietary bestatin led to strong suppression of CT development in male mice by 55% (0.60±0.21; p<0.01), & in the female mice by 59% (0.35±0.12; p<0.008) as compared to the controls.
- Bestatin administration was reduced CT incidence by 56% (p<0.001) in male and 52% (p<0.026) in female mice.
- SIPs were also significantly less in bestatin treated male mice (29% less; 21.67±2.32; p<0.006) while female showed 46% fewer SIP (16.00±1.98; p<0.0005) in comparison to controls mice.
- In PIRC rats also, bestatin treatment led to strong suppression of colonic polyps with ~72% less colonic polyps post-treatment period compared to pre-treatment.
- Pharmacokinetic analysis suggested dietary bestatin yielded substantial levels of agent in serum (15µg/mL) and colon content (up to 250 µg/g).
- LTB_4 levels in the plasma and colon tumors were also significantly lowered by ~70% (p<0.004) and ~26% (p<0.01).
- Colonic tumors from the treated animals also showed an increase in NK and NKT cells suggesting immune-modulatory effects of the agent.
- In summary, bestatin demonstrated excellent safety profile, and chemopreventive effects against CRC in preclinical models and warrants further validation clinically.

THE IMPACT OF GUT MICROBIAL TOXINS AND PGE2 ON IL-23 PRODUCTION AND ITS ROLE IN OBESITY ASSOCIATED COLORECTAL TUMORIGENESIS

Janani Panneerselvam[1], Venkateshwar Madka[1], Rajani Rai[2], Parthasarathy Chandrakesan[2], Courtney W. Houchen[2], Dharambir K. Sanghera[3], Katherine T. Morris[2], Chinthalapally V. Rao[1]
Janani-panneerselvam@ouhsc.edu
[1]Center for Cancer Prevention and Drug Development, [1,2]Stephenson Cancer Center, [3]Department of Pediatrics, University of Oklahoma Health Sciences Center, Oklahoma City, OK.

Colorectal cancer (CRC) is the second leading cause of cancer deaths in the United States. Studies indicate that excessive intake of high-fat diet (HFD) promotes CRC by modulating gut microbiome-associated inflammatory mediators. Recent evidence suggests that interleukin-23 (IL-23) plays an important role in the impact of a HFD on obesity, the gut microbiome and colon carcinogenesis. Our study aimed to elucidate the role of IL-23 in obesity associated CRC and explore an anti-IL-23 approach for prevention and treatment. First we profiled human plasma (n=15/arm) for circulating IL-23 levels and found significantly higher levels ($p<0.0001$) in obese individuals (BMI>30). In addition, IL-23 expression was evaluated in colonic tumors from both humans and preclinical rodent models. Data from the Cancer Genome Atlas showed significant over expression ($p<0.0001$) of IL-23A in CRC tumors (n=262) compared to normal tissue (n=41). This overexpression correlated with reduced disease free survival. Levels of both IL-23 and its receptor (IL23R) were evaluated in matched human CRC tissues and sporadic (AOM-induced rat CRC) rodent model when compared to matched normal mucosa by western blot and IHC and confirmed overexpression in CRC. These data reveal a clear association of IL-23 overexpression with both obesity and colonic tumorigenesis. To understand IL-23 production in the context of gut microbial toxins and PGE2 levels, we performed several mechanistic studies to mimic the tumor microenvironment. To elucidate PGE2-mediated regulation of IL-23 in colon tumorigenesis we studied both macrophages and dendritic cell lines in *in vitro* and *ex vivo* conditions. The immune cells treated with either PGE2 or bacterial toxins (LPS/LTA) showed a significant increase in IL-23 production which associated with macrophage polarization and dendritic cell phenotypic changes. Interestingly, when CaCo2 cancer cells were co-cultured with PGE2/LTA-LPS-educated macrophages or dendritic cells, the cancer cells displayed enhanced IL-23 along with increased tumor cell proliferation and self-renewal. Upon addition of human recombinant IL-23 directly to cancer cells (CaCo2 and HCT116), the cells exhibited increased IL-23R expression along with enhanced self-renewal, cell migration and invasive properties as well as loss of epithelial barrier permeability. In *ex-vivo* experiments we found that treatment of rat colon tumors with PGE2 increased the expression of IL-23 compared to normal mucosa. Overall our study results demonstrate that IL-23 is associated with both obesity and poor survival of CRC patients and that PGE2 and gut microbe toxins play an important role in IL-23-associated colonic tumor progression. This newly identified nexus represents a potentially important target for prevention of obesity associated colorectal cancer.

Funding provided by Kerley-Cade Chair Endowment and Stephenson Cancer Center.

The impact of gut microbial toxins and PGE_2 on IL-23 production and its role in obesity associated colorectal tumorigenesis

Janani Panneerselvam[1], Venkateshwar Madka[1], Rajani Rai[2], Parthasarathy Chandrakesan[2], Courtney W. Houchen[2], Dharambir K. Sanghera[3], Katherine T. Morris[2], Chinthalapally V. Rao[1]

[1]Center for Cancer Prevention and Drug Development, [1,2]Stephenson Cancer Center, [3]Department of Pediatrics, University of Oklahoma Health Sciences Center, Oklahoma City, OK

BACKGROUND

- Colorectal cancer (CRC) is the second leading cause of cancer deaths in the United States.
- Excessive intake of high caloric and/or high-fat diets (HFD) promotes obesity and risk of CRC by modulating gut microbiome-associated inflammatory mediators.
- Interleukin-23 (IL-23) is pro-inflammatory cytokine belongs to an IL-12 family consist of heterodimeric p40 and p19 subunits.
- Recent evidence show that IL-23 is highly expressed in a broad spectrum of cancers, including colon, ovaries, lung, breast, stomach, skin, liver, and head and neck.
- IL-23 plays an important role in the impact of a HFD on obesity, the gut microbiome and colon carcinogenesis.
- However, the underlying mechanism of obesity-associated inflammatory mediators and dysbiosis mediated activation of innate immunity and associated IL-23 secretion for colon tumor progression require more understanding.

OBJECTIVE

To determine the role of IL-23 in obesity associated CRC and explore mechanisms by which IL-23 is stimulated by gut microbes and colonic tumors. Design anti-IL-23 approaches to CRC prevention and treatment.

METHODS

TCGA Colon Cancer (COAD) Data:

The colon cancer (COAD) RNA-seq datasets (551 samples) from TCGA-COAD database were used.

Human Samples:

Serum samples from obese and non-obese patients were collected per IRB approval.

AOM-F344 rat study:

Colonic tumors and matched colonic mucosa from F344 rats (carcinogen-induced CRC) were collected and used for protein expression analysis.

In vitro study:

- Colon cancer cells were treated with recombinant human IL-23. Cells were used for organoid culture, migration, invasion assays, and cell lysates were prepared for western blotting analysis.
- THP-1 derived iDCs and macrophages were educated with Arachidonic acid (AA), (50μM), PGE_2 (10μM), LTA (10μg/ml) and LPS (1μg/ml) for 24 hours. The culture conditioned medium was collected for IL-23 (ELISA) analysis.
- Co-culture of educated DCs/macrophages with CaCo2 cells were carried out and the culture medium was collected for IL-23 (ELISA) analysis and tumor cells were utilized for organoid culture.

RESULTS

Fig. 1: Increased IL-23A expression in colon cancer is correlated with obesity and reduced disease-free survival

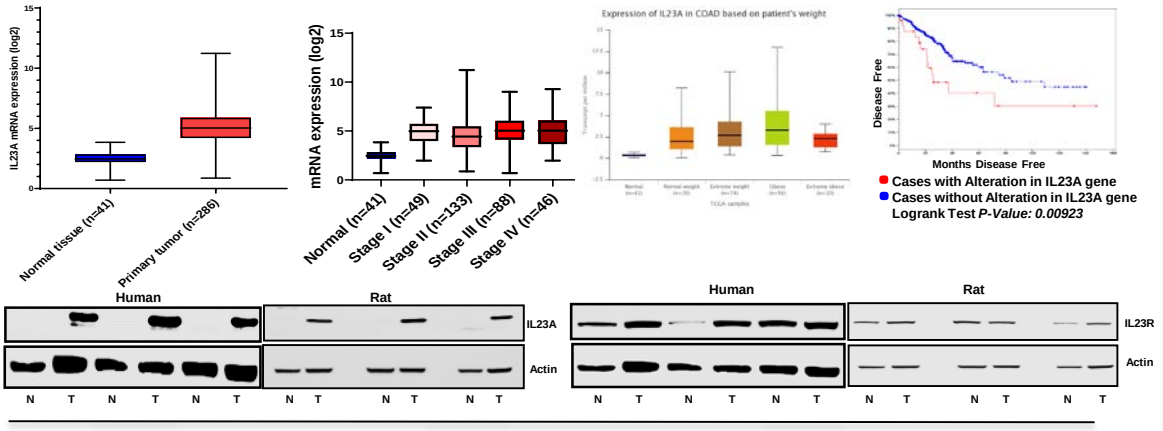

Fig. 2: IL-23 increases colon cancer progression

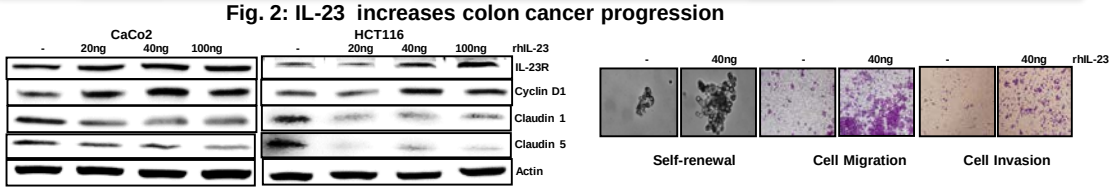

Fig. 3: Effect of AA, PGE_2, bacterial toxins on IL-23 production in dendritic cells

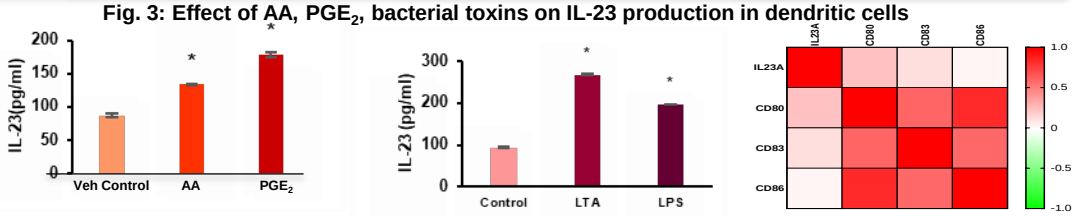

Fig. 4: Effect of AA, PGE_2, bacterial toxins on IL-23 production in macrophages

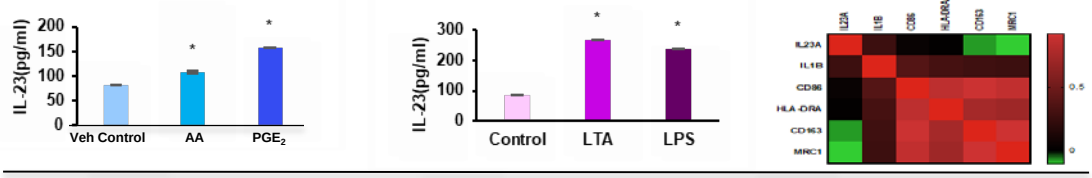

Fig. 5: IL-23 production by DCs/macrophages enhances colon tumor cell aggressiveness

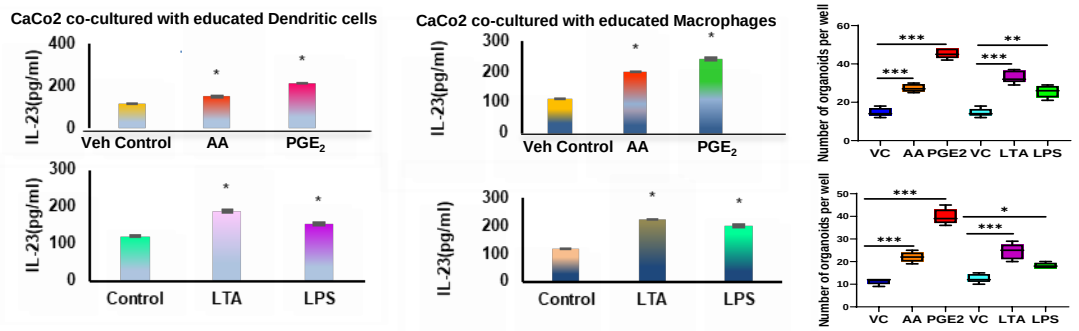

MAJOR FINDINGS AND CONCLUSIONS

- TCGA COAD data base demonstrated that IL-23A is highly expressed across all stages of primary colon cancer tissues than in the normal tissues. High expression of IL-23A is associated with increased bodyweight in colon cancer samples and reduced disease free survival.
- We observed a significant increase in the expression level of IL-23A and its receptor IL-23R in colon cancer tissues of human, and preclinical rodent colon cancer models.
- Our findings demonstrated that IL-23 directly enhances aggressiveness of colon cancer by increasing the proliferation, migration, invasion and self-renewal ability of colon tumor cells with loss of epithelial barrier function.
- Our in vitro study results demonstrated that obesity associated pro-inflammatory factors (AA, PGE2) and bacterial toxins (LTA, LPS) induces DC and macrophages mediated IL-23 production and its mediated colon cancer progression.
- Our results highlight the potential impact of obesity associated pro-inflammatory mediators and gut microbial toxins on innate immune cells to produce IL-23 for obesity-mediated colon cancer progression.

Funding provided by Kerley-Cade Chair Endowment and Stephenson Cancer Center

E-CIGARETTE AEROSOL ALTERS MITOCHONDRIA DNA DAMAGE AND BIOGENESIS

Balaji Sadhasivam[1], Vijay Raj[1], Elizabeth H. Hahn[1,3], Vengatesh Ganapathy[1,] Theodore L. Wagener[4.5] , Lurdes Queimado[1-3]
Balaji-sadhasivam@ouhsc.edu
Departments of [1]Otolaryngology- Head and Neck Surgery, [2]Cell Biology, [3]TSET Health Promotion Research Center, Stephenson Cancer Center, The University of Oklahoma Health Sciences Center, Oklahoma. [4]Center for Tobacco Research, The Ohio State University Comprehensive Cancer Center, and [5]The Ohio State University Wexner Medical Center.

Background: Mitochondria generates cellular energy through oxidative phosphorylation. Impaired mitochondrial function increases reactive oxygen species (ROS), and is associated with a wide range of disorders including cancer. Alterations in mitochondrial DNA (mtDNA) copy number, a biomarker of mitochondrial dysfunction, play a role in the progression of diverse cancers, including oral carcinoma. E-cigarettes are advertised as a safer alternative to combustible tobacco, and its use skyrocked among US teens and adults. Recently, we reported that e-cigarette increases ROS and oxidative DNA damage in oral epithelial cells. Herein, we performed a pilot study to assess the effects of e-cigarette use on mitochondrial DNA.

Aims: (1) To measure mtDNA damage in the oral mucosa of e-cigarette users. (2) To dissect the effect of e-cigarette aerosol on oral mtDNA damage and copy number using an *in vitro* model.

Methods: Oral epithelial cells were collected from 12 e-cigarette users before and after a 2 h *ad libitum* vaping session. To mimic users' exposure, cultured, oral epithelial cells (POE9n) were exposed for 2 h to e-cigarette aerosol extracts (~30 ng/ml nicotine) and samples were collected at various time points. mtDNA damage was quantified using LORD-Q. Relative mtDNA copy number was calculated using a nuclear gene as reference. Data were analyzed by student t-test.

Results: In the e-cigarette user group, 10 out of 12 vapers showed decreased mtDNA damage in oral epithelial cells after a 2 h vaping session compared with respective participants before vaping ($p<0.001$). *In vitro*, exposure of oral epithelial cells to e-cigarette aerosol extracts for 2 h lead to a significant ($p<0.05$) decrease in mtDNA damage 30 minutes post-exposure. No significant decrease in mtDNA damage was observed immediately after exposure. There was a significant increase ($p<0.01$) in mitochondrial copy number after 2 h of exposure, which persisted at 30 min post-exposure.

Conclusion: Our data reveal for the first time that exposure to e-cigarette aerosol decreases overall mtDNA damage levels in both user and tissue culture settings. Our *in vitro* data suggest that an increase in mitochondrial biogenesis accounts for the observed decrease in mtDNA damage. Further studies are warranted to fully understand the impact of e-cigarette use in mitochondrial biogenesis and the health implications of these findings.

Grant support: This work was supported by the NIH/NCI (R01CA204891, Wagener; R01CA242168, Queimado) and the Presbyterian Health Foundation (Queimado).

E-CIGARETTE AEROSOL ALTERS MITOCHONDRIA DNA DAMAGE AND BIOGENESIS

Balaji Sadhasivam[1], Vijay Raj[1], Elizabeth H. Hahn[1,3], Vengatesh Ganapathy[1], Mayilvanan Chinnaiyan[1], Theodore L. Wagener[4,5], Lurdes Queimado[1-3]

Departments of [1]Otolaryngology- Head and Neck Surgery, [2]Cell Biology and [3]TSET Health Promotion Research Center, Stephenson Cancer Center, The University of Oklahoma Health Sciences Center, Oklahoma. [4]Center for Tobacco Research, The Ohio State University Comprehensive Cancer Center, and [5]The Ohio State University Wexner Medical Center, Ohio.

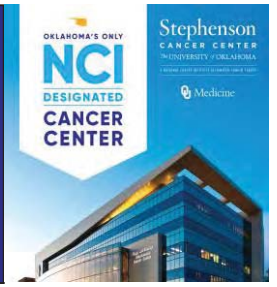

Background

- Mitochondria generates cellular energy through oxidative phosphorylation via respiration.
- Impaired mitochondrial function increases reactive oxygen species, and is associated with a wide range of disorders including cancer.
- Alterations in mitochondrial DNA (mtDNA) copy number, a biomarker of mitochondrial dysfunction, play a role in the progression of diverse cancers, including oral carcinoma.
- E-cigarette use has skyrocked among US teens and adults.
- E-cigarette increases ROS and oxidative DNA damage in oral epithelial cells.

Aims

(1) To measure mtDNA damage in the oral mucosa of e-cigarette users.
(2) To dissect the effect of e-cigarette aerosol on oral mtDNA damage and copy number using an *in-vitro* model.

Methods

- Oral epithelial cells were collected using cytobrush from 12 e-cigarette users before and after a 2 h *ad libitum* vaping session.
- To mimic e-cigarette users' exposure, cultured, oral epithelial cells (POE9n) were exposed for 2 h to e-cigarette aerosol extracts (~30 ng/ml nicotine).
- Tissue culture samples were collected immediately after the 2 h treatment and 30 minutes post-exposure (recovery time). A no exposure study group was used as control.
- Total genomic DNA was extracted as previously described. mtDNA damage was quantified using LORD-Q, a long-run real-time PCR-based DNA-damage quantification assay (Fig.1).
- Relative mitochondrial copy number was calculated using a standard formula [$2 \times 2^{(\text{nucDNA CT} - \text{mtDNA CT})}$].
- The human beta globulin gene HBB was used as the nuclear reference.
- Data shown as average ± SD. p-values from student-t test.

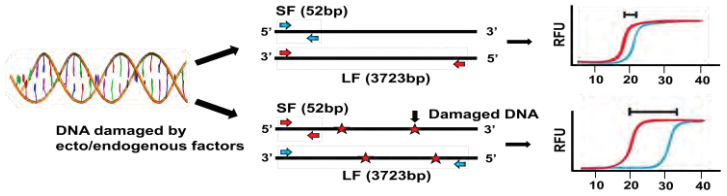

Fig 1. LORD-Q assay amplifies and measures DNA damage on a 3.7kb mtDNA genome (ND4-5) along with 55 bp fragment as a control. Schematic diagram adapted from Lehle *et al.*, NAR, 42: 6, e41, 2014.

Results

mtDNA damage in e-cigarette users before and after vaping

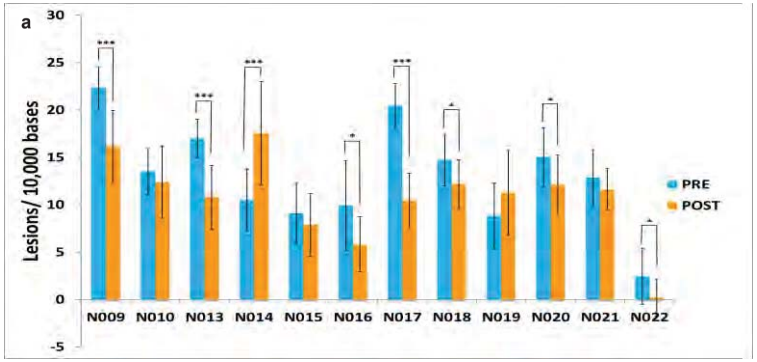

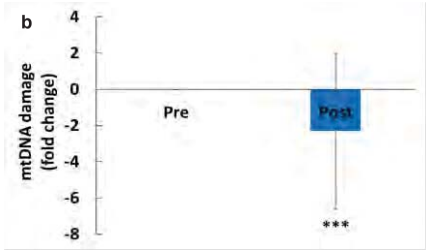

Fig 2. **mtDNA damage in the oral mucosa of e-cigarette users before (Pre) and after a 2 h (Post) vaping session.** A significant decrease in mtDNA damage is observed for several participants (a) and for the overall group (b). (* p≤0.05; ** p≤0.01; *** p≤0.001).

mtDNA damage and copy number in e-cigarette exposed cultured POE9n cells

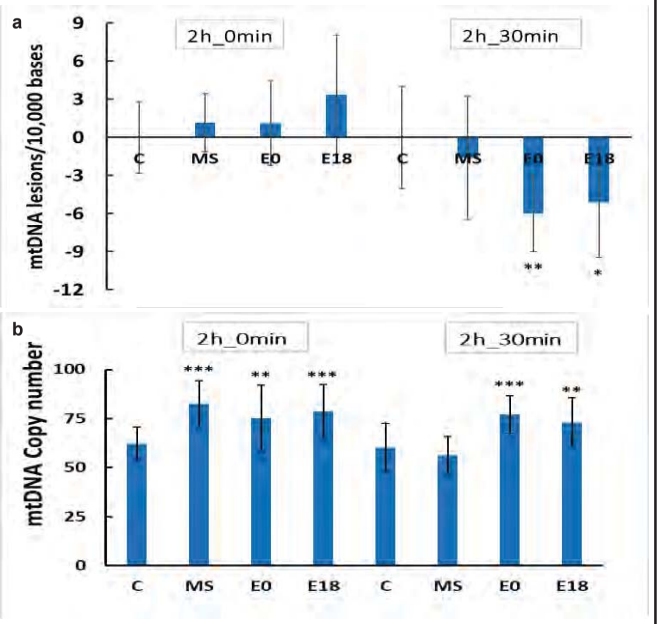

Fig 3. E-cigarette aerosol exposure for 2h, decreases significant level of mtDNA damage (a) and increases mtDNA copy numbers (b). (* p≤0.05; ** p≤0.01; *** p≤0.001).

Conclusions

- Our data reveal for the first time that exposure to e-cigarette aerosol decreases overall mtDNA damage levels in both vapers and *in vitro*.
- Our results suggest that an increase in mitochondrial biogenesis accounts for the observed decrease in mtDNA damage.
- Further studies are warranted to fully understand the impact of e-cigarette use in mitochondrial biogenesis and the health implications of these findings.

Grant support: This work was supported by NIH/NCI (R01CA204891, Wagener; R33CA202898, Queimado) and the PHF (Queimado). Dr. Queimado holds a PHF Endowed Chair in Otorhinolaryngology

Cancer Therapeutics

CANCER THERAPEUTICS POSTERS

POSTER PRESENTATION LIST

Listed A-Z by Presenter Last Name
Presenting*

CHEMOTHERAPY-INDUCED VASCULAR COGNITIVE IMPAIRMENT: ROLE OF ENDOTHELIAL SENESCENCE*
Chetan P. Ahire

ANTI-CANCER EFFECTS OF DANDELION'S EXTRACT ON CERVICAL CANCER CELLS*
Mahoon Ahsan

A LOCAL INTERVENTION-BASED THERAPY USING AN IMMUNOLOGICALLY MODIFIED NANOSYSTEM FOR MAMMARY TUMORS IN MICE
Wei R. Chen

PH-LOW INSERTION PEPTIDE PHARMACOKINETICS INFLUENCED BY SEQUENCE CHARACTERISTICS*
Alex N Frickenstein

OCCURRENCE AND TIMING OF ADVANCED CARE DISCUSSIONS IN RECURRENT OVARIAN CANCER PATIENTS PARTICIPATING IN CLINICAL TRIALS REMAIN TO BE OPTIMIZED*
Anjalika Gandhi

PLECTIN-1 CONTRAST AGENT IDENTIFIES PANCREATIC CANCER
Jordan Hagood

IL-1B PRODUCTION VIA STING SIGNALING ENHANCES ANTITUMOR MEMORY FORMATION*
Ashley R. Hoover

MODEL OPTIMIZATION AND CHEMOPREVENTION OF IPMN DRIVEN PDAC IN KPSD4 MOUSE MODEL*
Gaurav Kumar

SCRNASEQ ANALYSIS AND VISUALIZATION FOR BREAST TUMOR-INFILTRATING IMMUNE CELLS UPON LASER IMMUNOTHERAPY*
Kaili Liu

ACTIVE TARGETING FACILITATES PANCREATIC CANCER SPECIFIC UPTAKE OF NANOCONTRAST AGENTS*
William M. MacCuaig

MASS SPECTROMETRY METABOLOMICS STUDIES OF SINGLE CELL IN MULTICELLULAR SPHEROIDS*
Zongkai Peng

CANCER THERAPEUTICS POSTERS

THE EFFICACY OF EV ENCAPSULATED CHEMOTHERAPEUTICS IS ASSOCIATED WITH LOADING METHODS, EV SOURCES AND EV UPTAKE EFFICIENCY IN PANCREATIC CANCER CELLS*
Haoyao Sun

EXPLORING ASSOCIATIONS BETWEEN TUMOR MUTATIONAL BURDEN, MICROSATELLITE INSTABILITY STATUS AND TUMOR RESPONSE IN VARYING GYNECOLOGIC MALIGNANCIES*
Ana Valente

IN VIVO REAL-TIME VASCULATURE MONITORING IN CANCER THERAPIES USING OPTICAL COHERENCE TOMOGRAPHY ANGIOGRAPHY*
Feng Yan

ELTD1 AS A DIAGNOSTIC AND THERAPEUTIC TARGET FOR GBM: PRE-CLINICAL STUDIES*
Michelle Zalles

CHEMOTHERAPY-INDUCED VASCULAR COGNITIVE IMPAIRMENT: ROLE OF ENDOTHELIAL SENESCENCE

Chetan P. Ahire[1,2], Priya Balasubramanian[1], Stefano Tarantini[1], Tamas Kiss[1], Adam Nyul-Toth[1], Zoltan Ungvari[1], Anna Csiszar[1,2]

[1]Department of Biochemistry and Molecular Biology; [2]Department of Pathology, University of Oklahoma Health Sciences Center

Introduction: There is evidence from case studies on long-term cancer survivors that chemotherapy induces progressive adverse effects on cognitive function in 30 to 50% of patients. Although chemotherapy affects multiple cognitive domains, no strategies exist to prevent/reverse chemotherapy induced cognitive impairment (CICI). Progress in this field is hampered by the lack of adequately controlled clinical studies and preclinical models, making it difficult to investigate the underlying mechanisms of CICI. We have established an innovative mouse model, p16-3MR mice treated with the chemotherapeutic drug paclitaxel (PTX) to address this question.

Hypothesis: Although chemotherapeutics does not cross the blood-brain barrier; endothelial cells lining blood vessels are exposed to the highest concentrations of these drugs, making them uniquely vulnerable to drug-induced DNA damage and cellular senescence. Our working hypothesis is that chemotherapy-induced endothelial senescence is a major contributor to neurovascular dysfunction, dysregulation of cerebral blood flow and blood-brain barrier (BBB) disruption contributing to impaired cognitive function.

Results: Behavioral assessment with radial arm water maze test provided evidence for impaired cognitive function following chemotherapy ($p<0.05$). Endothelial vasodilator dysfunction affects cognitive function; thus, functional hyperemia responses and the BBB integrity were assessed in the somatosensory cortex. The results from control and PTX-treated animals showed that endothelial-dependent cerebral blood flow responses were markedly attenuated ($p=0.07$) and BBB integrity ($p=0.0412$) is compromised in PTX treated mice. Treatment with PTX has also been observed to cause vascular rarefaction in the somatosensory cortex ($p<0.05$). DNA damage was observed in the cortex of PTX treated mice quantitively. The number and activation level of microglia ($p=0.0001$) increased significantly in response to PTX treatment. Flow cytometry-based analysis of cerebrovascular endothelial cells proved that senescent endothelial cells have accumulated in the brain following chronic PTX treatment. Endothelial senescence has also contributed to inflammatory cytokine production and neuroinflammation.

Conclusion: Our results prove that PTX treatment induces cellular senescence in cerebromicrovascular endothelial cells via DNA damage response, which contributes to vascular rarefaction, decreased cerebral blood flow and loss of BBB integrity, thus inducing neuroinflammation and CICI.

Acknowledgment: This work was supported by the AHA 20PRE35211043, SCC Pilot Award, SCC Trainee and Travel Award.

Chemotherapy-induced vascular cognitive impairment: role of endothelial senescence

Chetan Ahire[1,2]; Priya Balasubramanian[1]; Stefano Tarantini[1]; Tamas Kiss[1]; Adam Nyul-Toth[1]; Jordan Delfavero[1]; Feng Yan[3]; Qinggong Tang[3]; Zoltan Ungvari[1] ; Anna Csiszar[1,2]

1. Department of Biochemistry and Molecular Biology; 2. Department of Pathology, University of Oklahoma Health Sciences Center; 3. Stephenson School of Biomedical Engineering, University of Oklahoma, Norman, OK, 73019

Background

Scientific premise: There is overwhelming evidence that cerebrovascular dysfunction could lead to cognitive decline. Although the BBB is impermeable to most of these compounds and the majority of chemotherapeutic drugs cannot cross this barrier, direct exposure to high concentration of circulating chemotherapeutic agents in the brain microvasculature can selectively affect cerebromicrovascular endothelial cells (CMVECS). CMVECS are sensitive to exogenous toxic agents and undergo rapid functional and phenotypic changes resulting in cellular stress-induced senescence.

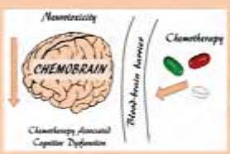

- 600 km of microvessels
- 20 m^2 surface area
- 1 capillary for each neuron

Chemotherapy → Alters cellular state of endothelial cell → Causing Cognitive impairment

The objective of this study is to reveal the mechanistic role of Chemotherapy Induced Endothelial Senescence (CIES) in the development of cognitive decline in a preclinical model of Chemotherapy Induced Cognitive Impairment (CICI).

Hypothesis

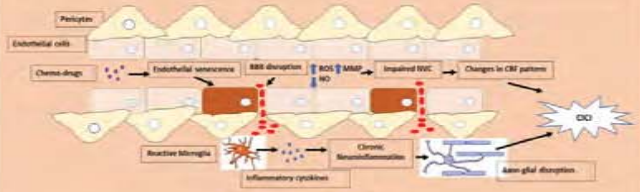

Research Design

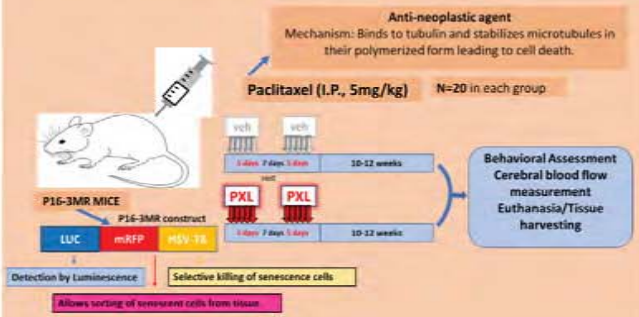

Results

Paclitaxel treatment (5mg/kg) induces cognitive impairment in mice

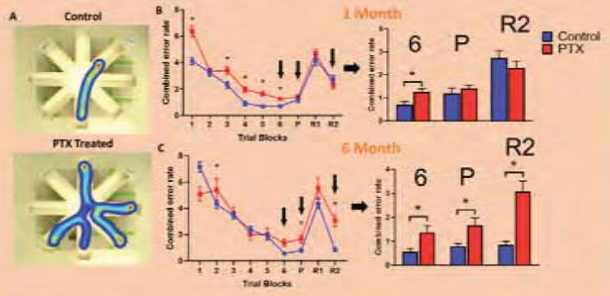

Figure 1: Paclitaxel (PTX) treatment associates with impaired radial arm water maze (RAWM) performance. Panel A: Representative RAWM figures of control and treated mice. Panel B: after 1 month of PTX treatment, Mice tends to have higher error frequency throughout learning phase. Panel C: After 6 Month of PTX treatment, Mice observed to have high error frequency at the end of learning, probe and reversal phase compared to control mice. *n = 10-15 for each data point. Unpaired t test; Data are mean ± S.D. (n = 20-60 for each data point). *P < 0.05 vs. control*

Paclitaxel treatment impairs neurovascular coupling in somatosensory region of the mice brain

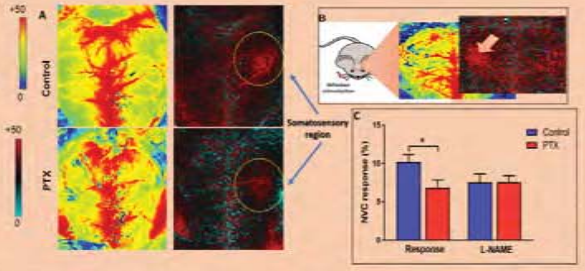

Figure 2: In PTX treated mice, Reduced neurovascular coupling responses associates with decreased radial-arm water maze (RAWM) performance. Panel A: Represent CBF changes in the whisker barrel field relative to baseline during contralateral whisker stimulation (right oval, 30s, 5Hz) in PTX treated and control mice. Color bar represents CBF as percent change from baseline. Panel B: Representative pseudocolour laser speckle flowmetry maps of baseline CBF Panel C: Time course of CBF changes after the start of contralateral whisker stimulation (horizontal bars). Summary data are shown. Data are mean ± S.E.M. (n = 6–8 in each group). Significant; *P < 0.05 v. s. control.

Paclitaxel treatment induces Blood-Brain Barrier (BBB) disruption

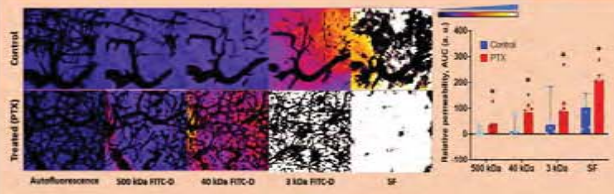

Figure 3: Two-photon-based imaging shows increase microvascular permeability in PTX treated mice compared to control mice. Extravascular intensity changes are quantified in PTX treated mice after the injection of tracers including 500 kDa FITC-D, 40 kDa FITC-D, 3 KDa FITC-D and SF. For both groups, graph on the right represents Area Under Curve (AUC)-based permeability indices, in which relative permeability of microvasculature is calculated for each of the tracers injected. Summary data are shown. Note the increase in permeability for each different sized tracers in PTX treated animals in compared to the control mice (n = 6–8 in each group). Significant; *P < 0.05 v. s. control.

PTX treatment causes vascular rarefaction and vessel dilation in the somatosensory cortex of brain

Figure 4: Imaging using Optical coherence tomography (OCT) highlights increased vascular rarefaction and decrease vascular density in PTX treated mice. Quantification of deep vascular skeleton density in PTX treated mice is performed by calculating ratio of the vasculature area to total imaged area (ROI). All data are presented as interquartile distributions with median. *P < 0.05 vs. control

Paclitaxel (PTX) Treatment can not only cause activation of microglia but also increases their number in cortex as well as hippocampus of PTX treated mice

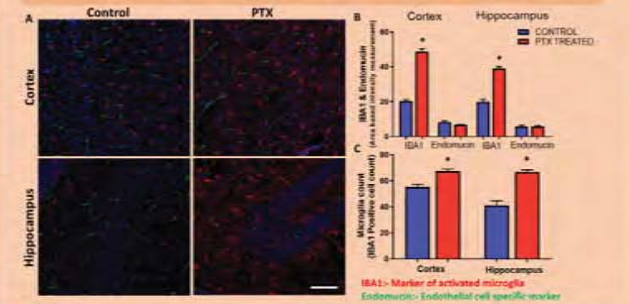

Figure 5: Paclitaxel treatment exacerbates neuroinflammation. Confocal images showing Iba1-positive activated microglia and Endomucin stained endothelial cells in the cortex and hippocampus of control and PTX treated mice. Blue fluorescence: Nuclei. (RArea: 202.272µm / z stack(35nm); n=5, 5 images each)

Chemotherapy (PTX) causes endothelial senescence

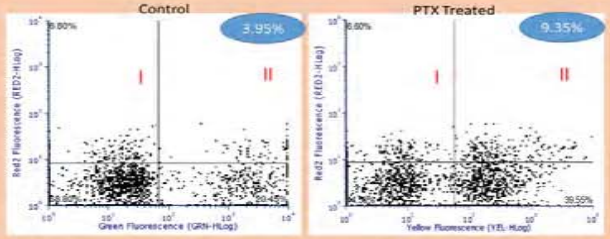

Figure 6: Paclitaxel treatment induces senescence in endothelial cells of brain microvasculature. (Analysis in progress)

Summary/Conclusion

Chemotherapy (Paclitaxel treatment) causes major structural and functional cerebrovascular changes leading to cognitive impairment:

1) Neuroinflammation

2) Disruption of Blood-Brain Barrier

3) Neurovascular coupling impairment

Acknowledgment

This work is supported by the AHA 20PRE35211043, R01AG068295-01, SCC Pilot Award, SCC Trainee and Travel Award.

ANTI-CANCER EFFECTS OF DANDELION'S EXTRACT ON CERVICAL CANCER CELLS

Mahnoor Ahsan, Kayley McBride, Melville Vaughan, and Christina Hendrickson
Center for Interdisciplinary Education and Research, and Department of Biology, University of Central Oklahoma

According to the American Cancer Society Journal, 1,806,590 new cancer cases and 606,520 cancer deaths are expected to occur in 2020 in the United States. Despite the development of many forms of cancer therapy, there continues to be a high rate of death among patients. Existing cancer therapies can be very expensive, placing immense economic distress on afflicted families who are coping with this disease. Certain plant-derived products have pharmaceutical uses due to their anti-cancer effects. Dandelion (*Taraxacum officinale*) could be one of them. Dandelion is widely accessible, it grows throughout the world and has long been consumed safely as part of Middle Eastern and Ancient Chinese Medicine due to its anti-inflammatory and anti-carcinogenic properties. The mechanism of its effect on cancer cells is still unclear. This study investigated the anti-cancer effects of Dandelion on cervical cancer cells known as HeLa cells. It was hypothesized that the anti-cancer activity of dandelion extract acts by disrupting key cellular processes in tumor cells, which could result in growth inhibition, cell death and an overall decrease in their invasiveness.

Dandelion Whole Extract (DWE) was prepared, filtered, freeze-dried and resuspended in cell-growth media. HeLa cells and normal human cervical cells (HCEC) were maintained under standard *in vitro* cell culture conditions, then treated with DWE concentrations between 8 to 0 mg/ml for 96 hours. For a more realistic 3-dimensional approach, cells were cultured into collagen lattices to form artificial tumors and treated with similar varying concentrations of DWE. Our results showed that DWE inhibited proliferation and invasion while promoting programmed cell death in HeLa cells, but did not have such effects on HCEC cells.

This study supports the possible use of dandelion as a natural source of anti-cancer compounds against cervical cancer. Screening compounds derived from herbal plants, like dandelion, is an exciting approach for discovering new anti-cancer drugs. This study could potentially improve cancer treatment by unveiling cellular and molecular mechanisms behind anti-proliferative and anti-invasion effects of dandelion that are getting popularized as a cancer treatment.

This research is funded by INBRE and UCO's STLR and RCSA.

Anti-cancer Effects of Dandelion's Extract on Cervical Cancer Cells

Mahnoor Ahsan, Kayley McBride, Melville B. Vaughan, and Christina Hendrickson
Center for Interdisciplinary Biomedical Education and Research
Biology Department, College of Mathematics and Science, University of Central Oklahoma

Abstract

Certain plant-derived products have pharmaceutical uses due to their anti-cancer effects. Dandelion (*Taraxacum officinale*) could be one of them. Dandelion is widely accessible, it grows throughout the world and has long been consumed safely as part of Middle Eastern and ancient Chinese medicine due to its anti-inflammatory and anti-carcinogenic properties. The mechanism of its effect on cancer cells is still unclear. This study investigated the anti-cancer effects of Dandelion on cervical cancer cells known as HeLa cells. It was hypothesized that the anti-cancer activity of dandelion extract acts by disrupting key cellular processes in tumor cells, which could result in growth inhibition, cell death and an overall decrease in their invasiveness.

Dandelion Whole Extract (DWE) was prepared, filtered, freeze-dried and resuspended in cell-growth media. HeLa cells and normal human cervical epithelial cells (HCEC) were maintained under standard *in vitro* cell culture conditions, then treated with DWE concentrations between 8 to 0 mg/ml for 96 hours. For a more realistic 3-dimensional approach, cells were cultured into collagen lattices to form artificial tumors and treated with similar varying concentrations of DWE.

Our results showed that DWE inhibited proliferation and invasion while promoting programmed cell death in HeLa cells, but did not have such effects on HCEC cells.

This study supports the possible use of dandelion as a natural source of anti-cancer compounds against cervical cancer. Screening compounds derived from herbal plants, like dandelion, is an exciting approach for discovering new anti-cancer drugs. This study could potentially improve cancer treatment by unveiling cellular and molecular mechanisms behind anti-proliferative and anti-invasion effects of dandelion that are getting popularized as a cancer treatment.

Hypothesis

Anti-cancer activity of *Taraxacum officinale* extract acts by disrupting key cellular processes to selectively target cancer cell vulnerabilities to induce apoptosis and impair proliferation.

Materials and methods

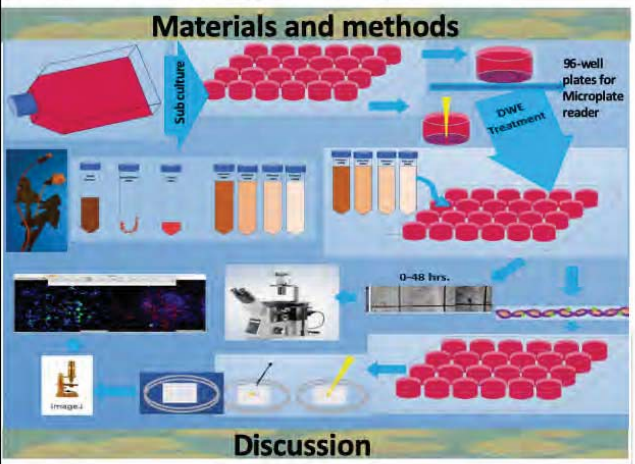

Discussion

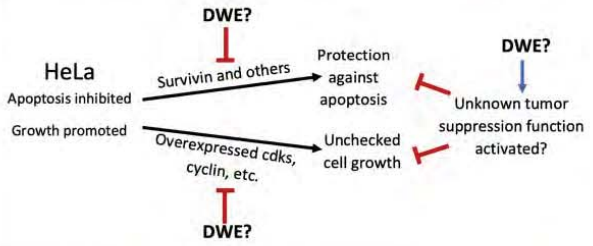

Results

Data exhibit a significant inhibition of proliferation and migration versus induction of apoptosis in HeLa cells. This anti-cancer effect is supported by data demonstrating no significant effect on normal human cell lines, HCEC & HDF's proliferation, migration and apoptosis at DWE concentration of 4 mg/mL and lower.

DWE Treated HeLa Cells Proliferation vs. Apoptosis

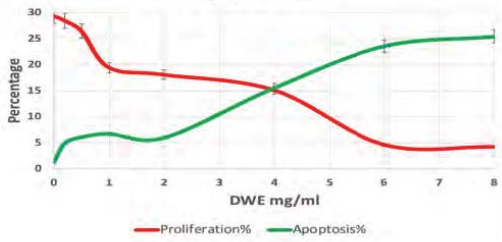

Daily Viability% of HeLa & HDF Compared to Day 1, @DWE 0 & 0.2 mg/mL

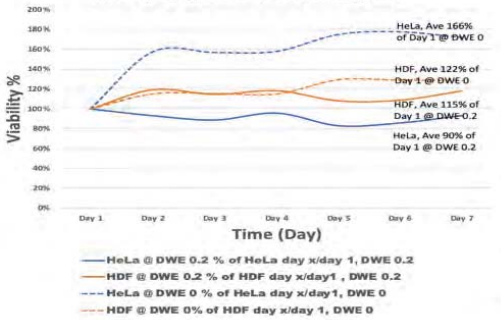

HeLa cells treated with DWE concentration of 0.2 mg/mL demonstrated an average of 10% reduction in cell viability over time compared to untreated control group (DWE 0 mg/mL at day 1). Human dermal fibroblast (HDF00703) cells' viability was increased by an average of 15% at the same concentrations of DWE.

Caspase 3, 8, and 9 Activation in DWE Treated HeLa & HCEC

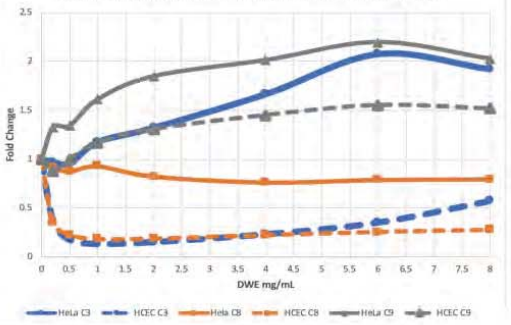

Caspases are differentially activated in HeLa and HCEC.

DWE Treated HeLa Cells (0-8 mg/mL)

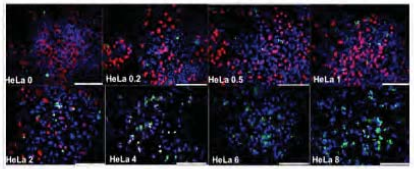

EdU denotes proliferation. Caspase 3 signifies cell death. DAPI is a counterstain to label all cells.

Artificial Tumors in Collagen Lattices

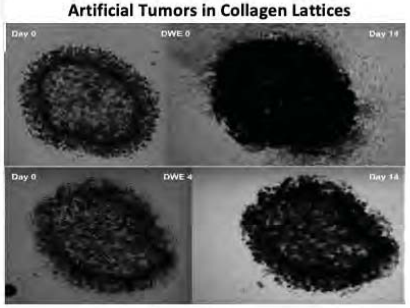

Invasion of HeLa cells artificial tumors nested in the collagen lattice and treated with DWE 0 and 4 mg/mL).

HeLa vs. HCEC JC-1 Assay

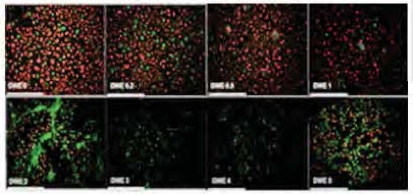

HCEC: Top, DWE 0, 0.2, 0.5, 1
Down, DWE 2, 4, 6, 8 mg mL

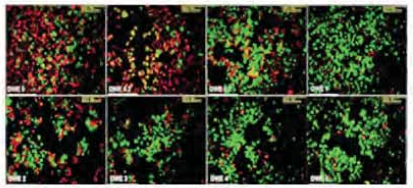

HeLa: Top, DWE 0, 0.2, 0.5, 1
Down, DWE 2, 4, 6, 8 mg/mL

DWE extracts affects HeLa cells mitochondria earlier and to a greater degree as compared to HCEC cells

96 Hours of DWE Treatment has Opposite Effects of Viability on HeLa and HCEC

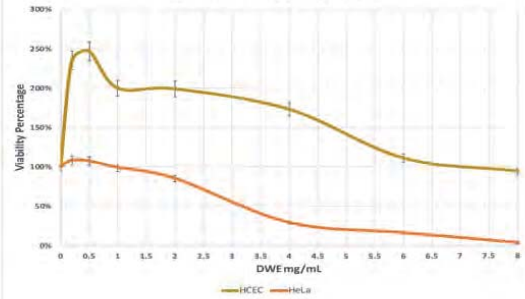

HeLa Cell Viability in Nested Matrix During 5-days of DWE Treatment

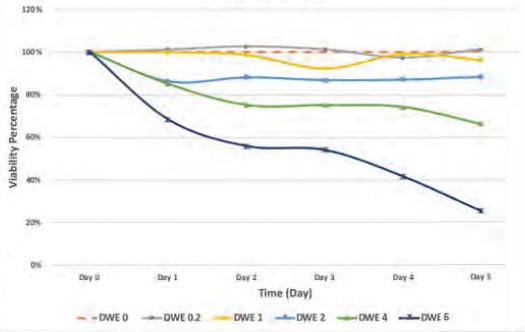

HeLa vs. HDF Migration

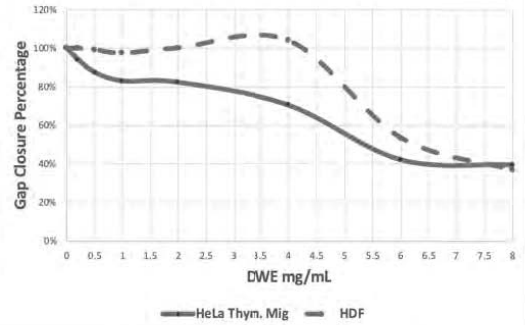

DWE differentially affects migration of HeLa and HDFs . At doses 1, 2 & 4 HDFs can migrate effectively unlike Hela cells.

References

Chatterjee, S. J., Ovadje, P., Mousa, M., Hamm, C., & Pandey, S. (2011). The efficacy of dandelion root extract in inducing apoptosis in drug-resistant human melanoma cells. Evidence-based complementary and alternative medicine : eCAM, 2011, 129045. doi:10.1155/2011/129045

Bray F, Ferlay J, Soerjomataram I, Siegel RL, Torre LA and Jemal A: Global cancer statistics 2018: GLOBOCAN estimates of incidence and mortality worldwide for 36 cancers in 185 coun- tries. CA Cancer J Clin 68: 394-424, 2018.

Ovadje, P., Ammar, S., Guerrero, J. A., Arnason, J. T., & Pandey, S. (2016). Dandelion root extract affects colorectal cancer proliferation and survival through the activation of multiple death signalling pathways. Oncotarget, 7(45), 73080–73100. doi:10.18632/oncotarget.11485

Acknowledgements

Dr. Nikki Seagraves for gifting HeLa cells,
Dr. Gloria Caddell for ID verification,
Mr. Ralph Jones for technical support

Funding

This work was made possible by INBRE funding (CGH & MBV), STLR (CGH), & UCO office of High Impact Practices (CGH & MBV).

A LOCAL INTERVENTION-BASED THERAPY USING AN IMMUNOLOGICALLY MODIFIED NANOSYSTEM FOR METASTATIC MAMMARY TUMORS IN MICE

Wei R. Chen, Ashley Hoover, and Kaili Liu
Stephenson School of Biomedical Engineering

Nanoparticles have great potential in biomedical applications as drug carrier and therapeutic agents. Specially synthesized nanosystems could integrate different therapeutic and diagnostic agents and synergize different treatment modalities. We developed an immunologically modified nanosystem for the treatment of metastatic cancers by synergizing photothermal therapy (PTT), chemotherapy, and immunotherapy. Specifically, we used reduced graphene oxide (rGO) as a platform to load mitoxantrone (MTX), a chemotherapeutic agent, and SB-431542 (SB), a transforming growth factor beta (TGF-β) inhibitor. In our in vivo studies using 4T1 mouse mammary tumor model, intratumoral administration of rGO/MTX/SB, followed by non-invasive irradiation of a near-infrared laser, could control both local primary tumors and inhibit distant metastases. Most treated mice resisted tumor rechallenge and developed tumor-specific immunity. We determined that rGO-based PTT induced immunogenic tumor cell death, providing tumor-specific antigens, using rGO as an immunoadjuvant. We also found that the use of SB changed the tumor microenvironment and improved the therapeutic effect of MTX-generated chemotherapy and rGO-based PTT. These effects were synergized to induce an effective antitumor immunity, as evidenced by the increased infiltration of tumor-specific cytotoxic $CD8^+$ T lymphocytes and decreased infiltration of regulatory T cells (Tregs) in distal tumors. This unique rGO/MTX/SB nanosystem, together with targeted laser irradiation, could present an effective clinical tool against metastatic cancers, particularly considering the fact that all the components of this specific nanosystem, as well as the near-infrared laser, have been used in humans.

Acknowledgement: This work was supported in part by the NIH/NCI (R01CA205348-01) and the Oklahoma Center for the Advancement of Science and Technology (HR16-085). The authors also acknowledge the support of the Charles and Peggy Stephenson Chair endowment fund.

A Local Intervention-based Therapy Using an Immunologically Modified Nanosystem for Metastatic Mammary Tumors in Mice

Wei R. Chen, Ashley Hoover, and Kaili Liu

Stephenson School of Biomedical Engineering, University of Oklahoma, Norman, OK, 73019

Stephenson CANCER CENTER
the UNIVERSITY of OKLAHOMA

Introduction

Nanoparticles can serve as excellent drug carriers and therapeutic agents. Immunologically modified nanomaterials can be used to synergize with chemotherapy, phototherapy, and immunotherapy for cancer treatment. We synthesized a unique immunologically modified nanosystem by loading mitoxantrone (MTX), a chemotherapeutic agent, and SB-431542 (SB), a transforming growth factor beta (TGF-β) inhibitor, onto reduced graphene oxide (rGO), which itself functions as a light-absorbing agent and immunostimulant. We combined intratumoral rGO/MTX/SB injection with non-invasive photothermal therapy (PTT) to treat metastatic mammary tumor, 4T1, in mice. We investigated the effects of laser+rGO/MTX/SB on tumor growth, animal survival, tumor microenvironment, and systemic antitumor immunity. The mechanism of laser+rGO/MTX/SB induced immune responses in treating metastatic tumors is given in Fig. 1.

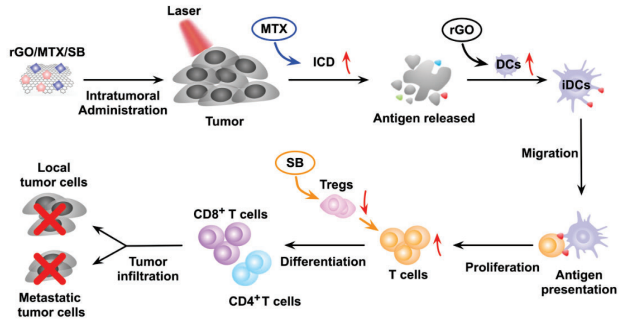

Fig. 1. The mechanism of antitumor immune responseinduced by laser+rGO/MTX/SB.

Synthesis of rGO/MTX/SB

Reduced graphene oxide (rGO) was conjugated with PEG2000-NH¬2 and purified by a 100 kDa filter through centrifugation. MTX and SB were then loaded onto rGO-PEG via π–π stacking interaction.

Treatment of Metastatic Tumors

4T1 cells (1x105 cells) suspended in 50 µl PBS were injected into the breast pad of Female BALB/c mice. Tumor-bearing mice were randomly divided into different treatment groups: PBS control, rGO, rGO/MTX, and rGO/MTX/SB, with or without laser irradiation. The mice were intratumorally injected with different components of rGO/MTX/SB, followed by laser irradiation (0.75 W/cm2 @5 min) 2 hours later.

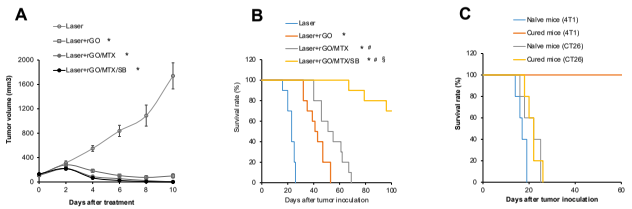

Fig 2. Therapeutic efficacy of laser+rGO/MTX/SB. A. Tumor growth curves of different treatment groups. (n=5, ∗P<0.05). B. Survival rates of tumor-bearing mice in different treatment groups. (n=10, *p<0.001 vs Laser; # p<0.05 vs Laser+rGO; § p<0.005 vs Laser+rGO/MTX). C. Survival rates of laser+rGO/MTX/SB cured mice after rechallenges by 4T1 or CT26 tumor cells.

Therapeutic Effects of Laser+rGO/MTX/SB Treatment

Laser irradiation alone did not have much impact on the tumor growth, while rGO-laser combination slowed down the tumor growth, as shown in Fig. 2A. However, only laser+rGO/MTX/SB resulted in long-term survival (Fig. 2B). Furthermore, the laser+rGO/MTX/SB-cured mice rejected challenge by 4T1 tumor cells, but not CT26 mouse colon tumor cells (Fig. 2C), indicating a laser+rGO/MTX/SB-induced tumor-specific immunity.

Except for the laser only treatment, other combinations have induced DAMPs, such as HSP70, CRT, ATP, and HMGB1, at different times after the treatment, as shown in Fig. 3A-B.

Laser+rGO/MTX/SB significantly increased mature DCs and decreased regulatory T cells in the tumor microenvironment 24 hour after the treatment (Fig. 3C).

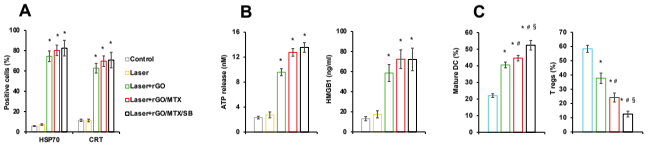

Fig 3. A. Surface expression of HSP70 and CRT on tumor cells 3 h after treatments. (n=4, *p<0.05). B. Extracellular ATP and HMGB1 released from tumor cells detected 12 h after the treatments. (n = 4, *P < 0.05). C. Infiltration of matured DCs and Tregs in tumor tissue 24 h after treatments. (n=4, *p<0.001 vs Laser; # p<0.05 vs Laser+rGO; § p<0.005 vs Laser+rGO/MTX).

Systemic Effects of Laser+rGO/MTX/SB Treatment

Laser+rGO/MTX/SB induced systemic immune responses, such as the increased IL-12 and IFNγ levels in the serum of mice 72 hours after treatment (Fig. 4A), as well as increased effector T cells in spleen (SPL) and draining lymph node (DLN) of laser+rGO/MTX/SB treated mice (Fig. 4B).

The abscopal effect (Fig. 5A) induced by laser+rGO/MTX/SB was also observed, including the suppressed the growth of the untreated second tumors after the treatment of the first tumor, as shown in Fig. 5B.

Furthermore, laser+rGO/MTX/SB significantly increased the infiltrating immune cells in the untreated second tumors, such as CD8+ T cells (Fig. 5C), and CD25+ cells (Fig. 5D).

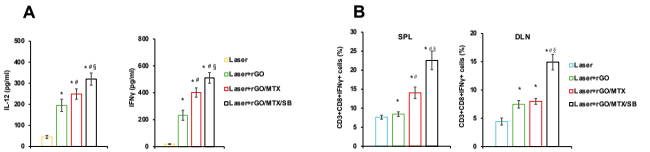

Fig 4. A. IL-12 and IFNγ levels in serum from mice isolated at 72 h post different treatments. (n=4, *p<0.001 vs Laser; # p<0.05 vs Laser+rGO; § p<0.01 vs Laser+rGO/MTX). B. The percentage of effector T cells (CD8+IFNγ+, gated on CD8+ cells) isolated from spleen (SPL) and draining lymph node (DLN) of mice, 7 days after the indicated treatments, (n=4, *p<0.001 vs Laser; # p<0.001 vs Laser+rGO; § p<0.001 vs Laser+rGO/MTX).

Acknowledgements

This research is supported in part by a grant from NIH/NCI (R01 CA205348) and by grants from the OCAST (HR16-085, HF20-019). The authors also acknowledge the support of the Charles and Peggy Stephenson Chair endowment fund.

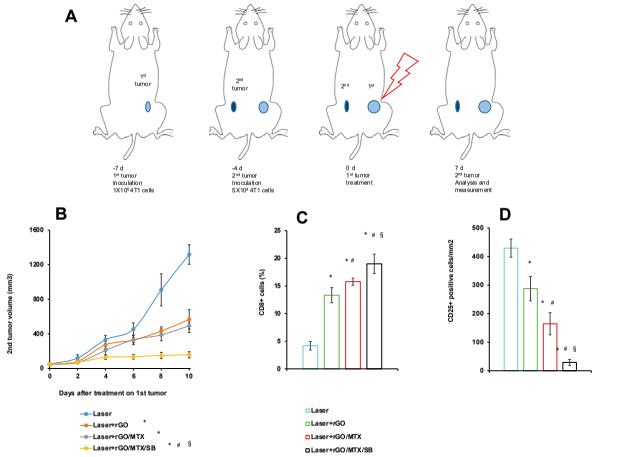

Fig 5. A. Schematic for abscopal effect of laser+rGO/MTX/SB. B. Volume of secondary untreated tumors after indicated treatments on the primary tumors in mice that inoculated with two tumors. (n=5, *p<0.001 vs Laser; # p<0.001 vs Laser+rGO; § p<0.001 vs Laser+rGO/MTX). C. Proportions of tumor-infiltrating CD8+ T cells (gated by CD3+) in secondary tumor. (n=4, *p<0.001 vs Laser; # p<0.05 vs Laser+rGO; § p<0.05 vs Laser+rGO/MTX). D. Numbers of tumor-infiltrating CD25+ cells in secondary tumor. (n=4, *p<0.01 vs Laser; # p<0.01 vs Laser+rGO; § p<0.001 vs Laser+rGO/MTX).

Discussion

Intratumoral administration of rGO/MTX/SB, followed by non-invasive irradiation of a near-infrared laser, destroyed local primary tumors and inhibited distant metastases in 4T1 mouse mammary tumor model, which is poorly immunogenic and highly metastatic. The hypothesized mechanism of laser+rGO/MTX/SB is as follows. rGO-based PTT provided an immunogenic antigen source, forming in situ vaccination with rGO as an immunoadjuvant. The use of SB changed the tumor microenvironment and improved the therapeutic effect of MTX-generated chemotherapy and rGO-based PTT. The immunological functions of MTX, SB, and rGO acted synergistically to induce an effective tumor-specific immunity (Fig. 1), as evidenced by the therapeutic effects and immune responses presented in this work.

Conclusion

In summary, we have developed an effective combination therapy for metastatic cancer, with the multi-functional rGO as a photothermal agent, an adjuvant, and a drug carrier, incorporating PTT, MTX chemotherapy, and TGF-β inhibition immunotherapy. The combination therapy induced a superior antitumor immunity, synergizing the tumoricidal and immunological processes, to trigger an effective CTL for metastasis control. This synergistic nanographene offered a new strategy for treating many metastatic cancers with primary tumors accessible by PTT.

References

Zhou F, et al. Synergistic nanographenes potentiate a local photo-chemo-immunotherapy for metastatic cancer by triggering host immunity. Biomaterials, 265, 2020.

Zhou B, et al. Immunologically modified MnFe2O4 nanoparticles to synergize photothermal therapy and immunotherapy for cancer treatment, Chemical Engineering Journal, 396, 125239, 2020.

Wang M, et al. NIR-triggered phototherapy and immunotherapy via antigen-capturing nanoplatform for metastatic cancer treatment", Advanced Science, 6, 1802157 (1-12), 2019.

PH-LOW INSERTION PEPTIDE PHARMACOKINETICS INFLUENCED BY SEQUENCE CHARACTERISTICS

Alex N Frickenstein[1,2,*], Abhi Sammykuty[2,3], Molly W McNally[2,3], Lacey R McNally[2,3]
[*]Presenting Author (africk256@ou.edu)
[1] Stephenson School of Biomedical Engineering, University of Oklahoma, Norman, OK 70319, USA, [2]Stephenson Cancer Center, University of Oklahoma, Oklahoma City, OK, 73104, USA, [3]Department of Surgery, University of Oklahoma, Oklahoma City, OK, 73104, USA.

Purpose: Pancreatic ductal adenocarcinoma (PDAC) is projected to be the second leading cause of cancer-related deaths in the United States. Curative options for PDAC remain limited due to patient incompatibility with therapeutic options and a lack of effective PDAC-targeting options. pH-low insertion peptide (pHLIPs) have been studied as molecular targeting agents for PDAC, responding to the acidic tumor microenvironment produced by tumor metabolism. While many pHLIP sequences have been assessed, the relation between pHLIP characteristics, such as hydrophobicity and estimated pK_a, and pharmacokinetic behavior is not well understood. Through approximating these trends, more effective pHLIPs may be designed. This study demonstrates the connection between pHLIP properties and pharmacokinetic behavior.

Methods: *In vitro*, PDAC cells from cell lines S2VP10L or S2013Q were plated with media of pH 7.4, 6.8, 6.6, or 6.4. Known pHLIP sequences V7, V3, and wild-type, alongside non-inserting negative control K7, were used to treat *in vitro* cells. Alternative pHLIP sequences possessing different hydrophobicity, aromaticity, and pK_a values from known sequences were similarly used. All pHLIPs were conjugated to fluorescent dye molecules before treating cells. pH-specific tumor targeting by each pHLIP was assessed by NIR fluorescent signal intensity from treated wells. *In vivo* pharmacokinetic modelling was performed in mouse models orthotopically implanted with S2VP10L cells. Dye-conjugated pHLIPs that demonstrated *in vitro* pH-targeting were administered by tail-vein injection. MSOT analysis was used to track fluorescent signal from the pHLIPs in organ and tumor tissue at rational time points. *Ex vivo* organ fluorescence was assessed for secondary pharmacokinetic data. Arterial input function and physiological compartment models were used to model pHLIP pharmacokinetics based on collected data.

Results: pHLIPs demonstrated pH-specific targeting *in vitro* and *in vivo*. pH limits of commonly used pHLIPs were established alongside pharmacokinetic restrictions.

Conclusions: The pharmacokinetic properties of select pHLIPs are innately favorable for *in vivo* tumor-targeting, though sequence modification may improve results.

Acknowledgement of Funding: This work was supported by NIH grants R01CA205941, R01CA212350, and R01EB020125.

pH-low Insertion Peptide Pharmacokinetics Influenced by Sequence Characteristics

Alex N Frickenstein[1,2], Abhilash Sammykuty[2,3], Molly W McNally[2,3], Lacey R McNally[2,3]

[1]Stephenson School of Biomedical Engineering, University of Oklahoma, [2]Stephenson Cancer Center, University of Oklahoma, [3]Department of Surgery, University of Oklahoma

ABSTRACT

Purpose: Pancreatic ductal adenocarcinoma (PDAC) is projected to be the second leading cause of cancer-related deaths in the United States. Curative options for PDAC remain limited due to patient incompatibility with therapeutic options and a lack of effective PDAC-targeting options. pH-low insertion peptides (pHLIPs) have been studied as molecular targeting agents for PDAC, responding to the acidic tumor microenvironment produced by tumor metabolism. While many pHLIP sequences have been assessed, the relation between pHLIP characteristics, such as hydrophobicity and estimated pKa, and pharmacokinetic behavior is not well understood. Through approximating these trends, more effective pHLIPs may be designed. This study demonstrates the connection between pHLIP properties and pharmacokinetic behavior.

Methods: *In vitro*, PDAC cells from cell lines S2VP10L or S2013Q were plated with media of pH 7.4, 6.8, 6.6, or 6.4. Known pHLIP sequences V7, V3, and wild-type, alongside non-inserting negative control K7, were used to treat *in vitro* cells. Alternative pHLIP sequences possessing different hydrophobicity, aromaticity, and pKa values from known sequences were similarly used. All pHLIPs were conjugated to fluorescent dye molecules before treating cells. pH-specific tumor targeting by each pHLIP was assessed by NIR fluorescent signal intensity from treated wells. *In vivo* pharmacokinetic modelling was performed in mouse models orthotopically implanted with S2VP10L cells. Dye-conjugated pHLIPs that demonstrated *in vitro* pH-targeting were administered by tail-vein injection. MSOT analysis was used to track fluorescent signal from the pHLIPs in organ and tumor tissue at rational time points. *Ex vivo* organ fluorescence was assessed for secondary pharmacokinetic data. Arterial input function and physiological compartment models were used to model pHLIP pharmacokinetics based on collected data.

Results: pHLIPs demonstrated pH-specific targeting *in vitro* and *in vivo*. pH limits of commonly used pHLIPs were established alongside pharmacokinetic restrictions.

Conclusions: The pharmacokinetic properties of select pHLIPs are innately favorable for *in vivo* tumor-targeting, though sequence modification may improve results.

pHLIP Insertion Behavior

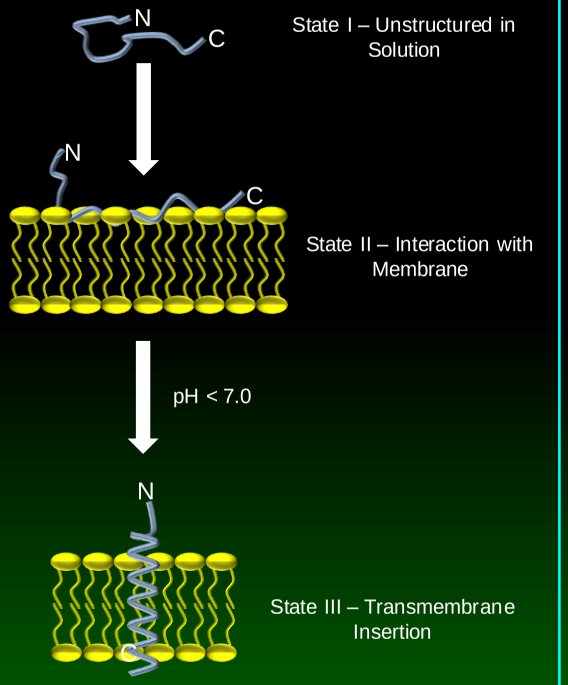

WT pHLIP Sequence

N- ACEQNPIY|WARYADWLFTTPLLLLDLALLV|DADEG -C

Figure 1: Schematic of pHLIP insertion across membrane with WT sequence.

Materials and Methods

- pHLIP peptides were conjugated overnight at room temperature to NIR 750 maleimide dye
- Following dialysis against ultrapure water, conjugation was confirmed through by spectrophotometer measurement
- S2VP10 in pH media were treated with pHLIP-dye probes and incubated for 2 hours
- Cell wells were washed with pH-specific PBS prior to NIR imaging to assess pH targeting of pHLIP-dye probes
- Chitosan coated MSNs were conjugated to pHLIPs for active targeting enabled theranostic nanovehicles
- NIR imaging and MSOT analysis confirmed pHLIP pH targeting

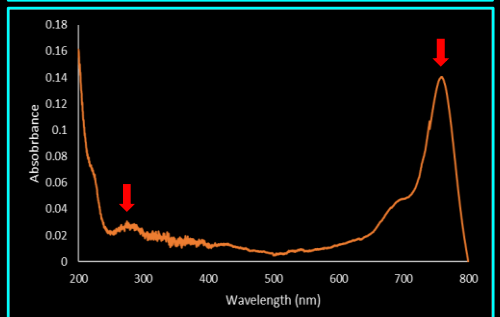

Figure 2: UV-vis spectrum of WT pHLIP conjugated with 750 maleimide dye. Conjugation occurs through disulfide bond formation between sulfur on the dye molecule and the cysteine residue in the pHLIP sequence. Red arrows highlight peaks for dye (750nm) and peptide (280nm).

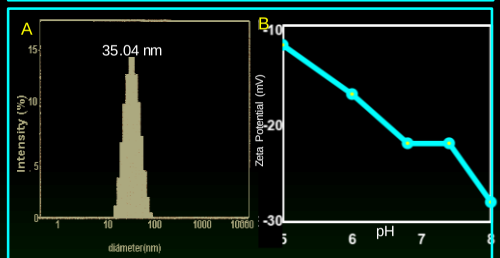

Figure 3: Dynamic light scattering and zeta potential analysis of synthesized MSNs. (A) DLS indicates 35 nm hydrodynamic MSN diameter with narrow size distribution (PDI<0.13). (B). Zeta potential measurements of chitosan-coated MSNs. Chitosan presence is verified by the decreasing measured voltage with increasing pH. This trend is produced by fewer protonation events of chitosan primary amine groups as pH is increased, decreasing overall net charge.

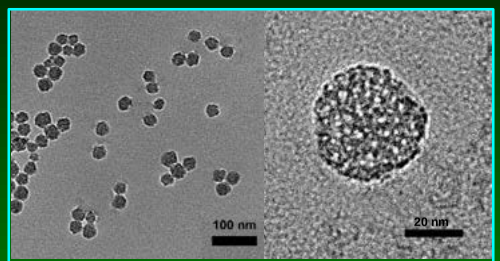

Figure 4: Synthesized MSNs were observed through TEM. Formation of mesoporous spherical particles of ~33 nm overall diameter and pore diameter of ~3 nm was confirmed, corroborating DLS measurements. TEM and DLS diameter difference is due to hydrodynamic radius.

RESULTS

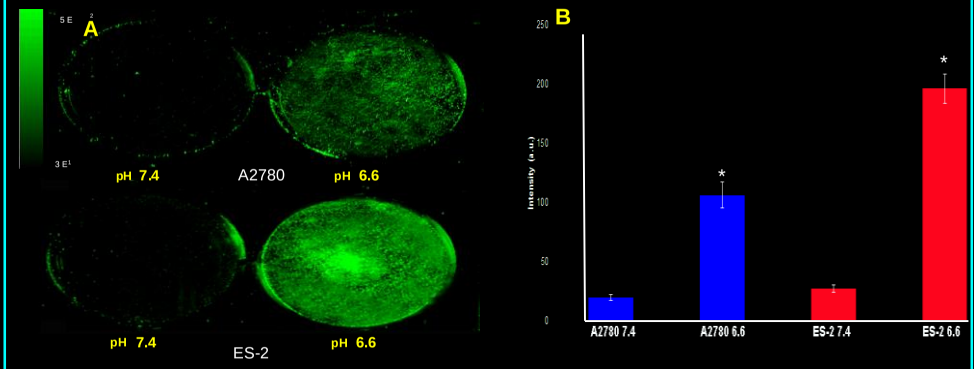

Figure 5: NIR fluorescent imaging of malignant cells treated with pHLIP-MSNs to demonstrate pH-specificity. pHLIP sequence variant V7 was used. $5.0*10^5$ ES-2 and A2780 ovarian cancer cells were plated in separate wells and treated with pH 7.4 and pH 6.6 media prior to incubation with fully conjugated pHLIP-MSNs. Plates were then washed using PBS at corresponding pH values and imaged. P<0.05

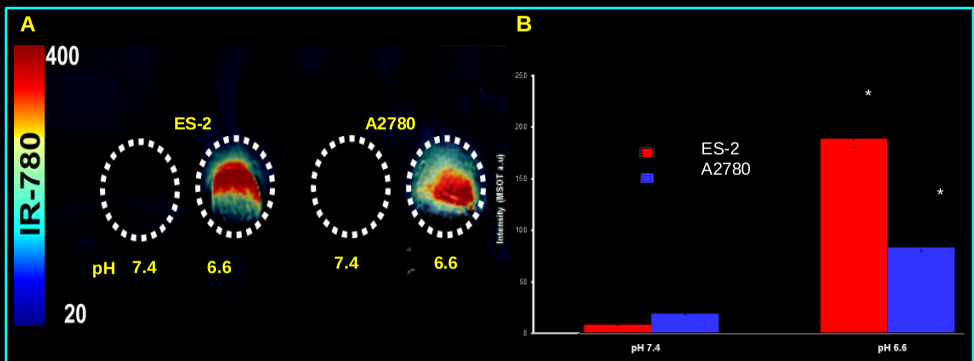

Figure 6: 3D analysis of dye-loaded pHLIP-MSNs by MSOT analysis. Cells treated with pHLIP-MSNs were scraped, centrifuged, and PBS washed before insertion into agar tissue phantoms. Tissue phantoms were imaged using multispectral optoacoustic tomography (MSOT). The observed nanoparticle uptake in both ES-2 and A2780 cells at pH 6.6 (205 a.u in ES-2 cells and 112 in A2780 cells) was in agreement with the NIR fluorescent images **(Figure 5).** Neither ES-2 nor A2780 had appreciable uptake of the nanoparticles at pH 7.4 (4 a.u in ES-2 and 7 a.u. in A2780 cells). P<0.05

CONCLUSIONS

- ❖ Acidic extracellular tumor microenvironment is a valid target for pH-sensitive probes, such as pHLIPs.
- ❖ Dye-conjugated pHLIPs can selectively insert across pancreatic cell membranes when in acidic environments, highlighting tumor cell presence.
- ❖ Decoration of nanoparticles, such as synthesized chitosan-coated MSNs, with pHLIPs permits pH-specific cell entry and controlled release of encapsulated molecules.
- ❖ Continued observation of sequence-specific parameters influencing pHLIP insertion behavior may expand the range of applications for pHLIP technology, such as demonstrating insertion across a wider pH range.
- ❖ With further analysis and implementation of this technology, there is potential to revolutionize the detection and treatment of pancreatic and ovarian cancer alongside other metastatic diseases.

ACKNOWLEDGEMENTS

This work was supported by NIH grants R01CA205941, R01CA212350, and R01EB020125

OCCURRENCE AND TIMING OF ADVANCED CARE DISCUSSIONS IN RECURRENT OVARIAN CANCER PATIENTS PARTICIPATING IN CLINICAL TRIALS REMAIN TO BE OPTIMIZED

Anjalika Gandhi MD, Blaire Scott, Spencer Hall, Sara Vesely PhD, Debra Richardson MD
Department of Gynecologic Oncology, Stephenson Cancer Center of OU Health

Objectives: In women with recurrent ovarian cancer (ROC), advanced care planning (ACP) such as advanced directives (AD), code status, and timely hospice referral should be addressed. In the clinical trial (CT) focused Stephenson Cancer Center (SCC), treatment with novel potentially life-prolonging therapies may alter timing of discussions. Our study compares patterns of ACP between CT and non-CT ROC patients.

Methods: All patients ≥18 years who had ROC and were ever treated at SCC for during the year of 2015 were reviewed. Patients who ever (n=84) versus never (n=41) participated in a therapeutic CT were compared. Chi-square or Fisher's exact tests and two sided t-tests or Wilcoxon Rank-Sum tests compared demographic data and ACP variables using an $\alpha=0.05$. Multivariable logistic regression estimated adjusted odds ratios (aOR) adjusted for CT participation, age, and Charlson comorbidity index.

Results: 125 patients were identified, 67% participated in CTs. Cohorts were similar in most demographic and histopathologic characteristics. Caucasian patients comprised 95% of the CT cohort vs 80% of non-CT patients (p=0.0205). Median duration of follow up after first recurrence was 856 days in trial patients vs 308 days in non-trial patients (p<0.0001). In unadjusted analyses, CT participants more frequently discussed AD (36% vs 17% non-trial patients, p=0.0321). Rates medical power of attorney (MPOA) discussion (54% in both), code status discussion (43% vs 27% in non-CT patients), and palliative care referral (49% vs 37% in non-CT patients) were similar. Median time between first recurrence and code status discussion was significantly longer in CT versus non-CT participants (731 days (IQR 102-1376) versus 57 days ((IQR 38-565), p=.0379). Of 81 deceased patients, though rates of hospice enrollment were similar (74% CT versus 71% non-trial), CT patients more frequently died in the hospital (22.8% vs 8.7%) or a care facility (14% vs 0%) (p=0.0311). ACP discussions and palliative care referrals tended to occur either during or after CT. In adjusted analyses, palliative care referral was the only significant predictor of discussions of code status (aOR 3.69, 95% CI 1.67-8.152), AD (aOR 14.46, 95% CI 5.04-41.49), and MPOA (aOR 8.71, 95% CI 3.66-20.73). Participation in neither late phase nor phase 1 trials significantly predicted the odds of ACP.

Conclusions: The time between the recurrence and code status discussions was significantly longer in CT participants, and ACP discussions occurred typically during or after a trial. ACP occurred more frequently when patients were referred to palliative care, independent of participation in either late phase or phase 1 CT. Prioritizing ACP and supportive care referral, especially in CT participants, may improve these rates and optimize end of life care.

Occurrence and Timing of Advanced Care Discussions in Recurrent Ovarian Cancer Patients Participating in Clinical Trials Remain to be Optimized

Authors: Anjalika Gandhi, MD MS; Blaire Scott; Spencer Hall; Sara Vesely, PhD; Debra Richardson, MD

Background:
- Ovarian cancer is the deadliest GYN cancer
- ROC is incurable
- Aggressive care still toward the end of life
- Timely palliative care services improve QOL and survival and reduce ICU admissions and hospital death
- CT participation may divert resources from ACP
- Phase 1 trial patients may have the biggest gap

Objectives:
To compare patterns of ACP between trial and non-trial ROC patients

Methods
- **Design:** retrospective cohort study
- **Patients:** ≥18 years who were treated at SCC for the diagnosis of OC during the year of 2015 and had ever recurred. Categorized based on ever participating in CT
- **Outcomes of interest:** MPOA, AD, and code status discussions and/or paperwork
- **Data sources:** EMR and Meditech
- **Statistics:** Chi-square or Fisher's exact tests and two sided t-tests or Wilcoxon Rank-Sum tests compared demographic data and ACP variables of interest using an α=0.05. Multivariable logistic regression estimated adjusted odds ratios (aOR) adjusted by CT participation, age, and CCI

RESULTS
- N=125, 67% participated in CTs
- Demographics similar except race: CT 95% Caucasian vs 80% in non-CT (p=0.0205)
- All ACP discussions, including code status, tended to occur during or after CT (Figure 1)
- Univariate outcomes in Table 1
- aOR for code status discussion in Table 2
- In all logistic models, palliative care referral was the only predictor of discussions of code status (table 2); AD (aOR 14.46, 95% CI 5.04-41.49), and MPOA (aOR 8.71, 95% CI 3.66-20.73)

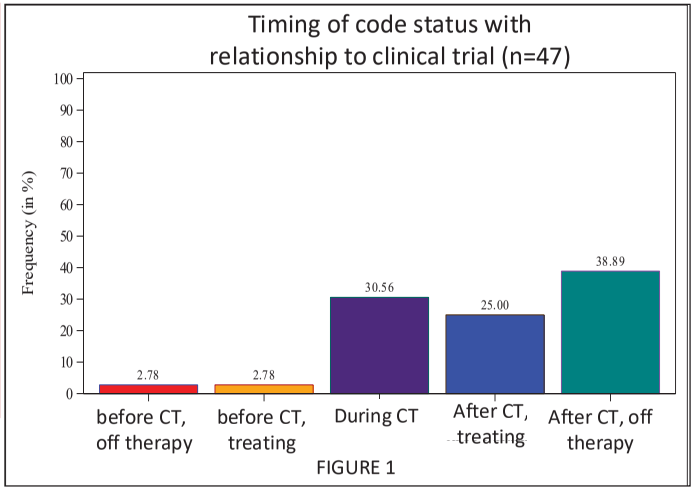

FIGURE 1

Recurrent ovarian cancer patients who participate in clinical trials tend to have longer intervals between diagnosis of recurrence and advanced care planning discussions. **Palliative care referral is the only significant predictor of advanced care planning. Early referral to palliative care, especially in clinical trial patients,** may optimize end of life care

Results

Table 1

Count (%) Or Median (IQR)	Non-CT (n=41)	CT (n=84)	p-value
Code status discussion	11 (27)	36 (43)	0.0824
MPOA discussion	22 (54)	45 (54)	0.9927
AD discussion	7 (17)	30 (36)	0.0321
Supportive or palliative care referral	15 (37)	41 (49)	0.197
Duration (days) of follow up after first recurrence	308 (91.5 - 640.0)	857.5 (437-1538)	<0.0001
Time (days) between first recurrence and code status discussion	57 (38-565)	731 (102-1376)	0.0379
Deceased	24 (56)	57 (68)	
Enrolled in hospice	17 (71)	42(74)	0.0384

Table 2 - aOR and Wald Cis for Code status discussion

	aOR	95% CI	
CT participant - only late phase (ref=non-CT)	1.833	0.651	5.16
CT participant - ever with history of phase 1 (ref=non-CT)	1.267	0.529	3.04
Referral to palliative care	3.686	1.666	8.15
Age at diagnosis	0.997	0.964	1.03
CCI	0.919	0.697	1.21

Abbreviations: GYN gynecologic, ROC recurrent ovarian cancer, QOL quality of life, ICU intensive care unit, CT clinical trial, ACP advanced care planning, MPOA medical power of attorney, AD advanced directive, CCI Charlson comorbidity index, aOR adjusted odds ratio, IQR interquartile range, CI confidence interval

OU Health | Stephenson Cancer Center

PLECTIN-1 CONTRAST AGENT IDENTIFIES PANCREATIC CANCER

Jordan Hagood,[1,2] William M. MacCuaig,[1,3] Catherine Vopat,[1,3] Alex Frickenstein,[1,3] Molly W. McNally,[1,2] Abhilash Samykutty,[1,2] Barish Edil,[1,2,3] Lacey R. McNally.[1,2,3]
Presenting author email address: Jordan-Hagood@ouhsc.edu
[1]Stephenson Cancer Center, University of Oklahoma, Oklahoma City, OK; [2]Department of Surgery, University of Oklahoma, Oklahoma City, OK; [3]Department of Biomedical Engineering, University of Oklahoma, Norman, OK.

Purpose: New methods in the imaging of pancreatic ductal adenocarcinoma can be used to improve diagnosis and treatment. Plectin-1 has been identified as an upregulated protein on the surface of pancreatic cancer cells. Our goal was to develop a plectin-1 targeted contrast agent to improve detection of pancreatic cancer.

Methods: We developed a plectin-1 contrast agent by combining a novel plectin-1 ligand conjugated to IR750-amine dye. The fluorescent and optoacoustic signal of the plectin-1 contrast agent was confirmed using UV-spectroscopy and multispectral optoacoustic tomography. Plectin-1 positive and negative cells were treated with the plectin-1 contrast agent *in vitro*. Near-infrared fluorescent imaging was used to compare the resulting signal. Plectin-1 contrast agent binding was confirmed using flow cytometry.

Results: In comparison to plectin-1 negative cells, plectin-1 positive cells treated with the fluorescent probe showed significant increase in signal $p<0.05$. The results of this study indicate that plectin-1 is a unique biomarker of pancreatic cancer cells and can be further used as a target for the imaging of pancreatic tumors *in vivo*.

Work funding provided by NIH grants R01-EB020125, R01-CA212350, and R01-CA205941.

Plectin-1 Contrast Agent Identifies Pancreatic Cancer

Jordan Hagood, William M. MacCuaig, Catherine Vopat, Alex Frickenstein, Molly W. McNally, Abhilash Samykutty, Barish Edil, Lacey R. McNally

Stephenson Cancer Center, University of Oklahoma Health Sciences Center

Abstract

Purpose: New methods in the imaging of pancreatic ductal adenocarcinoma can be used to improve diagnosis and treatment. Plectin-1 has been identified as an upregulated protein on the surface of pancreatic cancer cells. Our goal was to develop a plectin-1 targeted contrast agent to improve detection of pancreatic cancer.

Methods: We developed a plectin-1 contrast agent by combining a novel plectin-1 ligand conjugated to IR750-amine dye. The fluorescent and optoacoustic signal of the plectin-1 contrast agent was confirmed using UV-spectroscopy and multispectral optoacoustic tomography. Plectin-1 positive and negative cells were treated with the plectin-1 contrast agent *in vitro*. Near-infrared fluorescent imaging was used to compare the resulting signal. Plectin-1 contrast agent binding was confirmed using flow cytometry.

Results: In comparison to plectin-1 negative cells, plectin-1 positive cells treated with the fluorescent probe showed significant increase in signal $p<0.05$. The results of this study indicate that plectin-1 is a unique biomarker of pancreatic cancer cells and can be further used as a target for the imaging of pancreatic tumors *in vivo*.

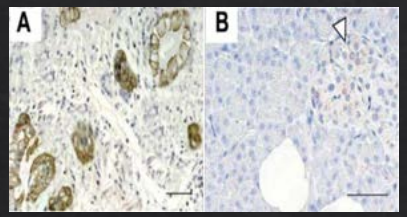

Figure 1. Immunohistochemistry shows plectin1 staining in human patient (A) pancreatic ductal adenocarcinoma (Stage IIB) and (B) non-involved which represents a surgically operative stage (arrow=islet). Bar=50µ Brown=positive staining.

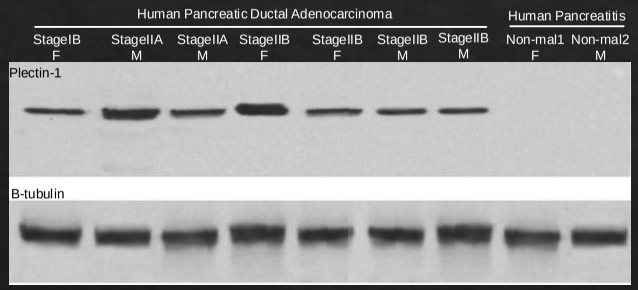

Figure 2. Western blot shows that each of the 7 human PDAC tumors (Stages 1B-IIB) surgically resected expressed plectin1 with 2 human pancreatitis (non-malignant controls). B-tubulin is a loading control.

Plectin-1 Contrast Agent Synthesis

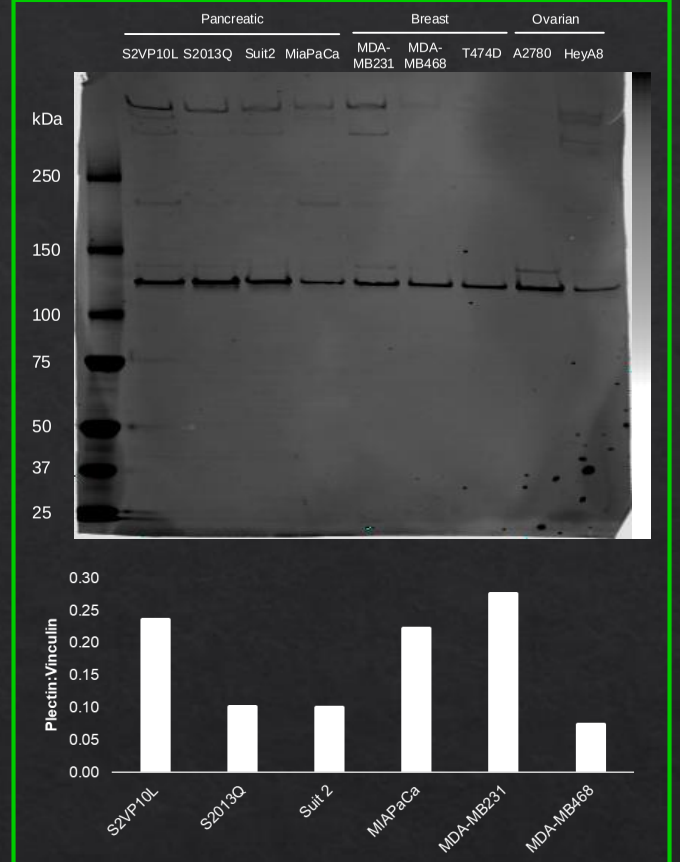

Figure 3. (A) Western blot probed for plectin-1 and vinculin using lysates from pancreatic, breast, and ovarian cancer cell lines. (B) Plectin-1 band normalization to determine relative plectin-1 expression. The ovarian cancer cell lines A2780 and HeyA8 are negative for plectin-1 protein expression.

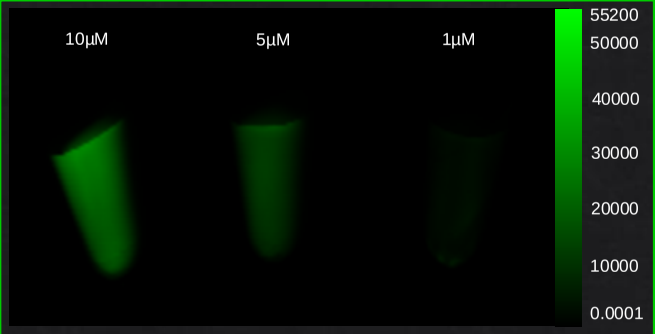

Figure 4. Plectin-1 contrast agent fluorescent signal at varying concentrations.

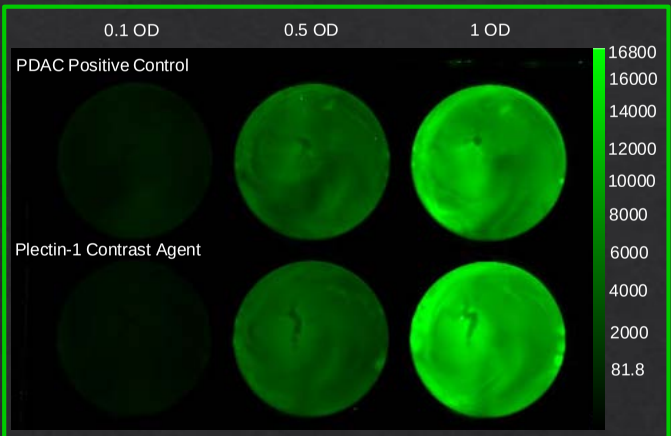

Figure 5. *In vitro* fluorescent imaging of pancreatic cancer cells treated with plectin-1 contrast agent compared to a PDAC positive control.

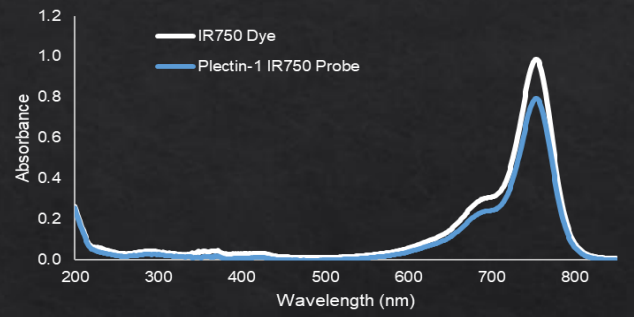

Figure 6. UV spectroscopy of IR750-amine dye and the plectin-1 contrast agent demonstrating that the conjugation process does not affect the fluorescent signal of the dye.

Conclusions and Future Studies

The results of this study indicate that the plectin-1 contrast agent allows specific targeting of pancreatic cancer cells for fluorescent imaging *in vitro*. The fluorescent signal of the IR750-amine is dependent on concentration, but is unaffected by conjugation to the plectin-1 ligand.

Western blot data indicates ovarian cancer cell lines negative for plectin-1 protein. These cell lines can be used as a negative control to further support plectin-1 contrast agent specificity. In addition to plate studies, flow cytometry and MSOT imaging can be used to confirm plectin-1 contrast agent binding.

Injection of the plectin-1 contrast agent subsequent to induction of PDAC tumors into mice could provide *in vivo* data regarding probe specificity, off target accumulation, and signal intensity over time.

Acknowledgements

Work funding provided by NIH grants R01-EB020125, R01-CA212350, and R01-CA205941.

IL-1B PRODUCTION VIA STING SIGNALING ENHANCES ANTITUMOR MEMORY FORMATION

Ashley R. Hoover[1,2], Kaili Liu[1], Xiao-Hong Sun[2], Wei R. Chen[1]
[1]University of Oklahoma, [2]Oklahoma Medical Research Foundation

To treat metastatic tumors, our lab has developed a unique approach that combines tumor ablative therapy with immunotherapy. We have termed this approach laser immunotherapy (LIT). LIT uses the combination of local laser ablation and local administration of an immunostimulant directly into the tumor to induce tumor-specific immune responses. Our pre-clinical studies and preliminary clinical trials demonstrated that the synergy of tumor ablative therapy and immunotherapy could not only destroy the treated primary tumors but also eradicate untreated metastases, leading to long-term survival and tumor resistance. Through single cell RNA sequencing (scRNAseq) on the tumor infiltrating leukocytes, we discovered that type I IFNs and the proinflammatory cytokine IL-1β are the dominant cytokines produced following LIT treatment. Further *in vivo* and *in vitro* analysis revealed that glycated chitosan (GC), the immune stimulating component of LIT, stimulates the production of type I IFN and IL-1β through STING signaling in dendritic cells (DCs). Furthermore, we discovered that the synergy of type I IFN and IL-1β production via STING signaling in DCs is crucial for the development of T cell memory following LIT and preventing tumor growth upon re-challenge of LIT cured survivors. The data presented within will reveal the role of IL-1β in enhancing anti-tumor memory responses generated via GC making it more suitable for immunotherapy than currently approved adjuvants.

Funding: R01CA205248-01A1 NIH

IL-1β Production via STING Signaling Enhances Antitumor Memory Formation Following LIT

Ashley R. Hoover[1,2], Kaili Liu[1], Xiao-Hong Sun[2], and Wei R. Chen[1]

[1]Stephenson School of Biomedical Engineering, University of Oklahoma, Norman, OK 73019
[2]Department of Arthritis and Clinical Immunology, Oklahoma Medical Research Foundation, Oklahoma City, Oklahoma 73104

Introduction

Laser immunotherapy (LIT) combines photothermal therapy (PTT) and an immunostimulant, N-dihydrogalactochitosan (GC) to generate effective antitumor immunity. LIT-induced immune responses can clear the treated tumor, its metastases, and prevent cancer relapse in human patients and animal models. The goal of the current study is to understand how LIT activates antitumor T cell immunity in order to eliminate poorly immunogenic metastatic tumors and prevent cancer relapse. GC induces a strong type I IFN and IL-1β response and type I IFNs are critical for the success of LIT as animals lacking the IFNaR1 are no longer responsive to LIT. In dendritic cells (DCs), GC requires STING signaling to produce type I IFN and IL-1β as DCs lacking STING no longer produce these cytokines. *In vivo*, there is no difference in survival between LIT-treated STING heterozygotes and STING deficient animals bearing B16-F10 tumors. However, while LIT-cured wild type animals rejected tumor re-challenges, when the LIT-cured STING deficient animals were re-challenged with B16-F10 tumor cells, the tumor growth was comparable to the untreated controls. This suggests that there is a memory defect in the STING deficient animals. Interestingly, STING heterozygous animals also have an immune memory defect upon B16-F10 tumor rechallenge. While type I IFN production between wild type and STING heterozygous bone marrow derived dendritic cells (BMDCs) stimulated with GC is comparable, IL-1β is dramatically reduced in the STING heterozygous BMDCs. IL-1β is a critical pro-inflammatory cytokine that enhances T cell activation, memory formation, migration, and effector function. To determine whether LIT STING heterozygous animals have a reduction in tumor specific CD8⁺ T cell development following LIT or in the development of CD8+ T cell memory formation, we assessed tumor specific CD8⁺ T cell responses via ELISPOT. In collaboration with Dr. William Hildebrand's group, we have identified several B16-F10 tumor specific peptides, a few of which initiate CD8⁺ T cell responses. LIT-cured tumor-rechallenged animals, that remain tumor free, have a strong response to 5 tumor specific peptides. Eight days post LIT treatment, both wild type and STING heterozygous animals have comparable splenic CD8⁺ T cell responses. However, both wild type and STING heterozygous animals, that were LIT cured and then rechallenged with B16-F10 tumors, failed to produce these same T cell responses. It is important to note, all LIT-cured STING heterozygous animals succumb to tumor growth while only 50% of LIT-cured re-tumor challenged wild type animals grow tumors. This posits that IL-1β plays a role in memory CD8+ T cell formation and will be further investigated using IL1R1 deficient animals. However, this does not explain why half of the LIT-cured tumor-challenged wild type animals, regrow tumors. This will be explored further by comparing the expression levels of these peptides on the B16-F10 tumors *in vivo*.

Results

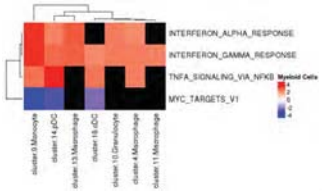

Figure 1. : Heat map of pathway enrichment for myeloid cell clusters induced by LIT. Single-cell RNA sequencing of PyMT breast tumors reveals dramatic upregulation pro-inflammatory pathways in LIT treated tumors compared to untreated tumors.

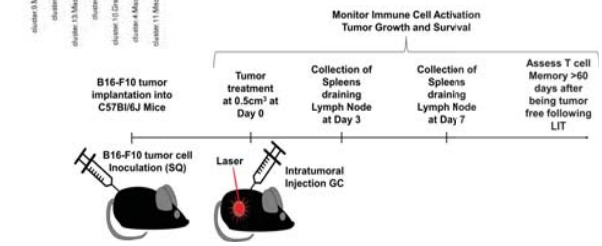

Figure 2. Schematic of LIT procedure and subsequent analysis.

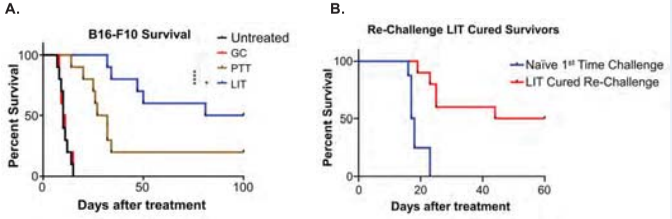

Figure 3. LIT successfully treats B1-F10 tumors. (A) Wild type C57Bl/6 mice were inoculated with B16-F10 highly metastatic tumors and then treated with GC, PTT, or PTT+GC (LIT) once the tumors reached 0.5cm³. After treatment, the animals were monitored for tumor growth and sacrificed when they reached ethical time points. (B) LIT cured animals that had been tumor free for >60 days were rechallenged on the opposite flank and monitored for tumor growth and were sacrificed once the animals reached ethical time points.

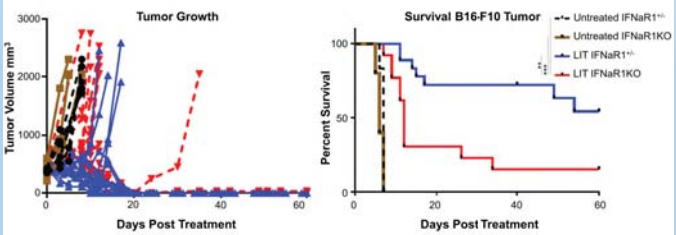

Figure 4. Type I IFNs are critical for the therapeutic effect of LIT. IFNaR1 heterozygous and deficient mice were inoculated with B16-F10 tumors. Once the tumors reached 0.5cm³ tumors were treated with LIT or left untreated. Tumor growth and survival was monitored for 60 days following treatment.

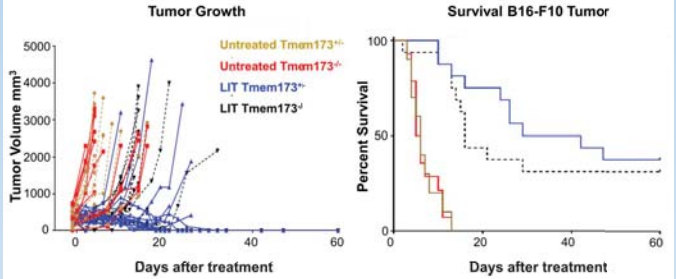

Figure 5. STING is dispensable for the successful treatment of B16-F10 tumors following LIT. Tmem173 heterozygous and deficient mice were inoculated with B16-F10 tumors. Once the tumors reached 0.5cm³ tumors were treated with LIT or left untreated. Tumor growth and survival was monitored for 60 days following treatment.

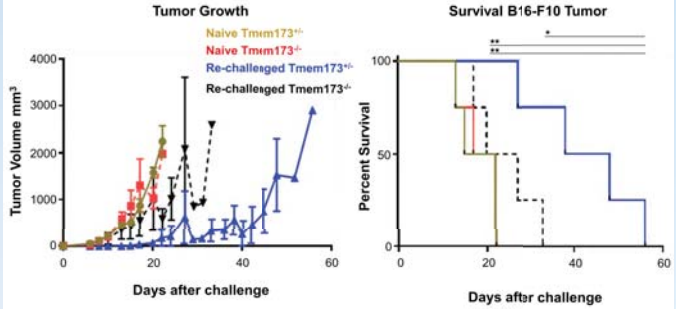

Figure 6. STING is required for the generation of immunological memory. LIT-cured STING heterozygous and deficient mice were re-challenged with B16-F10 tumors on the opposite flank. Naïve STING heterozygous and STING deficient animals (1st challenge) were used as positive controls for tumor growth. STING deficient re-challenged animals grew tumors at a similar rate as the untreated controls suggesting a memory defect.

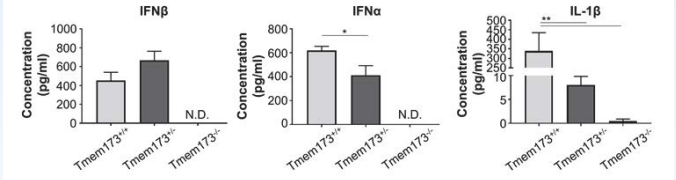

Figure 7. GC induces the production of type I IFN and IL-1β in bone marrow derived dendritic cells. BMDCs were stimulated for 24 hours with GC prior to harvesting of the supernatant for ELISA. Type I IFN production is nearly equivalent in Wild type and STING heterozygous BMDCs. IL-1β is dramatically reduced in the STING heterozygous mice.

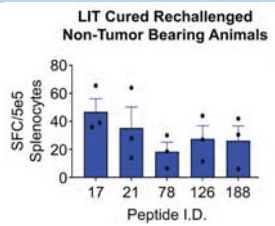

Figure 8. LIT-cured, tumor-rechallenged animals that remained tumor free develop a tumor specific CD8⁺ T cell response. LIT-cured wild type animals were rechallenged on the opposite flank with B16-F10 tumors. Tumor growth was monitored for 60 days. By the 60-day mark these animals (n=3) remained tumor free and the spleen was harvested for ELISPOTs using peptides that are expressed by specifically by B16-F10 tumor cells and not healthy mouse tissues (in collaboration with Dr. William Hildebrand's group).

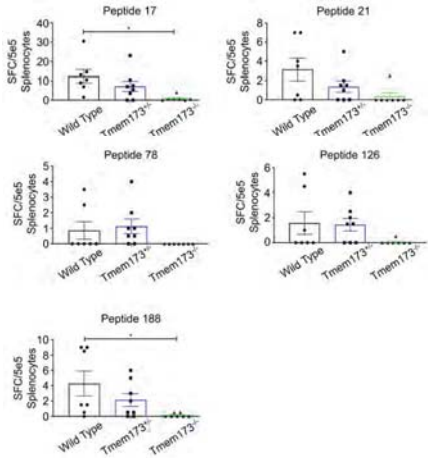

Figure 9. STING heterozygous animals develop tumor specific CD8⁺ T cells similar to wild type 8 days post LIT treatment. Animals were inoculated with B16-F10 tumor cells. Once the tumors reached 0.5cm³ they were treated with LIT. 8 days post treatment, spleens were isolated and used for ELISPOTs.

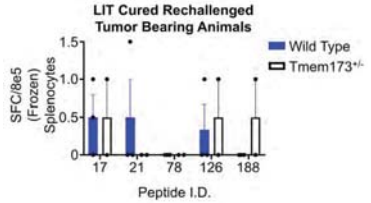

Figure 10. LIT-cured STING heterozygous and wild type animals that grow tumors upon rechallenge do not develop a CD8+ T cell specific antitumor response. After tumor challenge the animals were monitored for tumor growth. Once the tumor reached ethical endpoints, splenocytes were isolated and preserved for later use for ELISPOT.

Conclusion

- Type I IFNs are critical for the therapeutic effect of LIT as animals deficient in a type I IFN response are no longer protected from tumor progression.
- GC induces DC production of type I IFN and IL-1β through STING signaling.
- STING mediated IL-1β is involved in the generation of immunological memory following LIT.
- Current experiments are focusing specifically on IL-1β function in LIT antitumor immunity and tumor peptide expression levels.

Acknowledgements

This study was supported in part by grants from the U.S. National Institutes of Health (RO1 CA205348), and the Oklahoma Center for Advancement of Science and Technology (HR16-085).

MODEL OPTIMIZATION AND CHEMOPREVENTION OF IPMN DRIVEN PDAC IN KPSD4 MOUSE MODEL

Gaurav Kumar[1,2], Venkateshwar Madka[1], Anil Singh[1], Nandini Kumar[1], Nicole Stratton[1], Stan Lightfoot[1], Altaf Mohammed[3], Mark S. Miller[3], Rao CV[1,2]

[1]Center for Cancer prevention and Drug Development, Hem-Onc Section, Department of Medicine, Stephenson Cancer Center, University of Oklahoma Health Sciences Center, Oklahoma City, OK, [2] VA Medical Center, Oklahoma City, OK, and [3]Division of Cancer Prevention, Chemoprevention Agent Development Research Group, National Cancer Institute, Rockville, MD

Pancreatic ductal adenocarcinoma (PDAC) is a lethal cancer with one of the lowest five-year survival rates. Patients with intraductal papillary mucinous neoplasms (IPMN) or mucinous cystic neoplasms (MCNs) are at high risk for the development of PDAC and thus are target populations for intervention with chemopreventive agents. The lack of optimized animal models of IPMNs has limited the development of chemopreventive agents and vaccines. We have thus characterized the suitability of the Pdx1^{Cre}.LSL-*Kras*^{G12D}.SMAD4$^{flox/flox}$ (KPSD4) model for IPMN formation and their progression to PDAC. In addition, as a proof-of-principle we assessed the chemopreventive efficacy of gefitinib in the KPSD4 model. The development of IPMNs and PDAC were monitored up to 44 weeks of age by serial sacrifice at 6, 12, 18, 24, 36, and 44 weeks of age in male and female KPSD4 mice (n=6/time point), at which time the pancreata were analyzed for lesion development.

The KPSD4 mouse model developed both IPMNs and pancreatic intraepithelial neoplasia (PanINs) spontaneously. IPMNs were histologically classified as i) independent (single IPMN duct); ii) IPMN cluster/adenoma (multiple IPMN ducts as cluster or adenoma); iii) IPMN borderline (dysplasia with or without CIS); and iv) IPMN invasive carcinoma. At 6 weeks of age, the pancreata were normal in appearance (>94% in male; >97% female) with low frequency (Mean ± *SEM*) of PanINs (Male, 6.5±2.65; Female, 3.44±2.12) and IPMNs (Male, 5.5±2.21; Female, 2.56±0.96). At 12 weeks of age, there was a significant increase of IPMN number and their progression to borderline type that advanced to carcinoma by age 24 weeks. At 36 weeks of age, >80% of the KPSD4 mice developed carcinomas that rapidly spread to the entire pancreas by 44 weeks of age. Overall, IPMN progression to PDAC required somewhat less time than did the progression of PanINs to PDAC in the KPSD4 mouse model. A major limitation of the KPSD4 model was the mortality due to secondary phenotypes. In KPSD4 mice, ~40% mortality was observed between 6 and 18 weeks of age due to intestinal tumors leading to obstruction.

For the chemopreventive efficacy bioassay, 6 week old male and female KPSD4 mice (34/group) were fed diets containing 0 or 100 ppm of gefitinib for 18 weeks. Mice were euthanized at 24 weeks of age and pancreata were assessed for IPMNs, PanINs, and PDAC. Control-diet-fed male and female mice showed IPMN driven PDAC incidences of 83% and 100%, respectively, whereas male and female KPSD4 mice exposed to 100 ppm gefitinib showed PDAC incidences of 50% and 27% (p<0.0006), respectively. A significant reduction of IPMN individual ducts, adenoma, and IPMN borderline was observed in KPSD4 mice fed gefitinib, thus demonstrating a strong suppression of IPMN individual duct progression to more advanced lesions upon treatment with gefitinib. [Supported by NCI HHSN261201500038I].

Model optimization and chemoprevention of IPMN driven PDAC in KPSD4 mouse model

Gaurav Kumar[1], Venkateshwar Madka[1], Anil Singh[1], Nandini Kumar[1], Nicole Stratton[1], Stan Lightfoot[1], Altaf Mohammed[2], Mark S. Miller[2], Chinthalapally V Rao[1,3]

[1]Center for Cancer Prevention and Drug Development, Department of Medicine, Hem-Onc Section, Stephenson Cancer Center, University of Oklahoma Health Sciences Center (OUHSC), Oklahoma City, OK;

[2]Division of Cancer Prevention, National Cancer Institute, Bethesda, MD, [3]VA Medical Center, Oklahoma City, OK,

Rationale

- Pancreatic ductal adenocarcinoma (PDAC) is a lethal cancer with one of the lowest five-year survival rates.
- Projected to become the 2nd leading cause of cancer-related deaths in the United States by 2030 .
- 5-year survival rate still stands at 9% only.
- Pre-invasive lesions progression to PDAC varies in different types of preneoplasms (e.g., PanIN, IPMN, and MCN).

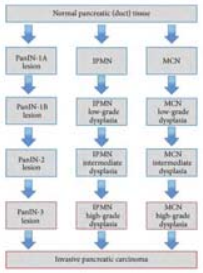

Specific Aim

- Characterize the development of precursor lesions (IPMN) and their progression to PDAC in genetically engineered mouse model (Pdx1$^{Cre/+}$.LSL-Kras$^{G12D/+}$.SMAD4$^{flox/flox}$; aka KPSD4).
- Evaluate chemopreventive efficacy of the EGFR inhibitor gefitinib (0, 100 ppm) in KPSD4 mouse model.

Experimental Design and Methodology

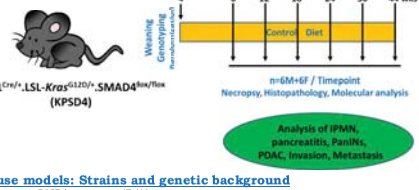

Mouse models: Strains and genetic background

LSL-*Kras*$^{G12D/+}$: *Kras*$^{tm4Tyj/J}$ (Stock:129S4 and C57BL/6)
SMAD4$^{fl/fl}$: Smad4$^{tm2.1Cxd}$ (Stock: 129S and C57BL/6)
***Pdx1*^{Cre}**: Pdx1$^{cre)6Tuv/J}$ (Stock: FVB/N6 and C57BL/6)

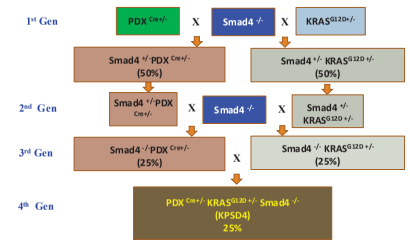

Results

Gross findings

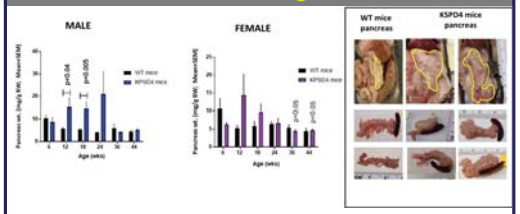

Histopathology

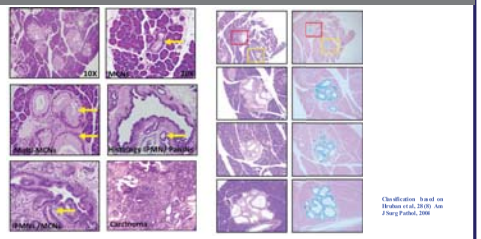

IPMN lesion development

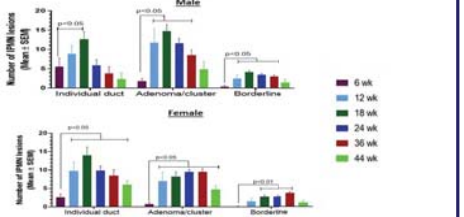

PanIN lesions development

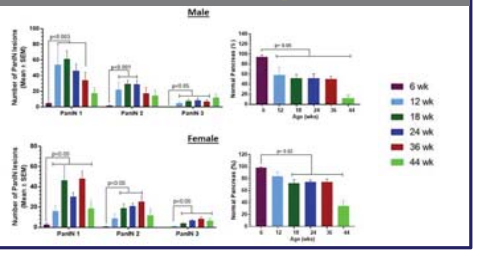

Carcinoma Incidence & spread

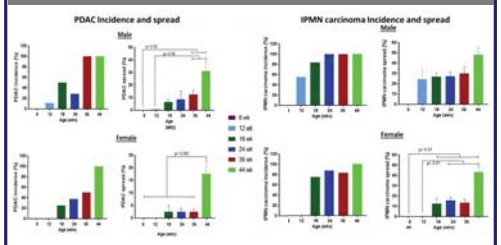

Other Abnormalities

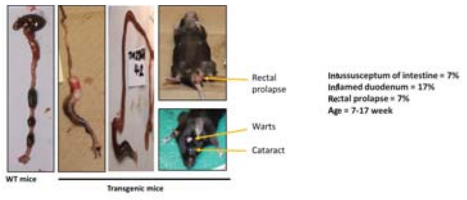

Efficacy of gefitinib (EGFR inhibitor)

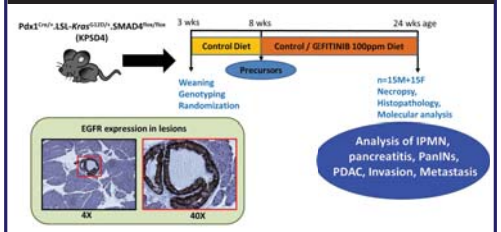

Effect of Gefitinib treatment

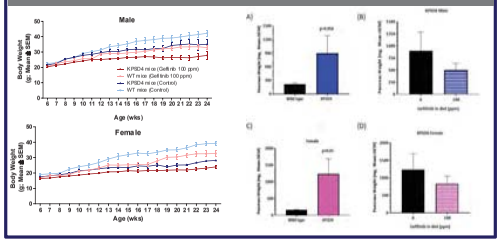

Gefitinib prevents lesions

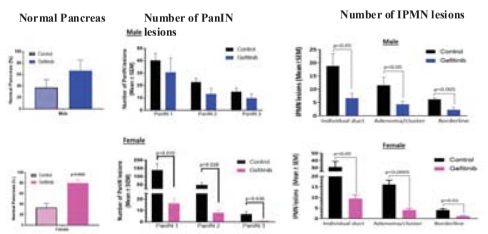

Gefitinib inhibits Carcinoma

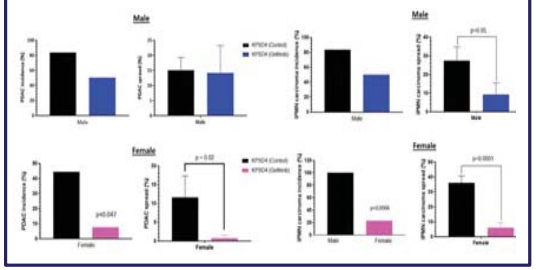

Conclusion

- Transgenic KPSD4 mice develop IPMN lesions that rapidly progressed to carcinoma.
- IPMN lesions were associated with mucin and EGFR expression.
- Control-diet-fed mice showed IPMN driven PDAC incidences of 83% - 100%, whereas mice exposed to 100 ppm gefitinib showed PDAC incidences of 27% - 50% (p<0.0006).
- A significant reduction of IPMN individual ducts, adenoma, and IPMN borderline was observed in KPSD4 mice fed gefitinib, thus demonstrating a strong suppression of IPMN individual duct progression to more advanced lesions upon treatment with gefitinib.
- Major limitation : In KPSD4 mice, ~30% mortality was observed between 6 and 18 weeks of age due to intestinal tumors leading to obstruction.

Acknowledgements:
HHSN261201500038i
Division of Cancer Prevention
National Cancer Institute
Rockville, MD

SCRNASEQ ANALYSIS AND VISUALIZATION FOR BREAST TUMOR-INFILTRATING IMMUNE CELLS UPON LASER IMMUNOTHERAPY

Kaili Liu[1], Ashley R. Hoover[1,2], Jason R. Krawic[3], Xiao-Hong Sun[2], William H. Hildebrand[3], and Wei, R. Chen[1]

[1] Stephenson School of Biomedical Engineering, University of Oklahoma, Norman, OK, 73019, [2] Arthritis & Clinical Immunology Research Program, Oklahoma Medical Research Foundation, Oklahoma City, OK, 73014, [3] Department of Microbiology and Immunology, University of Oklahoma Health Sciences Center, Oklahoma City, OK, 73014

Breast cancer is one of the most challenging human health burdens. Laser immunotherapy (LIT), using local administration of photothermal treatment (PTT) in combination with an immunoadjuvant, N-dihydrogalactochitosan (GC), has displayed promising capacities to impede tumor growth and suppress metastases in both animal experiments and preclinical studies. However, the atlas of host immune cell compositions and transcriptome changes in response to LIT in breast cancer have not been fully understood. Here, we used single cell RNAseq (scRNAseq) tools and analyzed nearly 50 thousand immune cells collected from mammary tumors in MMTV-PyMT mice across four treatment groups (Control, PTT, GC and PTT+GC). We revealed major immune cell clusters and performed cell identity annotations. We identified regulatory genes from different treatments in both myeloid and lymphoid cells and further conducted gene functional enrichment. We dissected the PTT+GC stimulated signaling pathways for each cell cluster and discovered ubiquitously upregulated pro-inflammatory cytokine pathways. Single cell trajectory inference was also employed to reveal the immune cell dynamics upon laser immunotherapy. These analyses and visualizations for the high dimensional data provided the cell landscape of breast tumor microenvironment and highlighted the critical roles of pro-inflammatory pathways elicited by laser immunotherapy.

Acknowledgement: This research is supported in part by a grant from NIH/NCI (R01 CA205348) and by grants from the OCAST (HR16-085, HF20-019). The authors also acknowledge the support of Charles and Peggy Stephenson Chair endowment fund.

ScRNA-seq Analysis and Visualization for Breast Tumor-Infiltrating Immune Cells upon Laser Immunotherapy

Kaili Liu[1], Ashley R. Hoover[1,2], Jason R. Krawic[3], Xiao-Hong Sun[2], William H. Hildebrand[3], and Wei, R. Chen[1]

[1] *Stephenson School of Biomedical Engineering, University of Oklahoma, Norman, OK, 73019*
[2] *Arthritis & Clinical Immunology Research Program, Oklahoma Medical Research Foundation, Oklahoma City, OK, 73104*
[3] *Department of Microbiology and Immunology, University of Oklahoma Health Sciences Center, Oklahoma City, OK, 73104*

Introduction

Breast cancer is one of the most fatal cancer subtypes due to its high recurrence rate, distant metastasis, and poor prognosis. Laser immunotherapy (LIT), combines photo-thermal therapy (PTT) with an immune stimulant, glycated chitosan (GC). LIT has demonstrated promising results in breast cancer treatment. We hypothesize that local tumor intervention by LIT induces a systemic, antitumor immunity as depicted in Figure 1, with activation of immune cells such as dendritic cells, macrophages, and T cells. An in-depth study is needed to fully understand the mechanism in which LIT activates the immune system, in order to improve its efficacy and pave the way for its future clinical applications.

The tumor microenvironment consists of an interplay between cancer cells, fibroblasts, and complex mixture of immune cells. Tumor infiltrating leukocytes consist of multiple individual cells with different cell states and functions. Traditional approaches for measuring gene expressions, such as microarrays and bulk RNA sequencing, require hundreds to millions of cells as input, resulting in only an average reading across cell populations. Single-cell RNA sequencing (scRNA-seq) revolutionized transcriptomic studies by disclosing the heterogeneity of individual cells with high resolution. It directly measures gene expressions at the single cell level to characterize cell types, cell states, and dynamic cellular transitions. It has great potential for unbiased identification of novel cell subtypes and rare cell populations, therefore enabling a better understanding of transcription dynamics and gene regulatory relationships within the tumor microenvironment.

Advances of scRNA-seq have allowed for comprehensive analysis of cancer and immune system. In this work, the infiltrating immune cells in PyMT breast tumors were analyzed by scRNA-seq after LIT treatment. LIT remodeled the immune cell subsets of the tumor microenvironment (TME) by inducing Type I/II related pro-inflammatory pathways and activation gene sets. This new technology has provided a broad cellular and transcriptional basis to understand the mechanism of LIT-induced immune responses.

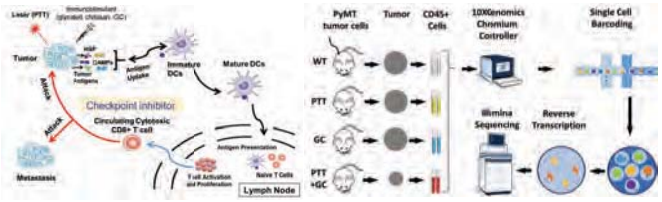

Figure 1. Schematic of laser immunotherapy mechanism

Figure 2. ScRNA-seq workflow

Results

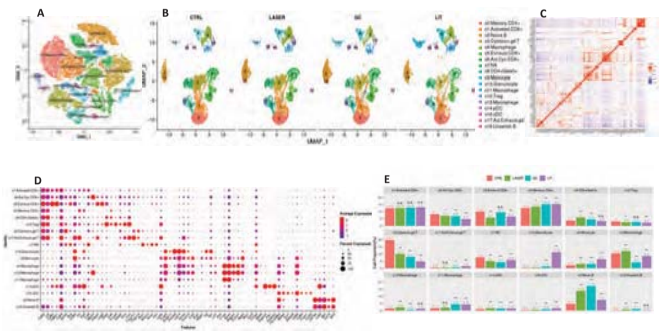

Figure 3. Atlas of tumor-infiltrating immune cells in treated tumors using scRNA-seq
(A)Two-dimensional visualization of single cell clusters using methods of t-distributed Stochastic Neighbor Embedding (t-SNE) from integrated immune cells of all four treatment groups. (B) Uniform Manifold Approximation and Projection (UMAP) plots for the immune cell atlas separated by each treatment group: untreated CTRL, PTT, GC and PTT+GC. (C) Gene-gene correlation heatmap of selected immune cell markers. (D) Validation of unsupervised clustering by using traditional immune cell markers. (E) Frequency of immune cell clusters in all four groups of treatments. Frequency was calculated for immune cells using immune cells in each cluster divided by total immune cells.

Methods

We divided mice bearing PyMT mammary tumors into four treatment groups: Control, PTT, GC, and PTT+GC, as shown in Figure 2. Treated tumors were collected and CD45+ immune cells were captured by flow cytometry. The 10XGenomics platform and Illumina NovaSeq 6000 were used for scRNA-seq. The *cellranger count* was used to take FASTQ files to performs alignment, filtering, barcode counting, and UMI counting (Figure 2). The *Seurat* and *Monocle2* were used for scRNA-seq data analysis. Statistical analysis and other visualizations were performed in R.

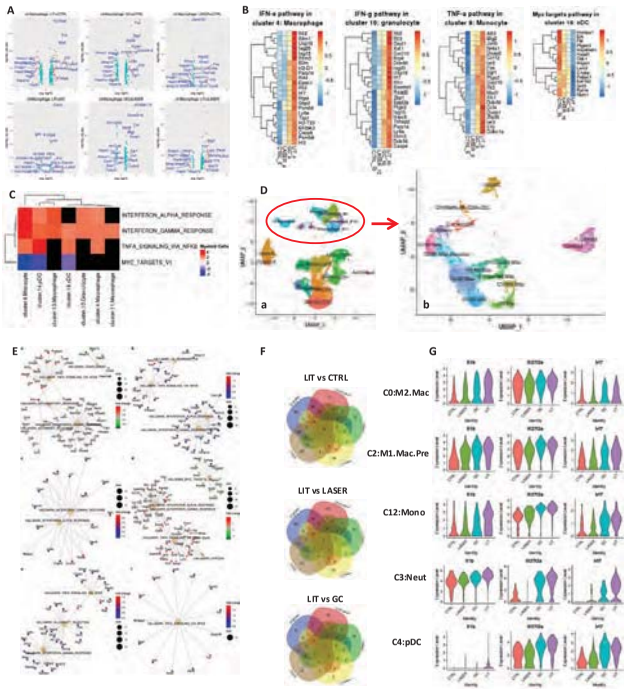

Figure 4. Immune responses of innate cells induced by PTT + GC
(A) Volcano plot for differential gene expression between various treatment groups in a representative myeloid cell cluster. (B) Heatmaps of normalized expression of treatment-induced pathway enrichment in selected myeloid cell clusters. (C) Heatmap of pathway enrichment for myeloid cell clusters induced by PTT+GC. (D) UMAP of re-clustered myeloid cells with higher shared-nearest neighbor (SNN) resolution. (a). Myeloid cell clusters within red dashed circle with default SNN resolution of 0.5. (b). Myeloid cell clusters in (a) with a higher SNN resolution of 0.7. (E) Gene-pathway network of LIT-induced DEGs in re-clustered myeloid cells. (F) Venn diagram showing the number of DEGs identified in each myeloid cell cluster. (G) Expression levels of representative Venn diagram-derived and myeloid cluster-shared DEGs in all four treatment groups.

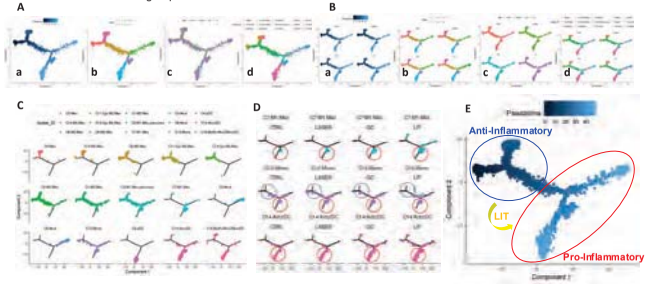

Figure 5. Cell trajectory inference of innate immune cells
(A) Branched trajectories of myeloid cells from four treatment groups colored by pseudotime (a), states (b), treatments (c) and annotated cell clusters (d). (B) Splitting of branched trajectories of (A) into each treatment group. (C) Branched trajectories of each myeloid cell cluster. (D) Splitting of selected myeloid clusters into each treatment group. Blue circles show reduction of cells and red circles show increase. (E) Schematic of anti- and pro-inflammatory trajectory regions.

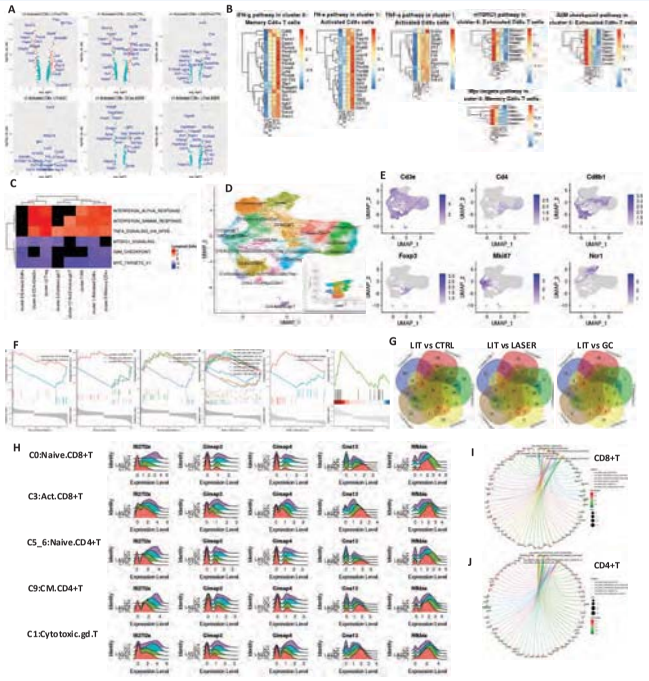

Figure 6. Immune responses of adaptive cells induced by PTT + GC
(A) Volcano plot for differential gene expression between various treatment groups in a representative lymphoid cell cluster. (B) Heatmaps of normalized expression of treatment-induced pathway enrichment in selected lymphoid cell clusters. (C) Heatmap of pathway enrichment for myeloid cell clusters induced by PTT+GC. (D) UMAP of re-clustered lymphoid cells with higher SNN resolution. (E) UMAP showing expression of selected T cell markers. (F) Pathway enrichment for selected re-clustered lymphoid cells induced by PTT+GC. (G) Venn diagram showing the number of DEGs identified in each lymphoid cell cluster. (H) Expression levels of representative Venn diagram-derived and lymphoid cluster-shared DEGs by in all four treatment groups. (I) Gene-pathway network of LIT-induced DEGs in all CD8+T cells. (J) Gene-pathway network of LIT-induced DEGs in all CD4+T cells.

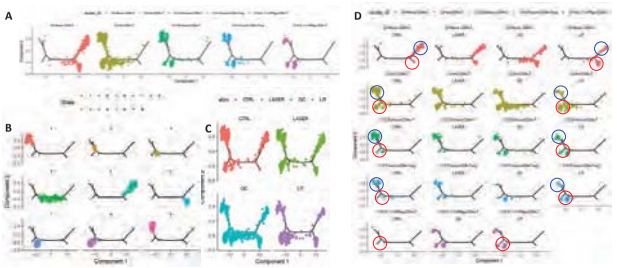

Figure 7. Cell trajectory inference of CD8+T cells
(A) Branched trajectories of each CD8+T subtype from four treatment groups. (B) Splitting of branched trajectories of all CD8+T into each state. (C) Splitting of branched trajectories of all CD8+T into each treatment group. (D) Splitting of (A) into each treatment group. Blue circles show reduction of cells and red circles show increase.

Conclusion

ScRNA-seq analysis (Figures 2 to 7) revealed induction of inflammatory phenotype in innate cells and activation of adaptive immune cells by laser immunotherapy, in order to induce and effective, long-term tumor-specific immunity. Further studies will provide a better understanding of the mechanism of LIT.

Acknowledgements

This research is supported in part by a grant from NIH/NCI (R01 CA205348) and by grants from the OCAST (HR16-085, HF20-019). The authors also acknowledge the support of Charles and Peggy Stephenson Chair endowment fund.

ACTIVE TARGETING FACILITATES PANCREATIC CANCER SPECIFIC UPTAKE OF NANOCONTRAST AGENTS

William M. MacCuaig,[1,2] Benjamin L. Fouts,[1] Molly W. McNally,[1,3] Abhilash Samykutty,[1,3] Min Li,[1] Lacey R. McNally.[1,2,3]

[1]Stephenson Cancer Center, University of Oklahoma, Oklahoma City, OK; [2]Department of Biomedical Engineering, University of Oklahoma, Norman, OK; [3]Department of Surgery, University of Oklahoma, Oklahoma City, OK.

Purpose: Inadequate early detection partially is responsible for the often-late stage diagnosis of pancreatic ductal adenocarcinoma resulting in an average survival of 14%-1% depending upon the stage at diagnosis. Nanoparticles containing either diagnostic or therapeutic agents offer an opportunity for improved delivery of agents to pancreatic tumors, however, the lack of tumor-specificity as a result of nanoparticle size and lack active targeting often diminishes overall efficacy.

Methods: We developed an acidic pH targeted mesoporous silica nanoparticles of three difference sizes, 26 nm, 45 nm, and 73 nm, to serve as a tumor specific nanocontrast agent (V7-TROS). TROS were capped with an acidic pH-responsive gatekeeper, and loaded with IR-780 reporter dye. Combinations of all-sized MSNs, both with and without V7, were compared *in vitro* and *in vivo* using near-infrared fluorescence and optoacoustic tomography. An orthotopic pancreatic cancer mouse model was used in these studies.

Results: Actively targeted nanoparticles via V7 peptide showed superior influence to tumor-specificity compared to size differences. Size exhibited a secondary, but still critical, influence on tumor-specificity. 26 nm V7-TROS showed 22-fold higher tumor-uptake, indicative of generated optoacoustic signal, compared to non-targeted 26 nm TROS. Similarly, 45 nm and 73 nm showed 6-fold and 4-fold increased signal over non-targeted counterparts. Uniquely, even the largest V7-TROS showed more signal than the smallest non-targeted nanoparticle. The results of our study indicate the potential of targeted acidic extracellular pH in pancreatic tumors and the greater importance of active targeting for improved *in vivo* pancreatic tumor accumulation.

Work funding provided by NIH grants R01-EB020125, R01-CA212350, and R01-CA205941.

Active Targeting Facilitates Pancreatic Cancer Specific Uptake of Nanocontrast Agents

William M. MacCuaig, Benjamin L. Fouts, Molly W. McNally, Abhilash Samykutty, Min Li, Lacey R. McNally

Stephenson Cancer Center, University of Oklahoma, Oklahoma City, OK

ABSTRACT

Purpose: Inadequate early detection is partially responsible for the often-late stage diagnosis of pancreatic ductal adenocarcinoma. Such diagnoses often result in an average 5-year survival rate of 14%-1% depending upon the stage of cancer progression. Nanoparticles containing either diagnostic or therapeutic agents offer an opportunity for improved delivery of agents to pancreatic tumors, however, the lack of tumor-specificity as a result of nanoparticle size and lack active targeting often diminishes overall efficacy.

Methods: We developed acidic pH targeted mesoporous silica nanoparticles of three difference sizes, 26 nm, 45 nm, and 73 nm, to serve as a tumor specific nanocontrast agents (V7-TROS). TROS were capped with an acidic pH-responsive gatekeeper, and loaded with IR-780 optoacoustic reporter dye. Combinations of all-sized MSNs, both with and without V7, were compared *in vitro* and *in vivo* using near-infrared fluorescence and optoacoustic tomography. An orthotopic pancreatic cancer mouse model was used in these studies.

Results: Actively targeted nanoparticles via V7 peptide showed superior influence to tumor-specificity compared to size differences. Size exhibited a secondary, but still critical, influence on tumor-specificity. 26 nm V7-TROS showed 22-fold higher tumor-uptake, indicative of generated optoacoustic signal, compared to non-targeted 26 nm TROS. Similarly, 45 nm and 73 nm showed 6-fold and 4-fold increased signal over non-targeted counterparts. Uniquely, even the largest V7-TROS showed more signal than the smallest non-targeted nanoparticle. The results of our study indicate the potential of targeted acidic extracellular pH in pancreatic tumors and the greater importance of active targeting for improved *in vivo* pancreatic tumor accumulation.

Synthesis Schematic of TROS MSNs

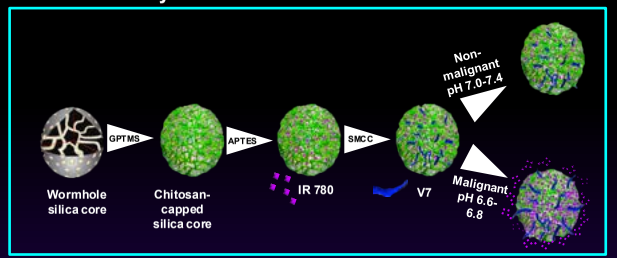

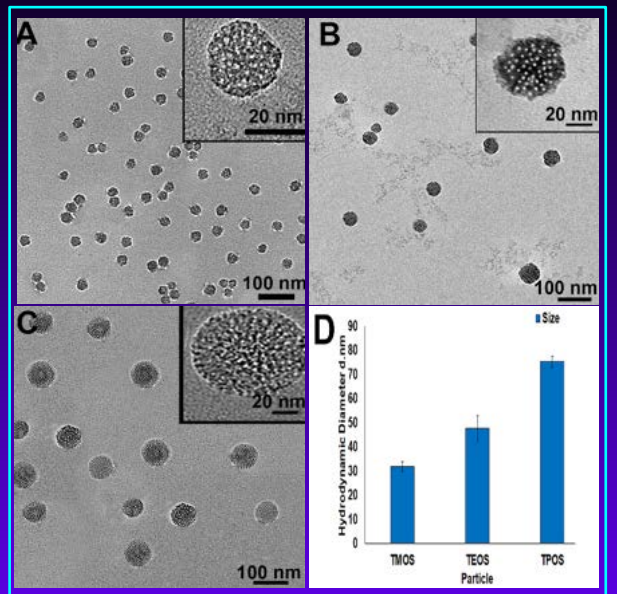

Figure 1: Transmission electron microscopy (TEM) images of A) TMOS, B) TEOS, and C) TPOS particles on lacey-carbon coated grids. Particles appeared as spherical structures with diameters of 26 nm, 45 nm, and 73 nm, respectively (D). All TROS pore sizes were measured at 1.5 nm.

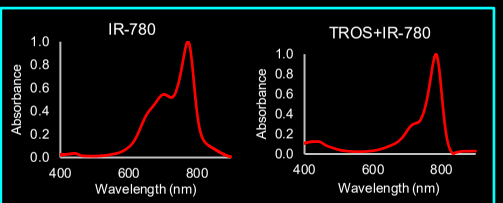

Figure 2: UV-Vis spectrum of IR-780 dye while and while not loaded inside of the MSN. Graphs show a similar spectra, including a peak at 780nm. Similar absorbance spectra of the two samples indicates the utilization of MSNs as a vehicle for IR-780 do not alter the spectrum, allowing MSNs to be utilized as a fluorescence/optoacoustic marker vehicle.

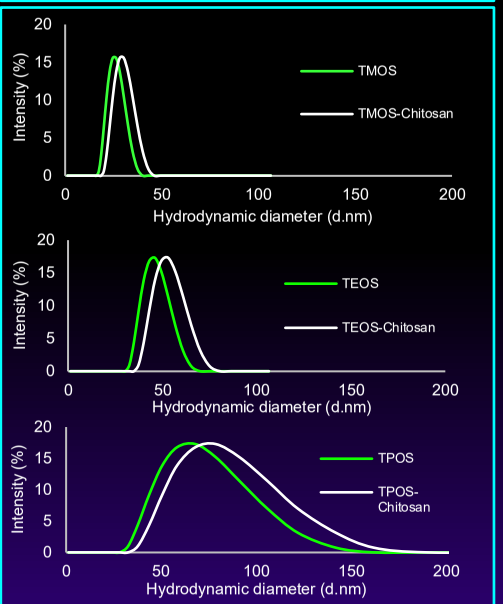

Figure 3: Dynamic light scattering (DLS) measurements showing the addition of the chitosan coat. Readings show the distribution of size for TMOS, TEOS, and TPOS before and after the addition of the chitosan coating. Chitosan shows to increase the size of TROS by 5-10 nm.

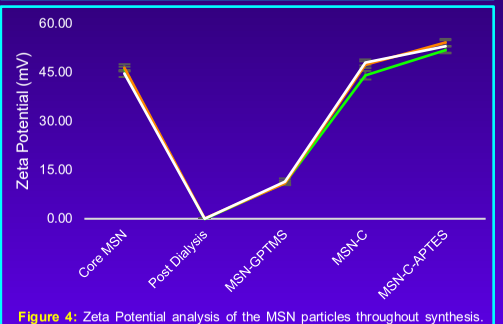

Figure 4: Zeta Potential analysis of the MSN particles throughout synthesis. Removal of CTAB drives a decrease in zeta potential. Conjugation of GPTMS, chitosan, and APTES adds positive charge to the MSN nanoparticles, resulting in a larger positive zeta potential when compared to the unconjugated MSNs.

RESULTS

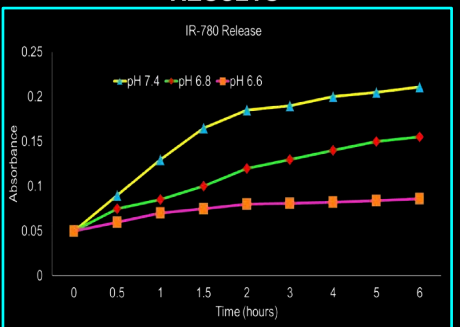

Figure 5: TMOS particles loaded with IR-780 dye were evaluated for pH specific dye release. Loaded particles were incubated in PBS solutions of pH 7.4, 6.8, or 6.6. Measurements of release were determined by absorbance measured (UV-Vis spectroscopy) over a 6 hour period. Increased absorbance of the PBS solution over time indicates the collection of free dye in the solution and released from the particles. TMOS particles at pH 6.6 were found to release ~2x the amount of cargo as compared to pH 7.4. All sized TROS exhibited similar release profiles.

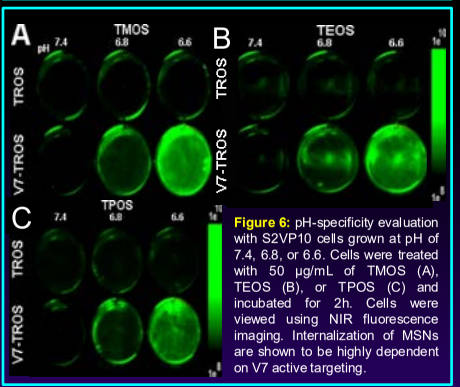

Figure 6: pH-specificity evaluation with S2VP10 cells grown at pH of 7.4, 6.8, or 6.6. Cells were treated with 50 µg/mL of TMOS (A), TEOS (B), or TPOS (C) and incubated for 2h. Cells were viewed using NIR fluorescence imaging. Internalization of MSNs are shown to be highly dependent on V7 active targeting.

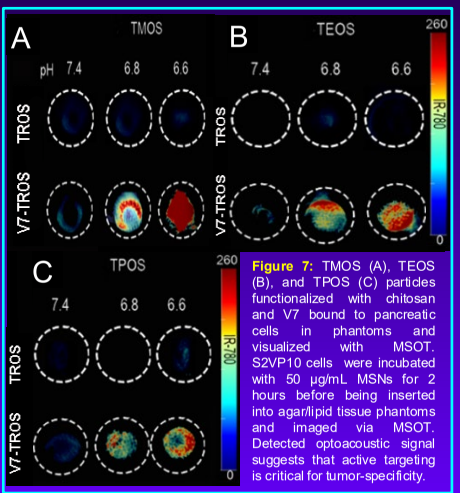

Figure 7: TMOS (A), TEOS (B), and TPOS (C) particles functionalized with chitosan and V7 bound to pancreatic cells in phantoms and visualized with MSOT. S2VP10 cells were incubated with 50 µg/mL MSNs for 2 hours before being inserted into agar/lipid tissue phantoms and imaged via MSOT. Detected optoacoustic signal suggests that active targeting is critical for tumor-specificity.

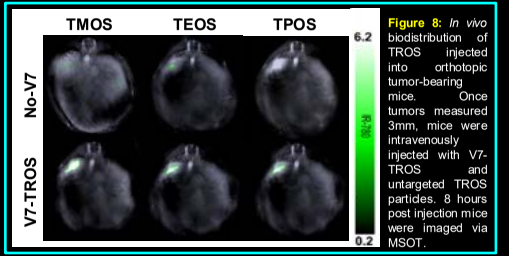

Figure 8: *In vivo* biodistribution of TROS injected into orthotopic tumor-bearing mice. Once tumors measured 3mm, mice were intravenously injected with V7-TROS and untargeted TROS particles. 8 hours post injection mice were imaged via MSOT.

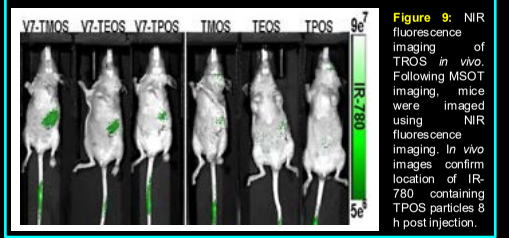

Figure 9: NIR fluorescence imaging of TROS *in vivo*. Following MSOT imaging, mice were imaged using NIR fluorescence imaging. *In vivo* images confirm location of IR-780 containing TPOS particles 8 h post injection.

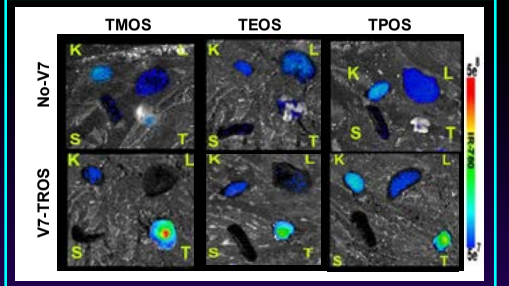

Figure 10: Secondary confirmation of IR-780 signal *ex vivo* within organs after 8 h post injection via NIR fluorescence. Kidney, liver, spleen, and pancreas tumor were imaged using AMI NIR fluorescence imaging. Signal uptake observed corresponded to MSOT/ fluorescent *in vivo* signals (Figs. 8 & 9)

CONCLUSION/FUTURE STUDIES

- Active targeting shows to be a critical component for tumor-specificity through use of V7 pH-low insertion peptide.
- Nanoparticle size shows to be an important factor in tumor specificity, but secondary to active targeting.
- TROS MSNs coated with chitosan and conjugated with V7 show tumor-specificity driven through pH-sensitivity.
- MSOT is capable of detecting IR-780 subsequent to release from the MSNs both *in vitro* and *in vivo*.
- Comparison of other types of mesoporous silica nanoparticles, as well as completely different nanoparticles could lead to potential characteristic optimization.
- Altering concentrations of chitosan, dye, peptide, etc. could lead to higher pH-specificity or more targeted particles.

ACKNOWLEDGEMENTS

This work was supported by NIH grants R01-EB020125, R01-CA212350, and R01-CA205941.

MASS SPECTROMETRY METABOLOMICS STUDIES OF SINGLE CELL IN MULTICELLULAR SPHEROIDS

Zongkai Peng; Advisor: Dr. Zhibo Yang

Multicellular spheroids are regarded as vivid models to represent the microenvironment of heterogeneous cells in *in vivo* tumors. As tumor grows, cancer cells far from the capillary supply lack nutrients and oxygen, and they possess different characteristics, such as with altered cell cycle distribution and reduced metabolite consumption, compared with others. Similar gradients of nutrients and oxygen have been found in spheroids. The conditions used to culture spheroids can be precisely controlled, while the metabolites in the microenvironment inside the spheroid can reflect these changes, making them a suitable study model to mimic the actual situation in tumors. Although metabolomics studies of spheroid models have been previously performed using traditional HPLC-MS (liquid chromatography–mass spectrometry) methods, cell heterogeneity that presents in different regions of spheroids cannot be studied using these conventional techniques. To further understand the activities of heterogeneous cells in spheroids, single-cell metabolomics analysis is an inevitable choice. The Single-probe, a microscale sampling and ionization device developed in our group can be coupled to mass spectrometer for versatile experiments such as single cell metabolomics studies.

In our studies, spheroids were cultured using HCT-116 cell line following the modified protocols. Cells at each layer were detached by incubating spheroids in trypsin solution assisted by an orbital shaker. The Single-probe was coupled to mass spectrometer to analyze these single cells. The metabolomics profiles of intracellular metabolites were visualized using principal component analysis (PCA), and analysis of variance (ANOVA) was used to determine the metabolites with significantly different abundances from cells at different layers. Our preliminary results indicate that cells in three different regions of spheroids show significantly different metabolomic profiles in PCA plots. To determine the metabolites with significantly different abundances in these regions, we performed ANOVA and tentatively labeled these species. Our results indicate a large number of lipids, including PC, DG, and MG, have different abundances in cells from different layers.

Single cell analysis of metabolites in tumor spheroids

Zongkai Peng, Mei Sun, Zhibo Yang*
Department of Chemistry and Biochemistry, University of Oklahoma, Norman, Oklahoma, 73019, USA
Corresponding author email: Zhibo.Yang@ou.edu

Introduction

1) Metabolites of cancer cells

- Intracellular metabolites reflect the cancer cell activities in different regions
- Extracellular metabolites are critical for cell-cell communication, tumor growth, and cancer cell migration

2) Spheroids obtained from 3D cell structure can be used for metabolites studies

- Better models of *in vivo* tumors compared with traditional 2D-culture cells
- Spheroids possess heterogenous cell populations in different regions
- Spheroids possess different intracellular metabolites in different regions due to the gradients of oxygen, nutrients, and energy

3) Single cell mass spectrometry (SCMS)

- A powerful tool to study cell heterogeneity
- Suitable for studies of rare cells
- Provide molecular compositions (e.g., metabolites and proteins) of cells

4) The Single-probe

- A microscale sampling and ionization device
- Allows for versatile experimental designs
- Can be coupled with MS for extracellular analysis of spheroids, SCMS, and MS imaging (MSI)

Experiments

1) Single-probe fabrication[1]

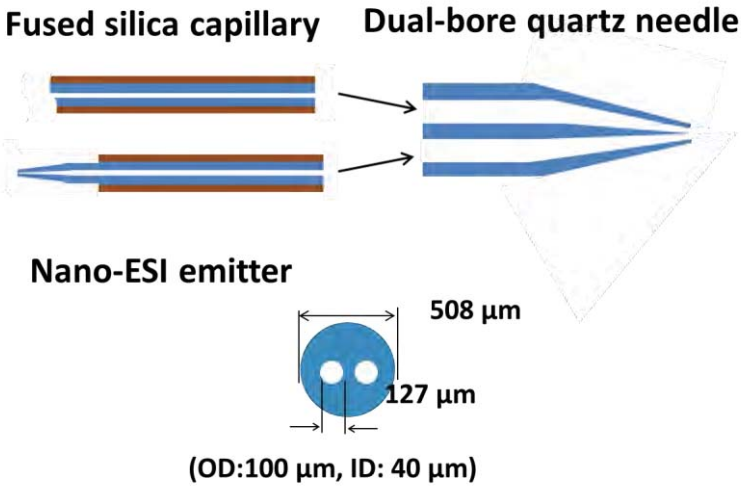

2) Single-probe SCMS setup

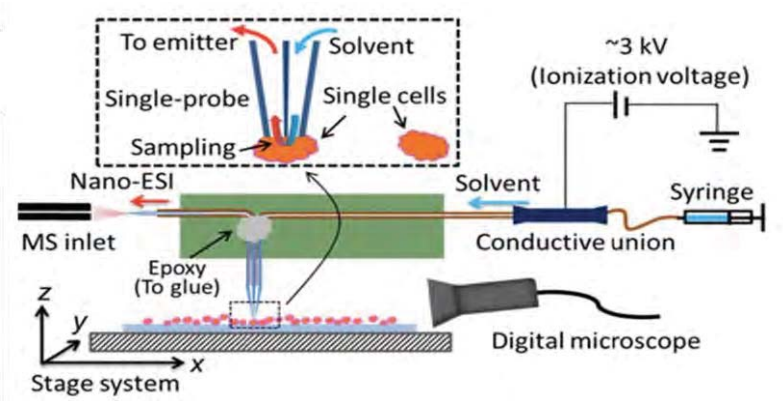

Results

1) Principal component analysis (PCA) results form different layer of spheroids

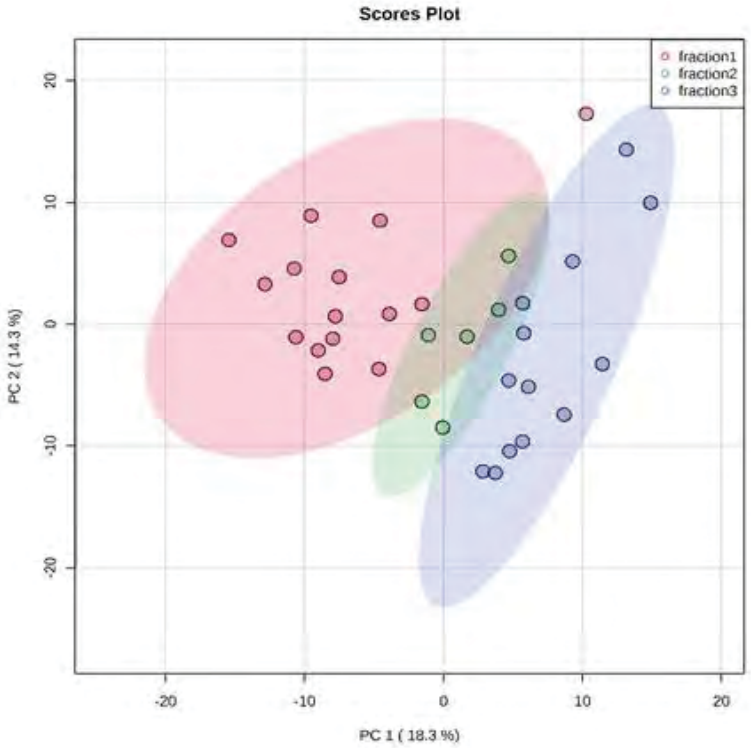

Conclusion

- Metabolites with significantly different abundances were observed in different layers of tumor spheroids
- By analyzing the metabolites results in these different regions, many fact acids are found changed significantly

([1]Mei Sun, et al., *Anal. Chem.* 2017, (89), 9069−9076.)

THE EFFICACY OF EV ENCAPSULATED CHEMOTHERAPEUTICS IS ASSOCIATED WITH LOADING METHODS, EV SOURCES AND EV UPTAKE EFFICIENCY IN PANCREATIC CANCER CELLS

Haoyao Sun[1,2], Kritisha Bhandari[1], Stephanie Burrola[1], and Wei-Qun Ding[1]
[1]Department of Pathology, the University of Oklahoma Health Sciences Center, Oklahoma City, USA,
[2] Department of Radiation Oncology, The Affiliated Suzhou Hospital of Nanjing Medical University, Suzhou, China

Background: Pancreatic cancer is the third leading cause of cancer related death in the United States and the overall 5-year survival rate is only around 9%. The therapeutic options against pancreatic cancer are rather limited compared with other solid tumors. New strategies in therapeutic development are desperately needed. Recent advancement in extracellular vesicle (EV) biology has indicated that certain type of EVs, such as small EVs, possess tumor homing propensity with lower immunogenicity, and are potential drug carriers to effectively deliver cancer therapeutics.

Objective: The aim of this study is to determine the efficiency of EV drug loading and the efficacy of EV encapsulated chemotherapeutics in pancreatic cancer cells.

Methods: Small EVs were isolated from culture medium of various human cell lines using an established protocol, and verified by nanoparticle analysis and western blot. Paclitaxel and Gemcitabine, two commonly used chemotherapeutics, were incorporated into small EVs via incubation, sonication, and electroporation. The loading efficiency was evaluated by spectrometric measurements. EV drug efficacy was analyzed by MTS assay. EV uptake was assayed by fluorescent microscopy of PKH-67 stained small EVs.

Results: Small EVs were successfully isolated and verified. Compared with incubation and electroporation, sonication was the most efficient method for the incorporation of chemotherapeutics into small EVs. However, the EV encapsulated drugs obtained with the incubation method were more efficacious in killing pancreatic cancer cells when applied at equivalent drug concentrations. This may be explained by the observation that the incubation method led to higher cellular uptake of the EV drugs, especially when the drugs were encapsulated by the small EVs derived from HPNE cells.

Conclusions: The efficiency of small EV encapsulation of chemotherapeutics varies among different loading methods, and the efficacy of EV encapsulated chemotherapeutics is associated with the loading methods, EV sources, and EV uptake efficiency.

The Efficacy of EV Encapsulated Drugs is Associated with Loading Methods, EV Sources and EV Uptake Efficiency in Pancreatic Cancer Cells

Haoyao Sun[1,2], Kritisha Bhandari[1] , Stephanie Burrola[1] , and Wei-Qun Ding[1]
[1]Department of Pathology, the University of Oklahoma Health Sciences Center, Oklahoma City, USA,
[2] Department of Radiation Oncology, The Affiliated Suzhou Hospital of Nanjing Medical University, Suzhou, China

Introduction and Objectives

Pancreatic cancer is a deadly disease with a 5-year overall survival rate around 9%. Therapeutic options against pancreatic cancer are rather limited compared with other solid tumors. New strategies in therapeutic development is desperately needed. Recent advancement in extracellular vesicle (EV) biology has indicated that certain type of EVs, such as small EVs, possess tumor homing propensity with lower immunogenicity, and are potential drug carriers to effectively deliver cancer therapeutics. The objective of this study was to determine the efficiency of EV drug loading and the efficacy of EV encapsulated drugs in pancreatic cancer cells.

Materials and Methods

- Small EVs were isolated from the cell culture media and purified by ultrafiltration plus membrane filtering.
- Three human pancreatic cancer cell lines (PANC-1, MIAPaCa-2 and BxPC-3), a normal human pancreatic duct cell line (HPNE), human embryonic kidney 293T cells and pancreatic cancer associated fibroblast (CAF19) cells were used for this study.
- EVs were verified by nanoparticle analysis (Nanosight) and Western blot.
- EV-drug concentrations were determined by spectrometric measurements.
- MTS was applied to analyze cell viability.
- EVs were stained with PKH-67 and fluorescent microscopy was applied to to evaluate EV uptake by pancreatic cancer cell lines.

Results

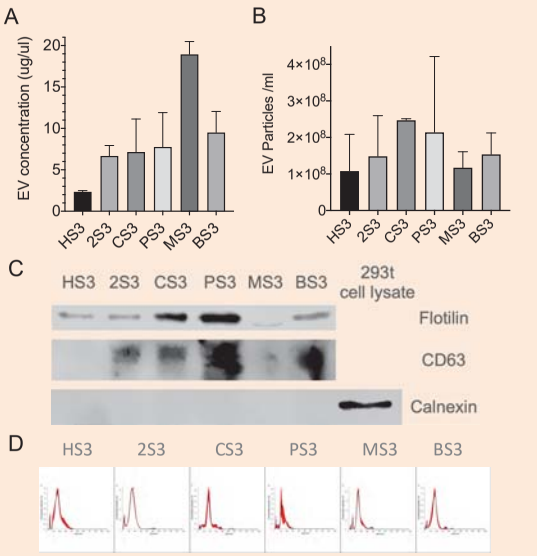

Figure 1. Verification of small EVs. (A) EV concentrations analyzed by BCA. EVs were derived from 20-mL medium of 6 different cell lines. **(B)** EV particle analysis by Nanosight (1:1000 dilution). **(C)** Small EV markers detected by Western blot. **(D)** Representative EV size and distribution analyzed by Nanosight. Abbreviations: HS3, HPNE sEV; 2S3, 293T sEV; CS3, CAF19 sEV; PS3, PANC-1 sEV; MS3, MIAPaCa-2 sEV, BS3, BxPC3 sEV.

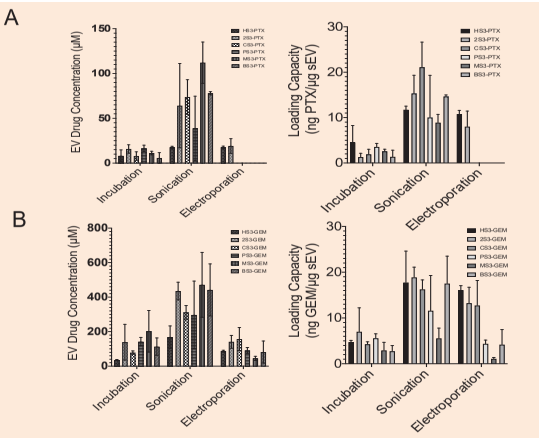

Figure 2. Sonication leads to higher efficiency of EV drug loading than incubation and electroporation (A) Paclitaxel (PTX) was incorporated into sEVs by 3 different methods. Drug concentration was determined spectrometrically. **(B)** Gemcitabine (GEM) was incorporated into sEVs by 3 different methods. Drug concentration was determined spectrometrically.
Abbreviations: HI-PTX, HPNE sEV incubated with PTX; HS-PTX, HPNE sEV sonicated with PTX; HE-PTX, HPNE sEV electroporated with PTX.

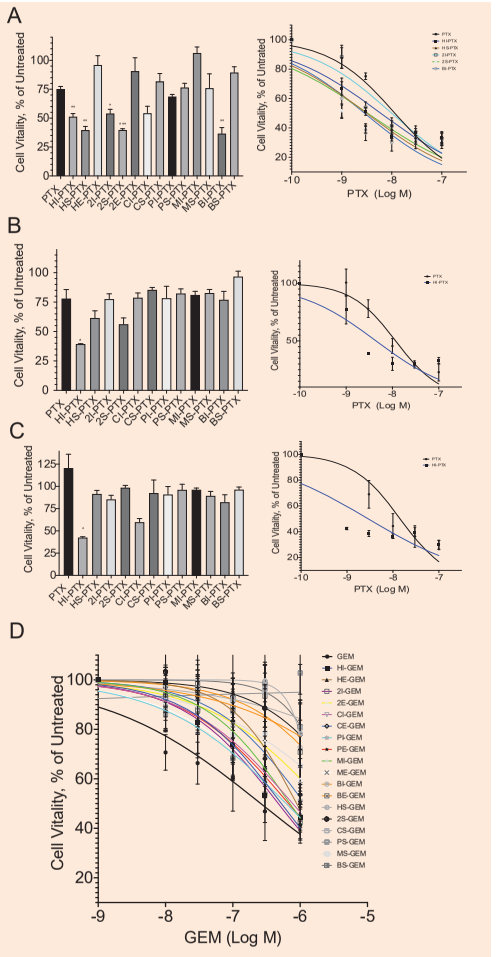

Figure 3. HI-PTX is more toxic than other EV-drugs in MTS assay. (A) Cell vitality of PANC-1 cells treated with equivalent 3nM EV free PTX and EV-PTX (left) or 1nM to 100nM PTX (right). **(B)** Cell vitality of MIAPaCa-2 cells treated with equivalent 3nM EV free PTX or EV-PTX (left) or 1nM to 100nM PTX (right). **(C)** Cell vitality in BxPC-3 cells treated with equivalent 1nM EV free PTX or EV-PTX (left) or 1nM to 100nM PTX (right). **(D)** Cell vitality of PANC-1 cells treated with equivalent EV free GEM or EV-GEM 10nM to 1uM. Statistical analysis was performed using one-way ANOVA. ***p<0.001, **p<0.01, *p<0.05 (n=3).

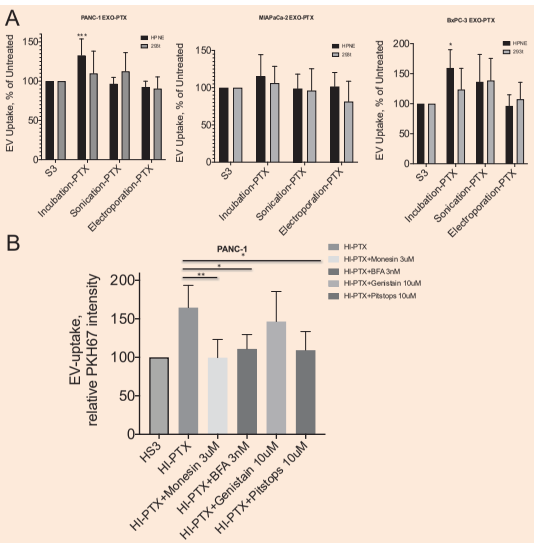

Figure 4. Endocytosis-mediated HI-PTX uptake in PANC-1 cells. (A) The uptake rate for HI-PTX is higher than for EV-PTX prepared by sonication and electroporation. **(B)** HI-PTX uptake by PANC-1 cells could be reversed by endocytosis inhibitors. Statistical analysis was performed using one-way ANOVA. ***p<0.001, **p<0.01 , *p<0.05 (n=3).

Summary

Our results demonstrate that while sonication leads to higher efficiency of drug loading than incubation and electroporation, EV-PTX derived from incubation is most efficacious in killing pancreatic cancer cells. It seems that the efficacy of EV encapsulated chemotherapeutics is associated with the loading methods, EV sources, and EV uptake efficiency.

Acknowledgement : This study was supported in part by grants from the National Institute of General Medical Sciences of the National Institutes of Health (P20GM103640), the National Cancer Institute (CA235208-01), the Presbyterian Health Foundation, and the Peggy and Charles Stephenson Cancer Center. We thank Dr. Priyabrata Mukherjee for kindly providing the CAF19 cell line, and the SCC core facility for supporting this study.

EXPLORING ASSOCIATIONS BETWEEN TUMOR MUTATIONAL BURDEN, MICROSATELLITE INSTABILITY STATUS AND TUMOR RESPONSE IN VARYING GYNECOLOGIC MALIGNANCIES

Ana Valente MD[1] (corresponding author: ana-valente@ouhsc.edu), Amy Gin[2], Allison Wells[2], Kai Ding[2], and Kathleen Moore MD[1, 2]

[1]University of Oklahoma/Stephenson Cancer Center Gyn Oncology, [2]University of Oklahoma Health Science Center School of Medicine

Funding: None

Objectives: Immune checkpoint inhibitors (ICI) are immunomodulatory antibodies that function by blocking key receptor-ligand interactions involved in immune checkpoint pathway activation. They are becoming more commonly used in solid tumors. Tumor mutations are key in the generation of anticancer immunity, and it is hypothesized that highly mutated tumors are more likely to harbor neoantigens that make them targets of activated immune cells[1,2,3]. Emerging data suggests that tumor mutation burden (TMB) determined by next generation sequencing predicts response to ICI monotherapy in melanoma and non-small cell lung cancer[4,5]. To our knowledge, this has not yet been reported across gynecologic (gyn) tumor types. Recent data among BRCA mutation carriers with ovarian cancer reported found no association between TMB and response to ICI[6]. This study aims to explore a correlation between TMB status and best response in gyn cancer population treated with ICI. Correlation with Micro satellite instability (MSI) status is also reported.

Methods: We conducted a retrospective review of 57 patients with gyn cancer at a single institution who received an ICI for management of recurrent or progressive disease. TMB was determined by next generation sequencing (via foundation testing) and reported as Very Low, Low, Intermediate or High. Complete response (CR), partial response (PR), stable disease (SD) and progressive disease (PD) were assessed by RECIST criteria. A Fisher's exact test was used to determine if correlation between TMB, MSI and response existed.

Results: Of the 57 patients identified, 20 patients (35.1%) had ovarian cancer, 13 patients (22.8%) had cervical cancer, 22 patients (38.6%) had uterine cancer and 2 patients (3.5%) had vulvar cancer. Mean age was 57. When grouped together by best response = PR/CR vs SD/PD, results revealed 42 SD/PD and 15 with CR/PR. A Fisher's exact test was used to determine if there was an association between TMB Low/Very Low and Intermediate/High and best response. No significant correlation was identified (p=.3807). 54 patients had MSI status available. A Fisher's exact test showed no association between MSI status and best response (p=.5021).

Conclusions: Our data suggests that there is no association between TMB status and response to ICI in gynecologic malignancies. Additional studies are needed to identify an optimal biomarker to identify patients who would benefit most from treatment w/ ICI. We were also unable to establish an association between MSI status and best response in this group of varying gyn malignancies. Our study is limited by small sample size.

Exploring Associations between Tumor Mutational Burden, Microsatellite Status and Tumor Response in Gynecologic Malignancies

Introduction

- Immune checkpoint inhibitors (ICPI) are immunomodulatory antibodies that function by blocking key receptor-ligand interactions involved in immune checkpoint pathway activation.
- Tumor mutations are key in the generation of anticancer immunity.
- Hypothesized that highly mutated tumors are more likely to harbor neoantigens that make them targets of activated immune cells.
- Not yet evaluated if tumor mutational burden correlate with response in GYN malignancy.
- Correlation with Microsatellite Status is also explored.

Methods

- Retrospective review of 57 patients with gynecologic cancer at a single institution who received an ICPI for management of recurrent disease
- TMB status was determined by next generation sequencing (via foundation testing) and reported as Very Low, Low, Intermediate or High.
- Complete response (CR), partial response (PR), stable disease (SD) and progressive disease (PD) were assessed by RECIST criteria.
- A Fisher's exact test was used to determine if correlation between TMB and response existed.

Valente A, Gin A, Wells A, Essel KG, Ding K, Moore K[1]

[1] *The University of Oklahoma, Stephenson Cancer Center, Oklahoma City, OK*

No association was found between Tumor Mutational Burden or Microsatellite Status and Response to Immune Checkpoint Inhibitors in our study population.

We are limited by small sample size.

Results

- Of the 57 patients identified mean age was 55.6 (SD 11.8, range 24-74).
- When grouped together by best response = PR/CR vs SD/PD, results revealed 42 SD/PD and 15 with CR/PR.
- The Fisher's exact test was used to determine if there was an association between TMB status (grouped into Low/Very Low and Intermediate/High) and best response.
- No significant correlation was identified (p=.3807).
- 54 patients had Microsatellite Status available. There was no association between Microsatellite status and best response (=.5021).

Conclusions

- Our data suggests that there is no association between TMB or MS status and response to ICPI in gynecologic malignancies.
- Additional studies are needed to identify an optimal biomarker to identify patients who would benefit most from treatment w ICPI.
- Our study is limited by small sample size.

Table 1: Patient Characteristics

Ethnicity	n(%)
Black/African American	6 (10.7%)
Caucasian	38 (67.9%)
Hispanic	5 (8.9%)
Native American	6 (10.7%)
Asian	1 (1.8%)
Cancer Type	
Ovarian	20 (35.1%)
Uterine	22 (38.6%)
Cervical	13 (22.8%)
Vulvar	1 (3.5%)
BMI	
<25	11 (19.3%)
25-30	19 (33.3%)
>30	27 (47.4%)
Best Response to ICPI	
CR	3 (5.3%)
PR	12 (21.1%)
SD	22 (38.6%)
PD	20 (35.1%)

Table 2: Tumor Mutational Burden vs Response

Tumor Mutational Burden	Best Response n(%)			
	PD	SD	CR/PR	Total
Very Low/Low	11 (34.4%)	14 (43.8%)	21 (23.5%)	32
Intermediate	8 (47.1%)	5 (29.4%)	4 (23.5%)	17
High	1 (12.5%)	3 (37.5%)	4 (50%)	8
Total	20	22	15	57

Table 3: Microsatellite Status vs Response

Microsatellite Status	Best Response n(%)			
	PD	SD	CR/PR	Total
High	3 (25%)	4 (33.3%)	5 (41.6%)	12
Stable	15 (35.7%)	17 (40.4%)	10 (23.8%)	42
Total	18	21	15	54

IN VIVO REAL-TIME VASCULATURE MONITORING IN CANCER THERAPIES USING OPTICAL COHERENCE TOMOGRAPHY ANGIOGRAPHY

Feng Yan[1], Chetan Ahire [2], Chen Wang [1], Anna Csiszar [2]*, Qinggong Tang [1]*
[1] Stephenson School of Biomedical Engineering, University of Oklahoma, Norman, OK, 73019
[2] Department of Biochemistry and Molecular Biology, University of Oklahoma Health Sciences Center, Oklahoma City, OK, 731042

Surgery, chemo, and radiation had been cancer treatment for several decades, and the current development of immuno-, hormone- and stem cell therapy has changed the era of precision medicine for cancer treatment. Evaluating the effectiveness of the treatment has become essential task to prolong the life and survival rate among cancer patients. Neovascularization of tumors is a critical bioimaging marker for evaluating the type and stage of cancer. Chemotherapy and targeted therapy, like antiangiogenic agents and vascular targeting agents, can inhibit neovascularization and selectively destroy tumor pathological vessels. Optical coherence tomography angiography (OCTA) is a new non-invasive imaging technique that employs motion contrast imaging to obtain high-resolution volumetric blood vessel information generating angiographic images in seconds. OCTA is a critical imaging tool for longitudinal observation of angiogenesis, vascular degeneration, and blood vessel ruptures. In this study, OCTA platform was developed to observe the changes of microvasculature following anti-cancer treatment in mouse brains treated by chemotherapy and targeted therapy. Eight parameters including vessel area density (VAD), vessel skeleton density (VSD), vessel diameter index (VDI), vessel perimeter index (VPI), and vessel complexity index (VCI) were quantified to describe the profile of microvasculature in different cerebral cortex layers to evaluate the performance of the chemotherapy and targeted therapy. We found that there was a significant difference in brain microvasculature before and after the chemotherapy and targeted therapy, and a significant difference existed among various cerebral cortex layers within/out anti-cancer treatment. The significant difference of parameters in microvasculature was used to evaluate the performance of cancer therapies. These results demonstrate that OCTA is a promising modality to monitor and evaluate the effectiveness of the chemotherapy and targeted therapy in anti-cancer according to the change of parameters in brain microvasculature.

Acknowledgement: This work was funded by 2020 Junior Faculty Fellowship from University of Oklahoma (Tang) and Startup Fund from University of Oklahoma (Tang).

In Vivo Vasculature Monitoring in Cancer Therapies Using Optical Coherence Tomography Angiography

Feng Yan [1], Chetan Ahire [2], Chen Wang [1], Anna Csiszar [2]*, Qinggong Tang [1]*

[1] Stephenson School of Biomedical Engineering, University of Oklahoma, Norman, OK, 73019

[2] Department of Biochemistry and Molecular Biology, University of Oklahoma Health Sciences Center, Oklahoma City, OK, 731042

Background

(1) Surgery, chemo, and radiation had been cancer treatment for several decades, and the current development of immuno-, hormone- and stem cell therapy has changed the era of precision medicine for cancer treatment. Evaluating the effectiveness of the treatment has become essential task to prolong the life and survival rate among cancer patients.

(2) Neovascularization of tumors is a critical bioimaging marker for evaluating the treatment response. Chemotherapy and targeted therapy, like antiangiogenic agents and vascular targeting agents, can inhibit neovascularization and selectively destroy tumor pathological vessels.

(3) Optical coherence tomography angiography (OCTA) is a new non-invasive imaging technique that employs motion contrast

Method

(1) Chemotherapy-induced cognitive impairment (CICI) animal models using cancer-free p16-3MR mice subjected to low doses of genetically designed drug ganciclovir (GCV) (25mg/kg) and pharmacological drugs ABT-263 (50mg/kg) were given treatments for 14 days routinely with the gap 5 rest days;

(2) A swept-source optical coherence tomography (SSOCT) system was used to obtain structural images of the animal brain;

(3) An OCT-based optical microangiography (OMAG) algorithm was developed and applied, as shown in Figure 1. With 200 X 200 pixels in 2mm X 2mm field of view, the 8 repeated B-frames at each location were used for OMAG calculation to obtain both the structure and blood flow images.

(4) Each layer was set ~100 μm thickness, the sorted summed intensity projection (SIP) algorithm for each layer where the summed intensity of flow was selected and mapped to an enface plane.

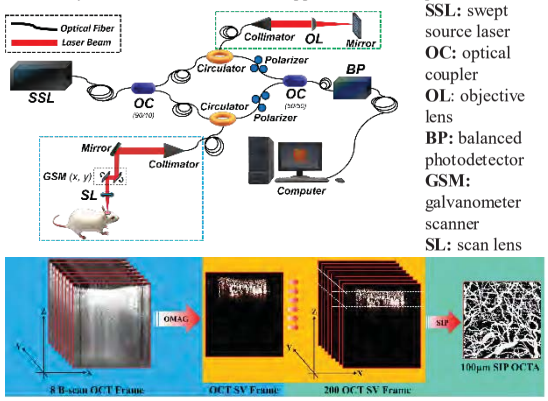

SSL: swept source laser
OC: optical coupler
OL: objective lens
BP: balanced photodetector
GSM: galvanometer scanner
SL: scan lens

Fig. 1. Schematic of OCT system and OMAG algorithm

Experimental Result

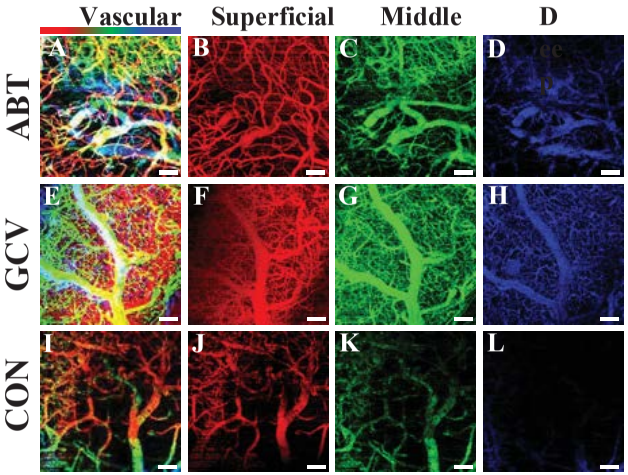

Fig. 2. Comparison of microvasculature between the treatments (ABT-263, GCV) and control (CON) in superficial (0-100μm), middle (100-200μm), and deep layers (200-300μm).Vascular images (0-300μm) are integrated by overlaying the superficial, middle, and deep layer figures. Scale bar is 150μm.

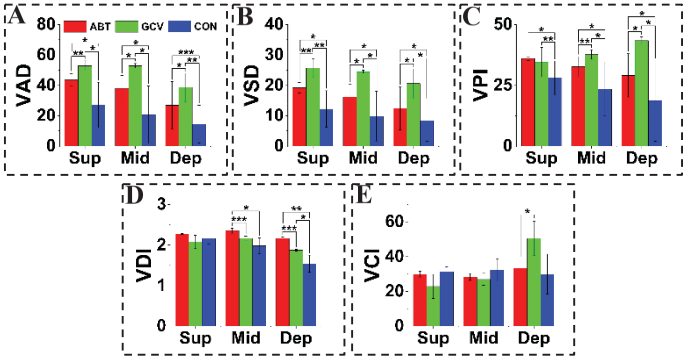

Fig. 3. Quantitative analysis of vasculature in vessel area density (VAD, %), vessel skeleton density (VSD, %), vessel perimeter index (VPI, %), vessel diameter index (VDI, %), and vessel complexity index (VCI, %). VAD presents the real density of vessel based on vessel length and size; VSD presents the vessel density through the vessel length; VPI includes the vessel length and diameter information; VDI presents the vessel size information regardless of the vessel length; VCI presents the morphological character. *: p<0.05, **: p<0.01, ***:p<0.001.

(1) From OCTA results, animals treated by ABT and GCV showed more and smaller capillaries compared to control group. (2) More capillaries existed in the superficial layer in ABT and GCV animal models compared to control group. The size of big blood vessels in ABT animals was much smaller than that in GCV and control mice. (3) There were larger blood vessels that existed in the middles layer of ABT mouse models compared to the superficial layer. GCV animals had smaller capillaries in the middle layer but still had some big blood vessels. (4) In the deep layer of CON animals, there were only a few capillaries. However, ABT animal models showed that many big blood vessels existed in the deep layer. Additionally, the deep layer of the GCV mouse brain still had many capillaries and some big blood vessels. (5) Except for the difference of VPI in the superficial layer, GCV animals had significantly higher VAD, VSD, and VPI than ABT and CON mouse models regardless of the three layers. Similarly, in all the three layers, CON animals had significantly lower VAD, VSD, and VPI than ABT and GCV mouse. (6) ABT mouse had a significantly higher VDI than GCV and CON animal models in the middle and deep layers. Furthermore, in the deep layer, the GCV mouse also showed a significantly higher VDI than the CON mouse. (7) Interestingly, there was only a significant difference in the VCI between the ABT and GCV mouse models with GCV had a significantly higher VCI than ABT mouse.

Conclusion & Expectation

(1) Animals treated by ABT and GCV exactly develop significantly higher vessels density and length in the brain; (2) ABT and GCV treatments can induce the mouse brain to produce larger blood vessels and more capillaries, especially in the deep layer; (3) The longitudinal investigation can be applied to observe the change of blood vessels with the time of treatment.

Acknowledgement

This work is supported by Startup Fund from University of Oklahoma (Tang) and University of Oklahoma Junior Faculty Fellowship Program (Tang).

Reference

[1] Chu, Z., Lin, J., Gao, C., Xin, C., Zhang, Q., Chen, C. L., ... & Wang, R. K. (2016). *Journal of biomedical optics*, *21*(6), 066008.

[2] Chang, J., Wang, Y., Shao, L., Laberge, R. M., Demaria, M., Campisi, J., ... & Zhou, D. (2016). Nature medicine, 22(1), 78-83.

ELTD1 AS A DIAGNOSTIC AND THERAPEUTIC TARGET FOR GBM: PRE-CLINICAL STUDIES

[1]Michelle Zalles, [1]Nataliya Smith, [1]Debra Saunders, [1]Rheal A. Towner
[1]Advanced Magnetic Resonance Center, Oklahoma Medical Research Foundation, Oklahoma City, OK USA.

Introduction: Glioblastoma (GBM) is the most aggressive malignant primary brain tumor in adults and has high recurrence and mortality rates. These high-grade gliomas undergo unregulated vascular angiogenesis, uncontrolled migration and cell proliferation allowing the tumor cells to evade cell-cycle checkpoints and apoptotic pathways.[1] The Epidermal growth factor, latrophilin, and seven transmembrane domain-containing 1 on chromosome 1 (ELTD1) is an angiogenic biomarker that is highly expressed in human GBM.[2] Novel treatments targeting ELTD1 with monoclonal and single chain variable fragment (scFv) antibodies were effective in increasing animal survival, decreasing tumor volume and normalizing the vasculature within the tumor region.[3] Due to the success of our antibody treatments on angiogenesis, we sought to whether our anti-ELTD1 treatments affected other aspects of tumorigenesis (cell proliferation, migration, and apoptosis).

Methods: Athymic Nude mice were intracerebrally injected with human G55 cells. Morphological MRI was used to monitor and calculate tumor growth. Tumors were treated with monoclonal or scFv anti-ELDT1 antibody via tail-injection every 3-4 days until tumor volumes reached 150 mm^3. The brain of each animal was removed, preserved in 10% neutral buffered formalin, and processed routinely. Immunohistochemistry (IHC) was used to assess cell proliferation (C-met and Ki-67), motility (CD44), and apoptosis (cleaved caspase-3). Aperio ImageScope was used to quantify IHC staining for each aspect of tumorigenesis. Cell migration chamber assays using G55 cells were done using six-well chambers with PDMS microchannels. The chambers were left untreated, or treated with mAb or scFv anti-ELTD1. Images of the cells inside of the channels were taken using a CK40 inverted microscope under 10x to measure the distance of the cells 16- and 44-hrs post-treatment.

Discussion: Previous studies have shown that targeting ELTD1 with varying antibodies results in an increase of survival, decrease in tumor volumes and a normalization of the tumor associated vasculature in a G55 xenograft GBM mouse model. Therefore, we decided to further examine other aspects of tumorgenesis. IHC analysis showed a significant decrease in both cellular proliferation and cellular migration. IHC staining against cleaved caspase 3, a marker for apoptosis demonstrated that our antibody treatments were also successful in increasing the overall apoptosis within the tumor region. Our data suggest that anti-ELTD1 therapies would be effective against glioblastomas by not only decreasing angiogenesis but by also targeting cell proliferation, cell migration/invasion, and increasing apoptosis within the tumor region.

Funding was provided by the Oklahoma Medical Research Foundation (OMRF).

ELTD1 as a Diagnostic and Therapeutic Target for GBM: Pre-Clinical Studies

[1]Michelle Zalles, [1]Nataliya Smith, [1]Debra Saunders, [1]Rheal A. Towner
[1]Advanced Magnetic Resonance Center, Oklahoma Medical Research Foundation, Oklahoma City, OK USA

INTRODUCTION

Glioblastoma (GBM) is the most aggressive malignant primary brain tumor in adults and has a high recurrence and mortality rate. These high-grade gliomas undergo unregulated vascular angiogenesis, and uncontrolled migration and cell proliferation allowing the tumor cells to evade cell-cycle checkpoints, and apoptotic pathways.[1] The Epidermal growth factor, latrophilin, and seven transmembrane domain-containing 1 on chromosome 1 (ELTD1) is an angiogenic biomarker and has shown to be highly expressed in human GBM.[2] Novel treatments targeting ELTD1 with polyclonal and monoclonal antibodies were effective as potential cancer therapies in a G55 xenograft mouse model.[3] While our studies have shown that the blood-brain barrier (BBB) was leaky at the tumor region, other studies have shown that the BBB is not equally disrupted in GBM patients.[4]Therefore, suggesting that our mAb may have difficulty crossing the BBB and infiltrating the tumor region due to its size. To overcome these limitations, we sought to use an optimized single-chain variable fragment (scFv) antibody fragment derived from our mAb against ELTD1. The scFv anti-ELTD1 treatment was successful in increasing animal survival, decreasing tumor volumes, and normalizing the vasculature within the tumor region. Additionally, molecular targeted MRI (mtMRI) using an scFv antibody treatment against ELTD1 demonstrated that our antibody-attached probe was successful in reaching extremely diffuse tumor regions that were otherwise undetectable via conventional MR imaging. Therefore, the aim of this study is to further assess other aspects of tumorigenesis (angiogenesis, cell proliferation, migration, and apoptosis) that are affected by our anti-ELTD1 treatments.

METHODS

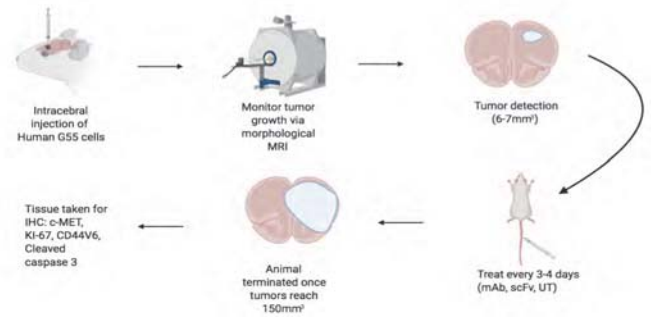

Athymic Nude mice were intracerebrally injected with human G55 cells. Morphological MRI (Bruker 7T) was used to monitor and calculate tumor growth. Tumors were treated via tail-injection until tumor volumes reached 150 mm^3. Perfusion images were obtained at tumor detection and before termination to determine microvasculature alterations. mtMRI on untreated G55 bearing mice were given either a non-specific mouse IgG, monoclonal, or scFv anti-ELTD1 fragment attached probes. Mouse brains were imaged at 0 (pre-contrast) and at 20 min. intervals up to 90 min post-contrast agent injection. The signal intensity values of 5 specified region-of-interest (ROI) were computed. Mice were euthanized after the last MRI examination. The brain of each animal was removed, preserved in 10% neutral buffered formalin, and processed routinely. Immunohistochemistry (IHC) was conducted to assess cell proliferation (C-met, KI-67), motility (CD44v6), and apoptosis (cleaved caspase-3). Aperio ImageScope was used to quantify IHC staining. Six-well chambers with polydimethylsiloxane (PDMS) microchannels seeded with G55 cells were used for cell migration chamber assays. The chambers were treated with mAb, scFv anti-ELTD1, or untreated. Cell velocity was measured.

RESULTS

Human mitochondrial antibody is decreased with anti-ELTD1 treatments

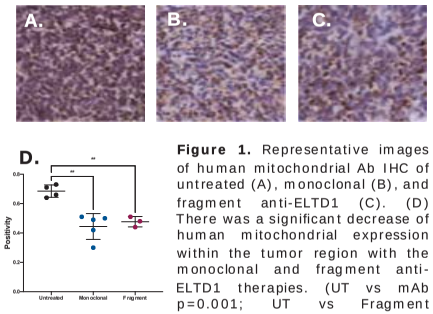

Figure 1. Representative images of human mitochondrial Ab IHC of untreated (A), monoclonal (B), and fragment anti-ELTD1 (C). (D) There was a significant decrease of human mitochondrial expression within the tumor region with the monoclonal and fragment anti-ELTD1 therapies. (UT vs mAb p=0.001; UT vs Fragment p=0.006)

Apoptosis is increased with anti-ELTD1 treatments

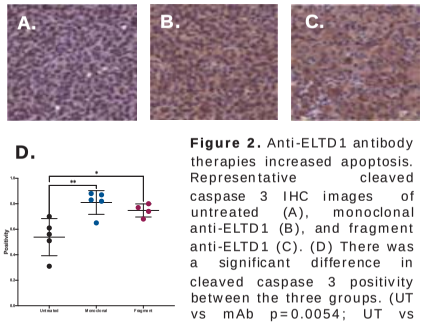

Figure 2. Anti-ELTD1 antibody therapies increased apoptosis. Representative cleaved caspase 3 IHC images of untreated (A), monoclonal anti-ELTD1 (B), and fragment anti-ELTD1 (C). (D) There was a significant difference in cleaved caspase 3 positivity between the three groups. (UT vs mAb p=0.0054; UT vs Fragment p=0.035)

Anti-ELTD1 therapies decrease cell proliferation.

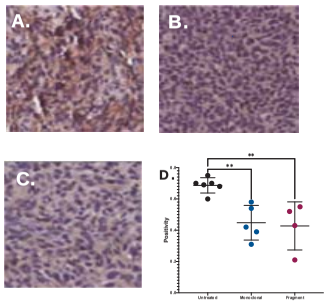

Figure 3. (Left) Representative images of c-MET IHC of untreated (A), monoclonal anti-ELTD1 (B), and fragment anti-ELTD1 (C). (D) Anti-ELTD1 groups significantly decreased c-MET positivity. (UT vs mAb p=0.0071; UT vs Fragment p=0.0063)

Figure 4. (Right) Representative images of Ki-67 IHC of untreated (A), monoclonal anti-ELTD1 (B), and fragment anti-ELTD1 (C). (D) Anti-ELTD1 groups significantly decreased Ki-67 positivity.(UT vs mAb p=0.0002; UT vs Fragment p=0.0001))

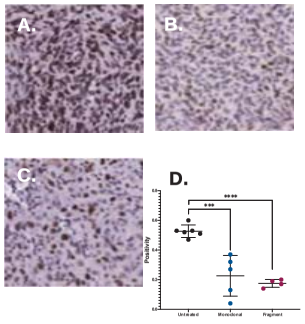

Anti-ELTD1 treatments significantly decrease *in vitro* cellular motility.

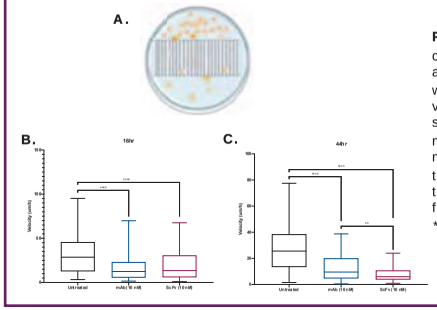

Figure 5. (A) Cartoon of migration chamber. (B) 16 hours post mAb and scFv antibody treatment. There was a significant decrease in cell velocity in mAb (C) There was a significant decrease in cellular motility 44 hrs after treatment of mAb and fragment anti-ELTD1 treatment. Fragment anti-ELTD1 therapy was significantly different from mAb. (***p<0.0001; **p=0.004)

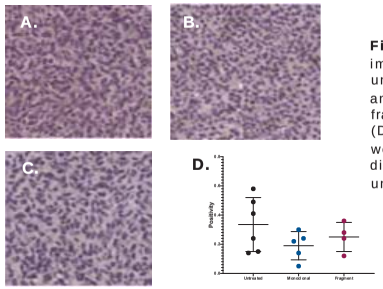

Figure 6. Representative images of CD44v6 IHC of untreated (A), monoclonal anti-ELTD1 (B), and fragment anti-ELTD1 (C). (D) Anti-ELTD1 groups were not significantly different than the untreated controls.

CONCLUSION

Previous studies have shown that by targeting ELTD1, a biomarker for angiogenesis, with varying antibodies there was a significant increase in survival and decrease in tumor volumes in a G55 xenograft GBM mouse model. Our antibody treatments were also successful in normalizing the vasculature back to contralateral healthy tissue levels.

Before examining the other aspects of tumorigenesis, we first wanted to see if our anti-ELTD1 treatment had a direct affect on the human tumor cells. Therefore, we stained against the human mitochondrial antibody and we saw a significant decrease of human cells within the tumor region with both our monoclonal and fragment anti-ELTD1 treatments. IHC staining against cleaved caspase 3 demonstrated a significant increase of apoptosis with both of our anti-ETLD1 treatments. We used two different cellular proliferation markers, c-MET and KI-67, to examine changes within the tissue and they both showed significant decreases in cell proliferation. Lastly, our anti-ELTD1 treatments showed a significant decrease in *in vitro* cellular motility. However, we will have to examine other stains of *in vivo* cell motility to validate our *in vitro* results.

GBMs are known to be extremely complex, they are known to evade apoptotic mechanisms, and promote unregulated cell growth and angiogenesis. Our data demonstrates that our anti-ELTD1 treatments are not only successful in completely normalizing the vascular structure within the tumor region, but can also target cell proliferation, cell migration/invasion, and apoptosis.

ACKNOWLEDGEMENTS

Funding was provided by the Oklahoma Medical Research Foundation (OMRF). We would also like to thank Dr. James Battiste and Dr. Anish Babu for their help with the migration chamber. Megan Lerner from Surgery Research Laboratory at the University of Oklahoma Health Sciences Center for the IHC staining. Cartoons created with BioRender.com